

# **MEMBRANE CHROMATOGRAPHY - HIGH THROUGHPUT SCREENING AND SIMULATIVE PROCESS DEVELOPMENT STRATEGIES**

Zur Erlangung des akademischen Grades eines/einer  
DOKTORS/DOKTORIN DER INGENIEURWISSENSCHAFTEN /

von der KIT-Fakultät für Chemieingenieurwesen und Verfahrenstechnik des  
Karlsruher Instituts für Technologie (KIT)  
genehmigte

DISSERTATION

von  
M. Sc. Dominik Marcel Stein  
aus Ellrich

Tag der mündlichen Prüfung: 12.01.2023

Erstgutachter/-in: Prof. Dr. Jürgen Hubbuch

Zweitgutachter/-in: Prof. Dr. Matthias Franzreb



## Danksagung

Die vorliegende Arbeit ist während meiner Tätigkeit als externer Doktorand am KIT-Fakultät für Chemieingenieurwesen und Verfahrenstechnik Sektion Molekulare Aufarbeitung von Bioprodukten (MAB) des Karlsruher Instituts für Technologie (KIT) in Kooperation mit Sartorius Stedim Biotech GmbH entstanden.

Nach Abschluss meiner Dissertation möchte ich allen Personen, welche mich bei der Durchführung und Fertigstellung meiner Arbeit unterstützt haben, herzlich danken.

Ich möchte im Besonderen meinem Doktorvater Prof. Dr.-Ing. Jürgen Hubbuch für die Ermöglichung dieser Arbeit danken. Darüber hinaus gilt meinem Doktorvater mein Dank für die Übernahme meiner Promotion in für mich ungewissen Zeiten, sowie für die stets konstruktiven Diskussionen und die umfassende und gute Betreuung. Dementsprechend danke ich Ihm nicht nur für seinen fachlichen Input, die eingeräumten Freiheiten und das entgegengebrachte Vertrauen, sondern auch für sein soziales Engagement, von welchem ich zusätzlich profitieren konnte.

Des Weiteren danke ich Herrn Prof. Dr. Harald Horn für die Übernahme des Vorsitzes der Prüfungskommission sowie Frau Prof.- Dr. Giesela Guthausen für die Übernahme der Prüferin und Herrn Prof. Dr. Matthias Franzreb für die Begutachtung dieser Arbeit.

Ich danke Dr. Louis Villain für die Ermöglichung der Kooperation mit Sartorius Stedim Biotech GmbH und Dr. Volkmar Thom für die Betreuung.

Den Kollegen Dr. Adrian Ley, Dr. Thomas Kruse und Dr.-Ing. Jan Schwellenbach danke ich für die gute Zusammenarbeit, das gute Arbeitsklima und die nötigen Ablenkungen neben dem Arbeitsalltag. Im Besonderen gilt mein Dank Dr. Adrian Ley für die ausgezeichnete Zusammenarbeit, fachlichen Diskussionen, interdisziplinäre Zusammenarbeit und privaten Ausgleich, zusammen mit Carina Ley.

Für Ihr fundiertes Fachwissen, handwerkliches Geschick und großen Arbeitseinsatz danke ich Philipp Werner Kirst, Robert Sperling, Peter Polossek, Thomas Krumbein, Jelena Kalinger, Nelli Marks und Nicole Linne.

Im Weiteren möchte ich Dr.-Ing. Steffen Zobel-Roos für die Betreuung während des Masterstudiums, der Masterarbeit, fachlichen Diskussionen während der Promotion und privaten Ausgleich, zusammen mit Lillan Roos, danken.

Alexander Langsdorf, Sebastian Hegner, Marvin Machava, Lucy Nisser, Lukas Schwetschenau und Niklas Eisele danke ich für Ihren guten Einsatz während ihrer Abschlussarbeiten, welche alle einen Teil zum Gelingen dieser Arbeit beigetragen haben.

Mein spezieller Dank gilt meinen Eltern Uwe und Pia Stein welche mich für diesen Weg gerüstet haben und mich zusammen mit meiner Schwester Michele immer unterstützt haben.

Ganz besonderer Dank gilt meiner Lebensgefährtin Kirstin Schneider für Beides, fachliche und private Unterstützung. Ihr bedingungsloser Rückhalt, Einfühlungsvermögen, Verständnis und Zuneigung neben Ihrer eigenen Promotionsphase ermöglichten die kontinuierliche Arbeit und den erfolgreichen Abschluss dieser Arbeit.

### Zusammenfassung

Die in dieser Dissertation durchgeführten Untersuchungen liefern einen Beitrag im Bereich der biopharmazeutischen Prozessentwicklung und Produktion, im Speziellen für die chromatographische Aufreinigung. Bedingt durch die weltweite SARS-CoV-2 Pandemie stand die biopharmazeutische Industrie im Mittelpunkt des Medieninteresses. Dies führte zu einer öffentlichen Diskussion der Entwicklung und Herstellung von biopharmazeutischen Produkten. Aufgrund des dringlich benötigten Impfstoffes sind auch die benötigten Prozessentwicklungszeiten dieses erörtert worden. Die schnelle Bereitstellung eines wirksamen Arzneimittels bzw. Impfstoffes unter Einhaltung der behördlichen Anforderungen erfordert eine modernisierte und effizientere Entwicklung. Hierbei birgt eine einseitige Fokussierung auf die reine Reduktion der Entwicklungszeit eines Prozesses jedoch Nachteile und Risiken. Die Effizienzsteigerungspotentiale ergeben sich vor allem aus Wissensmanagement bei der Übertragung von bekannten Prozessentwicklungen wodurch Neuentwicklungen durch vorhandenes Wissen beschleunigt werden können. Des Weiteren besteht das Risiko bei einer reinen Zeitfokussierung, dass neuer/alternativer Herstellungsverfahren vernachlässigt werden und die langfristige Wettbewerbsfähigkeit nicht gegeben ist.

Im Allgemeinen ist der pharmazeutische Aufreinigungsprozess in den vorgelagerten Upstream- (USP) und den daran angeschlossenen Downstream Prozess (DSP) unterteilt. Der USP verfolgt den optimalen Zellklon bzw. die optimalen Zellproduktionsbedingungen, wodurch eine stabile und hohe Produktivität erreicht wird. Im Gegensatz konzentriert sich das DSP auf die Produkt- und die Verunreinigungsprofile mit dem Ziel, eine hohe Reinheit und Ausbeute des Produktes zu erhalten. Aufgrund des hohen Standardisierungsgrades und der verfügbaren Informationen eignet sich die Herstellung von monoklonalen Antikörpern als Beispiel für einen Plattformprozess. Dieser Prozess umfasst im USP die Vorbereitung von Kulturen und Zellen sowie die Herstellung des Wirkstoffes in einem Fermenter. Anschließend erfolgt die Aufreinigung des Produktes im DSP durch die Zellabtrennung, zwei bis drei Chromatographieschritte, Virusinaktivierung und einen eventuellen Pufferaustausch. Dem angeschlossenen folgt die Virus- und Sterilfiltration in Vorbereitung auf die Abfüllung.

Das derzeitige Verfahren in der chromatographischen Prozessentwicklung ermöglicht den Maßstabstransfer vom Labor zur Produktion durch verschiedene Ansätze. Diese Ansätze beruhen auf experimentellen Informationen, Expertenwissen sowie mechanistischer und/oder statistischer Modellierung. Die Prozessentwicklung gliedert sich in eine erste statische Untersuchung, eine detailliertere dynamische Leistungsuntersuchung und Experimente. Das grundsätzliche Ziel ist eine erfolgreiche Ergebnisübertragung in den Produktionsmaßstab. In frühen Entwicklungsstadien stehen der Prozessentwicklung meist nur sehr geringe Mengen des potenziellen Wirkstoffes zur Verfügung. Dementsprechend werden die statischen Untersuchungen entweder manuell oder durch robotergestützte Pipettierschritte im Kleinstmaßstab durchgeführt. Dem angeschlossenen werden in Performance-Untersuchungen die ersten dynamischen Effekte ermittelt, typischerweise in automatisierten Robotersäulen im Mikrolitermaßstab. Bei ausreichender Verfügbarkeit werden detaillierte Experimente im Milliliter-Maßstab mit Flüssigchromatographie-Systemen im Labormaßstab durchgeführt. Die Laborsysteme weisen bereits einen mit der Produktion vergleichbaren Automatisierungsgrad auf. Dementsprechend bieten die detaillierten Experimente in der Regel die Grundlage für den Transfer in den Pilot- oder Produktionsmaßstab.

In aktuellen Studien wird der Entwicklungsprozess häufig durch mechanistische Modellierung (MM) unterstützt. Das Ziel dieser Arbeiten ist eine theoretische Repräsentation des betrachteten Schrittes unter Bildung eines digitalen Zwillings. MM bietet die Möglichkeit, zusätzliche Informationen über Eingangsstoffe, stationäre Phasen, Geräte und Prozessführungen zu generieren. Auf diese Weise könnte MM die heute bekannten Prozessentwicklungsansätze miteinander verbinden, zusammenfassen und eine lebende Prozessbibliothek schaffen. Eine solche Bibliothek könnte das Wissen aus verschiedenen Prozessen bündeln und auf neue Fragestellung übertragen. Durch eine solche Transferleistung würden sich Zeit- und Kostenaufwand reduzieren.

Die Entwicklung einer lebendigen Prozessbibliothek erfordert gleiche Untersuchungsansätze für alle stationären Phasen. Aufgrund der historischen Entwicklung besteht ein Ungleichgewicht zwischen partikulären/harzbasierter basiert Chromatographie und anderen stationären Phasen. Diese zumeist relativ neuen stationären Phasen werden nur selten für neue experimentelle Aufbauten, Prozessführungen und mechanistischen Modellierungsansätzen diskutiert.

In der vorliegenden Arbeit wird ein monoklonaler Antikörper-Aufreinigungsprozess zur Aggregatabtrennung untersucht. Hierbei wird zunächst die Angleichung der Prozessentwicklungsmethoden zwischen diffusiven harzbasierten- und konvektiven Membranadsorbentien (MA) als stationäre Phasen angestrebt. Dafür wird zunächst ein Aufbau für ein Hochdurchsatz-Screening entwickelt und mittels mechanistischer Modellierung die Ausarbeitung eines digitalen Zwillings angestrebt.

In vier maßgeblichen Fallstudien werden die unterschiedlichen Prozessentwicklungsansätze für konvektive stationäre Phasen an jene der partikulären Chromatographie angeglichen. Hierbei werden folgende Bereiche untersucht: Bestimmung des Prozessparameterbereichs, Einbeziehung neuer Prozessführungen, Vergleichbarkeit unterschiedlicher stationärer Phasen und Skalierbarkeit. Für die Untersuchung konvektiver stationärer Phasen wie MA, welche typischerweise einen hohen Stofftransport und geringen Druckverlust im Modul aufweisen, wurde ein HTS Modul im Kleinstmaßstab für eine skalierbare Prozessentwicklung entwickelt. Die Untersuchung fokussierte sich auf die Entfernung von Aggregaten aus einer fermentierten monoklonalen Antikörperlösung.

Die erste Fallstudie untersucht die experimentelle Anwendung des entwickelten HTS-Aufbaus und -Moduls. Hierbei werden der klassische Bindungs- und Elutionsmodus unter Variation des pH-Wertes und der Salzkonzentration angewendet. Dadurch lassen sich die Prozessfenster für die untersuchten Ionenaustausch-MA Sartobind® S und Q ermitteln. Des Weiteren wird mit Hilfe mechanistischer Modellbildung ein digitaler Zwilling erarbeitet. Die erhaltenen Ergebnisse bestätigen den erfolgreichen HTS-Aufbau und den entwickelten digitalen Zwilling. Im Ergebnisvergleich mit einer flüssigchromatographiebasierten Systemauftrennung zeigte der digitale Zwilling eine Signalübereinstimmung von über 80%. Des Weiteren wird für eine Maßstabsübertragung eines 0.42 mL Moduls auf ein 800 mL Modul eine Vorhersagegenauigkeit der dynamischen Durchbruchkonzentration von 90 % erzielt.

Im Rahmen der Angleichung von konvektiven zu harzbasierten stationären Phasen ist in der zweiten Fallstudie die Abbildbarkeit von neuen Prozessführungen untersucht worden. Unterstützt durch mechanistische Modellierung wurden zwei verschiedene Trennungen auf kompetitive Adsorption untersucht. Darauf aufbauend wurde ein neuartiges HTS-Screeningmethode entwickelt. Dieses Verfahren ermöglicht die Bestimmung von Verdrängungseffekten durch kompetitive Adsorption und liefert Schlüsselgrößen zur Identifizierung dieser. Die Untersuchungsmethode wird Überladungs- und

Elutionsverfahren (overload and elute mode, OBE) genannt und ebenfalls in der Aggregatabtrennung mit Sartobind® S untersucht. Basierend auf der im HTS angewandten OBE-Methode lassen sich sowohl klassische als auch dynamische Effekte bestimmen. Die Einführung des Verdrängungsidentifikators (displacement identifier, DI) ermöglicht eine Visualisierung von Verdrängungseffekten in einer Prozessparameterkarte. Auf Grundlage dieser Ergebnisse werden die Verdrängungseffekte in einem Recyclingexperiment angewendet. Dieses Recyclingexperiment weist durch die Ausnutzung der Verdrängungseffekte eine 45 % Reduktion der IgG- und 88 % höherer Aggregatbindungskapazität im Vergleich mit einem einfachen FT-Prozess auf.

Die zuvor angeführten Arbeiten haben die Unterschiede zwischen harzbasierten und konvektiven stationären Phasen reduziert. Dementsprechend erfolgten in der dritten Fallstudie die Untersuchung und der Vergleich von unterschiedlichen stationären Phasen. Hierbei wird eine Strategie zur Bewertung verschiedener Kombinationen von stationären Phasen, deren Grundgerüsten und Liganden, vorgestellt. Diese Strategie gewährleistet für die Erstellung einer Lebenden Prozessentwicklungsbibliothek die Untersuchung und Auswahl von passenden stationären Phasen. In dieser Fallstudie werden entwickelte Strategien an neuartigen MA behandelt, welche verschiedene chromatographische Effekte kombinieren (Mixed Mode, MiMo). Die Strategie beinhaltet theoretische Überlegungen sowie Untersuchungen der optimalen stationären Phasen hinsichtlich ihrer Selektivität und Bindungskapazität. Anhand der theoretischen Überlegungen lässt sich der experimentelle Raum, die möglichen Kombinationen aus stationären Phasen, deren Grundgerüst und Liganden reduzieren. Dafür wird jeder potenzielle MiMo MA Kandidat auf sein Potential zur Reduktion von Aggregaten in einer mAb Lösung untersucht und mit der Leistung der harzbasierten stationären Phase Capto™ Adhere verglichen. Die vorgestellte Strategie reduziert in einem frühem Untersuchungszeitpunkt die Reduktion von drei auf zwei mögliche stationäre Phasen reduzieren. Unter Berücksichtigung des untersuchten Einflusses der Ionenkapazität lässt sich ein finaler Kandidat ermitteln. Hierbei zeigt der Kandidat eine um 2 bis 3 Membranzvolumen höhere Bindungskapazität als die Referenz Capto™ Adhere. Unter Verwendung der vorgestellten Strategie und Einbindung in eine Lebende Prozessbibliothek lassen sich zeiteffizient optimale stationäre Phasen identifizieren.

Komplettiert wird die Arbeit in der letzten Fallstudie durch eine anwenderorientierte Maßstabsübertragung mittels mechanistischer Modellierung. Diese Arbeit beschreibt die typischen Modellierungsschritte mit Fokus auf der Maßstabsübertragung. Hierbei wird in der fluiddynamischen Beschreibung im Speziellen auf die Untersuchung und Optimierung von verschiedenen Modulen und deren Maßstabsübertragung eingegangen. Abweichend von der klassischen Isothermen-Parameterbestimmung werden historische HTS Daten verwendet, um die Isothermen-Parameter abzuschätzen. Dieses Vorgehen ermöglicht in einem Lebenden Bibliotheksansatz die Inklusion von historischen Daten. Abgeschlossen wird die Fallstudie durch die Maßstabsübertragung eines axial durchströmten 0,46 mL HTS-Moduls zu einem 150 mL radial durchströmten Modul im Pilotmaßstab.

Abschließend liefert diese Arbeit ein Verfahren zur Optimierung der Prozessentwicklung. Die verschiedenen Ansätze der Prozessentwicklung können in einem Lebenden Bibliotheksansatz zusammengeführt werden. Dieser Bibliotheksansatz umfasst Expertenwissen, Experimente sowie statistische und mechanistische Modellierung. In diesem Bestreben wurden zwischen harzbasierten und konvektiven stationären Phasen gleiche Wettbewerbsbedingungen geschaffen. Diese Vergleichbarkeit ermöglicht eine direkte Auswahl der stationären Phasen für eine bestimmte Trennaufgabe. Die anwenderorientierte Maßstabsübertragung bietet einen Leitfaden, wie durch mechanistische Modellierung die unterschiedlichen Prozessentwicklungsansätze zusammengeführt

werden können. In dieser Arbeit zeigt die mechanistische Modellierung, wie der Prozessentwicklungsprozess abgebildet, transferiert, konserviert und standardisiert werden kann. Dadurch entsteht ein kohärentes und übertragbares Verfahren zur Verfügung, wodurch die anstehenden Herausforderungen in der Prozessentwicklung überwunden werden können.

### Abstract

This thesis addresses the biopharmaceutical process development and production, particularly chromatographic unit operations. In the recent global SARS-CoV-2 pandemic, the biopharmaceutical industry was in the spotlight of media interest. As a result, the development and manufacturing of biopharmaceutical products were discussed broadly in the public sphere. Providing a potent vaccine or any other drug within a short timeframe and within the regulatory requirements urges the development to be streamlined from candidate screening to manufacturing. On the other hand, the shortened timescale raises the question of long-term competitiveness if alternative manufacturing processes are suppressed for the sake of speed. Maintaining sustainable drug production with the new timelines requires a fundamental change in product and process development.

Generally, the manufacturing process is divided into upstream (USP) and downstream processing (DSP). The candidate screening and USP target the optimal cell clone and cell production conditions, respectively, to achieve stable and high product output. In contrast, DSP focuses on the product and impurity profile aiming for high purity and yield of the product. The production of monoclonal antibodies is suitable as an example process for a state-of-the-art platform process in pharmaceutical processing. In this process, USP incorporates culture and seed/cell preparation and production in a fermenter. Subsequently, the DSP comprises two to three chromatography steps, virus inactivation, possible buffer exchange, virus, and sterile filtration to prepare the final fill and finish.

The current chromatography process development (PD) procedure facilitates the scale transfer from laboratory to production by incorporating several tools. These tools are based on pure experimental information, prior knowledge, mechanistic and or statistic modeling. In addition, some or all tools are applied or partially applied in the overall PD procedure following the initial static screening, performance screening, and detailed experiments to achieve a successful scale-up. In the early stage of PD development, the amount of available material is limited, and the experiments are performed either manually or by robot-assisted pipetting steps. Thereafter, initial dynamic effects are investigated through performance screening typically applied in automated robotic columns in a microliter scale. Finally, detailed experiments are performed by applying benchtop systems on a milliliter scale. These detailed experiments are commonly the basis for the pilot or production scale-up, allowing production-comparable signals. In recent publications, mechanistic modeling (MM) often supports this development process, aiming for a digital twin of the development phase step investigated.<sup>1-6</sup> MM delivers additional information containing different feed, stationary phase, device, and operation modes integrated. Thus, MM could connect and summarize today's available tools, enabling a living PD library and drastically reducing the timeline and costs.

The development of a living library urges a level-playing field for all stationary phases. Resin-based chromatography is exhaustively investigated and described in the literature. However, other stationary phases, e.g., membrane adsorber, monolith, and fibers, are getting more adapted in process development. These relatively new stationary phases are rarely discussed in experimental set-ups, process modes, and mechanistic modeling approaches.

The present work applies the state-of-the-art monoclonal antibody aggregate removal process to achieve a level-playing field for convective stationary phases, here membrane adsorber (MA). Initially,

a high throughput screening set-up is developed, employing mechanistic modeling to achieve a digital twin.

Four major case studies were performed with the aim of aligning high throughput screening (HTS) applications for MAs with those established for column chromatography: process parameter range determination, incorporation of new processing modes, comparison of different stationary phases, and scalability. In order to exploit the MA typically features, such as high mass transfer and low-pressure drop per device, an HTS scale-down device (SDD) for scalable PD was developed. Its applicability is confirmed for a monoclonal antibody aggregate removal step.

The first case study explores the experimental application of the SDD developed. It uses bind and elute mode and pH and salt concentration variations to obtain process operation windows for ion-exchange MAs Sartobind® S and Q. In the second case study, we successfully developed a mechanistic model based on parameters obtained from the SDD - HTS setup. The results proved to validate the use of the SDD developed for parameter estimation and thus model-based PD. Finally, the third case study shows the transferability and scalability of data from the SDD - HTS setup using both a direct scale factor and mechanistic modeling. Both approaches show good applicability with a deviation below 20% in predicting 10% dynamic breakthrough capacity and reliable scale-up from 0.42 mL to 800 mL.

In addition to aligning MA with the resin-based experimental set-up, competitive adsorption is investigated by evaluating new and existing processing modes. Here, a mechanistic model case study for the investigation of competitive adsorption was conducted for two different two-component solutions and confirmed prior evidence. With these outcomes, a novel HTS screening procedure was developed, including determining competitive adsorption-based displacement effects and key parameter identification. The screening procedure employing an overload bind and elute mode (OBE) is presented in a case study dealing with IgG aggregate removal in a typical monoclonal antibody purification step, applying a Sartobind® S membrane adsorber (MA). Based on a MA scale-down device, the OBE mode allows the determination of classical process parameters and dynamic effects, such as displacement effects. Competitive adsorption-based displacement effects are visualized by introducing a displacement identifier (DI), leading to a displacement process map. Based on this map, the approach is transferred to and confirmed by the OBE recycle experiments with 4.6 mL and 8.2 mL benchtop scale devices resulting in 45 % reduced IgG monomer, and 88 % increased HMWS binding capacities.

The previous investigations facilitated a level-playing field between resin and convective stationary phases. Accordingly, the third case study investigated and compared different stationary phases. Hereby, a strategy for evaluating different combinations of scaffolds, backbones, and ligands was introduced. This strategy ensures investigating and selecting suitable stationary phases for creating a living library in PD. The strategy was evaluated on novel mixed mode (MiMo) MA. In addition, the strategy includes theoretical considerations, investigation of optimal stationary phase selectivity, and binding capacity. Based on the theoretical considerations, the experimental space, the possible combination of scaffolds, their backbone, and ligands can be narrowed down. For this purpose, each potential MM membrane adsorber (MA) candidate is investigated in its high molecular weight species (HMWS) reduction potential for a given mAb feed stream and referenced to the performance of Capto™ Adhere. The presented strategy reduces the investigated stationary phases from three to two at an early study stage. In addition, a final candidate can be determined by accounting for the investigated influence of the ionic capacity. The strategy presented is supported by HTS investigation

and confirmed by benchtop experiments. Finally, the identified candidate presents a binding capacity of 2-3 membrane volume (MV) higher than the reference Capto™ Adhere. When the here applied strategy is integrated into a living library format, optimal stationary phases can be identified time efficiently.

In the final case study, the work is complemented by an application-oriented mechanistic modeling scale transfer approach. In general, the applied modeling steps are presented from lab to production scale focusing on the scale transfer. The fluid dynamic investigation explicitly addresses the investigation and optimization of different chromatographic devices and their scale transfer. Deviation from the state-of-the-art isotherm parameter determination, historical HTS data is used to estimate apparent isotherm parameters. This approach allows the inclusion of historical data in a living library. The case study is completed by the scale transfer from a 0.46 mL small-scale device with axial fluid flow to a 150 mL pilot scale device with radial fluid flow.

To conclude, this work provides a methodology for an optimizing PD workflow. The different tools in PD are combined in a living library approach. This library approach includes prior knowledge, experimentation, statistical and mechanistic modeling. Initially, a level-playing field was established between resin- and convective stationary phases. Following this, the selection of stationary phases for a dedicated separation task was facilitated. Finally, the presented application-oriented scale transfer guides how MM can link the different PD approaches. In this work, MM presents its ability to map, transfer, preserve, and standardize PD workflow. Furthermore, a coherent and transferable methodology results, which can be applied to overcome the upcoming challenges in PD.

## Content

1	Introduction.....	14
1.1	Chromatography in pharmaceutical production .....	17
1.1.1	Stationary Phase .....	17
1.1.2	Process modes .....	19
1.2	Downstream process development.....	22
1.2.1	Workflow.....	22
1.2.2	High throughput screening .....	24
1.2.3	Mechanistic modeling.....	28
2	Thesis Outline .....	52
2.1	Research Proposal.....	52
2.2	Manuscript overview and author statement.....	54
3	HTS setup of a Scale-down Device for Membrane Chromatography - Aggregate Removal of Monoclonal Antibodies .....	56
3.1	Introduction .....	56
3.2	Material and Methods .....	59
3.2.1	SDD characterization.....	59
3.2.2	HTS and benchtop chromatographic experiments .....	59
3.2.3	Analytical methods.....	60
3.2.4	Data handling, automation, and mechanistic modeling.....	60
3.2.5	Scale-down device – experimental setup .....	60
3.2.6	Case study 1: High throughput screening - Bind and elute mode .....	63
3.2.7	Case study 2: Scale-down device and mechanistic modeling .....	65
3.2.8	Case study 3: scale-up.....	67
3.3	Result and Discussion.....	68
3.3.1	SDD – experimental setup.....	68
3.3.2	Case study 1: High throughput screening - bind and elute mode .....	70
3.3.3	Case study 2: Scale-down device and mechanistic modeling .....	71
3.3.4	Case study 3: Scale-up.....	76
3.4	Conclusion.....	77
3.5	Acknowledgment .....	78

## Content

---

4	PD exploiting competitive adsorption-based displacement effects in monoclonal antibody aggregate removal - a new high throughput screening procedure for membrane chromatography .....	80
4.1	Introduction .....	80
4.2	Materials and Methods.....	82
4.2.1	Materials .....	82
4.2.2	Methods.....	83
4.3	Results and discussion .....	90
4.3.1	Mechanistic process understanding .....	90
4.3.2	High throughput screening - OBE mode .....	94
4.3.3	OBE recycle chromatography - case study.....	96
4.4	Conclusion.....	97
5	Streamlined PD procedure incorporating the selection of various stationary phase types established in a mAb aggregate reduction study with different mixed mode ligands .....	99
5.1	Introduction .....	99
5.2	Materials and Methods.....	103
5.2.1	Materials .....	103
5.2.2	Methods.....	104
5.3	Results & Discussion .....	111
5.3.1	Ligand densities – Coupling procedure.....	111
5.3.2	Biophysical characterization of the stationary phase .....	112
5.3.3	Initial process parameter – capacity and selectivity.....	113
5.3.4	Refinement of process parameter – High throughput screening.....	114
5.3.5	Confirmation of process parameter – Bench scale.....	117
5.4	Conclusions .....	118
6	Full train product development from lab 2 production procedure – incorporating a living library with mechanistic modeling - from HTS Scale to pilot scale of Membrane Chromatography in aggregate Removal of Monoclonal Antibodies .....	119
6.1	Introduction .....	119
6.2	Materials and Methods.....	122
6.2.1	Buffer preparation .....	122
6.2.2	Feed preparation.....	122
6.2.3	Full train product development from lab to production procedure.....	123
6.2.4	Analytical methods.....	134
6.2.5	Data handling, automation, and mechanistic modeling.....	135
6.3	Results and Discussion .....	135

6.3.1	Case study 1: Fluid dynamic scale transfer .....	135
6.3.2	Case study 2: Adsorption parameter determination .....	144
6.3.3	Case study 3: Approach evaluation and scale-up .....	151
6.3.4	Conclusion.....	155
7	Conclusion and Outlook .....	156
8	Verification of the contribution from the co-authors .....	159
10	References.....	162
11	Appendix.....	176
11.1	HTS setup of a Scale-down Device for Membrane Chromatography - Aggregate Removal of Monoclonal Antibodies .....	176
11.1.1	HTS set-up development of a scale-down device .....	176
11.1.2	Robotic parameters.....	178
11.2	Appendix - Full train product development from lab 2 production procedure – incorporating a living library with mechanistic modeling - from HTS Scale to pilot scale of Membrane Chromatography in aggregate Removal of Monoclonal Antibodies.....	180
11.2.1	Mechanistic modeling .....	180

## 1 Introduction

Throughout the recent global SARS-CoV-2 pandemic, the biopharmaceutical industry has been the focus of both media and public awareness.<sup>7</sup> The public has widely discussed the development and manufacturing of biopharmaceutical products. Providing an effective vaccine or other drugs within a short timeframe and compliance with regulatory requirements urges streamlining development from candidate screening through manufacturing.<sup>8-11</sup> Pharmaceutical product development (PD) involves screening drug candidates, developing cells that produce the drug, and transferring the single cells to a master cell bank. Furthermore, optimization of production conditions for large-scale fermentation and development of drug purification consists of a series of unit operations to achieve the required regulatory purity.<sup>12-15</sup> The manufacturing process is divided into upstream (USP) and downstream processing (DSP), see Figure 1.1.<sup>12,16,17</sup> Moreover, candidate screening and USP aim to identify the optimal cell clone and cell production conditions to achieve stable and high product output. In contrast, DSP focuses on the final product and impurity profile to achieve a high yield and purity. The production of monoclonal antibodies, presented in Figure 1.1, is ideally suited as an example process for pharmaceutical PD due to the state-of-the-art platform process. In monoclonal antibody production, USP incorporates culture, seed/cell preparation, and drug production in a fermenter, whereas DSP includes several chromatography steps. In between, unit operations such as virus inactivation, possible buffer exchange, and subsequent virus and sterile filtration are executed to prepare the final fill and finish.<sup>13,14,18,19</sup>

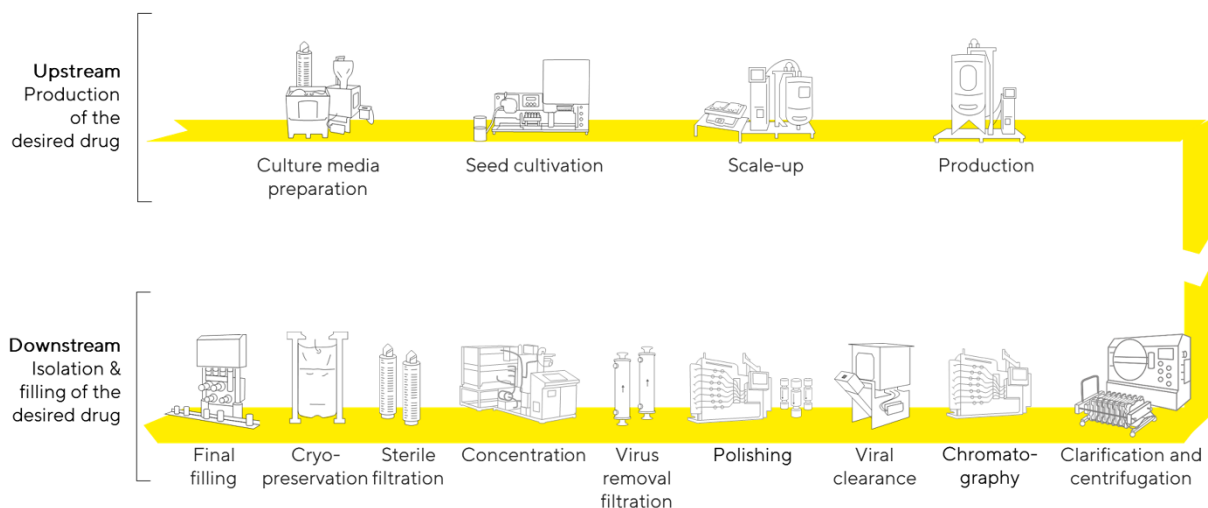


Figure 1.1: Exemplary mAb processing scheme, introducing process from cell cultivation in upstream to final fill and finish. The downstream process is divided in the clarification (cell removal), 1-3 chromatographic separation steps, in between virus inactivation, virus filtration, buffer exchange and sterile filtration.

Chromatography, with its various interaction/separation modes, typically offers high selectivity and purity, which can be associated with high costs and low productivity compared to other unit operations.<sup>20-22</sup> The chromatographic separation is a physical method exploiting the different distribution of components in either the mobile or stationary phases. Chromatography is applied in various industries and can be divided based on different characteristics. In the following, chromatography clustering is performed by the applied pressure. The liquid chromatography (LC) is operated in the range of 0–10 bar, and high-pressure liquid chromatography (HPLC) or high-

performance liquid chromatography applies typically pressure up to 400 bar. In comparison, the ultra-high performance liquid chromatography (UHPLC) is operated with pressure up to 1500 bar.<sup>23-26</sup> In a pharmaceutical environment, the HPLC and UHPLC is commonly applied for analysis, whereas liquid chromatography (LC) are used for manufacturing, although HPLC can be used in the production of small molecules or in the chemical industry.<sup>27-29</sup> In addition, chromatography can be classified according to the applied mobile phases such as gas chromatography (GC) and liquid chromatography (LC), gas, respectively liquid as mobile phase. However, in the pharmaceutical industry, GC is only relevant for analytical purposes. The stationary phase is typically a solid material. However, in some research areas, liquids are also used as a stationary phase.<sup>30,31</sup>

The chromatographic unit commonly used in pharmaceutical processes is LC, having a liquid mobile phase and a solid stationary phase.<sup>16,19,20</sup> The stationary phase is held in a device, such as a column or a capsule, and the liquid mobile phase flows through the device. Specifically, the mobile phase contains the molecules to be separated and is the so-called feed. The separation itself is performed by different interactions of the molecules between the mobile phase and the stationary phase. When the concentration of molecules in the liquid and stationary phase is constant, an equilibrium state is obtained. The interaction of the molecules with the stationary phase is induced by modification of the stationary phase, such as chemical coupling of certain molecules, the so-called ligands. Following the statute of the lowest energetical level, a molecule tends either to remain in the mobile or to adsorb on the stationary phase. Thereby, the feed is separated from the impurities/molecules, which are attracted to the stationary phase to different extents. The process mode nomenclature and phases differ whether the target molecule remains in the liquid or is bound to the solid phase. Following the process mode, the surrounding conditions, e.g., salt, H<sup>+</sup>, OH<sup>-</sup> concentration, can elevate or suppress the molecules preference of binding to the stationary phase. In general, the surrounding conditions are adjusted by changes in temperature, additional chemical components, or pressure, whereas the latter is usually not applied in pharmaceutical processes.

The complexity of drug products, the various process entities, and the high regulatory requirements issue high development and production costs within the range of 900 - 3000 million US dollars per drug.<sup>32,33</sup> These costs are incurred for drug discovery in the process of screening 10 000 molecules, toxicity testing, phase I to III clinical trials, registration, and PD to final production. This process takes ten to fifteen years. Consequently, PD evaluates the chromatographic processing types, stationary phases, and operation mode by separation success and commercial objectives.

Given these factors in chromatography PD, the demanded timeline and cost are typically overcome by applying platform approaches and robot-assisted high throughput screening. Platform approaches use a fixed set of unit operations and stationary phases, minimizing PD effort while simultaneously ensuring acceptable selectivity, capacity, and robustness. Platform approaches require thorough testing and qualification concepts for the involved operating units in advance. The advantage of such an approach lies in the expertise obtained by testing and qualifying a set of typical process parameters associated with materials that promise specific performance criteria.<sup>17,34</sup> Consequently, applying a platform technology enables time-saving knowledge- or experience-based PD of robust and productive processes. However, the application of platform technology often comes at the cost of a self-limitation to a few unit operations and well-characterized media.<sup>17,34</sup> This approach is only feasible for a set of molecules expressing high similarity, such as similar mAb molecules. However, platform development can be addressed by establishing PD tools of high throughput screening (HTS) robotic platforms for parallel, automated and standardized workflows to accelerate PD efforts. In addition,

applying scale-down devices (SDD) in these workflows reduces the usage of materials and costs.<sup>35-39</sup> HTS is applied among others for drug identification<sup>40-42</sup>, biological libraries<sup>43,44</sup>, cell cultivation<sup>45,46</sup>, aqueous two-phase systems<sup>47,48</sup>, and chromatography performance estimation.<sup>39,49-54,181</sup>

In HTS-based chromatography PD, the mode of parameter determination can be divided into the following: Batch isotherm determination<sup>49,55</sup>, process range evaluation<sup>35,53</sup>, scale dependency<sup>35,53,56,57</sup> and scale-down model development<sup>53,58</sup>. Typical formats for batch isotherm determination and process range evaluation are microtiter plates. Dynamic effects can be assessed in microtiter plates using micro pipetting devices and/or vacuum. The transfer from lab to production scale is called scale-up or scale transfer. Scale-up can only be successful if all significant parameters are known and well understood. Following this, allowing process predictions within HTS requires process-comparable operations and dynamic effects to be mimicked. Consequently, knowledge of scale-dependent variables is essential, and critical process parameters must be kept under control. Therefore, scale dependency of critical parameters and scale-down model development are highly connected.<sup>181</sup>

The solely experimental-based PD enables first process spaces determination and assessment of dynamic effects. However, fluid dynamic discrepancies, as well as wall and mass transfer effects, are known challenges for scale-up by existing HTS scale-down devices (SDDs) and lab-scale columns.<sup>35,51,56,59,60</sup> Reliable scale-up typically requires additional experiments on an LC system using lab-scale columns (1-10 mL) with process-scalable bed height. Solely experimental PD has been extended with mechanistic modeling (MM), a mathematical representation of the SDD, which enables a more profound understanding and facilitates a scale transfer from lab to production.<sup>1-6</sup> Mechanistic modeling consists of one or more mathematical descriptions of physic/chemical effects called models. The application of a model to a system or device considers all significant/relevant parameters. In addition, a digital twin is generated for models representing all process-relevant actions, such as pumping or waiting time, while a broad experimental range is also precisely represented.<sup>61</sup> Following this, a certain level of model detail is necessary when a digital twin mirrors a process and/or device such as HTS SDD. Eventually, a digital twin can be generated, revealing dynamic effects, and increasing the process understanding by allowing the transition from a unit operation to full-train PD. Thus, the predictive power - if given - of a scale-down model can overcome the limitations of a strictly experimental approach.

Admittedly, the methods mentioned above are state-of-the-art in resin-based chromatography. However, new and comprehensive methods are needed to comply with the shortened timescales and to facilitate long-term competitiveness. In this thesis, a new PD strategy is introduced that emphasizes a living library approach. Incorporating the living library approach, a new HTS SDD set-up is developed, characterized, and complemented by a model-assisted digital twin incorporating competitive adsorption processes. Finally, the HTS SDD is extended to investigate convective stationary phases facilitating a level-playing field with diffusive stationary phases. In the following, biopharmaceutical production is introduced in more detail, including the different chromatographic applications. Thereafter, process development, mechanistic modeling, and model/system characterization methods are described.

### 1.1 Chromatography in pharmaceutical production

The established monoclonal antibody process, as described in the introduction, typically consists of two to three chromatography unit operations after the fermentation and cell separation/clarification.<sup>13,14,18</sup> Thereafter, viruses are removed by filtration, the product is adjusted to the final concentration, and the final purity is achieved by sterile filtration. The process is completed by the fill and finish step of the final product in its dosage form. Measurements in quality standards ensure that the process delivers a constant drug product in accordance with the regulatory requirements. The regulatory guidelines have evolved with pharmaceutical manufacturing and processes, unfortunately, driven by adverse drug product reactions in the past. Accordingly, these guidelines envelop with new substances but also cover general aspects of drug product manufacturing to prevent incidents for existing and new substances. The urge for reliable quality is evident when considering that the receiving person is ill and the immune system is weakened. This weakened immune system is probably unable to respond to other threads, e.g., viruses or side effects. Hence, all steps during pharmaceutical manufacturing must ensure reproducibility and outstanding quality of the drug product. This quality is ensured by the regulatory requirements and guidelines, e.g., the food and drug administration (FDA) and the EMEA for the US or the EU market, respectively. During the process, impurities like host cell proteins, DNA, endotoxins, and impurities by the unit operation itself, as well as virus and cell fragments, need to be removed. Following this, practical examples apply two dedicated orthogonal steps for viral reduction (ICH Q5A) and a safety margin of 4-6 log<sub>10</sub> reduction of one virus molecule per dosage.<sup>13,62</sup> Specifically for a mAb process, aggregates of the single mAb pose a risk of adulterating the activity and can induce side effects.<sup>63,64</sup> The pharmaceutical industry addresses the regulatory requirements of such mAb processes by applying various unit operations.

The various chromatographic applications are described in the following section, detailing the typically stationary phases, interactions induced by the involved ligands, and process modes.

#### 1.1.1 Stationary Phase

In chromatography for pharmaceutical processes, four different scaffolds presenting different properties are frequently applied: a) bead, b) monolith, c) fiber, and d) membrane adsorber (Figure 1.2).<sup>216</sup>

Particulate/resin-based scaffolds usually have backbone structures consisting of particle diameters in the range of 50 – 500  $\mu\text{m}$  and pore diameters of 20 - 160 nm.<sup>21,22</sup> The resin scaffold typically possesses a high porosity obtaining a high internal surface area. A meso and macro pore structure can also characterize monoliths such as bead-based scaffolds. The monolith macro pores are called flow channels with a typical channel size of 1-6  $\mu\text{m}$ <sup>24-26</sup> while the meso pores are 2-50 nm.<sup>21,24,25</sup> Monoliths and beads tend to entail susceptibility to mechanical instability due to high internal porosity.<sup>21</sup> In addition, resins and monoliths are typically housed by a column applying mainly axial flow.<sup>216</sup>

Depending on the formulation and packing procedure, fiber-based backbone structures consist of flow channels in the range of 0.5 – 20  $\mu\text{m}$ . Membrane adsorber (MA) backbone structures with pore sizes of 2-4  $\mu\text{m}$  are known for their high applicable flow range with relatively low-pressure drop.<sup>31</sup> The fiber-based and MA backbones are typically housed in capsules employing radial flow through the stationary phase.<sup>216</sup>

## 1.1 Chromatography in pharmaceutical production

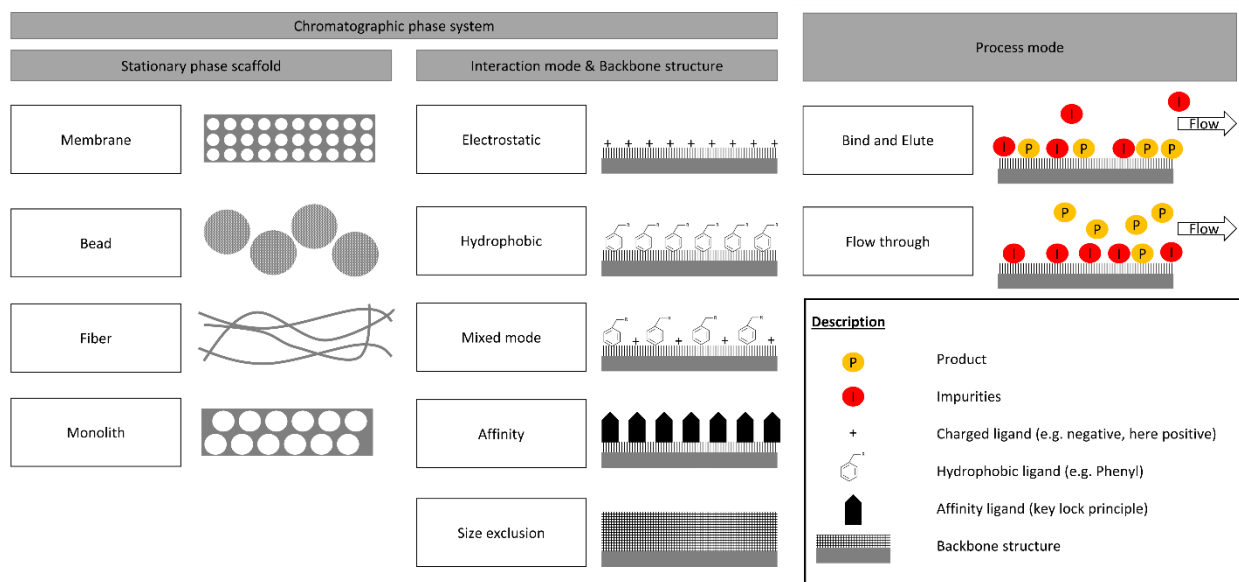


Figure 1.2: Exemplary chromatographic subgroups. Schematic representation of conventional subdivisions in chromatography using process mode, mode of interaction, and type of stationary phase scaffolds. The stationary phase is divided into the stationary phase scaffold as well as different ligand interactions and modifications. Stationary phases used in downstream processes are typically membranes, beads, fibers and monolith. Right-handed, the different process modes bind and elute as well as flow through represent additional processing modes.<sup>216</sup>

Subsequently, the general stationary backbone and the chromatographic interactions are described. The different stationary phases are chemically modified to facilitate chromatography interaction, except for size exclusion materials. For chromatography, the pharmaceutical industry commonly applies size exclusion, ionic, hydrophobic, affinity, and a combination of the aforementioned - so-called mixed mode (MiMo) - interactions.<sup>16,19,65,66</sup>

In the classical mAb process, size exclusion is usually limited to the use in analytical application.<sup>64,67</sup> In the interest of completeness, size exclusion separations shall be explained, wherein the separation is based on the size differences between two or more molecules. The porous backbone of the stationary phase for size exclusion is manufactured to have a similar pore size distribution between all particles. Following this, a molecule with a diameter below the pore diameter can penetrate the entire porous structure, while larger molecules can enter this volume only partially or not at all. Accordingly, the larger molecules have a shorter distance to the column outlet, while the smaller molecules have a longer distance based on the additional accessible volume.

The ionic interactions are based on the attractive force between two differently charged molecules.<sup>68,69</sup> Anion exchange chromatography consists of positively charged ligands while the dedicated molecule net charge is negative, and for cation exchange chromatography, it is vice versa. The application of anion- or cation exchange chromatography is typically decided by the pH value of the feed stream, considering the isoelectric point of the molecule that should be bound.<sup>69</sup> Below the isoelectric point, the molecule is positively charged. Above the isoelectric point, the molecule is negatively charged, allowing the properties of the molecule and process conditions to determine whether a cation exchanger or anion exchanger must be applied, respectively.

Hydrophobic chromatography interactions are present at or close to the pH value of the molecule isoelectric point, as well as a high salt concentration leading to the arrangement of ionic charges inside the protein structure.<sup>16,70</sup> This said, van der Waals forces and hydrogen bonds are thought to be the reason for

this hydrophobic interaction, although these interactions are not yet fully understood.<sup>68</sup> The affinity interaction is based on the biological induced fit concept, in which the enzyme and the substrate interact, changing the conformation and forming a protein-ligand complex. These ligands for affinity chromatography are the most selective but also most expensive ligands compared to classical ion exchange or hydrophobic ligands, see Figure 1.3. Following this, mixed mode (MiMo) ligands consisting of at least two different interaction modes were developed to overcome the single mode limitations and to reduce ligand costs.<sup>13,71-73</sup> However, up to now, affinity chromatography has not been replaced by MiMo in the mAb process but supplemented.

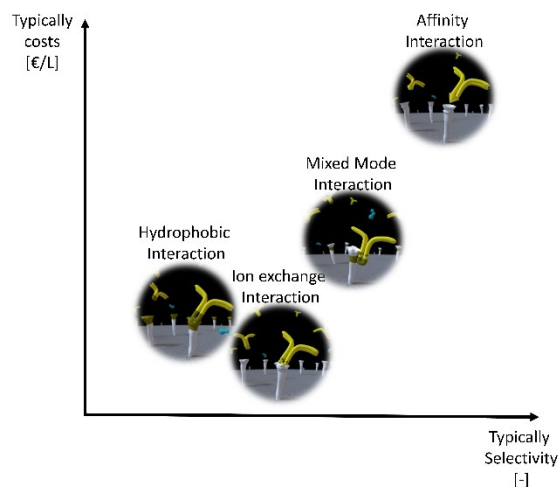


Figure 1.3: Exemplary cost and selectivity for different interaction modes / ligands.<sup>74-83</sup> The selectivity and costs increase from hydrophobic-, ion exchange-, mixed mode- and affinity interaction.

### 1.1.2 Process modes

In general, chromatographic process modes are bind and elute (BE), flow-through (FT), and subgroups thereof. These subgroups are characterized by different load, wash, and elution strategies. The classification of BE and FT depends mainly on the product behavior during the chromatographic process.<sup>16-18</sup> In BE mode, the product attaches to the stationary phase. At the same time, the impurities preferably either do not interact with the stationary phase or are separated from the product during elution, e.g., an ion exchange chromatography applying a salt or pH gradient. In mAb processing, bind and elute steps are typically the first chromatographic purification, named capture step, and the second chromatographic step, the so-called purification step. The product concentration in BE is typically higher when compared to the concentration in the feed. On the other hand, operating in FT mode is generally associated with binding the impurities and allowing the product to pass through the stationary phase with as little interaction as possible.<sup>19,20</sup> As a result of the impurity binding, the product concentration of the FT mode is limited to that of the feed. The FT mode is usually applied as the last chromatographic step in a mAb process; the latter is the so-called polishing step.

Subgroups of BE and FT mode apply more dynamic effects such as competitive binding. The weak partitioning, frontal-, overload- and displacement chromatography are exemplary listed for dynamic process modes.<sup>13,14,84-86,209</sup> For instance, overload and elute chromatography applies higher mass loading beyond the dynamic breakthrough concentration.<sup>8</sup> In FT mode, the overloading of the stationary phase implies that the higher attracted impurities displace the lower attracted product

## 1.1 Chromatography in pharmaceutical production

---

when competitive adsorption is present. Consequently, applying displacement effects in FT mode by overloading the stationary phase increases its utilization.<sup>209</sup>

In addition to the classification of BE and FT chromatography mode, batch and continuous processing categorization are possible. The batch process is defined by a distinct volume or time in which the process is completed. Thereafter, the next process is started, clearly distinguishing one run from another.<sup>12</sup> Continuous processes are constantly loaded with feed. At the same time, the product leaves the system continuously, with no clear division between one product sample to another possible, see Figure 1.4 simulated moving bed (SMB).

The only fully continuous chromatographic process is the SMB, which is derived from the concept of a theoretically true moving bed (TMB).<sup>68</sup> In addition to the SMB the continuous carousel chromatography (CAC) was developed to enable a continuous feed application.<sup>87</sup> However, various semi-continuous chromatography processes have been developed regardless of the exact definition for continuous processing. These processes apply multiple columns and switch the connection among these or the connected applied solution, partially comparable to the SMB. State of the art multi-column chromatography (MCC) is sequential multi column chromatography (SMCC)<sup>88</sup> or periodic counter-current chromatography (PCC)<sup>89</sup>, multi column counter-current solvent gradient purification chromatography (MCSGP)<sup>90</sup> and integrated counter-current chromatography (iCCC)<sup>91</sup>. These process modes are aimed either for recovery and purity or column utilization increase. Accordingly, the MCSGP and iCCC processing modes obviate the cut point predicament in either product loss or quality, see Figure 1.4. Consequently, when product and impurity overlap during elution, the aforementioned processing modes shift this change over fraction to a second identical or complementary interaction column. Following this, product recovery increases while purity is at least equal to the comparing batch processes. However, the utilization of the used columns will generally be comparable or lower compared to a batch process with the same columns. The SMCC/PCCC process shown in Figure 1.4 SMCC/PCCC is applied to maximize the column utilization. Comparable to the SMB process, the columns are willingly overloaded, and the subsequent column receives the feed breakthrough. The subsequent column will receive the feed solution directly in the next phase. Eventually, the SMB process mode presents a maximized purity and utilization but comes with the disadvantage of a binary separation. The SMCC/PCCC process mode increases the column utilization and can separate mixtures with more than two molecules. However, the SMCC/PCCC process has the drawback of increasing the number of columns or time required due to the three process phases a column needs to perform before the next loading step.

In general, (semi) continuous processes are beneficial for utilization, recovery, and purity, but they involve a more complex PD and system design. Furthermore, the initial costs for PD and system are higher when compared to a pure batch process, which is partially why continuous processing is rarely applied.<sup>92</sup>

# 1.1 Chromatography in pharmaceutical production

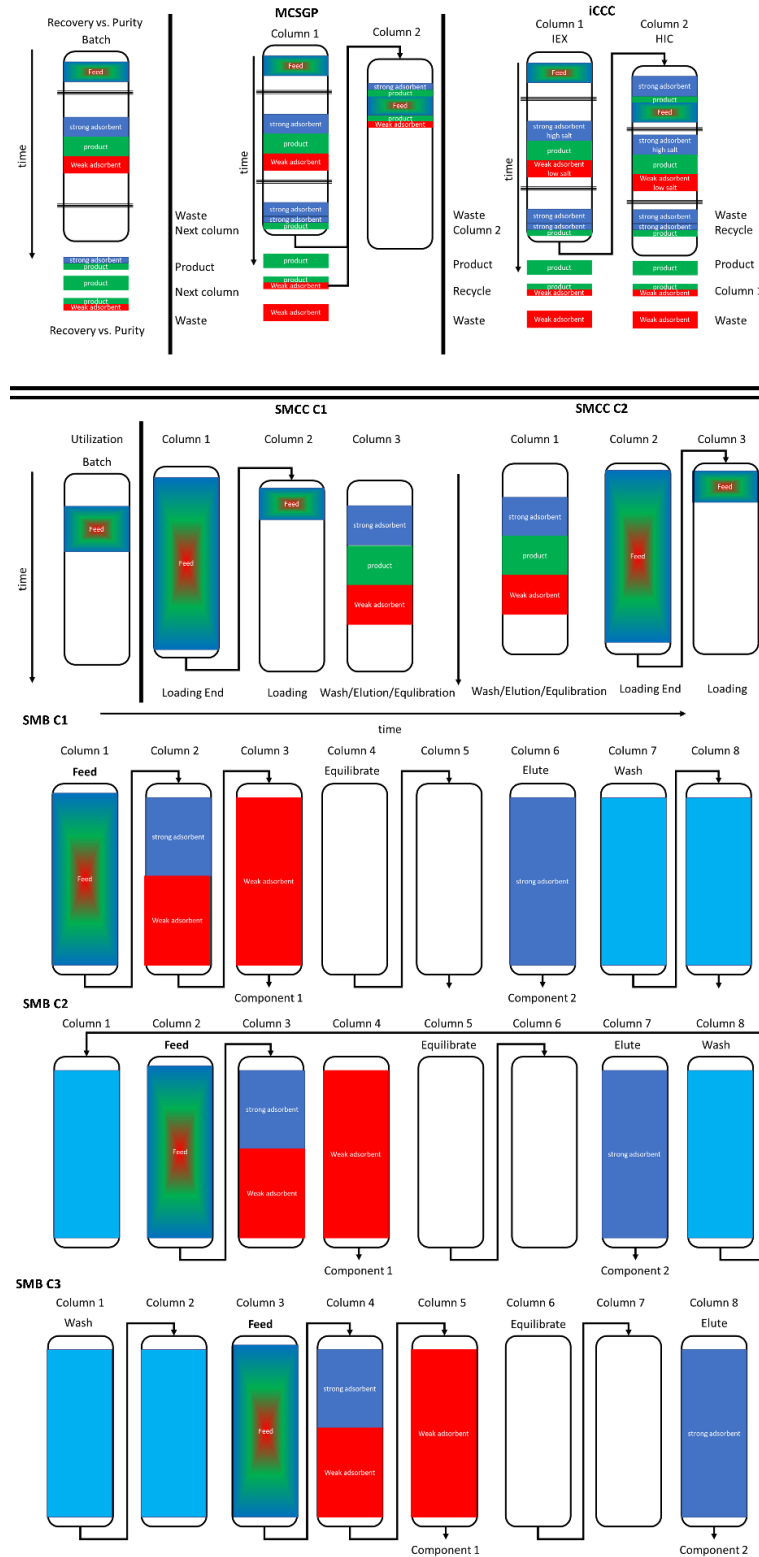


Figure 1.4: Exemplary batch and continuous processing. The figure comprises different process times over the column length or cycles. The feed mixture is indicated by a color mixture of red, green, and blue. In addition, weak binding components are indicated by the red color and strong binding components by dark blue. The MCSGP, iCCC are presented in the top. These two process schemes use parts of the fractionated product pool to either recirculate or reload a different column which theoretically facilitates a purity and recovery of 100%. Thereafter, the SMCC processing scheme with its higher stationary phase utilization is presented. Finally, the figure is completed by three SMB cycles.

### 1.2 Downstream process development

Several methods have increased the downstream PD efficiency and quality. These methods have been standardized into tools that accompanied the development from small-scale laboratory experiments at a microliter to milliliter scale, wet lab investigations within hundreds of milliliters of solutions, and liter-scale pilot testing up to production scale.<sup>35-39,49,50,53</sup> These tools are based on pure experiments, prior knowledge, mechanistic and/or statistic modeling. Prior knowledge includes the transfer of the feed, stationary phase, or similar processes information incorporation to the new separation task based on historical data or information. Statistical modeling, e.g., design of experiments (DoE), and mechanistic modeling tools enable preservation and generation of prior/new knowledge and scale transferability through mathematical equation representation of the system under study.<sup>1,58,93,94</sup>

#### 1.2.1 Workflow

The PD procedure faces the challenges of time to market, limited feed material availability, cost restrictions, and regulatory quality requirements. Initially, the upstream candidate screening will screen roughly ten thousand molecules for one medicinal drug product.<sup>95</sup> In the midway of candidate screening, the PD evaluates process range and critical process parameters in small-scale initial static experiments, see Figure 1.5. These initial experiments are conducted with early-stage molecules, which present a high likelihood of effectiveness, thereby reducing the development time. However, given the early stage, the available material is limited, and the experiments are performed either manually or with robot-assisted pipetting steps.<sup>35-39</sup> These experiments aim to create a process map presenting the correlation between process and target parameters, such as the separation effect of time, pH, or conductivity, onto the chromatographic performance. Thereafter, initial dynamic effects are investigated through performance screening typically applied in automated robotic columns.<sup>35-39</sup> On a milliliter scale, detailed experiments are performed applying benchtop systems. These detailed experiments are commonly the basis for the pilot or production scale-up. In recent publications, this development process is often supported by mechanistic modeling aiming for a digital twin of the development phase step investigated.<sup>2,6,61,181</sup> In PD, the described process can be reduced or expanded to the dedicated need and is not meant to represent a fixed static workflow.

According to the PD procedure described, the applied toolbox facilitates the screening methods strength while reducing the risk of their disadvantages in the next step by preserving the obtained knowledge. While the individual advantages and disadvantages of manual and HTS applications are a matter of preference - time, quality, amount of data, and data processing - the small-scale experiments are able to reduce the amount of feed needed to the range of microliters.<sup>35,49,55,181</sup> However, static experiments are not capable of representing the dynamic process. Therefore, the performance screening shall give a first glance of dynamic effects with as little as possible feed. Following this, in HTS employing robotic columns or devices, a flow is applied, interrupted by pipetting steps, that provides a first glance of dynamic effects.<sup>53,58</sup> The detailed experiments are the last PD step in the laboratory. In benchtop systems, the dedicated process is mimicked with processing-like conditions such as fluid conditions (e.g., flow) and hardware (e.g., sensors). Benchtop experiments are typically feed and time intensive but deliver comparable large-scale information (e.g., conductivity, pH, and UV signal).

## 1.2 Downstream process development

So far, the toolbox represents laboratory experiments that provide limited preservable prior knowledge. Admittedly, a mathematical abstraction of these experiments enables a more profound knowledge.<sup>1,4</sup> Following this, the simulation is an abstraction of the experiment and limited to the investigated and applied mechanism. Therefore, the simulation result relies on the experimental quality and quantity. Moreover, the advantages and disadvantages of the toolbox need to be known and considered in the simulation.

Applying mechanistic modeling emphasizes that time-consuming and material-intensive procedures such as initial static screening and detailed experiments might be reduced in the future. Furthermore, prior knowledge in chromatographic interaction enables access to an initial process range, while simulation can predict the sensor signals in detailed experiments and gain insightful information.

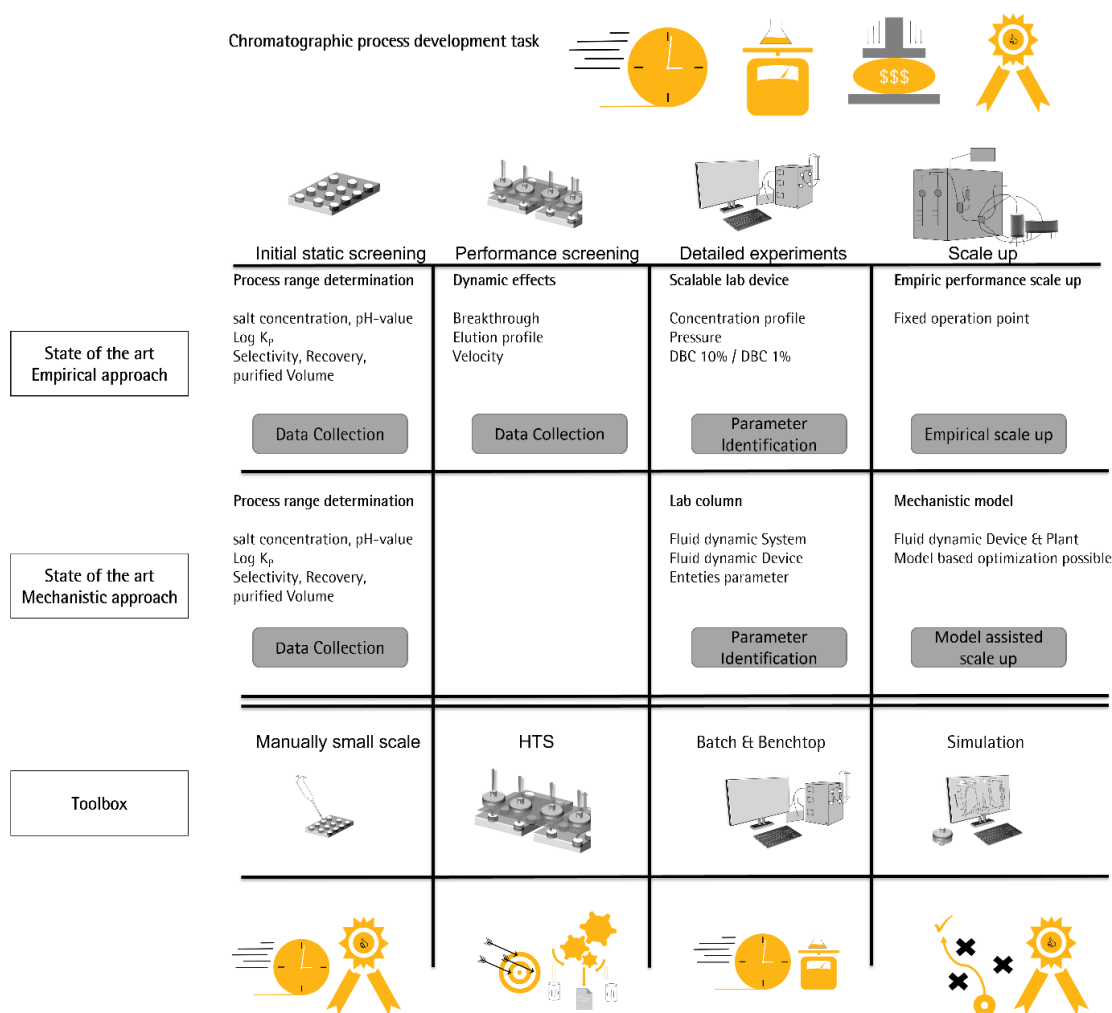


Figure 1.5: State of the art PD workflow and the available toolbox. Considering economic aspects of time, material availability, costs and quality, the PD workflow is divided into up to four steps. These four steps are an initial static screening for process range determination, a performance screening investigating dynamic effects, detailed experiments with measurements and automation level comparable to the production scale and the finale scale up. From top to bottom the state of the art empirical and mechanistic approach is compared. The Figure is completed by the available process development tools including the respective challenges. The initial screening is fast but the parameter significance/quality for scale up low. Applying an HTS in the performance screening reduces time, but accuracy may be compromised by SDD design. In addition, the high amount of data requires sufficient methodology. The detailed experiments apply benchtop systems which deliver in short time production comparable signals and automation degree but required a high amount of feed when compared to initial or performance screening tools. Simulation presents a variety of benefits, such as reduced experimental effort and transferability, but is also challenged by the model selection and definition at which point a model is good enough for its purpose.

## 1.2 Downstream process development

---

### 1.2.2 High throughput screening

Automated high throughput screening procedures were developed to overcome manual limitations such as time constraints as well as cost and quality variation due to different operators. In general, an automated HTS application consists of a programmed method of different pipetting steps, which are automatically performed when started. The method can be started when the automated platform is equipped, resulting in an almost working time independent processing. In the preparation, the operator verifies the condition of the platform, loads the recipe, equips the platform, and starts the experiment, which typically involves running multiple pipettes in parallel. Consequently, HTS reduces the experimental execution, and the operator can conduct other tasks. This parallel working reduces both experimental and working time, reduced by parallelization and automation, decreasing operational expenses.<sup>35-39,181</sup> Discussing the experimental results leads to either exclusion or further investigation of the unit operations or process modes studied. This said, the experimental quality of the results is crucial for the success of the process design.<sup>56,58</sup> Following this, experiments must be highly reproducible and comparable among each other, which can be achieved by automated robotic execution. However, the automated platform and the devices applied must be regularly maintained, evaluated, and audited.

The application for HTS is, for instance, identification of drugs<sup>40-42</sup>, biological libraries<sup>43,44</sup>, cell cultivation<sup>45,46</sup>, aqueous two-phase systems<sup>47,48</sup> and chromatography performance estimation.<sup>39,49-54</sup> In HTS-based chromatography PD the mode of parameter determination can be divided into the following: Batch isotherm determination<sup>49,55</sup>, process range evaluation<sup>35,53</sup>, scale dependency<sup>35,53,56,57</sup> and scale-down model development<sup>53,58</sup>. Typical formats for process range evaluation and batch isotherm determination are microtiter plates. If needed, fluid flow in microtiter plates is achieved by using micro pipetting devices and/or a vacuum. Process-comparable operations and dynamic effects need to be mimicked to allow process predictions. That said, knowledge of scale-dependent variables is essential, and critical process parameters must be kept under control. Therefore, scale dependency of critical parameters and scale-down model development are highly linked.<sup>58,181</sup>

The advantages and disadvantages of different PD scales can be categorized into material consumption, scale-induced deviation, standardization, and time. To summarize, usage of materials increases with the scale while potential deviations, e.g., in fractionation or analysis, will have less effect on the results.<sup>181</sup> On the other hand, small scales entail high standardization and availability as well as lower time and material consumption. Standardization refers to the methods and systems used when compared to manual handling.<sup>181</sup> Within a GMP-approved process, experimental and process standardization increase the likelihood that the regulatory requirements are satisfied.

#### 1.2.2.1 High throughput screening – Scale-down device

First and foremost, the automated HTS platform must be appropriate for the application and screening technique in question. The mechanical parts must be maintained, the pumps regularly checked for leakage, and the correct aspiration/dispensing speed and volume must be monitored. In addition, flushing/cleaning/rinsing procedures and void volumes must be considered to obtain accurate results. When operating with dispensing essays or needles, the sealing, positioning, and straightness need to be checked frequently.

## 1.2 Downstream process development

Developing a high throughput screening scale-down device requires the reflection of desired information. For instance, process range screening can be performed in the context of determining static binding capacities with static batch experiments applying a well plate format, see Figure 1.6 (1). This said, the stationary phase is placed in a well plate format. The HTS platform performs the experiment within buffer pipetting in the steps of equilibration, loading, wash, elution, regeneration, and storage.<sup>49,55</sup> After the pipetting steps, the well plate is usually shaken to prevent concentration gradients at the interface of the liquid and solid phases. The static binding capacity is reached when the concentration of the stationary phase and liquid phase is in an equilibrium state. Thus the concentration is then independent of time. Aiming for dynamic information and certain process-related information (scalability), the scale-down device must mimic the main effects in larger devices. Dynamic SDDs consists of a fluid inlet, providing a buffer that flows through the stationary phase and mimics the process steps. In robotic setups, the different process steps are typically performed in several pipetting steps, as shown in Figure 1.6 (2). The several pipetting steps correspond more closely to the real process condition when compared to static batch experiments but still exhibit a certain discontinuity between the individual steps.

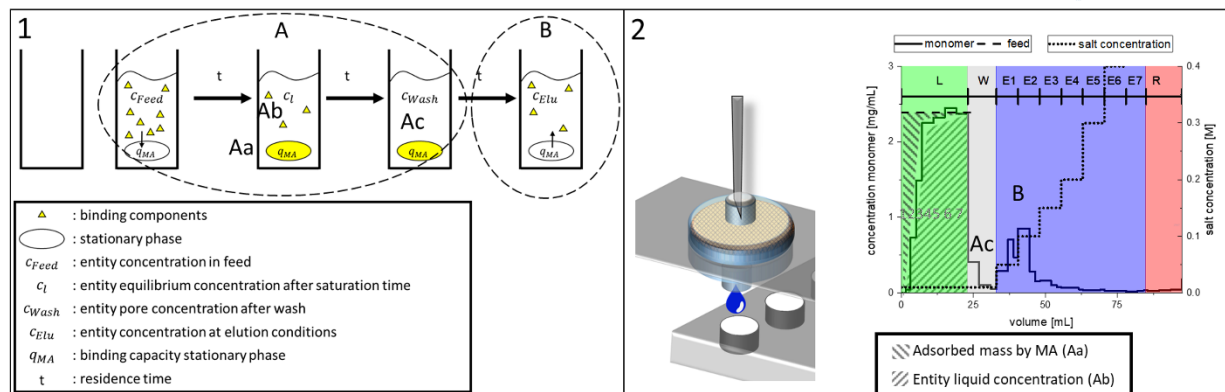


Figure 1.6: Exemplary static batch isotherm determination (1) and dynamic SSD process evaluation (2). Comparison of classical batch and dynamic isotherm determination/assessment. In 1) a general procedure of isotherm determination is presented. The equilibration, adsorption in 1) A, optional wash in B) and elution step. In contrast, the HTS BE method is presented in 2). The isotherm assessment is comparable in the loading phase, obtaining a full isotherm at different liquid feed concentrations. However, the stepwise step elution delivers only the saturation equilibrium concentration at the given salt concentration.<sup>181</sup>

The critical HTS SDD development parameters vary with the dedicated level of detail of information detailedness. Since the static SDD represents time-independent results, crucial parameters are residence time, liquid/solid ratio, and the accuracy of the pipetted volume/stationary phase. In addition, the number of measurement points, shaking speed, removal/exchange of the liquid, time, and dispersion of the stationary phase in the liquid must be considered.<sup>56</sup> This said, further consideration must be taken for different stationary phases such as resin suspension or membrane stamps. For instance, the correct suspension handling for resins is represented by a known solid-to-liquid ratio and particle diameter. At the same time, an interface between liquid, stationary phase, and well plate can impede the result for membrane stamps. In addition, dynamic SDDs additionally need sufficient mechanical development such as sealing, positioning, void volume consideration, and fraction handling. Furthermore, the dynamic SDD needs the best comparability to the dedicated large-scale device in terms of fluid distribution, residence time, and void volume, along with the ratio of contact interface between device wall and stationary phase.

## 1.2 Downstream process development

---

In any case, as the dedicated detail of information increases, so does the complexity of the SDD development. In addition, the SDD is an approximately large-scale device and process representation. Therefore, conducting HTS experiments typically compromises manufacturing and set-up related differences in flow and geometries between SDD and large-scale devices, such as disrupted flow and different ratio of contact interfaces.<sup>58</sup> This said, the deviation between SDDs and large-scale device must be considered in the transfer, either by knowledge and a reasonable safety margin or the application of mechanistic modeling resulting in a digital twin of the HTS SDD platform.

### 1.2.2.2 High throughput screening SDD operational procedure

The HTS SDD development includes constructional, methodological, and operational procedures. The platform and SDD are physically built/checked in the development phase to fulfill the specific screening purpose. In addition to the construction of additional devices for the existing HTS platform or integration of new devices into the platform, it is also necessary to incorporate dedicated screening techniques. The HTS platform layout is developed, and method programming, testing, and definition of wellness/calibration procedures are investigated. In addition, the method input and output parameters such as aspiration/dispensing speed, air gap above the sample, and waiting time before movement are determined.<sup>56,57</sup> Thereafter, external analytical evaluation/preparation, e.g., protein concentration determination UV reader or SEC, is integrated and the HTS platform verified.

The experimental or operational screening procedure development includes the performance of wellness procedures, initial preparation, conducting mechanical and methodological correctness checks, preparation of the HTS SDD set up, and the start of the procedure. In addition, the successful procedure provides samples and a used HTS set-up, which both need to be further processed. This said, the samples are subsequently treated and analyzed. In addition, the HTS data is exported and analyzed, while a post-check and cleaning of the HTS platform and SDD ensures the quality of the present and future experimental results. The typically large amount of data generated, and the small volume applied in HTS may lead to misinterpretation and discrepancies if no dedicated error investigation is performed.<sup>57</sup> The initial preparation of the platform includes assembling or disassembling of devices, preparation of consumables, buffers or buffer salts, storage solution, checking of robotic arm position, adjustment and loading of recipes, preparation of external analytics, and simulation of the recipe. In the case that subsequent analytical analysis is mandatory, e.g., IgG monomer and dimer determination by SEC, the robotic platform might also be used to pipette the needed solution into HPLC vials. Extended external analysis time facilitates data export of the HTS platform, such as the UV measurements, log file or recipe, preparation of new experiments, or evaluation of prior ones. Furthermore, the HTS platform and SDD should be investigated for abnormal behavior, like leakage or bent needles. The HTS platform and SDD shall be cleaned and transferred in storage conditions during downtimes.

### 1.2.2.3 High throughput screening Scale-up

The dynamic SDD data can be, to a certain extent, directly used to assess the dynamic breakthrough concentration of a larger-scale device.<sup>181</sup> The deviation would be low based on the assumption that the SDD and processing mode are a direct representation of the large-scale device. However, typical geometrically restrains in manufacturing and HTS procedure impede an exact scale transfer. For example, geometric length differences lead to differences in fluid dynamics, wall effects, and incomparable stationary bed properties, e.g., porosity, height, and packing quality. In addition, the

## 1.2 Downstream process development

---

unsteady HTS flow influences fluid dynamics, residence time, and concentration profile in the SDD.<sup>35,51,56,57,59,96</sup> Following this, the mass transfer may differ between the SDD and the large-scale device.

Nevertheless, for stationary phases and molecules with neglectable mass transfer restriction and a thoroughly SDD fluid distribution, the deviation between SDD and the large-scale device might be acceptable. Following this, the scale factor  $\Gamma$  might be used for the scale transfer. The scale factor  $\Gamma$  is calculated by the quotient of the volume at 10% dynamic breakthrough concentration (DBC)  $V_{DBC10}$ , and the stationary phase volume  $V_{MA}$ , lab device multiplied by the feed concentration of component  $i$  in Eq. (1.1). The scale factor can then be used to calculate the volume at the 10% DBC according to Eq. (1.2).<sup>181</sup>

$$\Gamma = \frac{V_{DBC10}}{V_{MA,lab\ device}} \cdot c_{Feed} \quad (1.1)$$

$$V_{DBC10,\Gamma} = V_{MA,\Gamma} \cdot \frac{\Gamma}{c_{Feed}} \quad (1.2)$$

In contrast to the ad-hoc procedure described above, the experimental scale transfer might be conducted by mechanistic modeling, considering the divergences between HTS SDD and larger-scale devices. The unknown differences can be overcome by reversed engineering.<sup>58</sup> Herein, a well-known process and larger-scale device are investigated, these findings are used to predict the SDD results, and the differences minimized by further parameter evaluation and/or adjustment of the SDD model. This said, the deviation can be observed by mathematical description of both SDD and larger-scale devices, revealing the differences between both and enabling a more precise transfer.<sup>181</sup>

## 1.2 Downstream process development

### 1.2.3 Mechanistic modeling

Comparable to the SDD as a more miniature representation of the large-scale device, the model mathematically represents the considered physic-chemical actions in the investigated operation. The investigated operation can be aggregated to the entire manufacturing process, segregated into a single unit operation or part of the unit operation as presented in Figure 1.7 A).<sup>97</sup> In chromatographic processes, the liquid phase, stationary phase, and the device itself are typically investigated.<sup>21,68</sup> The investigation includes the liquid and stationary phase, e.g., fluid dynamic and mass transfer. However, the used system to which the chromatographic device is attached for scale-up should also be considered.<sup>98</sup> This said, a representation and investigation for scale transfer, including deviations in operational parameters (e.g., discontinuous flow) or geometrical factors (e.g., device to stationary phase ratio), must be considered to reduce interpretation errors.

Following the general introduction in mechanistic modeling, the fundamental principles of modeling will be presented. This said, fluid dynamic description and mass transfer, as presented in Figure 1.7 D) and E) will be discussed.

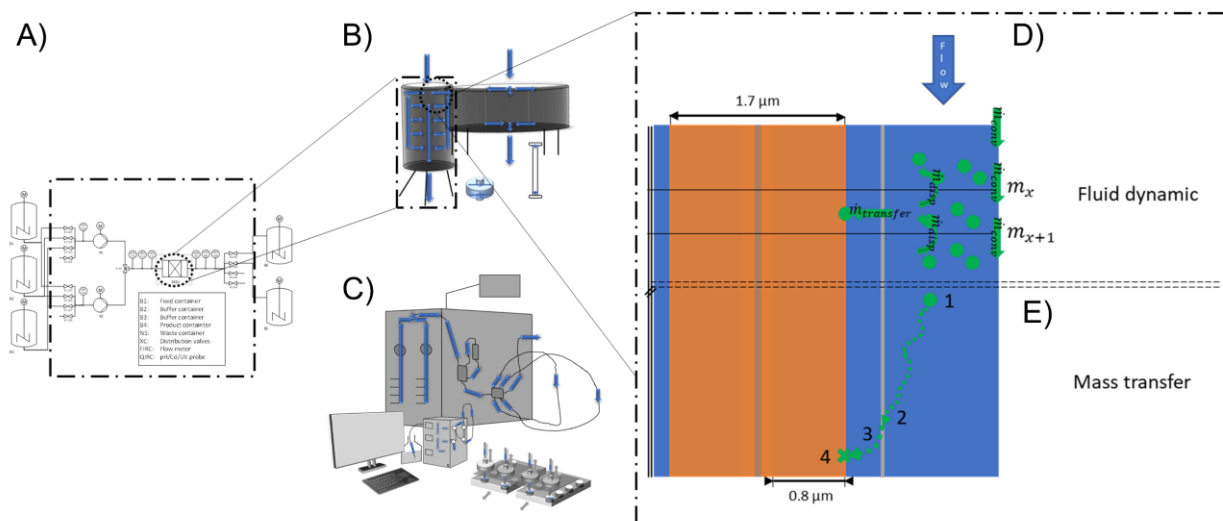


Figure 1.7: Exemplary chromatographic system segregated to the fundamentals in MA pores. A) describes the whole unit operation without supply, waste, and product tanks. The chromatographic device is shown in detail in B) for a membrane and C) for a column. The fluid dynamic and mass transfer processes for membranes are presented in D) and E), respectively.

#### 1.2.3.1 Fundamentals of mechanistic modeling in chromatography

Mechanistic modeling is typically performed by fundamental equations. These different equations describe mathematically the entities interactions between liquid and a general stationary phase and/or device resulting in the representation of the investigated system. The approach can be consulted in detail in the work of Guiochon et al.<sup>68</sup> and Schmidt-Traub<sup>99</sup>.

The chromatographic unit operation consists of a system and the chromatographic device, see Figure 1.7 B and C. This said, the system and the chromatographic device are flushed with a liquid. At the same time, the purification (adsorption) is only present in the chromatographic device, more precisely at the stationary phase integrated into the device. Following this, the fundamental fluid dynamics and mass transfer equations can only be described for the chromatographic device. Figure 1.7 D) and E)

## 1.2 Downstream process development

present the fluid dynamics and mass transfer schematically. The fluid dynamic change in component mass at the viewed discrete point  $m_x$  is the sum of mass received by the discrete point before  $m_{x-1}$  or emitted to  $m_{x+1}$ . Following this, the mass at  $m_x$  results from convective effects  $m_{conv.}$ , e.g. pumping and dispersive  $m_{disp.}$  effects such as back mixing induced, e.g. by deflections or wall effects.

In addition to fluid dynamics, mass transfer to the stationary phase  $m_{transfer}$  and final adsorption are also essential for modeling chromatographic separation. Figure 1.7 E) presents a simplified mass transfer scheme that can be formulated as the following: convective transport to the diffusive layer(1-2) followed by the diffusion towards the stationary phase surface (2-3) and subsequently, if present, pore diffusion, and final adsorption onto the stationary phase surface or pore (4). The mass binding to the stationary phase is represented by isotherms in which the concentration differences between liquid and stationary phase represent molecule and stationary phase properties. This said, the above-quoted interactions are part of the desorption in the elution step as well in the opposite direction.

### Equilibrium Dispersive model

Initiating the description of model equations with the equilibrium dispersive model is more comprehensive than the thereafter-described equations, facilitating the introduction of the modeling parameters and assumptions. The equilibrium dispersive model in Eq. (1.3) describes the time-dependent concentration change by convective, dispersive, and mass transfer concentration changes. First named convective concentration changes characterize the molecule concentration change through the column length / length coordinate, e.g., when pumping a liquid through a pipe. This said, the velocity  $u$  is divided by the porosity  $\epsilon$ , which is 1 for the device and smaller than 1 for the stationary phase. The dispersive term is represented by the diffusive-based apparent axial dispersion coefficient  $D_{ap}$  considering the change in concentration due to different resistance as wall effects, diffusion effects, or the separation of fluid elements by physical deflection in the device or in the stationary phase, thus broadening the concentration profile. The mass transfer term reflects the change in concentration over time by adsorption of the molecules onto the stationary phase represented by the binding capacity  $q$ . The binding capacity is corrected by the porosity  $\epsilon$  considering a lower stationary phase volume when reduced by the nonadsorptive pore volume. In Eq. (1.5), the porosity is determined by the interstitial porosity  $\epsilon_{Device}$ , representing, for instance different sized resin particles and the pore porosity of the individual particle  $\epsilon_p$ . In the equilibrium dispersive mode, the mass transfer is directly coupled to the stationary phase concentration and is represented by different isotherms and kinetic assumption, e.g. steric mass action mode (SMA) in Eq. (1.4.) The adsorption might be limited by summarized kinetic effects, formulated with  $k_{kin}$ , such as diffusion limitations or molecule relocation to facilitate binding. However, the molecules which are bound by the stationary phase result from the overall accessible ligands represented in the SMA by the ionic capacity  $\Lambda$ .<sup>100</sup> This said, these accessible ligands can interact with a certain number of molecules based on the size and charge of these molecules. The characteristic charge of a molecule  $v$  and the steric factor  $\sigma$  determine the stationary phase ligand occupancy. Following the concentration equalization principle, the pore concentration  $c_p$  influences the binding capacity / bound concentration.

$$\frac{\partial c_i}{\partial t} = - \underbrace{\frac{u}{\epsilon} \cdot \frac{\partial c_i}{\partial x}}_{convective} + \underbrace{D_{ap} \cdot \frac{\partial^2 c_i}{\partial x^2}}_{dispersive} - \underbrace{\frac{1 - \epsilon}{\epsilon} \cdot \frac{\partial q_i}{\partial t}}_{mass\ transfer} \quad (1.3)$$

$$k_{Kin,i} \cdot \frac{\partial q_i}{\partial t} = k_{Eq,i} \cdot \left( \Lambda - \sum_{i=2}^{n+1} (v_i + \sigma_i) q_i \right) \cdot c_{p,i} - c_{p,1}^{v_i} \cdot q_i \quad (1.4)$$

## 1.2 Downstream process development

---

$$\varepsilon = \varepsilon_{\text{Device}} + \varepsilon_p \cdot (1 - \varepsilon_{\text{Device}}) \quad (1.5)$$

The Danckwerts boundary conditions complete the model by adding inlet conditions in Eq. (1.6) and outlet conditions in Eq. (1.7).<sup>101</sup> Furthermore, the inlet concentration is described by velocity-induced dispersion with the quotient of velocity  $u$ , axial dispersion coefficient ( $D_{ax}$ ), the concentration difference between inlet concentration ( $c_{in}$ ) and concentration at the first length coordinate of the column ( $c(0,t)$ ).<sup>102</sup> The outlet concentration, e.g., at the stationary phase or device/investigated system end, is equal to that of the length coordinate before.

$$\frac{\partial c_i}{\partial x}(x = 0, t) = \frac{u}{D_{ax}} \cdot (c(x, t) - c_{in}) \quad (1.6)$$

$$\frac{\partial c_i}{\partial x}(x = L, t) = 0 \quad (1.7)$$

The assumptions of the equilibrium dispersive model can be grouped into stationary phase bed properties and mass transfer. The stationary phase bed properties include the assumptions of a uniform packed bed, e.g., no inconsistencies like wall effects or dead pockets exist. In addition, the overall concentration change of the fluid phase is summarized by the apparent axial dispersion coefficient. Furthermore, this model assumes linear adsorption, e.g., the application of a Freundlich isotherm.<sup>68</sup>

Eventually, this model simplifies the physical properties of the stationary phase, like fluid dynamics and adsorption properties. These simplifications will lead to deviation in the quality of representation/model and investigated system when significant parameters are merged. Specifically, the uniform and idealized bed are combined with the summarized apparent axial dispersion coefficient for the device and/or the stationary phase. Consequently, the geometry changes observed in a scale transfer will most likely result in a deviation and limit the model's purpose. Furthermore, the direct connection of mass transfer and isotherm narrows the application mainly to surface adsorptive stationary phases. In addition, the assumptions in mass transfer are only partially suitable for most complex molecules used in the biopharmaceutical industry, consisting of several amino acids and multiple binding sites. However, this model might be reasonable for different purposes such as initial system investigation, stationary phases with surface adsorption, or negligible mass transfer restriction such as MA. The fluid dynamics could be transferable with a linear scalable device and an exact packaging procedure.

### *Transport dispersive model*

Following the limitations in the equilibrium dispersive model, the transport dispersive mode in Eq. (1.8) splits the apparent axial dispersion coefficient into the axial dispersion coefficient  $D_{ax}$  and an effective mass transfer coefficient  $k_{eff}$ . In addition, the device porosity  $\varepsilon_{dev}$  is introduced to separate the device and stationary phase. Furthermore, the intrinsic velocity is  $u_{int}$  calculated by the quotient of linear velocity and device porosity. Finally, the mass transfer is modified considering the concentration exchange of fluid phase  $c$  and diffusive pore concentration  $c_p$  within the particle radius  $r_p$ .

## 1.2 Downstream process development

$$\frac{\partial c_i}{\partial t} = -u_{int} \cdot \frac{\partial c_i}{\partial x} + D_{ax} \cdot \frac{\partial^2 c_i}{\partial x^2} - \frac{1 - \varepsilon_{dev}}{\varepsilon_{dev}} \cdot \frac{3}{r_p} \cdot k_{eff} \cdot (c - c_p) \quad (1.8)$$

In conclusion, the transport dispersive model adds one additional parameter by specifying the apparent axial dispersion coefficient into two independent parameters facilitating a more detailed representation of fluid dynamics and mass transfer.

The effective mass transfer coefficient is difficult to determine directly and is typically assessed by heuristic equations. Exemplary, state-of-the-art heuristic equations for  $k_{eff}$  are the Wilson-Geankoplis<sup>103,104</sup> correlation in Eq. (1.9) as well as the Kataoka Correlation<sup>105</sup> for  $Re < 100$  in Eq. (1.10). These heuristic equations correlate fluid dynamics and diffusive molecule effects assessing  $k_{eff}$  by applying the Reynolds- and the Schmidt number in Eq. (1.11) and Eq. (1.12). In addition, the transport dispersive model is applied throughout all stationary phases and devices, and several modifications have been published.

$$Sh = \frac{k_{eff} \cdot \varepsilon_{dev}}{D_m} = \begin{cases} \frac{1.09}{\varepsilon_{dev}} Re^{0.33} \cdot Sc^{0.33} & \text{for } 1.5 \cdot 10^{-3} < Re < 5.5 \cdot 10^1 \\ \frac{0.25}{\varepsilon_{dev}} Re^{0.69} \cdot Sc^{0.33} & \text{for } 5.5 \cdot 10^1 < Re < 1.05 \cdot 10^3 \end{cases} \quad (1.9)$$

$$Sh = 1.85 \cdot \left( \frac{1 - \varepsilon}{\varepsilon} \right)^{\frac{1}{3}} \cdot Re^{\frac{1}{3}} \cdot Sc^{\frac{1}{3}} \quad (1.10)$$

$$Sc = \frac{\eta}{\rho \cdot D_m} \quad (1.11)$$

$$Re = \frac{\rho \cdot u \cdot d}{\eta} \quad (1.12)$$

### Lumped rate model

In contrast to the equilibrium transport dispersive model, the lumped rate model considers that the concentration in the pore volumes does not adsorb directly to the stationary phase. However, the lumped rate model in Eq. (1.13) further specifies the adsorption in diffusive pores considering the particle pore porosity  $\varepsilon_p$  in addition to Eq. (1.3).

$$\frac{\partial c_p}{\partial t} = \frac{3}{r_p} \cdot \frac{k_{eff}}{\varepsilon_p} (c - c_p) - \frac{1 - \varepsilon_p}{\varepsilon_p} \cdot \frac{\partial q_i}{\partial t} \quad (1.13)$$

In summary, the lumped rate model further specifies particle-specific adsorption. This said, the mass transfer is lumped into diffusion from the liquid phase to the pores, including the inside adsorption. Consequently, direct surface adsorption is not considered. This model is favored for resin-based and comparable stationary phases.

## 1.2 Downstream process development

---

### *General rate model*

Following the specification from the transport dispersive model and the lumped rate model towards particulate resin-based stationary phases description, the general rate model specifies the pore mass transfer effects. The effective mass transport coefficient is substituted by a film transfer coefficient  $k_{film}$  incorporating a possibility to consider hindered pore diffusion  $D_{pore}$  in Eq. (1.14). These mass transfer effects account for the concentration change within the particle radius. In addition to these new geometrical aspects, new boundary conditions are introduced. The pore concentration change at the particle center is set to zero. Furthermore, the adsorption term is divided into diffusion within the symmetric particle, diffusion towards the particle center, and the final adsorption in Eq. (1.15).

$$\frac{\partial c_p}{\partial r} = \frac{1}{D_{pore}} \cdot \frac{k_{film}}{\varepsilon_p} (c - c_p) \quad (1.14)$$

$$\frac{\partial c_p}{\partial t} = D_{pore} \cdot \left( \frac{\partial^2 c}{\partial r^2} + \frac{2}{r} \cdot \frac{\partial c}{\partial r} \right) - \frac{1 - \varepsilon_p}{\varepsilon_p} \cdot \frac{\partial q_i}{\partial t} \quad (1.15)$$

Finally, the general rate model precisely considers the molecular mass transfer into the stationary particulate phases. The model enables the geometrical induced mass transfer description by adding the film transfer coefficient  $k_{film}$  and pore diffusion effects  $D_{pore}$ . However, the model is explicitly designed for stationary particulate phases where the particle symmetry and concentration profile towards the particle center  $r$  is idealized. Considering the model depth, two additional model parameters are introduced, potentially three if the pore radius is also considered.

The different models described above are state-of-the-art and adjusted for different applications. This said, a broad variety of literature of models applied for the same stationary phase is available. Table 1.1 presents an overview of the model depth, the considered effects, and the model parameters to be evaluated.

## 1.2 Downstream process development

Table 1.1: Exemplary model parameter overview

Model	Number of parameters	Effects	Parameters
Equilibrium Dispersive model	3	Convective, dispersive, cumulative stationary phase mass transfer	$U, \epsilon, D_{ap}$
Transport dispersive model	4	Convective, dispersive, effective stationary phase mass transfer	$u, \epsilon, D_{ax}, k_{eff}$
Lumped rate model	5	Convective, dispersive, additional effective pore mass transfer	$u, \epsilon, D_{ax}, k_{eff}, r_p$
General rate model	6	Convective, dispersive, additional film pore mass transfer	$u, \epsilon, D_{ax}, k_{film}, k_{film}, D_{pore}, r$

While the presented models have different advantages and disadvantages, an initial assessment of the appropriate model is achievable by considering the system in question through theoretical evaluation, manufacturer information, and literature. Therefore, exemplary guidance is presented below, presenting the theoretical evaluation and manufacturer information.

Figure 1.8 exemplary describes column / resin and membrane-based differences in stationary phase and device. The resin chromatography is presented on the left side with the column device and particulate stationary phase. Membrane based stationary phase and device are right-handed in Figure 1.8.

The resin device consists of a fluid distribution part at the top and bottom. Following the homogenous liquid distribution at the top, the liquid flows axially through the device and is collected at the bottom outlet. The particulate stationary phase is a packed bed presenting a global porosity that includes the porosity of the stationary phase and an inter-particulate porosity and may include the device void volume. This said, the quality of the packed bed between different columns and sizes as well as wall effects can impede a sufficient mechanistic modeling scale transfer.<sup>56,57</sup>

The membrane capsule devices present a baffle plate after the inlet that distributes the fluid radially to the outer flow channel. Following the radial distribution of the liquid to the outer flow channel, the liquid is directed radial passing through the stationary phase. Finally, the liquid is pooled in the inner core of the device and exits the device at the outlet. The membrane porosity is fixed by the quality and properties, while the overall device description might be challenging for a model-based scale transfer.

For resin and membrane chromatography exist, typical performance statements can be retrieved from the literature and manufacturer information. These performance statements are high binding capacity, slow mass transfer, and limited suitability for separating large molecules (hydrodynamic diameter  $d_h > 20$  nm) for resins<sup>106-110</sup> and low binding capacity, fast mass transfer, and elevated suitability for the separation of large molecules for MA<sup>106,111,112</sup>. The characteristics of resin chromatography are due to

## 1.2 Downstream process development

the average particle size of  $\sim 80 \mu\text{m}$  and the high internal porosity of 90 % resulting in diffusive pores of  $\sim 45 \mu\text{m}$ . Following the diffusive pore lengths, a molecule needs a particular time to wander into the pore systems facilitating a high binding capacity by adsorption inside the particle. This said, the residence time needs to be sufficient for an adequate binding capacity resulting in a bigger column diameter for a larger scale and an overall small volumetric flow of  $\sim 1$  column volume per minute (CV/min) compared to membrane chromatography. The resin pore size is typical  $\sim 100 \text{ nm}$  resulting in size exclusion effects for a larger molecule such as viruses or bacteria. The membrane devices consist of several layers of a membrane sheet with a typical bed height of  $\sim 0.025 \text{ cm}$ . Membranes consist of convective or turbulent pores with a pore size of  $\sim 3000 \text{ nm}$  facilitating a better binding capacity for larger molecules when compared to resins. For membranes with an additional hydrogel, the diffusive and adsorptive layer is  $\sim 0.8 \mu\text{m}$  resulting in short diffusive layers. Thus, membrane devices are typically processed at high volumetric flows of  $\sim 10$  membrane volumes per minute (MV/min), resulting in short residence times. In conclusion, different chromatographic stationary phase parameter encourages different model approaches in fluid dynamics and mass transfer and will be further discussed in the chapter below.

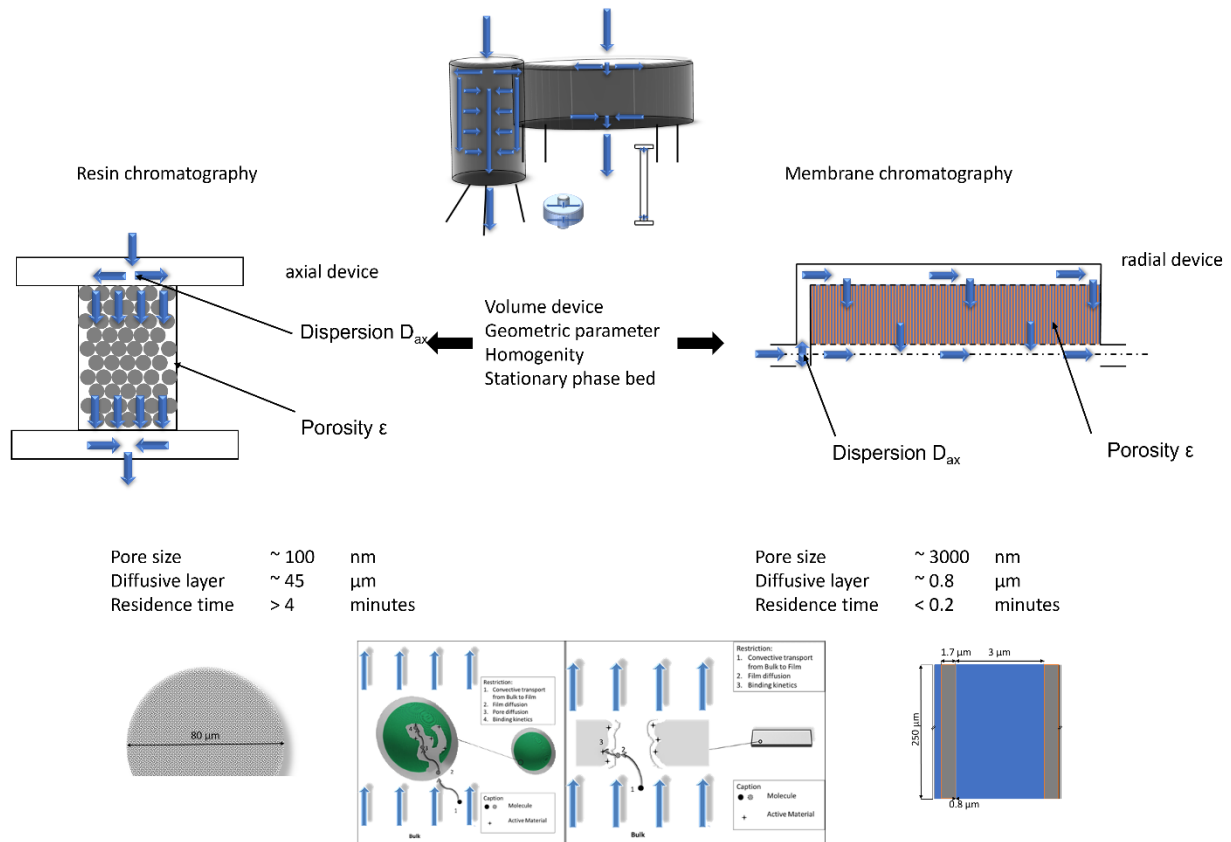


Figure 1.8: Exemplary Resin and MA differences in stationary phases and device properties. The centered top devices present different scales for Resin (axial flow) and MA (radial flow). In addition, a detailed description of the device, the properties of the stationary phase, and resulting effects are presented left for Resin and right for MA.<sup>216</sup>

## 1.2 Downstream process development

---

### 1.2.3.2 Model building

Investigating a system for model building is comparable to studying a new topic. Initially, the information is general and presents an overview. Following this, it might be compared with a black box model, e.g., mass in and out. Thereafter, the insight gains depth and more specific and related information are learned, e.g., the equilibrium dispersive model. In the further course of study, expertise is gained, and the detailed/specific interactions are investigated, leading to a specific view, e.g., resin-based mass transfer in the general rate model. The model depth might be comparable to the studying depth for different professions, e.g., a mechanical engineer does not need to be an expert in chromatography but needs the principal information about the process when designing a chromatography system. This said, the model development of a stationary phase with fast/neglectable mass transfer may not require particulate resin-based diffusive limitations as those presented in the general rate model. Following this, the model depth should be selected in accordance with the investigated system.

In the course of model building, several iterations of model selection and parameters determination, evaluation, and assessment are needed to be performed.<sup>94,113,114</sup> The parameter assessment includes the parameter determination within an error minimization procedure for parameters that are not directly accessible with experiments.<sup>115,116</sup> This said, increasing the model depth leads to additional parameters. Following this, a higher model depth with potential additional not needed/present parameter (NNP) will accumulate the model errors in these NNP if they are derived by error minimization. This said, these error minimizations will lead to an apparent accuracy between the model and experiments, which does not represent the correctness of the model. The overweight models will almost certainly fail when transferred to another scale; the hidden inaccuracy within the NNP is physically irrelevant and thus increases the inaccuracy in scale transfer.

Finally, aiming for a scalable representation of the investigated system includes continuously evaluating the selected model's adequacy.

#### *Fluid dynamics description*

When considering the development of an HTS membrane platform with a scale-down device, this device needs to provide representative and repetitive results. Aiming for a scalable model includes developing a device that minimizes the differences between small-scale and production scale while facilitating the advantages that result. This said, Figure 1.9 presents three different membrane devices. The laboratory module was modified for the HTS platform approach, and the modular membrane press was newly developed for the scale transfer from axial to radial fluid flow in commercial devices such as the Sartobind® Nano devices.

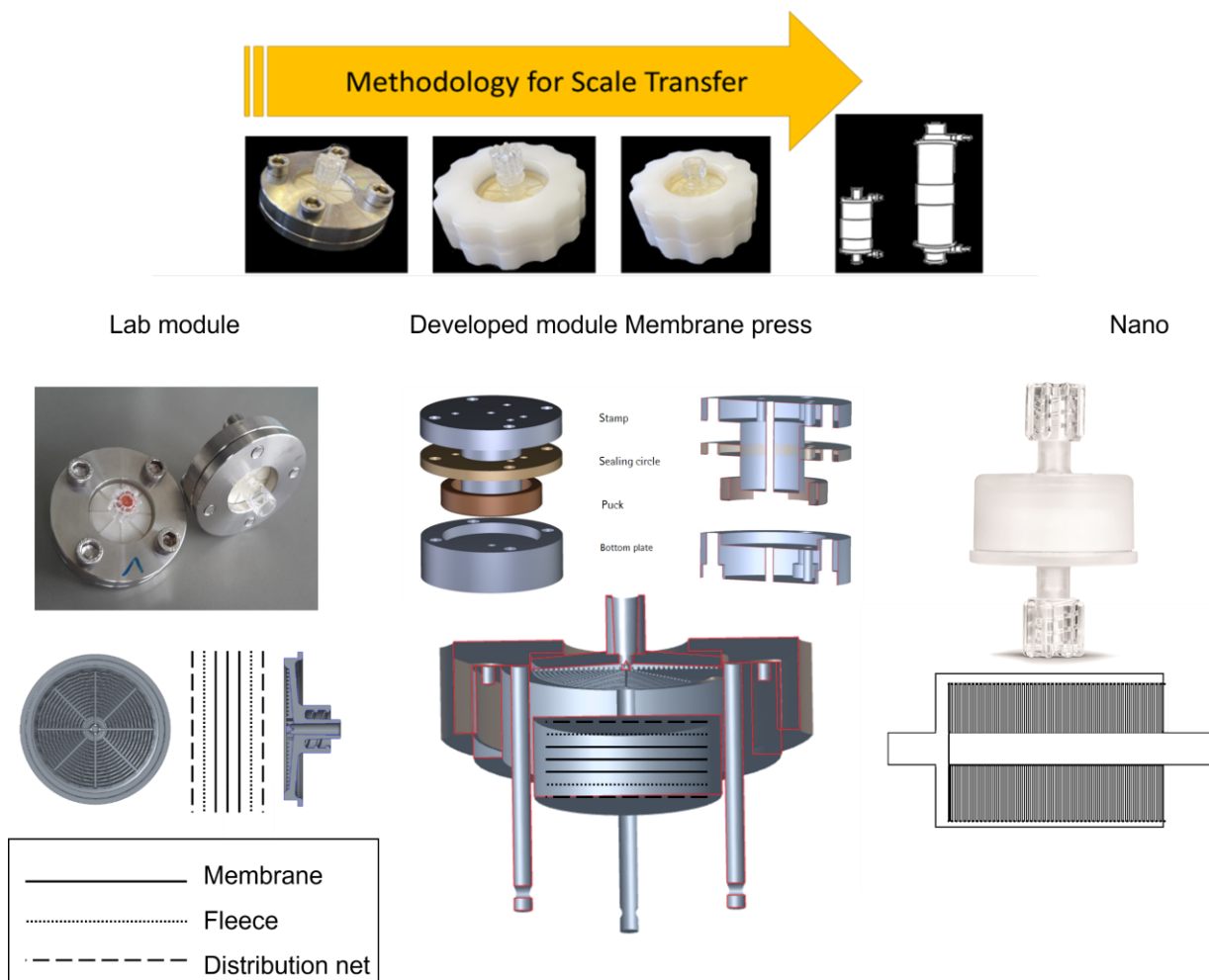


Figure 1.9: Different membrane devices for PD. The axial flow devices HTS SDD is shown on the left and the lab module is shown centered. In addition, the radial flow device Nano is presented right-handed. The SDD comprises a fluid distributor, followed by a distribution net, fleece and three layers of membranes. In contrast to the fixed layers of membranes in the SDD, the lab module can utilize up to 90 membrane layers. The distribution net, fleece and membrane layers are inserted into the lab module holder plate, which is surrounded by a plastic cylinder “Puck” and sealed with a sealing ring. Centering pins prevent movement of the membrane layer until the stamp is added. The stamp then presses onto the membrane layers, the centering pins are removed, and the sealing material is inserted from the outside through the sealing ring between the puck and the membrane layers.

Developing devices for a scale or geometrical transfer includes the investigation of fluid dynamics. Following this, the fluid dynamics are typically investigated by different qualitative dyeing or more quantitative tracer experiments. The dyeing experiments present the macroscopic view of the fluid distribution within a module. Here a dye is applied, which can visually present the qualitative homogeneity of the fluid distribution within the device. In case of process condition-related swelling of the stationary phase, e.g., due to different salt concentrations, these experiments are commonly conducted at a minimum and maximum swollen stationary phase.<sup>117</sup> Homogenous coloring represents a qualitative result for a device that can successfully distribute the fluid. Tracer experiments are performed with a non-adsorptive but detectable component. The tracer is injected either as a pulse or step function and results in a peak or sum functional signal. In Eq. (1.16), the total porosity is calculated by the ratio of detected tracer volume  $V_{\text{Tracer}}$  and membrane device volume  $V_{\text{MA}}$ . The tracer volume represents the mean residence volume/time of a molecule in the device and is determined by

## 1.2 Downstream process development

---

the signal centroid of the area. In addition, different accessible pore volumes and porosities can be determined by applying different tracer sizes and increasing the model accuracy.

$$\varepsilon_{Total} = \frac{V_{Tracer}}{V_{MA}} \quad (1.16)$$

In addition to the porosity determination, the tracer signal presents possible inaccuracy in the fluid dynamic. The inaccuracy in fluid dynamics is presented in a deviation of the Gaussian distribution of the peak. Tracer experiments are performed using the same device design when developing or optimizing a device but are repeatedly built to ensure reproducibility.

Developing devices for scalable results is typically performed with the same fluidic flow orientation. However, available membrane devices present a radial flow from the outer membrane towards the inner membrane layers. This design is barely technically feasible for an HTS dedicated scale-down device with less than 1 mL. The developed scale-down device will deviate from the large module, at least in the fluidal flow. Incorporating this fluidal flow, dividing the fluid dynamic contribution of device and membrane would simplify the model-assisted scale transfer. Using known dimensionless numbers such as the Bodenstein or Peclet number in Eq. (1.17) and Eq. (1.18), is a possible route transferring the fluid dynamic effects in scale. The actually for heat transfer applied Peclet number is here used for mass transfer effects, based on the similarity to mass transfer.

$$Bo = \frac{u \cdot L}{D_{ax}} \quad (1.17)$$

$$Pe = \frac{L \cdot u}{D} \quad (1.18)$$

The separation of the device and stationary phase combines several challenges: How many models are needed for the separations? Which models should be considered? How to separate the impact between device fluid distribution at the inlet and the dependent on the fluid dynamic distribution of stationary phase and outlet? These questions have been answered differently within the chromatography modeling community. Generally applied models in fluid dynamic investigations are typically achieved with a derivative description of constantly stirred tank reactors or dispersed plug flow reactor. For instance, the equilibrium dispersive model<sup>68</sup> without a mass transfer term, the Roper and Lightfoot model<sup>118</sup>, and the Zonal rate model<sup>119</sup> might be examples in the fluid dynamic description progress.

Following the different approaches, exemplary investigations are presented. Zobel-Roos et al. investigated a dedicated membrane module by splitting it into five different models.<sup>120</sup> Here, the different device sections obtained their axial dispersion coefficient, which was determined by error minimization. In addition, the separation of membrane and device was recently investigated with computational fluid dynamic simulation.<sup>98</sup> However, while suitable for dedicated investigations, the

## 1.2 Downstream process development

---

feasibility for scale-up parameter determination is missing in both examples. This said, the discussed applied models consist of a significant number of parameters that are not directly accessible.

All things considered, for a successful model-based scale-up, the fluid dynamic of the device and stationary phase needs to be characterized. In addition to the typical characterization, further investigation of the device's suitability for scaling is needed. A scale transfer between different device flow patterns and stationary phase properties, such as swelling, must be considered. The number of models and model parameters must be minimized for the specified target investigation.

### *Adsorption*

Following the fluid dynamic description and the need for a scalable device and model development, the chromatographic interaction, e.g., mass transfer, is considered in the model building. The mass transfer from the fluid phase towards the stationary phase is typically considered diffusion hindered. This said, the effect of diffusion on the required residence time depends on the length that a molecule wanders until it binds towards a free ligand. Following this, the mass transfer restriction relevance depends on the stationary phase properties.

The mass transfer coefficient  $k_{\text{eff}}$ , first introduced in chapter 1.2.3.1, is commonly assessed with the dimensionless Sheerwood Sh number applying the Peclet Pe number in the range of  $0.0016 < \text{Re} < 55$ . In addition to the presented correlation, further application within different fluid dynamic arrays is described by Dwivedi et al. and Williamson et al..<sup>121,122</sup>

In addition to general mass transfer restrictions, the pore diffusion induced mass transfer limitation, represented by the pore diffusion coefficient  $D_p$ , might be considered for porous spherical stationary phases. The pore diffusion can be derived with correlations introduced by Carta and Jungbauer in Eq. (1.19).<sup>123</sup> Following this proposed correlation, the pore diffusion coefficient is calculated by the product of pore porosity  $\varepsilon_{p,i}$ , molecular diffusion coefficient  $D_{m,i}$ , and diffusive hindrance coefficient  $\psi_{p,i}$  divided by the tortuosity factor  $\tau_{o,i}$ . The diffusive hindrance coefficient is presented in different ranges depending on the ratio of pore and molecule radius, considering size exclusion/hindrance. The tortuosity factor represents the uneven diffusion in real particles with stochastically pore size distribution. Following this, the tortuosity factor is a factor that is determined by geometrical rules of thumbs or parameter assessment between modeling and experimental results.

$$D_{p,i} = \frac{\varepsilon_{p,i} \cdot D_{m,i}}{\tau_{o,i}} \cdot \psi_{p,i} \quad (1.19)$$

The experimental determination, apart from model parameter assessment of mass transfer effect, has been constantly focused on in recent research.<sup>51,103,105,121,122</sup> Thus, dyed proteins and/or stationary phases were examined in a confocal laser scanning microscope to evaluate the feasibility of determining size exclusion and mass transfer restrictions.<sup>124-126</sup> However, this new application presents challenges in the experimental set-up, such as correct protein/dye concentration and general preparation.

The pore diffusion implied mass transfer restriction might not be dominant for stationary phases diverging from particulate resin-based stationary phases. Due to their convective pore structure, MAS

## 1.2 Downstream process development

---

are not considered mass transfer-limited stationary phases.<sup>106,127</sup> Following this, the mass transfer restriction is often simplified in MA models reducing the model complexity.

Following the molecule route towards the stationary phase, the adsorption process description remains open. The state-of-the-art descriptions of adsorption processes onto a stationary phase in chromatography are isotherms such as the steric mass action model (SMA) and the Langmuir Isotherm. In addition to those two isotherms, derivative and/or specific Isotherms, e.g., modified Langmuir Isotherms, are applied in chromatographic models.

The SMA is capable of representing molecular properties in Eq. (1.20), while the Langmuir Isotherm in Eq. (1.21) is limited to more general parameters. In contrast, the Langmuir Isotherm can also be applied to hydrophobic adsorption in Eq. (1.22). However, the Langmuir Isotherm does not deliver a direct linkage of the applied parameter to stationary phase properties.<sup>128,129</sup> Consequently, investigating and comparing the adsorption process on different stationary phases is facilitated by the SMA isotherm compared to the Langmuir isotherm.

In Eq. (1.23), the equilibrium concentration  $c_{eq,i}$  results from the stationary phase, process parameters and molecule properties. This stationary phase and molecule properties are steric hindrance  $\sigma$ , characteristic charge  $v$ , binding capacity  $q$ , equilibrium constant  $k_{eq}$ , and ionic capacity  $\Lambda$  representing the number of available ligands. The SMA is applicable for ion exchange interaction which is why the salt concentration  $c_1$  represents process conditions. The Langmuir isotherm in Eq. (1.21) describes the competitive binding capacity with the ratio of maximum binding capacity  $q_{max,i}$ , equilibrium constant, as well as the equilibrium concentration reduced by the sum of competitive effects/molecules. This said, the sum of competitive effects is represented by the sum of equilibrium constant and concentration of these molecules. For multi-layer adsorption, the Langmuir isotherm is typically extended to a linear function considering the equilibrium and salt concentration as well as a multi-layer coefficient  $c_i$ . Following the PD route for different stationary phases and molecules, the SMA is applied and investigated throughout this work.

$$c_{eq,i} = \frac{q_i}{k_{eq}} \cdot \left( \frac{c_1}{\Lambda - \sum_{i=2}^{n+1} (v_i + \sigma_i) q_i} \right)^v \quad (1.20)$$

$$q_{i,j} = \frac{q_{max,i} \cdot k_{eq,i} \cdot c_{eq,i}}{1 + \sum_{j=1}^n k_{eq,j} \cdot c_{eq,j}} \quad (1.21)$$

$$q_{i,j} = \frac{q_{max,i} \cdot k_{eq,i} \cdot c_{eq,i}}{1 + \sum_{j=1}^n k_{eq,j} \cdot c_{eq,j}} + c_{eq,i} \cdot c_1 \cdot C_i \quad (1.22)$$

The ionic capacity summarizes the bound counter ions  $q_1$  and the sum of bound components in Eq. (1.23). The accessible salt ions  $q_1$  are represented by the overall bound salt ion capacity  $\bar{q}_1$  considering the adsorbed component properties including the characteristic charge and steric hindrance parameter in Eq. (1.23) to Eq. (1.25).

$$\Lambda = q_1 + \sum_{i=2}^{n+1} (v_i + \sigma_i) q_i \quad (1.23)$$

$$\Lambda = q_1 + \sum_{i=2}^{n+1} v_i \cdot q_i \quad (1.24)$$

$$q_1 = \bar{q}_1 - \sum_{i=2}^{n+1} \sigma_s \cdot q_i \quad (1.25)$$

The charge and equilibrium constant for a single component solution can be determined by curve evaluation of  $\log k$  applying Eq. (1.26) and Eq. (1.27). This said, isotherms are experimentally determined and in the following, the capacity factor  $k'$  is calculated. The SMA parameters can then be derived by plotting the logarithm capacity factor against the logarithm of the mobile phase salt concentration.<sup>100</sup> In multi-component evaluation, this linear approach can be applied for initial isotherm parameter assessment while refining the isotherm with error minimization.<sup>181</sup>

$$k' = \frac{1 - \varepsilon}{\varepsilon} \cdot \left( \frac{q_i}{c_i} \right) \quad (1.26)$$

$$\log k' = \log \left( \frac{1 - \varepsilon}{\varepsilon} \cdot k_{eq1,i} \cdot \Lambda^{v_i} \right) - v_i \cdot \log(c_1) \quad (1.27)$$

Following the statement of negligible mass transfer restriction for convective material, the adsorption process for MAs urges accurate description. The model simplification for MA shifts the sensitivity towards fluid dynamics and adsorption processes. In addition, MAs typically consist of high ionic charges while presenting a lower surface area when compared to resins. This said, competitive adsorption processes such as the displacement effect might be a pronounced effect on MAs.

Several researchers have comprehensively described the principle description of displacement effects as e.g. the Steven Cramer group<sup>84,130-132</sup>, among others as the Georges Guichon group<sup>133-135</sup> and the Massimo Morbidelli group<sup>136-138</sup>. In displacement chromatography, components of a mixture, which are bound to the stationary phase, are selectively eluted by applying a specific displacer. Then, the specific displacer is characterized and selected by calculating the separation factor  $\alpha$  in Eq. (1.28). The displacer dynamic affinities  $\lambda$  are calculated in Eq. (1.29).

$$\alpha = \frac{\lambda_i}{\lambda_j} \quad (1.28)$$

## 1.2 Downstream process development

$$\lambda_i = \left( \frac{K_i}{\frac{q_{Displacer}}{c_{Displacer}}} \right)^{\frac{1}{v_i}} \quad (1.29)$$

The previous work of Cramer et al. can also be applied to identify competitive binding-based displacement effects. This said, the rearrangement of the SMA in Eq. (1.30) displays three groups (T1, T2, and T3) representing the different interactions. The ligand availability for the component m is represented in term T1; term T2 can be described as the reduction of available ligands by the bound component m, and T3 includes competitive adsorption depending on the surface charge, the sum of steric hindrance  $\sigma$ , and characteristic charge  $v$  of each component.

$$q_m = \frac{\Lambda}{\frac{(v_m + \sigma_m)}{T_1}} - \frac{q_m^{v_m} \cdot c_s}{\underbrace{\left( c_{eq,m} \cdot K_{eq,m} \right)^{\frac{1}{v_m}} \cdot (v_m + \sigma_m)}_{T_2}} - \frac{\sum_{j=2}^n (v_j + \sigma_j) \cdot q_j}{\frac{(v_m + \sigma_m)}{T_3}} \quad (1.30)$$

Applying Eq. (1.30) for a two-component system simplifies the identification of competitive adsorption-based displacement effects in Eq. (1.31) to the differences in steric effect and characteristic charge of the two components.

$$q_1 = \frac{\Lambda}{\frac{(v_1 + \sigma_1)}{T_1}} - \frac{q_1^{v_1} \cdot c_s}{\underbrace{\left( c_{eq,1} \cdot K_{eq,1} \right)^{\frac{1}{v_1}} \cdot (v_1 + \sigma_1)}_{T_2}} - \frac{(v_2 + \sigma_2) \cdot q_2}{\frac{(v_1 + \sigma_1)}{T_3}} \quad (1.31)$$

The relevant terms for competitive adsorption processes T2 and T3 can be evaluated within the typical component parameter range, as exemplary presented in Table 1.2. In addition, the binding capacity and equilibrium concentration of component 1 need to be set, here  $6.7 \cdot 10^{-6}$  and  $3.3 \cdot 10^{-7}$  with 0.05 M salt. In addition, the binding capacity range might be set from  $1.0 \cdot 10^{-5}$  M to  $2.0 \cdot 10^{-5}$  M doubling the component 2 binding capacity. Following this, the effect on the component 1 isotherm can be investigated at different T2 and T3 combinations (low, medium, and high values) in Figure 1.10.

Table 1.2: Parameter range applied for the T2 and T3 analysis.

Parameter	$v_1$	$\sigma_1$	$K_2$	$v_2$	$\sigma_2$
Value [-]	4,6,8	250, 500	1, 5, 10, 100, 10000	4,6,8	250, 500, 10000

The binding capacity of component 1 increases with the T2 term in Figure 1.10. In addition, the component 1 binding capacity does not decrease with increasing component 2 bound. Following this, T2 is not necessarily suitable for competitive adsorption process identification.

Observing T3 in Figure 1.10 reveals a decrease in the binding capacity for component 1 through the increase in the concentration of component 2 as T3. However, the examination of term T3 also presents indifferences in the maximum binding capacity values of component 1. Here, an explicit correlation statement of component 1 binding capacity and T3 is not possible, indicating the mutual impact of T1 and T2.

## 1.2 Downstream process development

Following the T2 and T3 interactions, any change in these affects the binding capacity of component 1. However, the competing effects are exclusively present with high values for T3, enabling a clear interaction strength description.

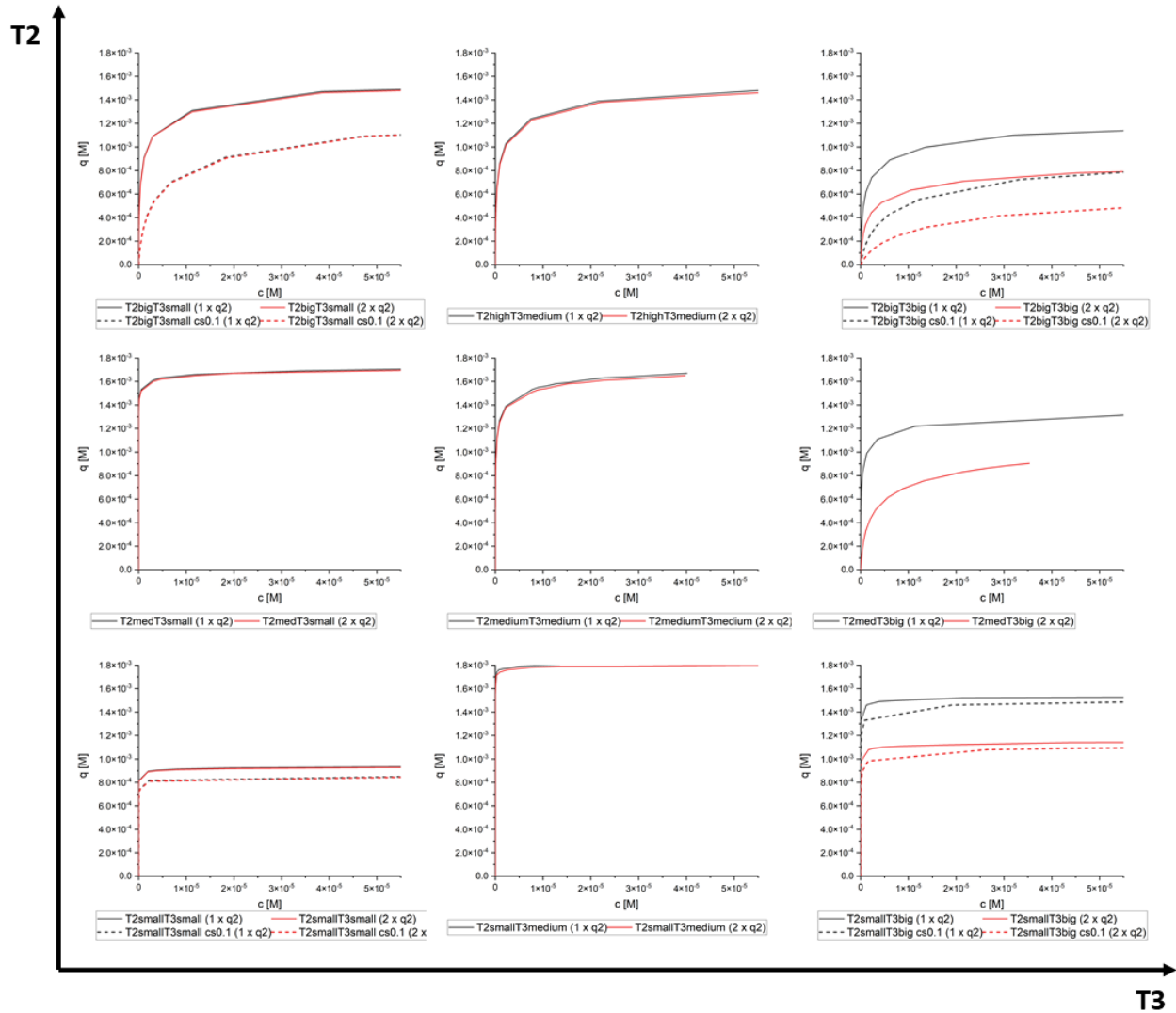


Figure 1.10: Parameter screening for the rearranged SMA equation terms T2 and T3 at different component 2 concentrations. With increased T2, the binding capacity of component 1 increases whereas the binding capacity of component 2 at increasing concentration remains constant. With increased T3, the binding capacity of component 1 is dominated by other parameters rather than T3. However, the binding capacity of component 1 decreases with increasing component 2 binding capacity and T3. For increasing T2, the salt-induced component 1 binding capacity reduction increases. Following this, the displacement observations might be concealed by T2. However, T3 can be identified as displacement identifier and thus as interaction strength.

The descriptions above present no significant salt dependence of displacement effect, which is not confirmed by the already published displacement chromatography investigations. This said, different salt concentrations, for this introduction 0.05 M – 0.16 M, should be considered when investigating competitive adsorption processes, see Figure 1.11. Following the description of T2 in Eq. (1.31), the non-linear correlation between equilibrium concentration, binding capacity, and salt concentration enables a possible shift in the competitive adsorption processes. This effect is represented in Figure 1.11. Furthermore, increasing salt concentration decreases the isotherm slope change. Following this, the salt concentration can facilitate or impede displacement effects.

## 1.2 Downstream process development

In summary, the competitive adsorption investigation by mechanistic modeling allows a deeper understanding of the interactions. Consequently, process effects and new operation modes can be considered in PD based on isotherm data. Furthermore, the investigation can lead to the competitive adsorption identification upfront, thus avoiding scale-transfer challenges. These opportunities will be discussed in detail in chapter 4.

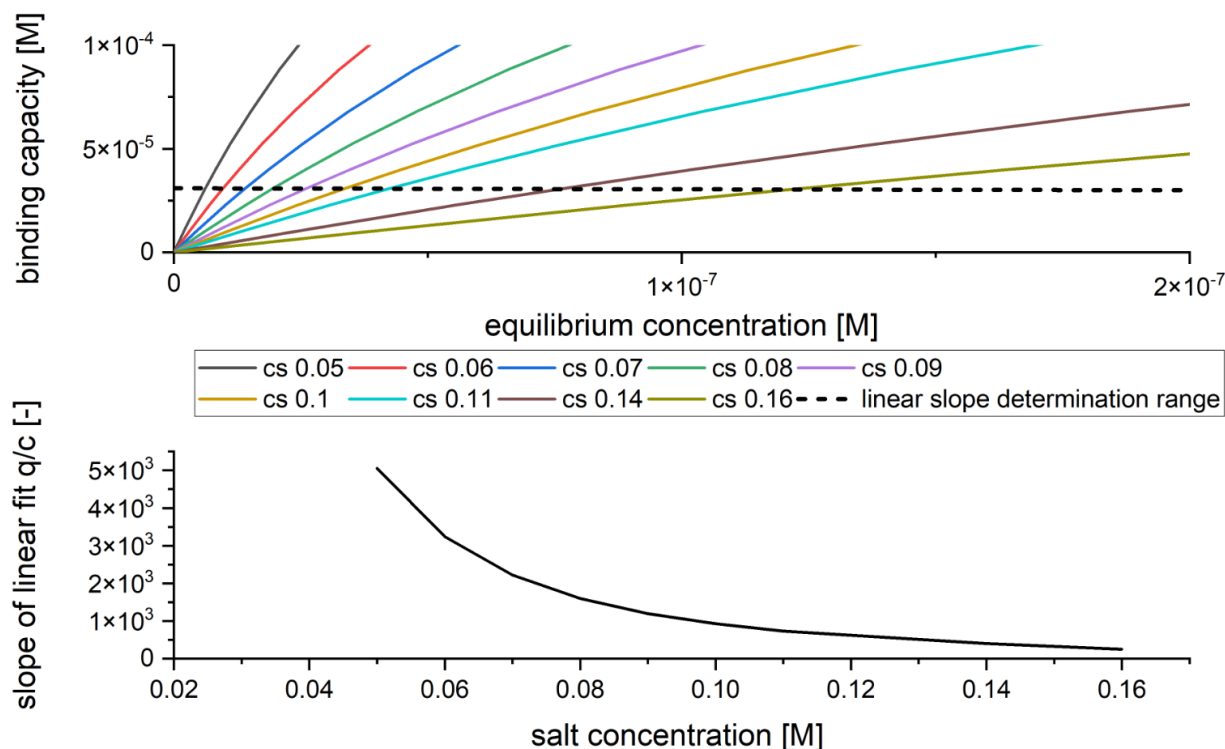


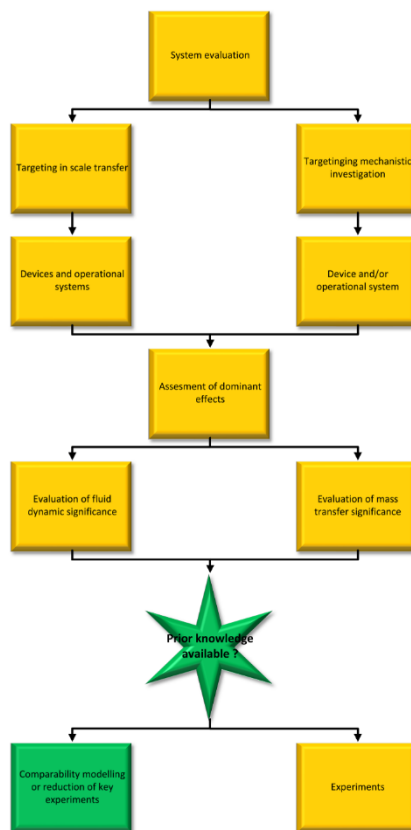
Figure 1.11: Investigation of salt-induced nonlinear change in the isothermal slope. Upper graph isotherms at different salt concentrations and the applied range for slope determination. The salt-dependent isotherm slope, resulting from the upper graph, is shown in the lower graph. Following the nonlinear isotherm slope, the different affected components equilibrium concentrations and binding capacities state the salt dependency of displacement effects.

### Procedure and industrial significance

The model building procedure can be manifold. In general, the first step is evaluating the dedicated system with regard to the aim. Markedly, the fluid dynamic optimization of a device or the scale transfer will need a different level of detail while the system observed is the same. Figure 1.12 A) presents a schematic representation of the system evaluation. Following the aimed result, as previously described, different models and model depths need to be investigated. This said, assessment of the relevant parameters would reduce the effort and enable the focus on in-depth needed parameters, exemplary presented for the mass transfer in Figure 1.12 B). The prior knowledge of either fluid dynamic or mass transfer effects, represented by device and stationary phase information, is needed. The current publications in modeling focus shifts from specialized models to reviewing existing and new model approaches.<sup>61,113,139</sup> However, the industrial application is hindered by broad model approaches occasionally including extensively parameter determination, while the significance of the dedicated system is unknown. Contrary to presenting a new model building approach, the development of a model library incorporating existing and new approaches is missing. Developing a new model applying mechanistic modeling is time-consuming and will only gain weight in the industry when existing models and parameters can be applied to new challenges.

## 1.2 Downstream process development

A)



B)

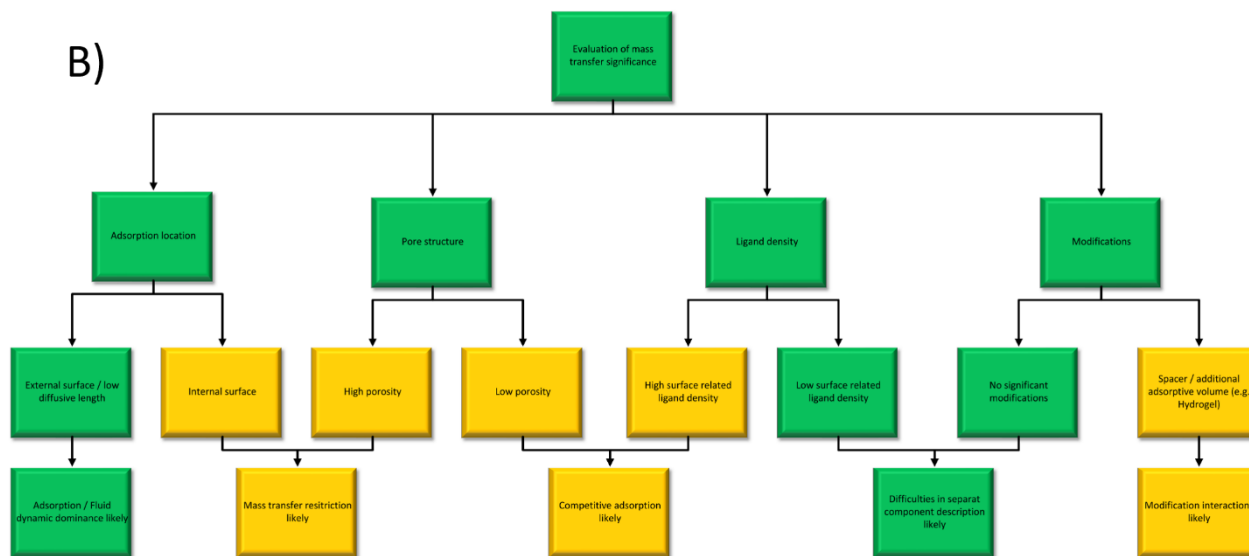


Figure 1.12: Schematic system evaluation for reduction in modeling effort within prior knowledge library. Following the overview in A), the experimental and modeling depth can be assessed with the in B) identified significant effects. Depending on the modeling depth defined in A), different foci may initially be relevant for scale transfer or mechanistic studies. Furthermore, investigating the relevance of fluid dynamic and mass transfer presents the need for detail of the respective effects. The model building procedure could be further accelerated with available prior knowledge/models. In addition, B) presents stationary phase properties and estimation of dominant effects.

Following the prior knowledge library approach for mass transfer restriction in Figure 1.12 B), the stationary phase properties can be used to assess significant effects. This approach is already established for empirical chromatographic PD reducing the experimental variables of stationary phase

## 1.2 Downstream process development

---

characteristics, ligands, and process parameters.<sup>49,140</sup> However, in empirical PD, this approach is only feasible for a set of molecules expressing high similarity, such as the classical mAb purification processes. The typical classification scheme for chromatographic steps employs a) chromatographic processing mode, b) stationary phase scaffolds, c) backbone structures, and d) chromatographic interaction mode. This said, the library approach can be applied to modeling receiving assessments of diffusive length, porosities, ligand densities, and channel sizes. The benefits are, among others, model building and identification of the best suitable stationary phase. This said, a standardized approach and screening procedure are needed to characterize stationary phases towards a streamlined PD incorporating existing and new process procedures.

Developing a standardized approach utilizing the benefits of high throughput screening could consist of manufacturer stationary phase and devices information supplemented by experiments and modeling information for PD.

The manufacturing information for a possible process mode is a function of scaffold, backbone, interaction mode, and feed stream composition. To sort the various properties of the scaffolds, they are grouped into: a) bead, b) monolith, c) fiber, and d) MA (Figure 1.2). Bead-based scaffolds usually have a backbone structure consisting of particle diameter in the range of 50 – 500  $\mu\text{m}$  and pore diameter of 20 - 160 nm.<sup>106,107</sup> These scaffolds are usually based on silica, polysaccharides, acrylates, or methacrylate and can exhibit additional surface modifications.<sup>141</sup> Numerous researchers have shown a close relationship between molecular size, optimal pore diameter, and achievable binding capacity.<sup>108,109,142</sup> Hunter et al and Svec, among others, point towards an ideal particle pore to protein diameter ratio of about 10-12.<sup>110,143-147</sup> This rule of thumb correlates to the molecule specific accessible surface area and thus available binding sites, nearly independent of the overall ligand density. A meso and macro pore structure can characterize monoliths as bead-based scaffolds. The monolith macro pores are called flow channels with a typical channel size in the range of 1-6  $\mu\text{m}$  <sup>148-150</sup>, while the meso pores are in the range of 2-50 nm.<sup>106,148,149</sup> The scaffold of monoliths consists of different materials like silica, polyacrylamide, cellulose, styrene, and polyglycidylmethacrylate.<sup>148,151</sup> Monoliths and beads tend to express mechanical instability due to the high internal porosity.<sup>106</sup> Depending on the formulation and packing procedure, fiber-based backbone structures consist of flow channels in the range of 0.5 – 20  $\mu\text{m}$  and a surface area of 2-20  $\text{m}^2/\text{g}$ . The scaffold can be compared to monoliths and membrane material, e.g., polyethylene terephthalate, and cellulose.<sup>152-154</sup> MA backbone structures with pore sizes of 2-4  $\mu\text{m}$  are known for their high applicable flow range with relatively low-pressure drop.<sup>111</sup> These MA backbones are usually made of organic material such as cellulose and its derivatives, polyethersulfone, polypropylene, and polyvinylidene fluoride, exhibiting a surface area of 0.6 – 3  $\text{m}^2/\text{g}$ .<sup>153,155</sup> In summary, the stationary phase properties provided by the manufacturer can be applied to assess the diffusive length, adsorption location, and stability. Furthermore, the physical protein properties were investigated heuristically by several researchers. These physical properties are related to the schematic investigation in Figure 1.12 B), facilitating the integration of stationary phase information in the PD workflow.<sup>216</sup>

Thereafter, the stationary phase manufacturer typically provides information such as the ionic capacity and ligand attached to the stationary phase. However, the ligand density is typically provided as the amount of ligand per stationary phase volume, which neglects the distance from ligand to ligand. Following this, the protein accessible specific surface area should be considered. The specific surface, if not available, can be assessed within the BET (Brunauer, Emmett, and Teller) or microscopic measurement, while the molecular accessibility is typically investigated with tracer experiments

## 1.2 Downstream process development

applying different sizes of reference molecules, e.g., dextran or pullulan.<sup>21,117,120,156</sup> This said, besides the accessible specific surface area for a given molecule – mostly determined by the chosen backbone structure - the ionic capacity or density can be a variable influencing the binding capacity, selectivity, and the mass transfer rate.<sup>141,144,146,157</sup> Thus, various backbone structure modifications are available to influence the ionic capacity distribution and/or distance between ligands of a stationary phase, such as a) surface modification, b) grafted polymers, and c) gel in a shell.<sup>141</sup> The various modifications can influence the binding capacity and/or mass transfer by changing the ionic forces or ionic charge distribution.<sup>216</sup>

After all, the manufacturer information already provides valuable information in assessing relevant processes and model parameters. Even so, mechanistic modeling publications in PD have increased in the last few years, but unsorted procedures hinder the broad application and use. However, a possible solution might be the development of a living process and model library which would, in the future, also need to incorporate molecular information, correlation in separation -molecular similar charge/size distribution - and ionic stationary phase density distribution and correlation for each dedicated process type. Consequently, this model parameter determination could be integrated into the PD experiments with the streamlined approach presented in Figure 1.12.

### 1.2.3.3 Modeling characterization

#### *Characterization of systems*

The model building is typically performed on a lab scale by applying HPLC and LC benchtop systems. These systems consist of different buffer containers, several meters of tubing, at least two pumps, a kind of injection loop, mixing chambers, different detectors, and fractionation devices, see Figure 1.7.

In addition to the desired model selection and mode depth, the system geometry should be considered for a suitable model. For example, the model parameter velocity and axial dispersion consider the geometry in length, diameter, and volume. For a detailed fluid dynamic description, mixing points such as mixing chambers or redirection of liquid, axial or radial, might be a reason to increase the model depth. Following the theoretical/physical investigation of the system, the model parameters such as mixing tank size and mixing factor for CSTR or axial dispersion for PFR model approaches are evaluated.<sup>118,119,158,159</sup> The fluid dynamic evaluation is typically performed by tracer experiments in inject and/or step gradient experiments, see Figure 1.13 A).

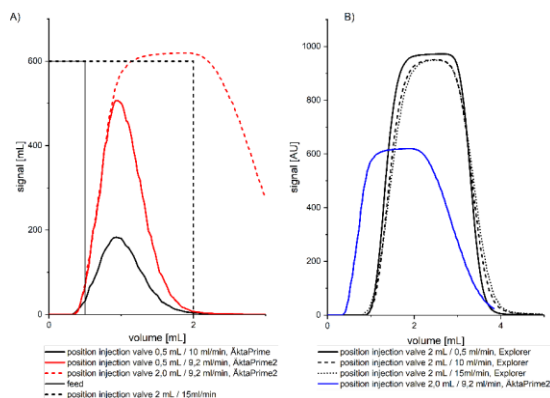


Figure 1.13: Exemplary acetone tracer experiments for different injection volumes, velocities, and systems. In A) different velocities and injection volumes are compared. The differences between various flow rates and systems at 2 mL injection volume are presented in B.

## 1.2 Downstream process development

---

In addition to model-assisted parameter assessment, the overall axial dispersion coefficient of the device can be derived by calculating the Bodenstein number / Peclet number based on the experimental results.<sup>58,68,102</sup> This said, the overall device axial dispersion coefficient merges all system and/or device effects. Following this, the system and the device are typically segregated into one or more system and device models. In addition, the different buffer flow paths used in experiments are also considered in modeling when a gradient or step function of feed is performed by one of the buffer pumps. The tracer experiments discussed earlier are also applied to determine the residence time or volume of the molecules transitioning the system, as presented in Figure 1.14. This said, more detailed fluid dynamic procedures and descriptions might be found in the work of Octave Levenspiel.<sup>102</sup>

Following the procedure in Figure 1.14, the raw data selection in A) is transferred to a homogenous signal by integration or differentiation of the injection/peak or step/sum function, respectively. The sum function's first derivative will determine the average residence time/volume at the peak maximum. Following this, the calculated and experimentally derived peaks are areas normalized, preserving the peak shapes and allowing comparability. In Figure 1.14 B), the centroid of the area is used to normalize the abscissa values to the average residence time/volume. The different system signals in Figure 1.14 B) of Äkta® Prime, Äkta® Prime 2 and Äkta® Explorer are now directly comparable. The peak width is marginal, increasing from the system Äkta Explorer < Äkta Prime2 < Äkta Prime1. However, the comparison of different signal types requires sufficient methodology. Following this, the injection mode, adequate injection volume, and concentration must be investigated to obtain valid results. The step injection mode, however, reveals further information, such as switching to a different pump line, as presented in Figure 1.14 C). Following the observation in C), the normalized sum function data present significant differences between the systems of Äkta® Explorer and Äkta® Prime when comparing the increasing and decreasing signals. The Äkta® prime presents a narrow peak form in the increasing sum function while a wider peak form in the decreasing sum function analysis when compared with the Äkta Explorer. In addition, the Äkta Explorer presents a comparable peak width in increasing and decreasing sum function analysis. In summary, the detailed system analysis revealed the requirement to build a model for each system. In addition, modeling each system would not only increase the simulation reliability of the simulation but also allow the integration of each system into a model library.

## 1.2 Downstream process development

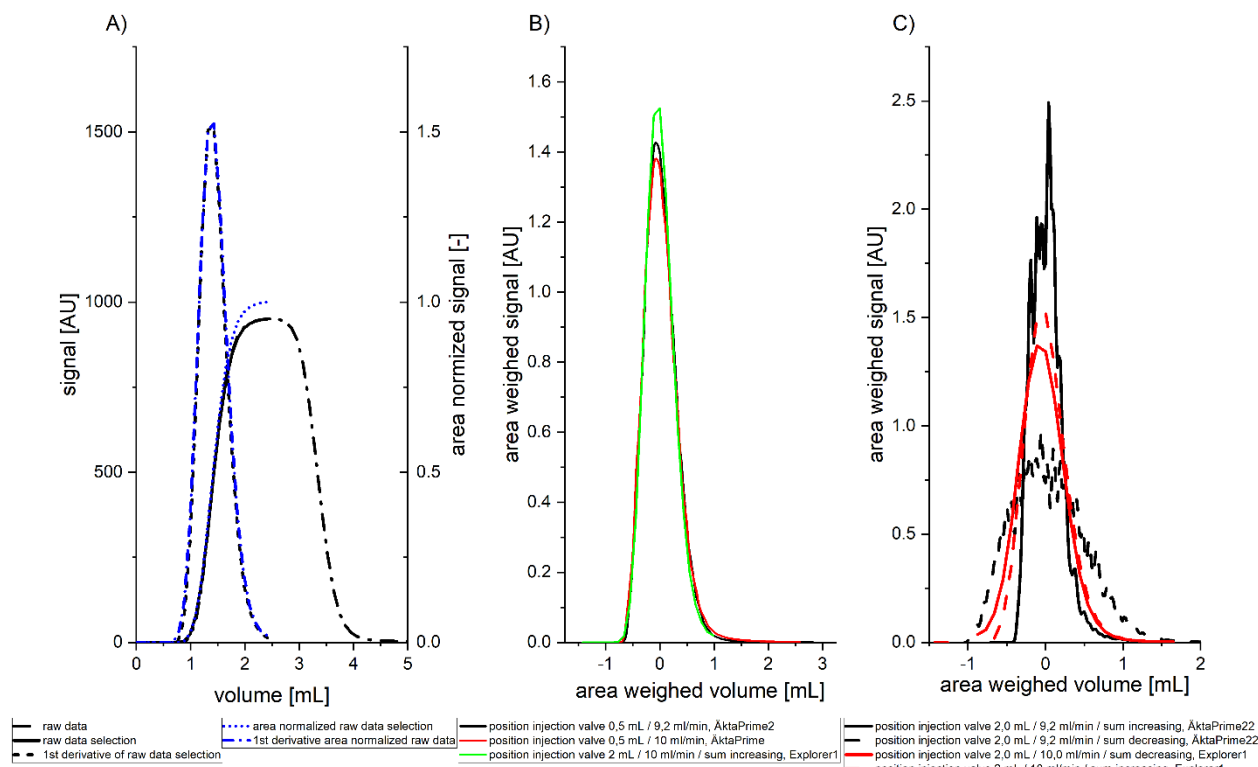


Figure 1.14: Exemplary area weighed fluid dynamic investigation of different tracer signals and systems. The data handling is described in A, beginning with the raw data selection in the increasing tracer sum function and transferring it to the peak function within the first derivative revealing the average residence time/volume at the peak maximum. Following this, the derived peak is integrated, the area normalized, and the first derivative obtained. In B, different system tracer injection peaks for the Äkta Prime, Äkta Prime 2, and in A) obtained sum function signals are presented, normalized to the obtained area weighed volume. This said, the system fluid dynamic is comparable, presenting systems with the same capillary diameter and comparable length while small differences are presented in the peak width. The peak width increases from the system Äkta Explorer < Äkta Prime2 < Äkta Prime1. The injection mode requires a sufficient investigation of injection volume and concentration to obtain valid results. In addition, the step injection typically reveals further information, such as switching to a different line, as presented in C. Following the observation in C, the sum increasing and decreasing signal of Äkta Explorer and Äkta Prime shows significant differences between the systems. The Äkta prime presents a narrow peak form in the increasing sum function, while a width peak form in the decreasing sum function analysis when compared with the Äkta Explorer. In addition, the Äkta Explorer presents a comparable peak width in increasing and decreasing sum function analysis.

### Characterization devices

Devices typically consist of the device inlet, a type of fluid distribution for homogeneous concentration profile, the stationary phase, as well as fluid collector and outlet. The separate device description without the stationary phase might be possible but can also present wrong assumptions/parameters. Therefore, fluid distributors are developed for a dedicated application. The missing resistance, e.g., stationary phase induced back pressure, can present an inaccurate fluid dynamic representation when the device is investigated without the stationary phase. Following this, fluid dynamic device investigations, including the stationary phase, are typically performed.<sup>106,118,120</sup> However, the system's geometrical parameters, and previous investigation also apply to the device. In addition to the geometrical parameter and tracer experiments, the porosity and stationary phase-induced changes might be considered. The chemically modified stationary phases can consist of spacers, additional binding volume, or hydrogels that change with the surrounding conditions, as presented exemplary in Figure 1.15. This said, the porosity and/or void volume depends on the process conditions and can promote fluid dynamic changes in addition to adsorption.

## 1.2 Downstream process development

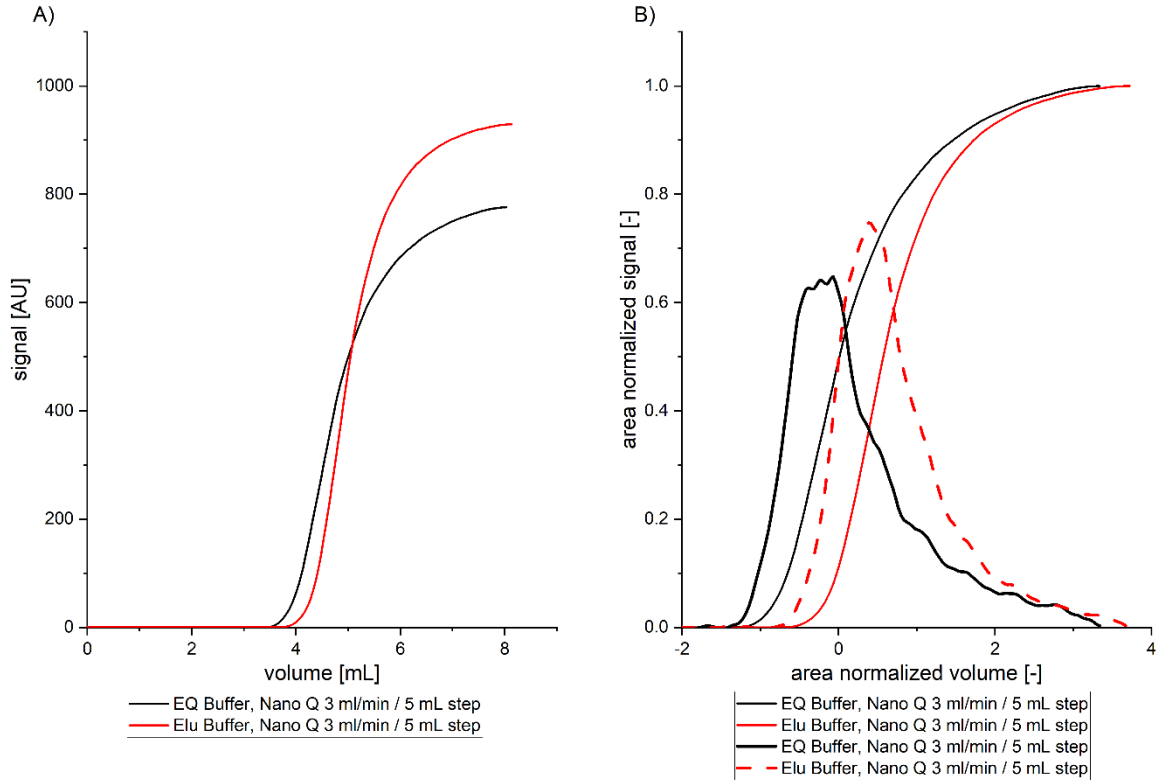


Figure 1.15: Exemplary device fluid dynamic deviation at different process conditions. In A), the raw data of a Sartobind Q Nano device is presented at equilibration and elution conditions. The different process conditions are leading to changes in peak width and retention time/volume, as presented in B).

### Characterization stationary phases

In addition to the manufacturer stationary phase information presented in chapter 1.2.3.2, the experimental model parameter determination can be divided into additional physical/molecular and adsorption parameters.

The physical/molecular parameter determination describes the evaluation of porosity and molecular accessible pore structure. Therefore, the stationary phase porosity is determined by applying BET measurements. The BET measurement generally describes the desorption behavior of liquid nitrogen in the stationary pores, which is then selectively evaporated by defined pressure ramps.<sup>160,161</sup> Furthermore, the in chapter 1.2.3.2 discussed that tracer experiments typically apply tracers of different sizes, e.g., pullulan and dextran.<sup>1,21,120</sup> Doing so results in a molecular size-related accessible pore volume. The accessible porosity is then calculated for the stationary phase or device according to Eq. (1.32) and (1.33). Deducing the difference of the tracer retention volume  $V_{ret,tracer}$  and the external retention volume of the device and/or system -  $V_{device}$ ,  $V_{System}$  - divided by the stationary phase volume  $V_{MA}$  provides the tracer-related porosity.

$$\varepsilon_{Stationary\ Phase,i} = \frac{V_{ret,tracer,i} - V_{Device} - V_{System}}{V_{MA}} \quad (1.32)$$

$$\varepsilon_{Device,i} = \frac{V_{ret,tracer,i} - V_{System}}{V_{Device}} \quad (1.33)$$

As previously described, the SMA model parameters are ligand density, represented by the ionic capacity, the isotherm parameter, and the kinetic parameter.<sup>100</sup> As said, the ionic capacity is typically

## 1.2 Downstream process development

assessed by titration. Following the titration of an ionic charged stationary phase, the stationary phase is preconditioned with the counter ion of the stationary phase (acid or base). Thereafter, the stationary phase is washed with purified water and subsequently flushed with a step signal of the oppositely charged acid or base, washed, and repeated. The conductivity signal is evaluated within the difference of the stationary phase-related titrated mass in the two titration steps according to Eq (1.34).<sup>181</sup> The ionic capacity is calculated by deducting each titration's acid/base titration mass corrected by the porosity  $\varepsilon$  corrected stationary phase volume  $V_{MA}$ .

$$\Lambda = \frac{\int c_{Titration\ 2} \cdot \partial V_{Titration\ 2}}{V_{MA} \cdot (1 - \varepsilon)} - \frac{\int c_{Titration\ 1} \cdot \partial V_{Titration\ 1}}{V_{MA} \cdot (1 - \varepsilon)} \quad (1.34)$$

Next to the ionic capacity determination, the isotherm adsorption parameters are assessed. The experimental evaluation is typically performed with batch experiments.<sup>57,162,163</sup> This said, a known portion of the stationary phase is placed into several containers, equilibrated, loaded with different feed masses, and shaken/mixed until an equilibrium state is achieved. Thereafter, the liquid concentration is measured and either corrected by the theoretical pore volume in Eq. (1.36) or the stationary phase transferred to a second vessel with equilibrium buffer washing out the unbound molecules in Eq. (1.37). Subsequent to the wash step, the elution is performed, and the mass balance is closed. The two presented procedures have other inaccuracies. Applying the theoretical stationary phase volume requires an exact knowledge of the stationary phase properties and can result in deviations due to the usually small sample volumes. The second approach, applying a wash and elution step, affects the equilibrium concentration by diluting the surrounding conditions. Following this, the equilibration buffer will reduce the overall liquid phase concentration and induces an elution. In this approach, the mass found in the wash step would then be added to the equilibrium mass. Consequently, the partially eluted mass would be wrongly added to the equilibrium concentration. The binding capacity  $q_{MA,i}$  is then calculated by the difference of feed applied  $m_{Feed,i}$  and the residual liquid feed  $m_{Equilibration}$  relative to the porosity corrected stationary phase volume  $V_{MA} \cdot (1 - \varepsilon_{Total})$  in Eq. (1.35). This procedure is then repeated at different process conditions, such as pH value and/or conductivity.<sup>181</sup>

$$q_{MA,i} = \frac{m_{Feed,i} - m_{Equilibration,i}}{V_{MA} \cdot (1 - \varepsilon_{Total})} \quad (1.35)$$

$$m_{Equilibration,i} = V_{liquid,load} \cdot c_{liquid,load} + V_{MA} \cdot (1 - \varepsilon_{Total}) \cdot c_{liquid} \quad (1.36)$$

$$m_{Equilibration2,i} = V_{liquid,load} \cdot c_{liquid} + V_{liquid,wash} \cdot c_{liquid} \quad (1.37)$$

The isotherm parameters are determined with the batch experiment results using error minimization. This said, the in Eq. (1.4) introduced parameters - steric hindrance  $\tau$ , characteristic charge  $\nu$  and equilibrium constant - are derived.

The isotherm determination is sensitive to several experimental parameters, which need to be evaluated in advance: The time until an equilibrium state is achieved must be evaluated, possible liquid evaporation considered or prevented, the stationary phase properties and masses must be known.<sup>68</sup> In addition, the binding capacity of the stationary phase must be sufficient to enable a reliable detection, the number of batch experiments must be sufficient to represent the isotherm, and high experimental care must be considered in the experimental set-up. Furthermore, competitive binding changes the shape of the isotherm as a function of component concentration. Following this, different

## 1.2 Downstream process development

---

approaches were investigated to mitigate the isotherm parameter determination, e.g., additional breakthrough experiments and/or model-assisted isotherm parameter determination.

Dynamic HTS screening should be a supplementary possibility for convective stationary phases to assess additional isotherm parameters.<sup>55</sup> This said, a process comparable in HTS set-ups could be applied to estimate additional isotherm measurement points provided that the various injections applied to satisfy certain constraints. Such constraints result from the time necessary to achieve an equilibrium state. Following this, either the injection rate is small enough to reach an equilibrium state or the time step between the pipetting steps is large enough. Each fraction would represent an isotherm measurement, while an inter-column concentration gradient might illuminate competitive binding, comparable to Figure 4.4. The Yamamoto method applies different salt gradients at a barely loaded stationary phase and provides the linear isotherm information such as characteristic charge  $v$  and equilibrium constant  $K_{eq}$ .<sup>164</sup> Thereafter, the kinetic constant and steric hindrance parameter can be assessed with model-assisted error minimization of the same or additional experiments, including breakthrough experiments.

## 2 Thesis Outline

### 2.1 Research Proposal

During the last years, increasing interest in the pharmaceutical industry was shown towards industry 4.0, including mechanistic modeling. In addition, the COVID pandemic presented the pharmaceutical industry as one of the core business areas in providing health and although economic growth. The recent development has presented the need to speed up PD times. While upstream PD and processing have transformed in screening and processing efficiency, batch downstream processing has become the bottleneck.<sup>16,66,113,165</sup> The unit operation most often relied upon in DSP for separation efficiency and reliability is chromatography. Despite the frequent use of chromatography, PD is challenging owing to the many different types of chromatography, processing modes, and process parameters. These challenges have been overcome by applying different PD tools, e.g., experimental, prior knowledge, mechanistic, and/or statistic modeling.

However, the different tools developed mainly for one stationary phase impede a level-playing field for all stationary phases, which is why these tools are only partially intertwined. Following this, a fast and effective scale transfer is impeded by the lack of harmonization in development tools and standardized procedures. The scale-down devices (SDD) typically applied in HTS are miniaturized robotic columns of 0.2-1 mL bed volume.<sup>35,39,56</sup> While column chromatography is a standardized and widespread application; this is only conditionally true for convective chromatography such as membrane chromatography. MAs have long been recognized as offering significant advantages over resin-based chromatographic processes when used for contaminant removal in a flow-through (FT) mode.<sup>166,167</sup> However, due to high mass transfer rates observed in MAs and, thus, significantly elevated productivity, their use can also be advantageous in capture steps. However, what is considered the established toolbox in chromatography - i.e., robotic columns, model-based PD - has yet to be developed and established for MA-based PD. In addition to the lack of a small-scale experimental setup, SSD is, in principle, able to provide a first appreciation of dynamic effects.<sup>53,57,59</sup> However, fluid dynamics abbreviations, as well as wall and mass transfer effects, are known challenges between existing SDDs and lab-scale columns.<sup>35,51,56,59,96</sup> This said, direct transfer from small-scale laboratory experiments to production scale is hardly possible. Mechanistic modeling (MM) is considered a possible bridging technique between small-scale laboratory experiments and a successful scale transfer. In combination with mechanistic modeling (MM), a digital twin (SDD – MM) can be generated, which based on deeper understanding, allows the transition from a unit operation to full-train PD. Thus, the predictive power - if given - of a scale-down model can overcome the mentioned limitations of a purely experimental approach. However, mechanistic modeling and the facilitation of a small-scale digital twin/model-assisted support are currently published only for resin-based approaches.<sup>35,39,56,58,168</sup>

In addition to the harmonization in screening techniques and description between different stationary phases, different adsorption phenomena can facilitate or hinder different processing modes. Following this, a fast and cost-effective PD conditions the consideration of the present adsorption processes to utilize the best processing mode. Simplified, competitive adsorption is present when the mixture's higher attracted component is less proportional. This said, the binding capacity depends on the concentration/ratio of the individual component. Following this, the competitive binding will not only

## 2.1 Research Proposal

---

affect the best suitable process mode but also change process outcomes when not considered. Different operation modes utilizing competitive adsorption have been utilized in the past. In the case that the feed mixture itself exhibits competitive binding components and the product is displaced from the stationary phase by the impurities, a typical frontal chromatography (FC) mode is used.<sup>85,136</sup> However, the determination of competitive adsorption/displacement effects and the dedicated laboratory small-scale determination are rarely recognized. This said, the early investigation, description, and transfer of the present adsorption phenomena is a piece of important information when a PD in general or a PD including a living library approach is performed.

Developing a state-of-the-art process, e.g., mAb purification, typically involves the standardization by process library implementation/usage enabling certain cost efficiency and time-saving.<sup>17,34,169,170</sup> Platform processes use a fixed set of unit-operation and stationary phases, minimizing PD effort while at the same time ensuring acceptable selectivity, capacity, and robustness. This approach, however, is only feasible for a set of molecules expressing high similarity, such as the classical mAb purification processes. Accelerating time to market demand with different entities, generic products, and new processing modes requires a more dynamic strategy. The typical (static) platform PD only focuses on a few process parameters, limiting itself in transferability, and its success relies on fragile individual knowledge. Future strategies need to rely on standardized strategies for choosing various unit operations, allowing a more dynamic PD leading to diverse but highly robust and productive processes. Therefore, a PD strategy is needed that emphasizes a living library approach comprising the development of an HTS SDD set-up considering various stationary phases and is complemented by a model-assisted digital twin incorporating competitive adsorption processes.

## 2.2 Manuscript overview and author statement

The in this work performed research is represented by three manuscripts subsequent listed. These manuscripts are ordered by the chapter and page number, followed by a brief summary. In addition, a not yet published fourth manuscript is presented.

This work aims to enable a living library approach for different stationary phases, processing types, and tools. This living library approach is initialized by facilitating a level-playing field for convective material and utilizing mechanistic modeling for the early development phase at small-scale laboratory experiments.

### **Chapter 3. HTS setup of a Scale-down Device for Membrane Chromatography - Aggregate Removal of Monoclonal Antibodies.....54**

Dominik Stein, Volkmar Thom, Jürgen Hubbuch

*Biotechnology Progress (2020) Volume 36, Issue 6, e3055*

Chapter 3 presents the developed HTS SDD setup for convective material, here MA. Three case studies for a monoclonal antibody aggregate removal were performed with the aim of aligning HTS applications for MAs with those established for column chromatography: process parameter range determination, mechanistic modeling, and scalability. The first case study explores the experimental application of the SDD developed. Following this, bind and elute mode is applied, exploring different variations of pH and salt concentration to obtain process operation windows for ion-exchange MAs Sartobind® S and Q. In the second case study, the developed mechanistic model is compared to experimental data with the parameters obtained from the SDD - HTS setup. Finally, the third case study investigates the transferability and scalability of data from the SDD - HTS setup using both a direct scale factor and mechanistic modeling.

In addition to the harmonization in screening techniques and description between different stationary phases, present or different adsorption phenomena enable or impede different processing modes.

### **Chapter 4. PD exploiting competitive adsorption-based displacement effects in monoclonal antibody aggregate removal - a new high throughput screening procedure for membrane chromatography.....78**

Dominik Stein, Volkmar Thom, Jürgen Hubbuch

*Biotechnology and applied biochemistry (2021)*

The study mentioned above investigates competitive adsorption processes and new processing modes. Therefore, the adsorption processes are investigated and supported by mechanistic modeling, aiming for a key parameter to identify competitive adsorption. In addition, the new HTS screening procedure overload bind and elute (OBE) is employed to verify competitive adsorption experimentally. The OBE mode is investigated in its ability to deliver classical process parameters, e.g., process maps and dynamic effects, such as displacement effects. In addition, the derived information is used to employ a new processing mode in which the feed passes through the column and is then recirculated to the feed tank.

The previous work enables a level-playing field in small-scale evaluation and processing, which can be used to implement a living library and identify suitable stationary phases for a given separation task.

### **Chapter 5. Streamlined PD procedure incorporating the selection of various stationary phase types established in a mAb aggregate reduction study with different mixed mode ligands.....97**

Dominik Stein, Volkmar Thom, Jürgen Hubbuch

*Biotechnology Progress (2021) Volume 38, Issue 2, e3230*

The in chapter 5 work presented extends the previously harmonized stationary phases screening techniques with the selection of stationary phases and process modes in PD. Furthermore, the introduction of a living library proposes harmonizing different information types. Therefore, a rigorous strategy will be pursued to reduce the various experimental design space resulting from possible combinations in scaffolds, backbones, and ligands. The strategy is based on theoretical considerations, identification of stationary phase selectivity, and capacity for identifying a suitable stationary phase system, here MA. For these systems, five mixed mode ligands and various MA candidates are investigated in their high molecular weight species (HMWS) reduction potential for a given mAb feed stream and referenced to the performance of Capto™ Adhere. The procedure guides the integration from initial theoretically/manufacture-guided information, initial ionic capacity to the verification in HTS while enabling the integration in a living library.

### **Chapter 6. Full train product development from lab 2 production procedure – incorporating a living library with mechanistic modeling - from HTS Scale to pilot scale of Membrane Chromatography in aggregate Removal of Monoclonal Antibodies.....117**

Dominik Stein, Volkmar Thom, Jürgen Hubbuch

In preparation

Finally, the study mentioned above-investigated PD tools' linkage to a universal approach. A procedure is introduced guide PD to transit from partially connected development tools to a fully integrable process development living library approach. Therefore, the investigated process tools are linked by three sub-case studies in which mechanistic modeling enables the link, preservation, and further investigation of process information. The approach is divided into fluid dynamic investigations, integration of historical data including isotherm information, and kinetic transfer, including scale-up verification. Following the fluid dynamic investigation, new devices are developed to separate stationary phase and device effects. In addition, historical information from different stationary phases can be integrated into the living library. The second part of this work focuses on integrating historical data by assessing apparent isotherm parameters from existing data, in this case, HTS data. Finally, the kinetic effects are evaluated, and a scale-up experiment verifies the approach. Generally, the approach uses thoroughly engineering and commonly known dimensionless numbers for the scale transfer linked by mechanistic modeling. The approach guides PD to develop a living library approach, linking the previous studies with a workflow to the final scale-up. Consequently, the transitioning from partially connected PD to a fully integrated PD strategy by applying mechanistic modeling linked living library is presented.

### 3 HTS setup of a Scale-down Device for Membrane Chromatography - Aggregate Removal of Monoclonal Antibodies

Dominik Stein<sup>1,2</sup>, Volkmar Thom<sup>2</sup>, Jürgen Hubbuch<sup>1</sup>

<sup>1</sup> Karlsruhe Institute of Technology (KIT), Institute of Process Engineering in Life Sciences, Section IV: Biomolecular Separation Engineering, Karlsruhe, Germany

<sup>2</sup> Sartorius Stedim Biotech GmbH, August-Spindler-Str. 11, D-37079 Goettingen

#### Abstract

In biopharmaceutical PD, resin based high throughput screening (HTS) is well known for overcoming experimental limitations by permitting automated parallel processing at miniaturized scale, which results in fast data generation and reduced feed consumption. For membrane adsorber (MA), HTS solutions have so far only been available to a partial extent.

Three case studies were performed with the aim of aligning HTS applications for MAs with those established for column chromatography: process parameter range determination, mechanistic modeling, and scalability. In order to exploit the MA typically features, such as high mass transfer and easy scalability, for scalable high throughput PD, a scale-down device (SDD) for MA was developed. Its applicability is confirmed for a monoclonal antibody aggregate removal step.

The first case study explores the experimental application of the SDD developed. It uses bind and elute mode and variations of pH and salt concentration to obtain process operation windows for ion-exchange MAs Sartobind® S and Q. In the second case study, we successfully developed a mechanistic model based on parameters obtained from the SDD - HTS setup. The results proved to validate the use of the SDD developed for parameter estimation and thus model-based PD. The third case study shows the transferability and scalability of data from the SDD - HTS setup using both a direct scale factor and mechanistic modeling. Both approaches show good applicability with a deviation below 20% in the prediction of 10% dynamic breakthrough capacity and reliable scale-up from 0.42 mL to 800 mL.

#### 3.1 Introduction

PD for chromatographic separation in the bio-pharmaceutical industry is challenged by high cost, limited availability of the target entity and shortened timelines. The abundance of available chromatographic media and the broad range of possible process parameters result in high experimental effort for their determination.<sup>35,49,140</sup>

These challenges can be addressed by the established PD tools of high throughput screening (HTS) robotic platforms for parallel, automated and standardized workflows to accelerate PD efforts and to use scale-down-devices (SDD) in these workflows to reduce usage of materials and cost.<sup>35-39</sup>

The fields of application for HTS are, for instance, identification of drugs<sup>41,42,171</sup>, biological libraries<sup>43,44</sup>, cell cultivation<sup>45,46</sup>, aqueous two-phase systems<sup>48,172</sup> and chromatography performance estimation.<sup>39,49-53,173</sup> In HTS-based chromatography PD the mode of parameter determination can be divided into the following: Batch isotherm determination<sup>49,55</sup>, process range evaluation<sup>35,53</sup>, scale

### 3.1 Introduction

dependency<sup>35,53,56,57</sup> and scale-down model development<sup>53,58</sup>. Typical formats for process range evaluation and batch isotherm determination are microtiter plates. If needed, fluid flow in microtiter plates is normally achieved by using micro pipetting devices and/or vacuum. Process-comparable operations and dynamic effects need to be mimicked in order to allow process predictions. That said, knowledge of scale-dependent variables is essential and especially critical process parameters need to be kept under control. Therefore, scale dependency of critical parameters and scale-down model development are highly connected.

The advantages and disadvantages of different PD scales are shown in Figure 3.1. To summarize, usage of materials increases with the scale, while potential deviations, e.g., in fractionation or analysis, will have less effect on the result. On the other hand, small-scales entail high standardization and availability, as well as less time and usage of material. The standardization shown in Figure 3.1 refers to the methods and systems used. Within a GMP approved process the standardization is high to meet the regulatory requirements. However, the process is designed specially to meet the desired criteria and thus is not easily to transfer. For example, the used system to perform a chromatographic step is usually customized engineered for the needs of the process and differs between the processes between pumps, piping and thus dead volumes, detectors, automation platforms and data transfer rates are used, which is less true for laboratory equipment which is usually built in a standardized way.

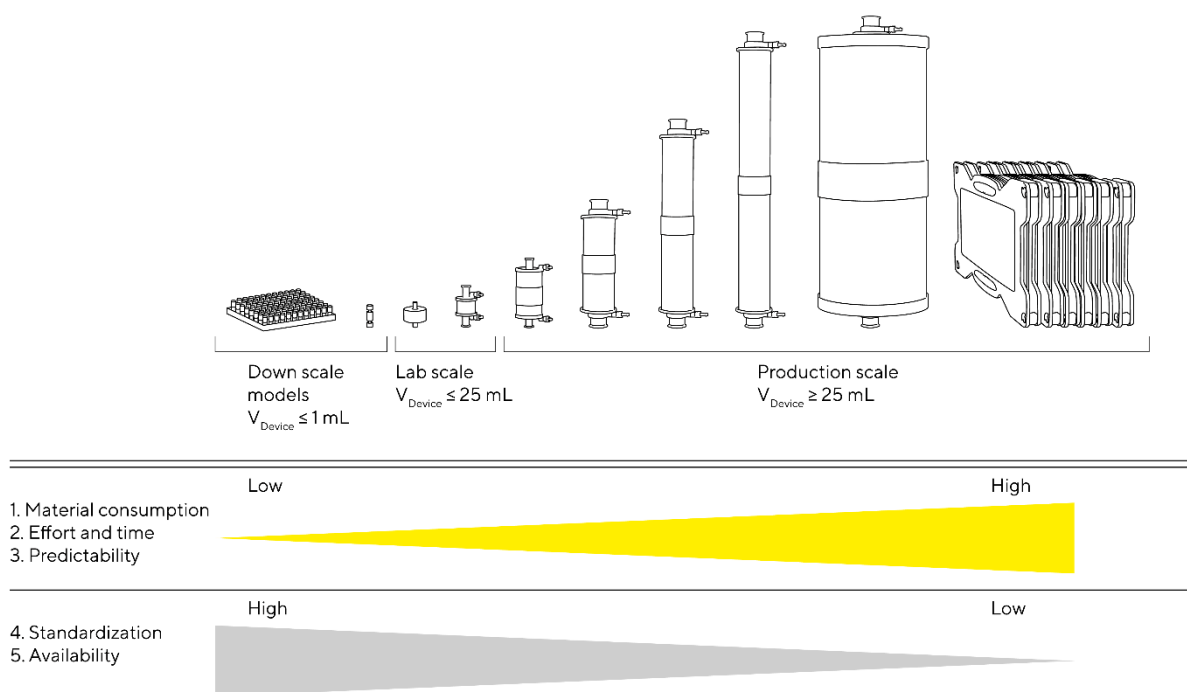


Figure 3.1: Comparison of different standard scales. Comparison regarding material usage, effort, time, predictive power, degree of standardization, and availability

SDD in column chromatography for resin and process window determination are commonly miniaturized robotic columns of 0.2-1 mL bed volume<sup>35,39,56</sup>, in addition, these SDDs can offer a first appreciation of dynamic effects.<sup>53,57,59</sup> However, fluid dynamics abbreviation as well as wall and mass transfer effects are known challenges between existing SDDs and lab-scale columns.<sup>35,51,56,59,96</sup> Reliable scale-up typically requires additional experiments to be performed on a liquid chromatography system using lab-scale columns (1-10 mL) with process-scalable bed height.

In combination with mechanistic modeling (MM), a digital twin (SDD – MM) can be generated, which based on deeper understanding, allows transition from a unit operation to full-train PD. Thus, the predictive power - if given - of a scale-down model can overcome the mentioned limitations of a purely experimental approach.

While column chromatography is a standardized and widespread application, this is only partially true of membrane chromatography. MAs have long been recognized as offering significant advantages over resin-based chromatographic processes when used for contaminant removal in an flow-through (FT) mode.<sup>166,167</sup> However, due to high mass transfer rates observed in MAs and, thus, significantly elevated productivity, their use can also be advantageous in capture steps. Processing in a fast-cycling mode at reduced membrane bed volume lends itself towards single-batch-use of the ready-to-use MAs, reducing cost of goods by full utilization of the MA lifetime, mitigating bioburden risks, and making cleaning and cleaning validation efforts obsolete. However, what is considered the established toolbox in chromatography - i.e., robotic columns, model-based PD, etc. - has yet to be developed and established for MA-based PD.

In this paper, we are introducing a robotic HTS platform based on a newly developed SDD MA PD to overcome the gap in HTS applications between resin chromatography and MA. To illustrate the applicability of this SDD, a process is investigated for aggregate removal of a recombinant monoclonal antibody (mAb) immunoglobulin G (IgG) feed stream by MA-based anion-exchange (AEX) and cation-exchange chromatography (CEX) processes. The objective is to align column- and membrane-chromatographic based HTS by considering the process parameter range, scale dependence and MM studies. Therefore, three case studies are carried out: SDD - HTS process map determination, the use of MM to create a digital twin (SDD - MM) of the process in question and scalability considerations of data obtained by the SDD – HTS setup. During these studies, we thus applied the bind and elute (BE) mode for process map determination in which the MA is equilibrated, loaded, washed, and eluted in a step-wise manner. The fraction concentration obtained in step-wise loading is used to characterize the breakthrough curve at the initial solution conditions, comparable to common liquid chromatography (LC)-BE experiments. The fully loaded MA is washed and subsequently eluted in fractions using increasing salt concentrations in step-wise elution. Assuming that the decreased binding capacity at higher salt concentration also holds true in an FT mode of operation, a process map with respect to the pH and salt concentration can be determined. Targeted levels of purity and yield define the available process window. The SDD - HTS setup generates process data that is directly comparable to a liquid chromatography system and thus should allow for direct scale-up based on HTS data. Parameters obtained from the SDD – HTS setup were used to compare model descriptions based on these parameters with obtained process data. Conformity of the SDD – HTS and SDD – MM is assessed by scale-up experiments with different scale factors.

### 3.2 Material and Methods

The applications for material used in this study are subdivided into the following: SDD characterization, HTS and benchtop chromatographic experiments, analytics, and data handling, automation, and MM. A full list of abbreviations, symbols and indices used throughout this paper is presented at the end (Table 3.7, Table 3.8 and Table 3.9).

## 3.2 Material and Methods

---

### 3.2.1 SDD characterization

SDD characterization includes fluid dynamic investigations with qualitative dyeing- and acetone tracer experiments as well as determination of the overall binding capacity with lyophilized BSA for Sartobind® Q and lysozyme for Sartobind® S. The dye used was coomassie blue from Thermo Fisher Scientific and acetone is purchased from VWR Chemicals. The binding capacity experiments were used to evaluate the mass balance between bound and eluted mass. BSA supplied by Kraeber, and lysozyme purchased from Sigma Aldrich were utilized. The Sartobind® MAs employed in our studies are manufactured by Sartorius Stedim Biotech GmbH. The inline fluid dynamic experiments with acetone were measured by a prototype UV flow cell with a 60 µL void volume and a 1 mm path length. This cell was connected to UV/VIS diode array detector supplied by J&M Analytik AG. The wavelength used were 220 nm and 280 nm.

### 3.2.2 HTS and benchtop chromatographic experiments

HTS was carried out with a Lissy® 2002 GXXL/8P HTS robot manufactured by Zinsser Analytic, and the FT experiments were performed using Äkta Prime™ and Äkta™ Explorer supplied by GE Healthcare. The two MA devices used were prototype setups, with three flat-sheet-stacked MAs of a diameter of 2.8 cm in a plastic housing or with 20 flat-sheet-stacked MAs in a silicon housing stabilized by a plastic jacket. Cellstar® 12-wellplates supplied by Greiner Bio-one International GmbH were used for fractionation of process streams in the

SDD – HTS setup. Buffer was prepared by dissolving buffer salts in purified water produced by the arium® lab water purification system manufactured by Sartorius Stedim GmbH.

The CHO-fermented monoclonal antibody was an internal Sartorius Stedim Biotech GmbH feed solution. Further purification was done by using a MabSelect™ Sure™ lab column (5 cm diameter, 192 mL volume) provided by GE Healthcare and by an Äkta Prime™ system. The eluate contained about 18 g/L mAb and a mAb aggregate level of about 0.5-1%. Enrichment of the aggregate content of the clarified mAb solution to 2-6% was done by a pH shift process. Aggregation by a temporary pH shift is a commonly used method for aggregation.<sup>64,174,175</sup> After diluting the 0.1 M pH 3 glycine-buffered mAb solution three times with KPi buffer, the pH was adjusted to 3 with 0.5 M HCl. The aggregation time was set to 3 h with stirring at 150 rpm. Afterwards, the pH was readjusted to pH 7 with 0.5 M NaOH, which resulted in an aggregate content between 6-12 %. Afterwards, the aggregated mAb solution was diafiltrated against the desired buffer using the Sartoflow® Smart system (Sartorius Stedim Biotech GmbH) using a 200 cm<sup>2</sup> Sartocon® Slice 200 Hydrosart® 30 kDa cassette. Diafiltration was carried out until the buffer conductivity and/or pH of the diafiltered solution reached a constant value. These solutions exhibited a mAb concentrations of up to 10 g/L. The final feed solutions were prepared by diluting of the 10 g/L aggregated mAb solution with the corresponding buffer. Each buffer at each pH was prepared using 0 mol/L and 1 mol/L NaCl. The pH and conductivity (CD) were adjusted by mixing the solution with the corresponding buffer, followed by an incubation period of one hour at room temperature. For the screening procedures, different protein feed solutions were used: (1) 1-5 g/L bovine serum albumin dissolved in KPi buffer at pH 7 with an NaCl concentration of 0-0.3 mol/L, (2) 1-3 g/L lysozyme dissolved in 10 mmol KPi buffer at pH 7 with an NaCl concentration of 0-0.3 mol/L and (3) 1-6 g/l diafiltered mAb solution with a 0-0.3 mol/L NaCl concentration. The buffer preparation and therefor used consumables are presented in the supplement.

### 3.2.3 Analytical methods

The overall protein concentration was measured by a UV spectrometer at a wavelength of 280 nm using the VivaSpec<sup>®</sup> UV reader provided by Sartorius Stedim Biotech GmbH. IgG and its HMW concentration were measured using a Yarra<sup>™</sup> 3  $\mu$ m SEC 3000 column of 300 x 7.8 mm supplied by Phenomenex using the Thermo Scientific<sup>™</sup> Dionex<sup>™</sup> UltiMate<sup>™</sup> 3000 HPLC System from at a flow rate of 1 mL/min.

### 3.2.4 Data handling, automation, and mechanistic modeling

Automated HTS was performed using Zinsser Analytic WinLissy (version 7). UNICORN<sup>®</sup> supplied by GE Healthcare was used for FT experiment recipe writing and chromatographic analysis. The concentration of IgG and of its HMW aggregates were quantified by the Dinox Chromleon<sup>™</sup> 6.80. Evaluation of the experimental results and analysis of the chromatographic curve were performed using Origin<sup>®</sup> 2018b software supplied by OriginLab Corporation. MM was done by ChromX<sup>™</sup> provided by GoSilico GmbH.

### 3.2.5 Scale-down device – experimental setup

Each SDD contained a membrane bed consisting of three flat-sheet membrane discs with a 27 mm diameter and a thickness of 230  $\mu$ m to 260  $\mu$ m, resulting in bed volumes of 0.40 mL to 0.46 mL respectively, as illustrated in Figure 3.2 A. Two different membrane types were used: Sartobind<sup>®</sup> S membrane (CEX) and Sartobind<sup>®</sup> Q membrane (AEX) with a mean pore diameter of 3  $\mu$ m to 5  $\mu$ m and a ligand density of 2  $\mu$ eq/cm<sup>2</sup> to 5  $\mu$ eq/cm<sup>2</sup>. Each SDD exhibited a septum port, through which a robotic needle could penetrate to inject solution with a positive pressure into the device. To test and confirm the targeted average pipetted volume accuracy of less than  $\pm$  3% for an injection velocity of 500  $\mu$ L/s, a volume calibration routine for reducing the deviation between the set and measured dispensed volumes was established using 200, 400, 800, 1500, 2500 and 4000  $\mu$ L water in triplicate for each needle prior to each experiment as presented in the supplement. If the targeted accuracy could not be reached, the volume correction factors of the robotic system were adjusted in the HTS robotic software. The HTS setup was comprised of eight SDDs attached to a holder plate for parallel operation; see Figure 3.2 B. Below the SDD holder plate, four movable 12-well plates collected the fractions of the eight devices, where each well held a maximum of 5 mL of solution for completing SDD - HTS.

### 3.2 Material and Methods

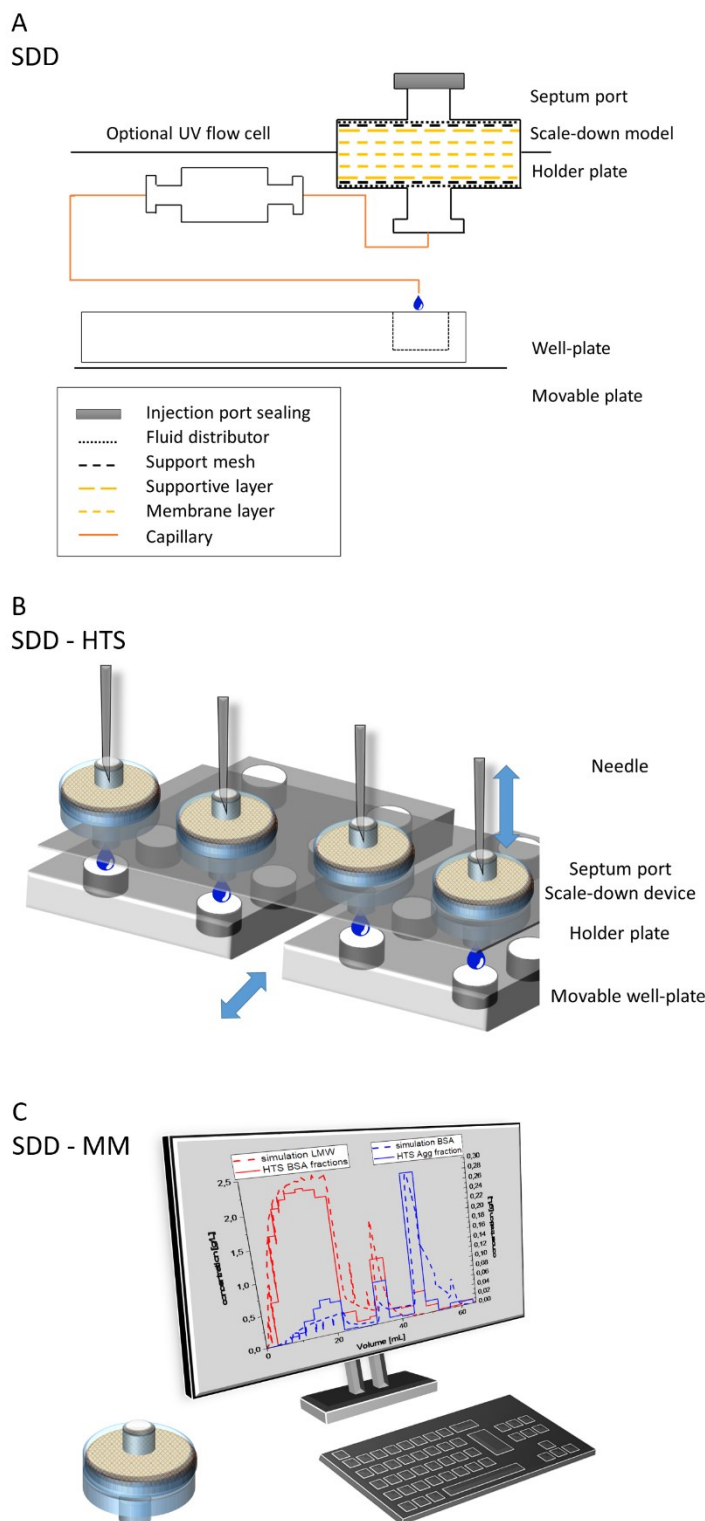


Figure 3.2: Schematic view of SDD, SDD-HTS and SDD-MM. (a) Scale-down device (SDD) setup: side view with optional UV flow cell, (b) SDD-HTS setup: a needle injects the liquid through the septum port into the membrane device, which is attached to a holder plate. The liquid passes a fluid distributor first, then through a support mesh and the three membrane layers. The holder plate accommodates eight membrane devices. Four movable well plates are used for fractionation, while each well plate collects the fraction from two membrane devices, (c) Combination of an SDD and MM results in an SDD-MM. HTS, high throughput screening; MM, mechanistic modeling; SDD, scale-down device

To ensure appropriate comparison between lab scale and production scale, the SDD needed to exhibit certain fluid dynamic and mass transfer properties. The fluid dynamic behavior of the SDD - HTS was characterized by performing dyeing experiments and breakthrough tracer experiments as well as by directly comparing a model protein breakthrough curve obtained with the SDD - HTS setup with that obtained using a benchtop system for Sartobind® S and Q MAs. Kinetic experiments regarding the residence time were conducted with IgG monomer and its HMW binding capacity at different velocities. The dyeing experiments were employed for qualitative fluid dynamic analyses and performed by injecting either 1 mL or 4 mL 0.1-1g/L of coomassie blue dye in 10 mM KPi HCl buffer at a velocity of 500  $\mu\text{L/s}$  into each SDD at a level that would only partially dye the available membrane volume. Afterwards, the respective SDD was dismantled and the distribution of dye on the consecutive membrane layers was optically analyzed. The color pattern on the membrane layers indicated the fluid flow and thus the quality of the fluid distribution within the device and throughout the membrane layers of the membrane bed. The residence time influence was investigated by injection of a 3 g/L IgG feed solution with 8% HMW in 10mM KPi at pH 5 in an injection volume of 1 mL to 4 mL at a velocity of 100 and 500  $\mu\text{L/s}$ . The 3% to 5% acetone in 10mM KPi buffer tracer and the 2 g/L lysozyme in 10 mM KPi buffer protein breakthrough curve experiments were carried out with the respective SDD - HTS setup shown in Figure 3.2 A at a velocity of 500  $\mu\text{L/s}$  an injection volume of 0.5 mL to 2 mL. For direct continuous on-line measurement of the resulting concentration profiles, a prototype UV flow cell was connected by a luer lock fitting and a 0.75 mm inner diameter capillary to the downstream port of the scale-down model. The raw data of the HTS UV flow cell signal was corrected by the pipetting time and smoothed by a mean average and a window size of 60 points using origin® 2018b software. The resulting data was differentiated, simulated by the modified Gaussian function, and finally compared with the respective LC experiments. The lab scale LC experiments were conducted with the SDD using the same solutions on an Äkta™ Explorer benchtop system at 5 MV/min and allowed a direct comparison between the two setups employed.

## 3.2 Material and Methods

### 3.2.6 Case study 1: High throughput screening - Bind and elute mode

The BE mode provides process parameter information, such as the dynamic breakthrough concentration profile, binding capacities and resulting process map. Applying the BE mode allows rapid determination of dynamic  $q_{1/10\%}$  and static binding capacity  $q_m$  for a range of salt concentrations and pH values. Assuming that the calculated IgG monomer and dimer binding capacity of every salt step also applies to the FT mode, this results in a corresponding FT process map. The MA is loaded to saturation, followed by wash steps and several elution steps with conductivity increasing in steps, as shown in Figure 3.3.

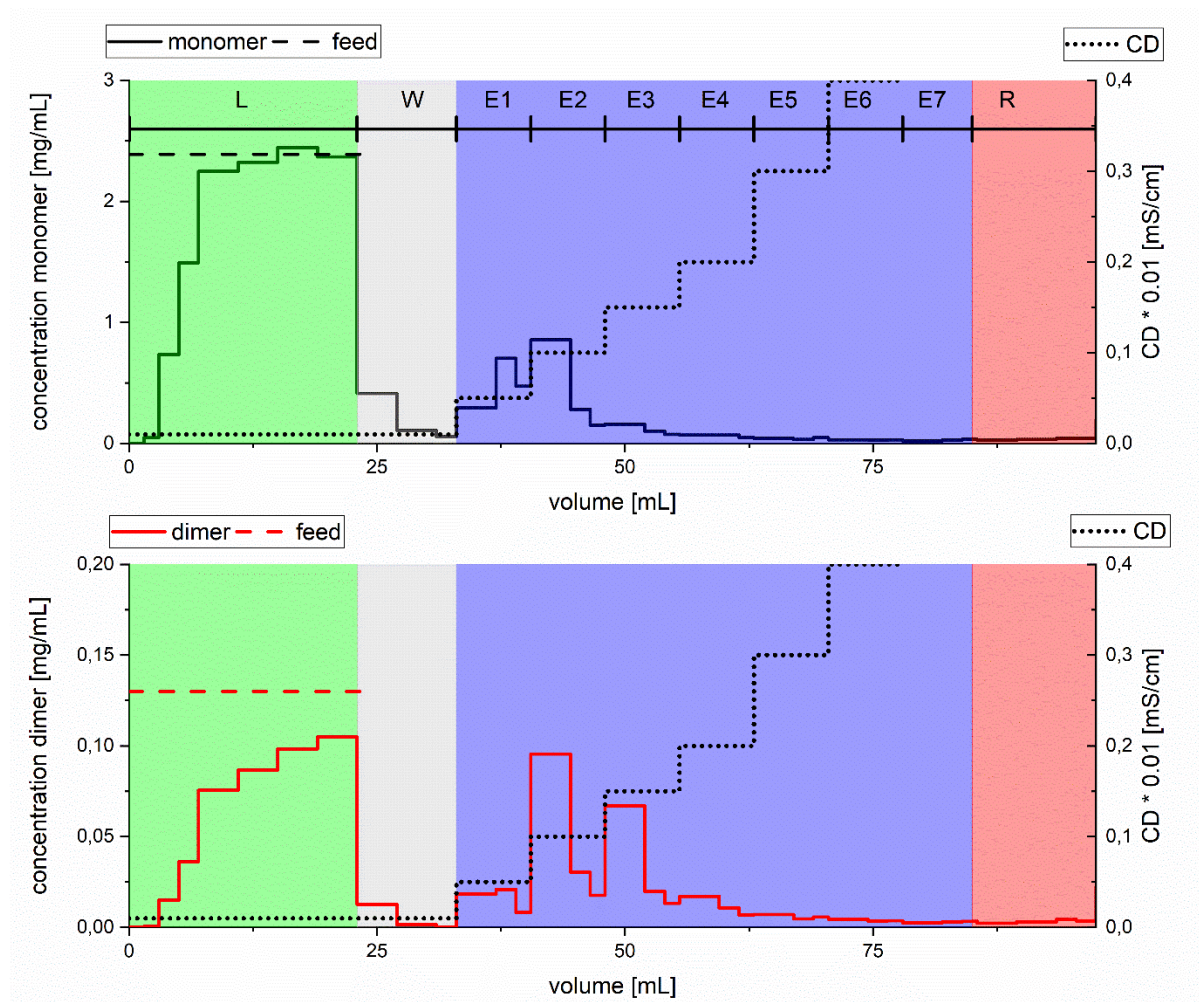


Figure 3.3: Example of the BE SDD-HTS approach and experimental results for Sartobind® S. Color-coding of the steps: green for loading steps L, gray for wash steps W, blue for elution steps E, and red for regeneration step R. The top fraction concentration profile shows IgG monomer and the bottom fraction concentration profile IgG dimer. BE, bind and elute; HTS, high throughput screening; SDD, scale-down device.

The single SDD of the SDD - HTS setup is equilibrated with the respective buffer system containing no additional salt to cover different pH values and then loaded in steps with protein containing feed solution as shown in Figure 3.3 (green-colored area). During the loading phase used for breakthrough curve determination, aliquots of 1 mL, 1.5 mL and 2 mL were pumped through the device for each liquid-dispensing step until 80 % of the expected maximum binding capacity is reached. For the remaining 20%, the aliquot volume applied was then increased to 2 mL, 3 mL, or 4 mL. After a wash

with at least 8 mL, the MA was sequentially eluted using elution buffers with a conductivity increasing in steps from 2 mS/cm to 45 mS/cm and with a maximum dispensed volume of 14 mL in 2 mL or 4 mL steps, as shown in Figure 3.3 (blue-colored area). Subsequently, the MA is regenerated with at least 80 mS/cm and re-equilibrated with equilibration buffer and washed using storage buffer, with a volume of 14 mL in 4 mL steps for each phase. Every pipetting step represents an individual fraction that is collected in a separate well of the movable well plate. Afterwards, 500  $\mu$ L of each fraction is drawn automatically from each well by the robotic HTS system and analyzed for mAb concentration via SEC. The parameters of binding capacity and selectivity for each salt step are determined by totaling the data obtained for all subsequent elution fractions. Assuming that the determined IgG dimer selectivity, calculated from binding capacity, also holds true for the MA FT mode, the screening procedure will automatically generate a respective FT process map.

In order to validate the results obtained, LC experiments were carried out with an Äkta™ Explorer with MA prototype lab-scale devices with a bed volume of 4.5 mL and a diameter of 2.8 cm at pH 8.8, 9.5 and 10 and at a CD of 8.8 mS/cm, 12 mS/cm, and 14 mS/cm, respectively. The volumetric flow rate was 13.5 mL/min, and 5 mL and 10 mL fractions were collected and analyzed using SEC.

### 3.2.6.1 Mass balance

In order to assess the experimental results, the resulting mass balance for each run was calculated according to Eq. (3.1). Here, index  $i$  is the observed component in the pipetting step. The deviation  $D$  is determined by the ratio of loaded feed mass to the accumulated mass determined in eluate, wash, and elution step in Eq. (3.2).

$$0 = m_{Loading,i} - \sum_{k=1}^n m_{k,i} \quad (3.1)$$

$$D_i = \frac{m_{Loading,i}}{\sum_{k=1}^n m_{k,i}} \quad (3.2)$$

### 3.2.6.2 Binding capacity and selectivity

The HTS results yield the static binding capacities for process maps. The maximum binding capacity at the initial CD at a given pH is calculated by Eq. (3.3) and Eq. (3.4). In Eq. (3.3), the difference between the loaded and the accumulated mass in the flow-through fraction mass of each component equals the static binding capacity. Likewise, the sum of the mass elution fraction is used to determine the static binding capacity. Both procedures should lead to the same results and indicate a closed mass balance. The HTS – SDD approach also includes several elution salt steps, which are generally used for process maps. Static binding capacity at a given pH and as a function of CD is determined by the sum of component eluate masses including the elution fraction.

$$q_{MaxLoad,i} = \frac{1}{V_{MA}} \cdot \left( c_{Feed} \cdot V_{Feed} - \sum_{k=1}^l \sum_{i=1}^n c_{i,k} \cdot V_k \right) \quad (3.3)$$

$$q_{MaxElu,i,k} = \frac{1}{V_{MA}} \cdot \sum_{k=1}^l \sum_{i=1}^n c_{i,k} \cdot V_k \quad (3.4)$$

Selectivity is calculated by the ratio of the bound dimer mass and bound monomer mass in elution step  $i$  in Eq. (3.5). Besides selectivity, product recovery is a parameter of interest for PD, which is calculated by Eq. (3.6).

$$Selectivity_i = \frac{m_{Dimer,i}}{m_{Monomer,i}} \quad (3.5)$$

$$Recovery_i = \frac{m_i}{m_{MA,i}} \quad (3.6)$$

### 3.2.7 Case study 2: Scale-down device and mechanistic modeling

For early or integrated PD, a simulative interpretation of data reduces the experimental effort and enables the integration of process step interactions. In addition, the main disadvantages of the SDD involving an unsteady and intermittent flow pattern, several injections and mixed concentration due to fractionations are corrected. During this study, we thus applied a simplified MA model to describe the screening results and enable SDD - MM investigations as illustrated in Figure 3.2 C).

#### 3.2.7.1 System characterization

The performance of the SDD - HTS is described by two equilibrium models; the second model represents the respective membranes and the first model all other parts of the SDD - HTS setup. The void volume of the membrane layers with 0.42 mL is known, and the total column porosity  $\varepsilon_{Total}$  in Eq. (3.7) is determined in a breakthrough tracer experiment performed with 3% to 5% acetone in 10 mM KPi buffer using a benchtop system. The retention volume is corrected by the previously determined void volume, calculated by the first derivative of the acetone breakthrough curve. The axial dispersion of models one and two are estimated as well as the void volume of model one. The void volume and axial dispersion of the SDD is described by an error-minimized axial dispersion coefficient based on the benchtop experiment. Therefore, the SDD - HTS setup with a UV flow cell is used to apply 3% acetone in 10 mM KPi tracer in ten 1 mL steps.

$$\varepsilon_{Total} = \frac{V_{Tracer}}{V_{MA}} \quad (3.7)$$

#### 3.2.7.2 | Batch isotherm

Batch isotherms for lysozyme and BSA are determined for Sartobind® S and Sartobind® Q. The MA stamp with a 2 cm diameter is equilibrated in buffer solution, wiped with tissue, and transferred with the respective feed solution to a 12-well plate. The Sartobind® Q 4 mL feed solutions with concentrations of 3, 1.5, 0.75, 0.5, 0.4, 0.3, 0.2 and 0.1 g/L BSA were prepared in KPi buffer with a pH of 7.0 at 0.01, 0.06 and 0.16 M NaCl concentrations. The Sartobind® S isotherm was determined by using lysozyme in the same feed concentration, amount, and salt concentration, but with a pH value 7.2 and the buffer system KPi. The solution was equilibrated over at least 10 h, preferably overnight, in an enclosed 12-well plate. Afterwards, the MA is isolated, wiped again and transferred in a new well plate with 4 mL of wash solution. Elution was performed with 4 mL of 1 M NaCl. The binding capacity of each component  $q_{MA,i}$  is calculated using Eq. (3.8). Where the binding capacity equals the mass differences between feed  $m_{Feed,i}$  and equilibration  $m_{Equilibration,i}$  is divided by the chromatographically active volume which is determined by membrane volume  $V_{MA}$  times one minus the membrane porosity  $\varepsilon$  in.

$$q_{MA,i} = \frac{m_{Feed,i} - m_{Equilibration,i}}{V_{MA} \cdot (1 - \varepsilon_{Total})} \quad (3.8)$$

### 3.2.7.3 | Ionic capacity

The ionic capacity is determined using a lab-scale device with a 0.42 mL ( $V_{MA}$ ) bed volume. The MA is preconditioned for 10 MV with 1 M NaOH. Subsequently, equilibration is carried out with water for injection and titrated with 10 mM HCl. Afterwards, the MA is washed with water for injection and the titration procedure is repeated. In Eq. (3.9), the difference between the resulting CD areas is used to calculate the amount of titration substance used.

$$\Lambda = \frac{\int c_{Titration,liquid,2} \cdot \partial V_{Titration,liquid,2}}{V_{MA} \cdot (1 - \varepsilon)} - \frac{\int c_{Titration,liquid,1} \cdot \partial V_{Titration,liquid,1}}{V_{MA} \cdot (1 - \varepsilon)} \quad (3.9)$$

### 3.2.7.4 SMA parameter determination

Eq. (3.10) to Eq. (3.12) show the ionic capacity in dependence on the steric factor  $\sigma$ , characteristic charge  $\nu$  and binding capacity of counter ions  $q_1$  as well as the binding capacity  $\bar{q}$  of the components  $q_i$ . For a rapid equilibrium or in equilibrium state, the SMA isotherm can be expressed as shown in Eq. (3.13).

$$\Lambda = q_1 + \sum_{i=2}^{n+1} (\nu_i + \sigma_i) q_i \quad (3.10)$$

$$\Lambda = q_1 + \sum_{i=2}^{n+1} \nu_i \cdot q_i \quad (3.11)$$

$$\bar{q} = q_1 - \sum_{i=2}^{n+1} \sigma_i \cdot q_i \quad (3.12)$$

$$c_{eq,i} = \frac{q_i}{k_{eq}} \cdot \left( \frac{c_1}{\Lambda - \sum_{i=2}^{n+1} (\nu_i + \sigma_i) q_i} \right)^\nu \quad (3.13)$$

The charge and equilibrium constant are determined by the curve evaluation of  $\log k$  using Eq. (3.14) and Eq. (3.15). Using a linear regression of logarithmic capacity factor over the logarithmic salt concentration results in the charge  $\nu$  and equilibrium  $k_{eq}$  constant by slope and intercept. Multi-components were adjusted by error minimization, using the one component result as the initial value.

$$K = \frac{1 - \varepsilon}{\varepsilon} \cdot \left( \frac{q_i}{c_i} \right) \quad (3.14)$$

$$\log k' = \log \left( \frac{1 - \varepsilon}{\varepsilon} \cdot k_{eq,1,i} \cdot \Lambda^{\nu_i} \right) - \nu_i \cdot \log(c_1) \quad (3.15)$$

### 3.2.7.5 Equilibrium-dispersive model

MAs are known for their high mass transfer rate. Assuming negligible mass transport effects, the equilibrium-dispersive model is used in Eq. (3.16) and Eq. (3.17). The kinetic constant  $k_{kin}$  describes the adsorption and desorption processes.

$$\frac{\partial c_i}{\partial t} = -u_{int} \cdot \frac{\partial c_i}{\partial x} + D_{ax} \cdot \frac{\partial^2 c_i}{\partial x^2} - \frac{1 - \varepsilon}{\varepsilon} \cdot \frac{\partial q_i}{\partial t} \quad (3.16)$$

$$k_{Kin,i} \cdot \frac{\partial q_i}{\partial t} = k_{Eq,i} \cdot \left( \Lambda - \sum_{i=2}^{n+1} (v_i + \sigma_i) q_i \right) \cdot c_{P,i} - c_{p,1}^{v_i} \cdot q_i \quad (3.17)$$

#### 3.2.8 Case study 3: scale-up

The SDD experiments result in a range of applicable process parameters. The ability to transfer this information to a larger scale has been investigated by two approaches: a) SDD direct parameter transfer by applying a scale factor, b) mechanistic modeling(SDD – MM).

##### 3.2.8.1 Direct scale factor

The scale dependency of the HTS data is investigated in scale-up experiments using Sartobind® Q and S using the breakthrough curves obtained. The study is carried out using the 0.42 mL SDD and based on the comparability of the 10% dynamic breakthrough capacity (DBC). HTS data is interpolated to predict the DBC independently of the fraction volume. Afterwards, the scale factor  $\Gamma$  is calculated using Eq. (3.18). The scale-up volume  $V_{DBC10,\Gamma}$  is calculated using Eq. (3.19), considering the feed concentration and MA volume.

$$\Gamma = \frac{V_{DBC10}}{V_{MA,lab\ device}} \cdot c_{Feed} \quad (3.18)$$

$$V_{DBC10,\Gamma} = V_{MA,\Gamma} \cdot \frac{\Gamma}{c_{Feed}} \quad (3.19)$$

Lysozyme, BSA and IgG solutions were used to investigate scale dependency from 0.42 mL SDD to lab and production scale with 4.7 mL, 8.3 mL, and 800 mL. In this study, a protein solution with 2.3 g/L BSA containing 4.2% HMW, was used to scale the SDD results from lab to production scale with a maximum scale factor of over 1900. For IgG and lysozyme, the SDD results were scaled up to a lab device using a scale factor of 10. The experimental conditions for scale-up investigations with lysozyme were 2.8 g/L and for IgG the following: a monomer of 2.7 g/L, aggregates of 0.15 g/L at a pH 6.5; a monomer of 6.8 g/L, aggregates of 0.67 g/L at a pH 8.8 and a monomer of 5 g/L, aggregates of 0.66 g/L at a pH 9. Flow rates were 10.5 and 22 mL/min.

##### 3.2.8.2 Mechanistic modeling (SDD – MM)

The transferability and scalability of the SDD by a mechanistic model was tested using at Sartobind® S and Q. The solutions used were the same as for the direct scale factor. The investigations were performed in single-component and multi-component simulations. Therefore, bind and elute experiments were carried out with lysozyme on Sartobind® S and BSA and its HMW on Sartobind® Q. The lab scale MA device prototype used consisted of a 4.7 mL bed volume. The MA device prototype was designed to have an axial flow path through 30 membrane layers. Therefore, the membranes were stacked between a comparable SDD - HTS fluid distributor and sealed with silicone. The volumetric flow used for lysozyme was 14 mL/min and for BSA 22 mL/min.

### 3.3 Result and Discussion

#### 3.3.1 SDD – experimental setup

Data validity of an SDD is a critical part of any screening procedure during PD. For parameter estimation and scalability, the SDD needs to display all key effects of a large-scale device. This prerequisite also enables parameters to be determined for simulative model development. In the course of SDD development we thus investigated: a) robotic parameters, b) SDD fluid distributor, c) comparability experiments with a UV flow cell direct after the SDD and d) chromatography performance.

##### 3.3.1.1 SDD fluid distributor

Qualitative fluid dynamic dyeing experiments were used to optimize the SDD. In this study we injected 1 mL 10 mM KPi pH 7 containing 0.1 – 1 g/L Coomassie brilliant blue with 0 - 0.2 M sodium chloride with 500  $\mu$ L/s in the SDD. Following this, the SDD is disassembled, and the membrane layers qualitatively visualized with a camera. The SDD fluid dynamic development is shown in Figure 4. Intermittent dyeing at the beginning of SDD development was improved with adding a support net and support fleece before and after the membrane layers in Optimization 1 (Figure 3.4). In the second optimization phase, the inconsistent dye dead areas could be avoided with an improved fluid distributor design. Based on the mass balance of a single elution step of Lysozyme with Sartobind® S, the improvement of the SDD is confirmed (data not shown).

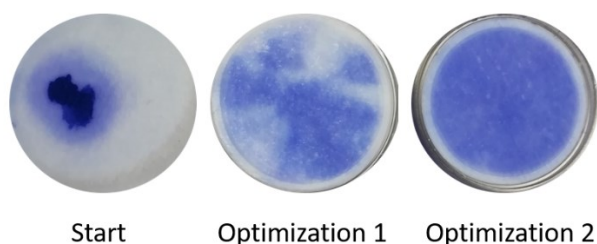


Figure 3.4: Exemplary SDD fluid distributor optimization progress. Experiments conducted by injections of dyed buffer solution at 0.2 M sodium chloride. SDD, scale-down device.

##### 3.3.1.2 Comparability experiments with a UV flow cell direct after the SDD

Additional fluid dynamic investigations were carried out by implementing an inline UV flow cell direct at the outlet of the SDD - HTS setup. Inline measurement enables the differences between SDD - HTS and LC fluid dynamics to be determined. The SDD - HTS setup with UV flow cell is used for 5 % acetone tracer and 2 g/L BSA breakthrough curves. Subsequent, the SDD without flow cell is then connected to a LC system equipped with a UV sensor at 280 nm wavelength detection and the experiments repeated, for acetone tracer experiments a 500  $\mu$ L injection volume was used. The HTS UV flow cell signal raw data is corrected by the dispensing and needle wash time and smoothed by mean average and a window size of 60 points with the software origin® 2018b. Comparing SDD - HTS with UV flow cell and LC experiments in Figure 3.5 A and B, based on the shown HTS – SDD data in Figure 3.5 C, shows the

### 3.3 Result and Discussion

deviations in half peak height, right peak width and left peak width of 3.9%, 5.9% and 17.7%, respectively. This indicates that disrupted fractionated chromatographic operation performed by robotic needles yields in comparable results to those of a continuous LC system, when keeping the fraction size during the HTS mode reasonably small to prevent mixing effects (data not shown).

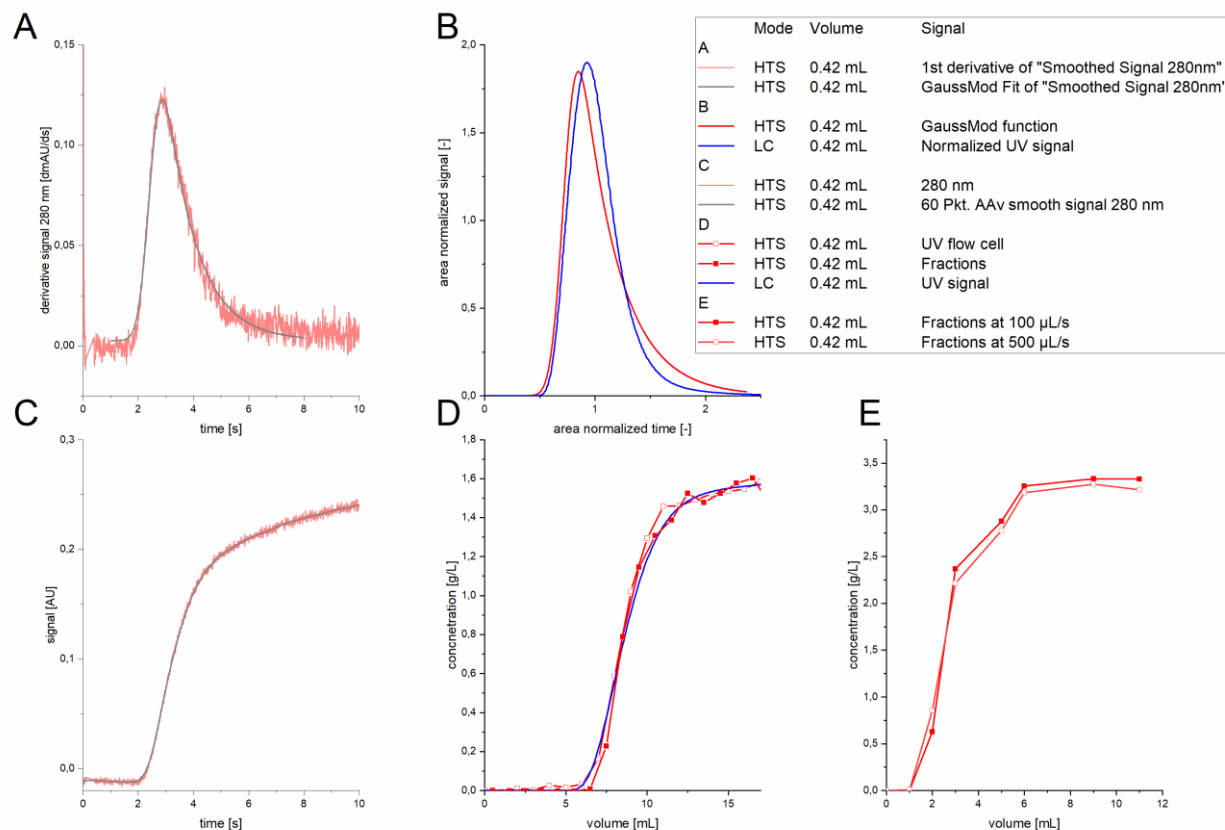


Figure 3.5: Comparison between SDD-HTS and benchtop system. SDD-HTS with UV flow cell and Sartobind® Q membrane, (a): Differentiated smoothed acetone step function, (b): Comparison of HTS-differentiated step function and acetone tracer of the same device with the benchtop system, (c): Sixty points smoothed acetone step function, (d): Comparison of HTS fractions, HTS with UV flow cell and benchtop concentration converted signal of BSA breakthrough curve, (e): IgG monomer breakthrough curves at different injection speeds for Sartobind®. BSA, bovine serum albumin; HTS, high throughput screening; SDD, scale-down device.

#### 3.3.1.3 Chromatographic performance

A direct comparison of the BSA breakthrough concentration between SDD - HTS and benchtop SDD setup illustrates the comparability in Figure 3.5 D. Residence time investigations were carried out by loading experiments at 100  $\mu$ L/s and 500  $\mu$ L/s, resulting in 0.8-seconds and 4-seconds residence time; at the dispensing speeds tested, no effect on binding capacity was determined for IgG and IgG HMW aggregates measured at 18.27, 18.92 mg/mL and 2.35, 2.79 mg/mL. The breakthrough concentration profile comparison shows only slight differences, which are depicted in Figure 3.5 E. Thus, at production scale, mass transfer restrictions do not limit adsorption, which is a boundary condition, considering the transferability of data from the SDD - HTS setup.

## 3.3.2 Case study 1: High throughput screening - bind and elute mode

The SDD - HTS BE mode comprises information of load capacity or product breakthrough and implicitly a process map. Applying the BE mode provides values for dynamic  $q_{1/10\%}$  and static binding capacity  $q_{Max}$  at a broad range of salt concentrations and pH values. HTS BE results are shown in Figure 3.6. For Sartobind® Q, the overall protein binding capacity increases as the pH rises. Figure 3.6 (A, B) displays only slight differences in IgG monomer and aggregate binding capacity. The CEX Sartobind® S results in Figure 3.6 (C, D) exhibit a high binding capacity at a wide pH range and salt concentration below 10 mS/cm. As the pH decreases, the overall binding capacity increases. Differences at a pH of 5 can be charge effects caused by the protein surface or the proximity to the pKa region of the ligand. Comparable to Sartobind Q, the binding capacity for dimers increases towards the isoelectric point of the monomer. The mass balance can be closed with a deviation of less than 10% for the IgG monomer and less than 35% for the IgG dimer.

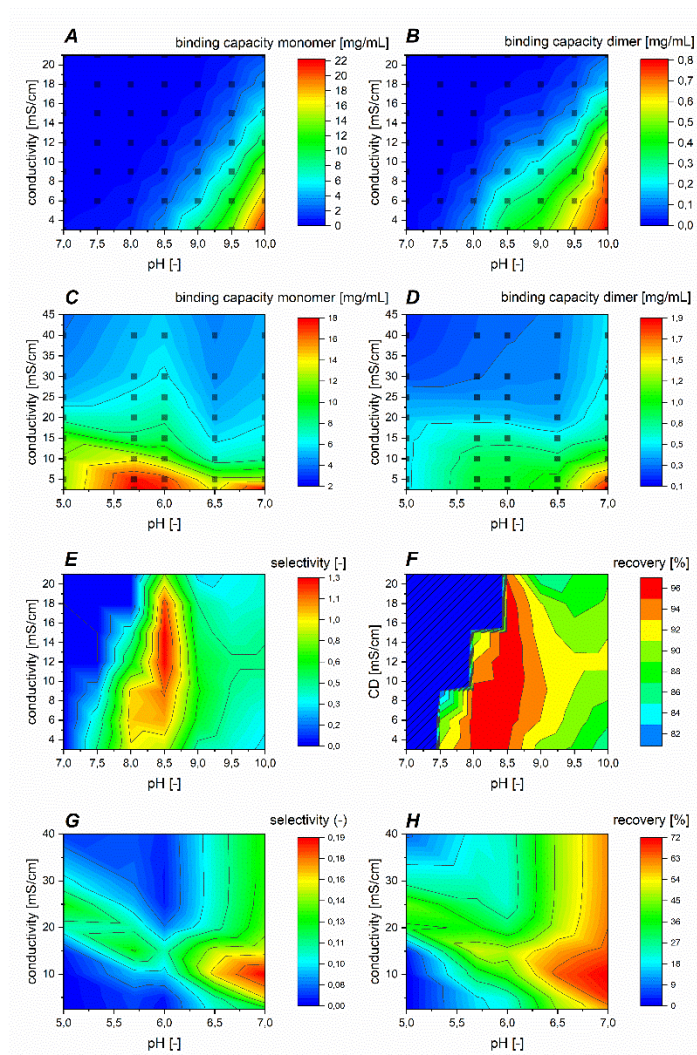


Figure 3.6: Response surface for IgG monomer and dimer binding capacity, selectivity, and recovery by Sartobind® Q (A, B, E, F) and Sartobind® S (C, D, G, H). Sartobind® S feed concentration and aggregate mass content for the different pH values was: pH 5.0, 2.7 g/L with 4.3%; pH 5.7, 2.7 g/L with 4.3%; pH 6.0, 2.8 g/L with 4.9%; pH 6.5, 2.7 g/L with 4.0%; and pH 7.0, 2.6 g/L with 5.8%. Sartobind® Q feed concentration and aggregate mass content for the different pH values was: pH 7, 5.0 g/L with 1.4%; pH 7.5, 4.9 g/L with 1.6%; pH 8, 4.5 g/L with 1.7%; pH 8.5, 4.9 g/L with 1.8%; pH 9, 5 g/L with 1.8%; pH 9.5, 5.0 g/L with 1.7%; and pH 10.0, 4.8 g/L with 1.5%. The color change from red to blue indicates decreasing values.

### 3.3 Result and Discussion

Selectivity of IgG aggregates for Sartobind® Q and S are shown in Figure 3.6 (E, G). The area of the highest binding selectivity for Sartobind® Q is in the pH range of 8.5 to 9.0 and a conductivity of 6 mS/cm to 18 mS/cm. The highest selectivity at pH 8.5 relies on the isoelectrical point of the IgG at 8.6-8.8. While the binding capacity for CEX chromatography material is low, the differences between the IgG monomer and IgG aggregates may be prominent. Sartobind® S reaches the highest selectivity at pH 5 to 6 in the range of 5 mS/cm to 15 mS/cm. Sartobind Q in Figure 3.6 (E) compared to Sartobind S in Figure 3.6 (G) enables higher maximum selectivity. The recovery of Sartobind® Q is more than 80% as shown in Figure 3.6 (F). This corresponds to a higher selectivity caused by the fact that more IgG monomer can flow through the MA without IgG dimer breaking through. Due to higher binding capacity of IgG monomer by Sartobind® S, the recovery in Figure 3.6 (H) without an additional elution step is below 80%. Overall, Sartobind® Q shows better selectivity and recovery than Sartobind® S for IgG dimer removal. However, for process management, the CEX could be favorable due to the ability to operate below the isoelectric point of the protein. Furthermore, the operation window shows a selectivity line at Figure 3.6 (G) over all pH values. The results obtained for selectivity and recovery of Sartobind® S in the overlapping region are comparable to the results of Vogg et al. for a 100 kDa monovalent antibody<sup>136</sup>.

LC experiments with MA devices of a 4.5 mL bed volume were carried out to determine the difference for HTS prediction. Recovery and selectivity of IgG monomer in Table 3.1 are in good agreement with the HTS results. The experimental deviation in recovery for HTS and LC is below 2%. For selectivity, the deviation in the HTS and LC results is below 20%. Hence, the results demonstrate the suitability of the HTS – SDD for determining process windows not only for FT applicability but also for scale transfer.

Table 3.1: Sartobind® Q HTS and LC comparison of recovery and selectivity at no aggregate breakthrough

pH [-]	Conductivity [mS/cm]	Recovery [%]		Selectivity [-]	
		HTS	LC	HTS	LC
8.8	12.0	97.8	95.0	0.94	0.99
9.5	9.8	81.3	81.3	0.45	0.31
10.0	9.5	72.8	72.4	0.47	0.33

#### 3.3.3 Case study 2: Scale-down device and mechanistic modeling

The SDD - HTS setup is affected by unsteady and intermittent flow pattern which reduces the comparability to benchtop or production runs.<sup>176</sup> The different fraction sizes, which are applied for optimal usage, and the usually higher velocities in the SDD - HTS setup could cause high deviations by kinetically limited components. Therefore, the simulation of lysozyme and BSA and its aggregates, their higher molecular weight (HMW) component, is used to investigate the capability of determining simulation parameter and the transferability of the SDD - HTS setup. The simulation takes unsteady flow into account by implementing the needle washing times as downtime with no flowrate. In an expanded simulation approach, the SDD - HTS setup results could be used to integrate different chromatographic operation modes. The equilibrium model parameters used are shown in Table 3.2.

Table 3.2: Model parameters for SDD - HTS setup and FT simulation

		SDD - HTS lysozyme Sartobind® S	FT lysozyme	SDD - HTS BSA Sartobind® Q	FT BSA
<b>Model 1</b>					
Length	[mm]	22	22	22	22
Volume	[mm <sup>3</sup> ]	0.76	0.51	0.76	0.51
$\varepsilon_{\text{Total}}$	[-]	1	1	1	1
$D_{\text{ax}}$	[mm <sup>2</sup> /s]	1.65	96.4	1.65	96.4
<b>Model 2</b>					
Length	[mm]	0.84	7.5	0.84	7.5
Volume	[mm <sup>3</sup> ]	0.42	4.66	0.42	4.66
$\varepsilon_{\text{Total}}$	[-]	0.75	0.75	0.75	0.75
$D_{\text{ax}}$	[mm <sup>2</sup> /s]	0.06	0.028	0.06	0.028
$\Lambda$	[M]	0.71	0.71	0.5	0.5

The parameters for models 1 and 2 are kept equal for both SDD - HTS and for the lab prototype simulations. These parameters were determined by batch isotherm experiments (Table 3.3). The kinetic parameter K is obtained by an error minimization fit using the ChromX® L2Error in the SDD - HTS setup simulation, the value can be found in Table 3.3.

Table 3.3: Model component parameters for SDD - HTS setup and FT simulation

		lysozyme	BSA	BSA HMW
K	[s]	0.1	1	1
$K_{\text{eq}}$	[-]	4.4	5.8	9.9
$\nu$	[M]	1.6	1.37	2.3
$\sigma$	[M]	42	132	486
$C_{\text{Feed,SDD - HTS}}$	[g/L]	2.6	2.4	0.1
$C_{\text{Feed,FT}}$	[g/L]	2.6	1.8	0.2

In Figure 3.7 the isotherm experimental data and SMA fit are presented for Sartobind® S with Lysozyme and Sartobind® Q with BSA and aggregates. The SMA fit represents the experimental data, while for BSA aggregates the saturation state was not measured. In respect to the case study the obtained SMA fit is considered adequate.

### 3.3 Result and Discussion

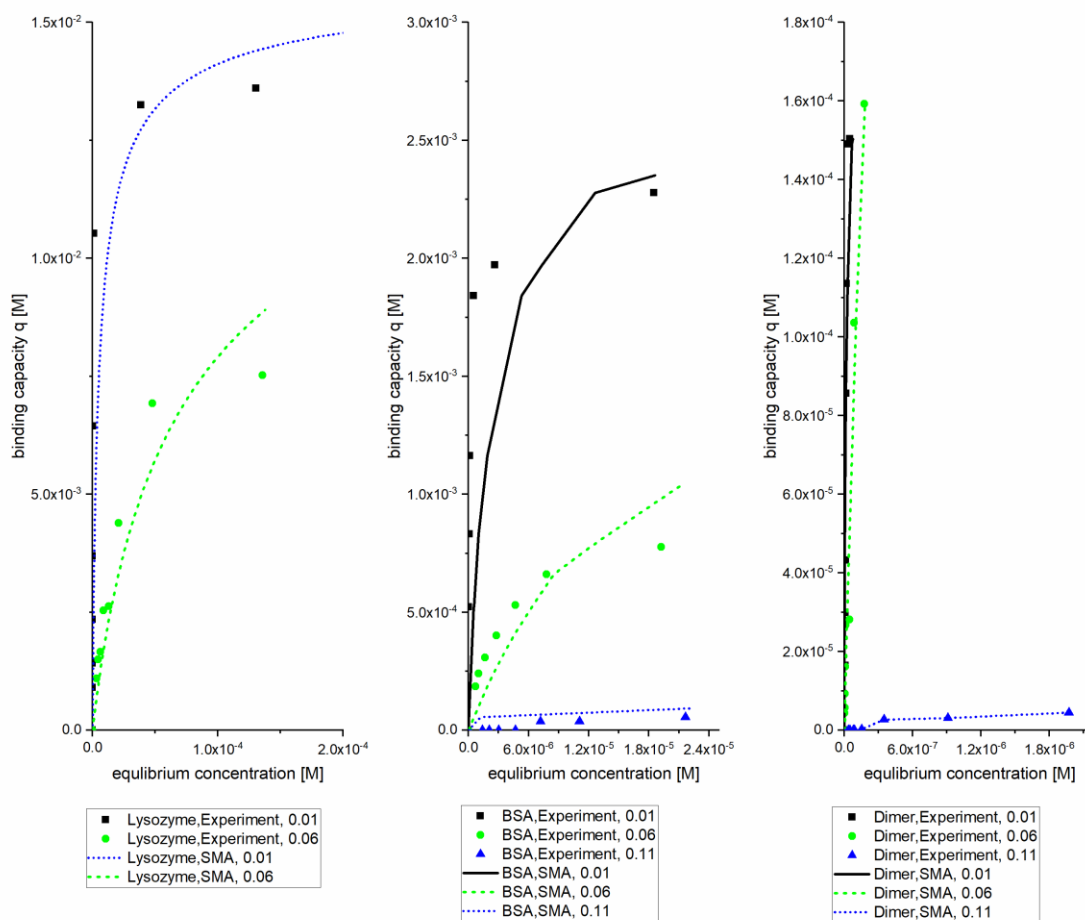


Figure 3.7: Experimental and SMA fit function comparison for Sartobind® S with Lysozyme and Sartobind® Q with BSA and BSA aggregates. BSA, bovine serum albumin; SMA, steric mass action model.

The SDD - HTS setup simulation for Sartobind® S using lysozyme is shown in Figure 3.8 A. For this experiment, the equilibration phase is followed by a loading phase, a subsequent wash phase and a one-step elution phase. The lysozyme breakthrough simulation is in good agreement with the experimental concentration profile. Due to time-based simulation, the concentration profile decreases when the flow stops. The disruptive flow describes the robotic needle wash after each injection. During breakthrough, the concentration profile mentioned is present until saturation is reached. The wash fraction at 40 mL is also in good agreement with the simulation. For the elution fraction, the simulation does not fully cover the two fractions. The simulation peak is sharper than the one obtained in the SDD - HTS setup experiment. This indicates an experimental deviation, e.g. mass overtake during fractionation, or a model deviation induced by a salt-dependent change in the hydrogel<sup>85,177-179</sup>, that collapses, or even a simulative abbreviation in fluid dynamics or thermodynamics. However, the SDD - MM simulation parameters in Table 3.4 show a deviation below 6% mass and are accordingly used for the benchtop prototype lab experiment in Figure 3.8 B. The prototype lab device bed volume is 10 times higher than in the SDD - HTS setup. Qualitatively, all simulations are comparable to the SDD - HTS setup, showing deviations in the elution peak.

Table 3.4: Comparison between SDD - HTS and SDD - MM

Parameter	Unit	Value for fraction until 19 mL	Value for fraction until 40 mL	Value for fraction until 56 mL
Mass HTS lysozyme	[mg]	30.1	81.5	103.8
Mass Simulation lysozyme	[mg]	28.4	80	102
Deviation	[%]	6	2	2
Mass HTS BSA	[mg]	31.4	44.8	47.7
Mass Simulation BSA	[mg]	35.4	49	49.1
Deviation	[%]	11	9	3
Mass HTS HMW	[mg]	0.47	1.02	2.27
Mass Simulation HMW	[mg]	0.3	0.7	2.2
Deviation	[%]	36	31	3

### 3.3 Result and Discussion

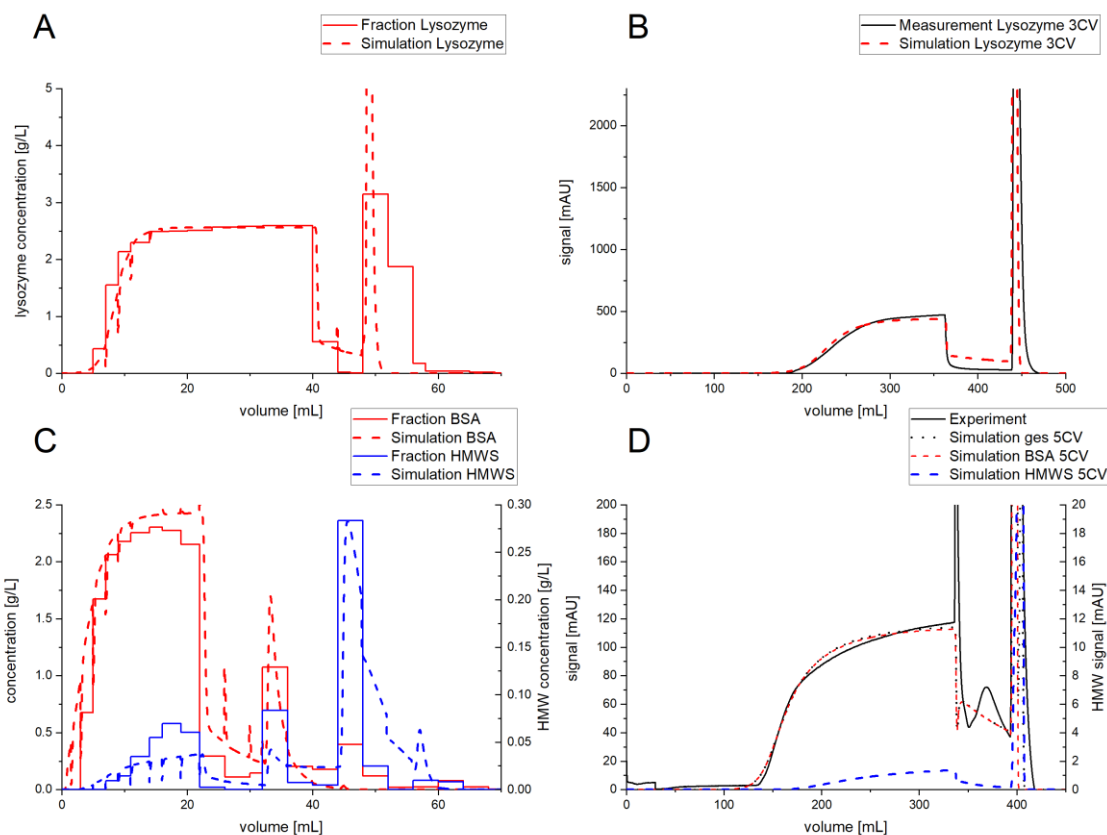


Figure 3.8: Comparison of SDD-HTS setup simulation and experiments as well as the corresponding FT experiments with a 10 times higher membrane volume. (a): Comparison of SDD-HTS setup experiments and simulation with lysozyme; (b): Comparison of FT experiments and simulation with lysozyme; (c): Comparison of SDD-HTS setup experiments and simulation with BSA and HMW; (d): Comparison of FT experiments and simulation with BSA and HMW. BSA, bovine serum albumin; FT, flow-through; HMW, higher molecular weight; HTS, high throughput screening; SDD, scale-down device.

For Sartobind® Q, the SDD - HTS setup for BSA and BSA aggregates (HMW) is investigated in Figure 3.8 C. In the experiment, the equilibration phase is followed by a loading phase and subsequent wash phase. Elution is performed as a three-step elution procedure with 0.1 M, 0.2 M and 0.3 M sodium chloride solutions followed by a 1 M sodium chloride regeneration phase. The simulated breakthrough concentration profile for BSA and HMW appears earlier than is seen in the experimental run. For the breakthrough concentration profile, the BSA-simulated concentration exceeds the experimental concentration, while the HMW concentration remains below the experimental concentration. A deviation in the measured feed composition could explain the mismatch. The simulation of the wash fraction is in good agreement with the experimental data. Overall, the elution concentration profile of BSA matches the first elution profile. In the second and third elution phases, the simulation is lower or no BSA concentration is observed. The simulation of the HMW concentration profile is in good agreement with the experimental results in all elution fractions but shows a deviation up to 37% in the mass (see Table 3.4). The deviations could indicate different HMW species. The elution profile in lab-scale experiments shows a double to triple peak at gradients above 10 column volumes. In each fraction of the different elution peaks, SEC shows BSA, which indicates charge variants (data not shown). Due to the lack of charge-variant information, this effect cannot be depicted in the simulation. Figure 3.8 D shows simulation and experimental data of the benchtop lab device. In general, simulation

and experimental data are in good agreement. However, the graphic does not show the experimental double peak, which is not depicted by the simulation results.

The simulated elution peak is always smaller than that observed in the experiment. A collapse of the MA hydrogel could be the cause for this observation. However, the simulation does always correctly indicate the breakthrough concentration, both in the SDD - HTS setup and in the benchtop lab experiment. The simulative study enables transfer from HTS to lab-scale and should also be applicable for pilot or production scale - resulting in early integrated PD. This case study is intended to close the gap between resin and MA chromatography PD. Within this study, state-of-the-art resin HTS setup and MM are implemented for MA. The MM will be investigated more precisely in further investigation which are not part of this study.

### 3.3.4 Case study 3: Scale-up

The different process design and transfer methods used in this co-study are a direct scale factor and the use of SDD - MM. Afterwards, a straightforward approach for a direct scale factor based on the separation of IgG monomer and HMW by Sartobind® S and Q will be discussed. Applying the direct scale factor to the SDD - HTS leads to a deviation of between 4% and 19% in Table 3.5. The experimental results are in an acceptable range for direct SDD – HTS scale-up and would be capable for the process by applying a 20% safety margin. The previous conclusions apply to a scale factor of 10; for production-scale experiments with BSA and Sartobind® Q a deviation of 12% was obtained (see Table 3.6).

Table 3.5: SDD - HTS IgG scale factor transferability

Parameter	Unit	Sartobind® S		Sartobind® Q		
		IgG	IgG	IgG HMW	IgG	IgG HMW
Component	[-]	6.5	8.8	8.8	9.0	9.0
pH	[-]	28	5.0	5.0	4.9	5.3
DBC experiment	[mL]	Lab	Lab	Lab	Lab	Lab
Device	[-]	26.9	4.2	4.1	4.1	4.7
Scaled estimated	[mL]	4	16	18	16	11
Deviation	[%]					

Considering the higher deviations for aggregates with the direct scale factor, a mechanistic model should be able to provide a more accurate prediction. The SDD – MM-based approach is further used to verify the feasibility of utilizing HTS data for modeling (Table 3.6). For all combinations considered, the SDD – MM-based approach shows a smaller deviation than that obtained using the direct scale factor at a scaling factor of 10. Breakthrough of lysozyme with Sartobind® S is predicted 3% earlier than achieved in the experiment.

Table 3.6: Comparison of SDD - HTS and SDD - MM scalability

Parameter	Unit	Sartobind® S			Sartobind® Q	
		lysozyme	lysozyme	lysozyme	BSA	BSA
Component		6	7	7	7	7
pH	[-]	122.9	79.9	11.8	11.8	11.8
DBC experiment	[mL]	Lab	Lab	Production	Production	Production
Device	[-]	Scaled	SDD - MM	Scaled	SDD - MM	Scaled
Type of prediction	[-]	115.2	126.1	91.0	76.1	10.4
Estimated volume	[mL]	6	-3	-14	5	12
Deviation	[%]					

#### 3.4 Conclusion

Three case studies were carried out with the aim of aligning HTS applications for MA with those of column chromatography. Therefore, a SDD - HTS setup was created, validated, and used for mAb aggregate removal. The dynamic SDD - HTS setup based on positive pressure was characterized in terms of robotic parameters. In the first case study, the BE mode was used to estimate a process parameter range, assuming that the decreased binding capacity at higher salt concentration also applies in an FT mode of operation. The BE mode results in a process map showing different pH values and salt concentrations. LC experiments confirmed the assumption that the binding capacity obtained in the elution steps of the SDD - HTS setup is transferable to FT processing. In a next step, the SDD - HTS data obtained was used for MM. This application led to a deeper understanding, enabling the experimental effort to be reduced. The analysis of SDD - HTS by MM and thus the determination of the fluid dynamics allows the HTS results to be transferred to benchtop experiments. The third case study demonstrated the transferability of the SDD - HTS experiments using a direct scale factor and an SDD – MM based approach. Both approaches show good applicability with a deviation below 20%. The dynamic SDD - HTS setup with comparable process behavior allows reliable scale-up from 0.42 mL to 800 mL. In contrast to the increased deviation of the direct scale factor for secondary components, the SDD - MM improved the precision of the experimental scale predictions for the observed data. A direct comparison between the two methods, direct scale factor and MM, would require a discussion of effort, accuracy and information content which is not in the scope of this study. However, the good agreement between simulation and experimental results, especially in the analysis of the breakthrough curve, enables integrated PD. The simulative approach permits observation of process deviation through process variation and increases the information content for process designing. In conclusion, the gap between HTS resin chromatography and MA was narrowed. Following the first step towards HTS harmonization, further investigations should follow with regard to the mechanistic model and transferability, thus improving the results. For aggregate removal, the SEC analysis time is the limiting factor and should be reduced by a UHPLC or DLS plate reader. Deviations in parameter determination could be reduced by smaller fraction volumes and/or usage of the directly implemented HTS UV detector flow cell.

#### 3.5 Acknowledgment

The authors wish to acknowledge the Membrane Chromatography & Modification team, especially Nicole Linne for robotic instructions and Patrick Adametz for the scale-up Sartobind® Q data set. Furthermore, we acknowledge Marek Hoehse and Alexander Graf from the Process Analytical Technologies group for analytical support, as well as Peter Polossek for construction engineering support and the Device Development for 3D printing support of the HTS scale-down model. Our thanks also go to the BioProcessing Group for providing the mAb feed solution. The authors also would like to acknowledge Tobias Hahn from GoSilico GmbH Karlsruhe for his helpful discussions and support in chromatographic simulations. In addition, we especially acknowledge the students Alexander Langsdorf and Lucy Nisser for their dedicated effort and excellent laboratory work.

Table 3.7: Abbreviations

Abbreviations	Meaning	Unit
AEX	Anion exchange chromatography	[-]
BE	Bind and elute	[-]
BSA	Bovine serum albumin	[-]
CD	Conductivity	[-]
CEX	Cation exchange chromatography	[-]
CV	Column volume	[-]
DBC	dynamic breakthrough capacity	[-]
FD	Fluid distributor	[-]
FT	Flow-through	[-]
HMW	Higher molecular weight molecules	[-]
HTS	High throughput screening	[-]
IEX	Ion exchange chromatography	[-]
IgG	Immunoglobulin G	[-]
LC	Liquid chromatography	[-]
MA	Membrane adsorber	[-]
mAb	Monoclonal antibody	[-]
MM	Mechanistic modeling	[-]
MV	Membrane volume	[-]
SDD	Scale-down device	[-]
SDDs	Scale-down devices	[-]
SEC	Size exclusion chromatography	[-]
SMA	Steric mass action model	[-]

Table 3.8: Symbol

Abbreviations	Meaning	Unit
A	Area	[cm <sup>2</sup> ]
A <sub>1</sub>	Constant describing the concentration profile	[mg/mL]
A <sub>2</sub>	Constant describing the concentration profile	[mg/mL]
C <sub>i</sub> <sup>*</sup>	Concentration of component i	[mg/mL]
C <sub>Feed</sub>	Feed concentration	[M]
C <sub>i</sub>	Concentration of component i	[M]
C <sub>Norm</sub>	Feed-normalized concentration	[-]
D	Deviation	[%]
D <sub>ax</sub>	Axial dispersion coefficient	[mm <sup>2</sup> /s]
DI	Displacement identifier	[-]
k'	Capacity factor	[-]
K <sub>Eq</sub>	Equilibrium constant	[-]
k <sub>Kin</sub>	Kinetic constant	[s((M) <sup>y</sup> )]
K <sub>P</sub>	Partitioning coefficient	[-]
M	Molar mass	[g/mol]
m <sub>i,k</sub>	Mass of component <i>i</i> und fraction <i>k</i>	[mg]
MV	Membrane volume	[MV]

### 3.5 Acknowledgment

n	Control variable	[-]
q	Binding capacity	[M]
Q <sub>1</sub>	Salt-binding capacity, stationary phase salt concentration	[M]
Q <sub>m,Elu,i,k</sub>	Static binding capacity calculated by the eluted concentration for each elution fraction	[M]
Q <sub>m,Load,i</sub>	Static binding capacity calculated by the difference between loaded and unbound mass	[M]
Recovery	Recovery of MA	[-]
Selectivity	Selectivity/Utilization of MA	[-]
u	Velocity	[mm/s]
V	Volume	[mL]
x	Rate	[mm]
Γ	Scale factor	[-]
ε <sub>total</sub>	Total MA porosity	[-]
Λ	Ionic capacity	[M]
v	Characteristically charge	[-]
σ	Steric factor	[-]
$\bar{q}$	Binding capacity non hindered molecules	[M]

Table 3.9: Indices

Abbreviations	Meaning	Unit
i	Component	[-]
DBC <sub>10</sub>	Value at 10% dynamic breakthrough concentration	[-]
Dimer	IgG HMW	[-]
Eq	Value at equilibrium state	[-]
Int	Interstitial	[-]
j	Fraction	[-]
k	Fraction / dispensing step	[-]
Kin	Kinetic	[-]
Liquid	Identifier for the titration substance	[-]
MA	Membrane adsorber	[-]
Mas	Membrane adsorbers	
Monomer	IgG monomer	[-]
P	Pore	[-]
Titration	Value obtained due to titration	[-]
Total	Overall value	[-]
Γ	Scale factor, value corresponding to scale level	[-]

## 4 PD exploiting competitive adsorption-based displacement effects in monoclonal antibody aggregate removal - a new high throughput screening procedure for membrane chromatography

Dominik Stein<sup>1,2</sup>, Volkmar Thom<sup>2</sup>, Jürgen Hubbuch<sup>1</sup>

<sup>1</sup> Karlsruhe Institute of Technology (KIT), Institute of Process Engineering in Life Sciences, Section IV: Biomolecular Separation Engineering, Karlsruhe, Germany

<sup>2</sup> Sartorius Stedim Biotech GmbH, August-Spindler-Str. 11, D-37079 Goettingen

### Abstract

High throughput screening (HTS) approaches are commonly used to accelerate downstream PD. While most HTS approaches use batch isothermal data ( $K_p$  screen) or bind and elute mode as screening procedure, different or new process designs are rarely investigated. In this paper a mechanistic model case study for the separation of two different two-component solutions was conducted and confirmed prior evidence. With these outcomes, a novel HTS screening procedure was developed including the determination of competitive adsorption-based displacement effects and key parameter identification. The screening procedure employing an overload bind and elute mode (OBE) is presented in a case study dealing with IgG aggregate removal in a typical monoclonal antibody purification step, applying a Sartobind<sup>®</sup> S membrane adsorber (MA). Based on a MA scale-down device, the OBE mode allows the determination of classical process parameters and dynamic effects, such as displacement effects. Competitive adsorption-based displacement effects are visualized by introducing a displacement identifier (DI) leading to a displacement process map. Based on this map, the approach is transferred to and confirmed by the OBE recycle experiments with 4.6 mL and 8.2 mL benchtop scale devices resulting in 45 % reduced IgG monomer and 88 % increased HMWS binding capacities.

### 4.1 Introduction

Downstream PD faces increasing diversity of therapeutic modalities, shortened timelines, high cost, and limited availability of the target entity.<sup>35,180</sup> With regard to the classic purification process, the chromatographic PD is challenged by the following aspects: a) abundance of different ligands, b) different stationary phase, c) a range of potential process parameters, and d) new process designs resulting in a high experimental effort.<sup>36,180</sup> High throughput screening (HTS) on robotic platforms typically addresses the challenges posed by the abundance of the different ligands and a range of possible process parameters. These platforms are established PD tools and allow parallel, automated, and standardized workflows. Scale-down devices (SDDs) operated in a HTS regime accelerate PD efforts and workflow at reduced material consumption.<sup>36-39</sup> Beside model assisted scale transfer publications<sup>35,39,56,58,168</sup>, investigations of HTS are usually limited to batch isotherm determination and/or  $K_p$  screenings. In addition, studies on HTS membrane chromatography applications are rarely found when compared to resin based HTS applications. These limitations have been addressed earlier.<sup>181</sup> However, optimal PD, scale-up and novel process designs depend on the limitation of the screening method used.

## 4.1 Introduction

---

Displacement chromatography add a dedicated displacer which compete with at least one component and induce a partial elution and thus separation of the stationary phase bound components. In the case that the feed mixture itself exhibit competitive binding components and the product is displace from the stationary phase by the impurities a typical frontal chromatography (FC) mode is used.<sup>85,136</sup> The presented overload bind and elute (OBE) now follows the same principle as FC but consist of product binding and an additional elution step. Both process modes, FC and OBE mode apply higher mass loading beyond the dynamic breakthrough concentration.<sup>86,182,183</sup> Consequently, the application of components with similar binding properties and thus competitive adsorption-based in displacement effects occur. Thereby, FC and OBE overloading the stationary phase and thus increases its utilization and productivity.<sup>86,136,183,184</sup>

In the light of the above, given typical multi-component process streams competitive adsorption-based displacement effects can only be considered for PD if the screening method identifies those. Especially in separation tasks with closely similar molecules as monomer and aggregates such as higher molecular weight species (HMWS), OBE chromatography offers the advantage of an increased productivity avoiding the implementation of narrow cut points or extended gradients (i.e. pH value, conductivity) leading to product dilution.

For monoclonal antibodies (mAbs), aggregates in the final formulation pose a risk due to various influences on the activity and stability of the product.<sup>63,64</sup> In the established platform process for the purification of mAbs, the typical Protein A capture step is followed by one or two additional chromatographic purification steps.<sup>13,14</sup> High purity of active pharmaceutical ingredients are obtained by separating HCP, DNA, leached Protein A, viruses and HMWS aggregates in these chromatography steps. For the separation of mAbs and their HMWS, cation and hydrophobic interaction chromatography are established methods.<sup>13,14,185</sup> In addition, ceramic hydroxyapatite and mixed mode<sup>185,186</sup> chromatography are also used for the removal of aggregates<sup>14</sup>. The different chromatographic types for the reduction of HMWS can be applied in bind and elute, flow through, weak partitioning chromatography, FC or OBE.<sup>13,14,84-86</sup> When separating HMWS with a chromatographic mode that contains high salt concentration or varying pH values, the risk of new aggregate/HMWS formation during the step is highly probable.<sup>63,64</sup> Given the widely constant conditions, OBE chromatography offers the advantage of a stationary state with regard to salt load and pH value and should thus suppress new aggregate formation. The significant advantages of membrane adsorber (MA) over resin-based chromatographic processes when used for contaminant removal in FT mode<sup>166,187</sup> underline their application for OBE chromatography. In addition, the high mass transfer rates observed in MAs furthermore promote competitive binding-based displacement effects and maintain the typically high productivity. During the last decades several efforts in research and PD were carried out investigating competitive based displacement effects and its use.<sup>84-86,183,184,188-192</sup> However, currently no screening strategy exists to investigate potential displacement effects applying membrane chromatography on a robotic screening platform.

In this paper, we introduce a PD strategy for the determination of competitive binding-based displacement effects in monoclonal antibody aggregate removal. Initially, principles behind competitive binding-based displacement effects are investigated and verified by mechanistic modeling of two different two-component mixtures. Subsequently, a new robotic HTS screening procedure is developed and evaluated in the light of a novel process design. The newly developed robotic HTS screening procedure is applied for aggregate removal PD when processing mAbs. To illustrate its applicability towards PD using OBE chromatography, a Sartobind® S a cation exchange (CEX) MA is

investigated. Specifically, during the HTS OBE mode, the CEX MA is loaded until saturation, washed, and partially eluted in repeating cycles at stepwise increased salt concentrations. In addition, the method can be used to identify the potential presence of competitive binding-based displacement effects and predict the optimum process condition. The process parameter and displacement effects are confirmed with benchtop recycle experiments. In the recycling experiments, at least 60 times loading volume was passed twice over a Sartobind S MA and the displacement effects were analyzed with size exclusion chromatography (SEC) in the breakthrough. Finally, this processing mode is shown to elevate yield and enhances selectivity when comparing to a classical FT mode which is typically stopped at a HMWS product content below 1%.

### 4.2 Materials and Methods

#### 4.2.1 Materials

The applications for material used in this work can be divided into a) HTS and benchtop chromatographic experiments, b) benchtop recycle experiments, c) analytics, d) data handling, automation, and mechanistic modeling.

##### a) HTS and benchtop chromatographic experiments

The HTS is carried out with the HTS robot Lissy<sup>®</sup> 2002 GXXL/8P from Zinsser Analytic. FT and OBE chromatography experiments were performed using Äkta Prime<sup>™</sup> and Äkta<sup>™</sup> Explorer from Cytiva. The used MA devices were prototype set-ups, based on three flat sheet-stacked MAs with a diameter of 2.9 cm in a plastic housing, resulting in a liquid accessible diameter of 2.7 cm for the then 0.025 cm  $\pm$  0.003 cm bed height and 0.43 cm<sup>3</sup>  $\pm$  0.05 cm<sup>3</sup>. Cellstar<sup>®</sup> 12-wellplates from Greiner Bio-one International GmbH were used for the fractionation of the SDD - HTS. The buffer preparation is done by dissolving the buffer salts in purified water which is provided by an Arium<sup>®</sup> Water Purification System from Sartorius Stedim GmbH. The used salts were weighed with Sartorius Master<sup>pro</sup> LP 12000S balance or Sartorius Expert LE225D-OCE from Sartorius Stedim Biotech GmbH with the components: sodium chloride (NaCl), hydrochloric acid (HCl), glycine, sodium acetate (NaAc), acetic acid, dipotassium hydrogen phosphate, potassium dihydrogen phosphate, disodium hydrogen phosphate dihydrate and sodium di-hydrogen phosphate di-hydrate from Carl Roth, trisodium citrate di-hydrate and acetone from VWR chemicals, citric acid monohydrate from Alfa Aesar, ethanol from Sigma Aldrich. For pH value adjustment sodium hydroxide (NaOH) or hydrochloric acid (HCl) were used. Each buffer and load solution are pre-filtered with a 0.45  $\mu$ m Sartopure<sup>®</sup> and a 0.2  $\mu$ m Sartolab<sup>®</sup> RF vacuum filter from Sartorius Stedim Biotech GmbH. The CHO fermented monoclonal antibody is a Sartorius Stedim Biotech GmbH internal load solution. Further purification was done with a MabSelect<sup>™</sup> Sure<sup>™</sup> lab column (5 cm diameter, 192 mL volume) provided by Cytiva and an Äkta Prime<sup>™</sup> system. The eluate contained approximately 18 g/L mAb and a mAb aggregate level of approximately 0.5-2 %. Enrichment of the aggregate content of the clarified mAb solution to 2 % - 8 % is done with a pH shift. Aggregation with a temporary pH shift is a commonly used method for aggregation.<sup>64,174,193</sup> After diluting the 0.1 M pH  $\sim$ 3 glycine buffered mAb solution three times with KPi buffer, the pH value is adjusted to pH 3 with 0.5 M HCl or 0.5 M H<sub>3</sub>PO<sub>4</sub>. The aggregation time was set to 2 h with stirring at 150 rpm. Finally, the pH is readjusted to pH 7 with 0.5 M NaOH. Following this, the respective aggregated mAb solution is again purified with the protein A column fractionated in a pre-, high concentration and post fraction. The pre- and post-fractions of all chromatographic runs are pooled, and pH adjusted again loaded to the

## 4.2 Materials and Methods

---

protein A column. Resulting in pooled high concentration fraction solutions which exhibit mAb concentrations of up to 22 g/L. The final load solutions were prepared by diluting the high concentrated aggregated mAb solution with the respective buffer, with a minimum dilution ratio of one to three. Each dilution buffer at each pH value was prepared with 0 mol/L and 1 mol/L NaCl to achieve appropriate salt concentrations. The pH value and conductivity (CD) was adjusted by mixing the solution with the respective buffer followed by an incubation period of one hour at room temperature. In a pH range of 5 - 7, the feed solution was diluted to 1 g/L - 6 g/L with 0 M - 0.3 M NaCl concentration. The used load and buffer stock solution for the HTS screening are sodium acetate (pH range 5 - 5.5) and potassium phosphate (pH range 6 - 7).

### b) Benchtop recycle experiments

The benchtop OBE chromatography experiments in recycle mode were carried out with a mAb solution of 2 g/L - 6 g/L monomer and 2 % - 8 % HMWS in 20 mM sodium acetate buffer at pH 5 or 5.5 and a sodium chloride adjusted conductivity of 10 mS/cm and 18 mS/cm, respectively. The benchtop experiments were conducted applying a MA in a silicon housing stabilized with a plastic jacket with 20 or 40 stacked flat sheet Sartobind® S membranes resulting in a bed volume of 4.6 mL ± 0.2 mL and 8.4 mL ± 0.3 mL, respectively.

### c) Analytics

Overall protein concentration was measured at 280 nm wavelength with a VivaSpec® UV reader from Sartorius Stedim Biotech GmbH. The IgG and its HMWS concentration were measured with a Yarra™ 3 µm SEC 3000 column of 300 x 7.8 mm from Phenomenex using Dionex™ UltiMate™ 3000 HPLC System from Thermo Scientific™ at a flowrate of 1 mL/min.

### d) Data handling, automation, and mechanistic modeling

The HTS method automation was done with WinLissy (version 7) from Zinsser Analytic. UNICORN® from Cytiva was used for FT experiment recipe writing. The IgG and its HMWS concentration were quantified with the Chromeleon™ 6.80 from Dionex. Experimental results evaluation and chromatographic data analysis was done with Origin® 2018b from OriginLab Corporation. Mechanistic modeling was done with ChromX™ provided by GoSilico GmbH.

## 4.2.2 Methods

A full list of abbreviations, symbols and indexes used throughout this work is presented at the end of this manuscript.

### 4.2.2.1 Scale-down device – experimental set - up

Each SDD contains a membrane bed consisting of 3 flat sheet membrane discs with 27 mm diameter and 240 µm to 280 µm thickness resulting in a bed volume of 0.41 mL to 0.48 mL, respectively, as illustrated in Figure 4.1 A. A Sartobind® S membrane with a mean pore diameter of 3 µm - 5 µm and a ligand density of 2 µeq/cm<sup>2</sup> - 5 µeq/cm<sup>2</sup> is used in this work. Each SDD exhibits a septum port, through which a robotic needle can penetrate to inject solution with a positive pressure into the device. To test

and assess the targeted average pipetted volume accuracy of less than  $\pm 3\%$  for an injection velocity of  $500\ \mu\text{L/s}$ , a volume calibration routine to reduce the deviation between set and measured dispensed volume was established using  $200\ \mu\text{L}$ ,  $400\ \mu\text{L}$ ,  $800\ \mu\text{L}$ ,  $1500\ \mu\text{L}$ ,  $2500\ \mu\text{L}$  and  $4000\ \mu\text{L}$  water in triplicate for each needle prior to each experiment. In case the targeted accuracy could not be reached, the volume correction factors of the robotic system are adjusted in the HTS robotic software. The HTS set-up comprises eight SDDs fixed on a holder plate to be operated in a parallel fashion, see Figure 4.1 B. Below the SDD holder plate, four movable 12 well plates collect the fractions of the eight devices where each well can hold a maximum of 5 mL solution and complete the SDD - HTS.

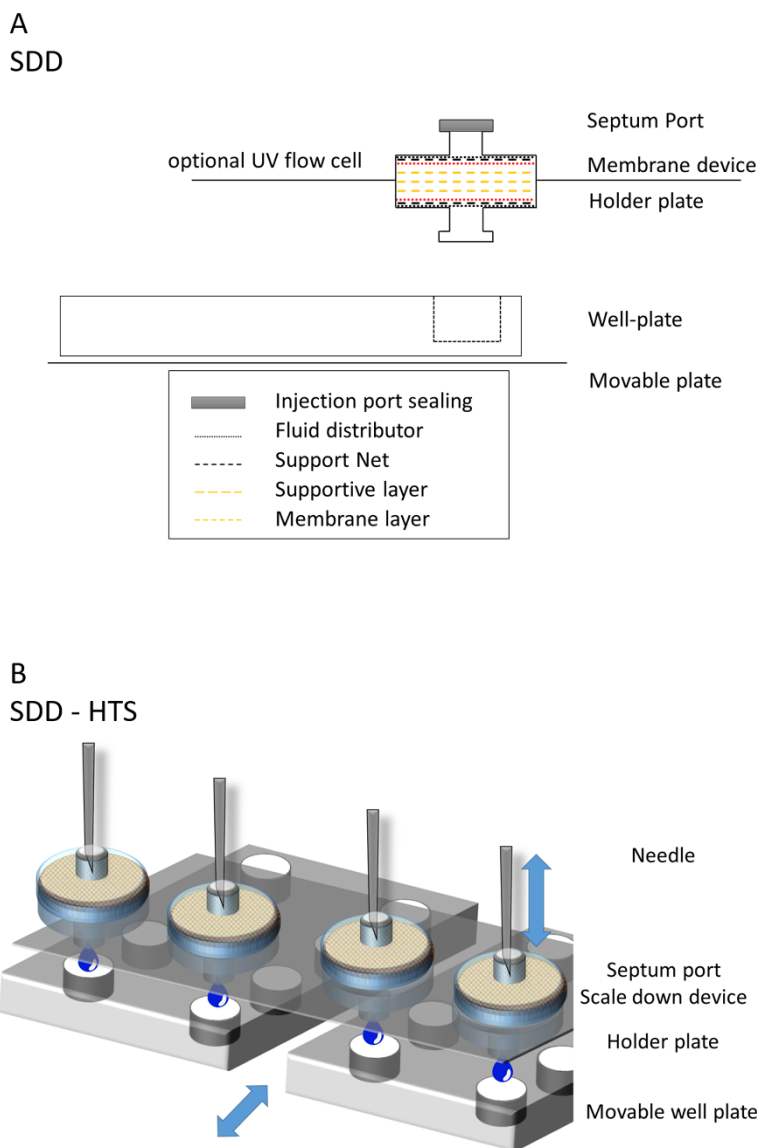


Figure 4.1: (A) SDD setup in which the liquid passes a fluid distributor followed by a support net and the three membrane layers, (B) SDD-HTS setup: needle injects the liquid through the septum port into the SDD, which is fixed to a holder plate. The holder plate holds eight membrane devices. Four movable well plates are used for the fractionation while each well plate collects the fraction for two membrane devices

### 4.2.2.2 Competitive adsorption-based displacement - delta interaction strength

Displacement effects have been exhaustively investigated by several researcher as e.g. the Steven Cramer group<sup>84,130-132</sup>, among others as Georges Guichon group<sup>133-135</sup> and Massimo Morbidelli group<sup>136-138</sup>. In displacement chromatography, components of a mixture, which is bound to the stationary phase, are selectively eluted by applying specific displacer. Selection and characterization of a possible displacer can be achieved calculating the separation factor  $\alpha$  in Eq. (4.1) based on the dynamic affinities  $\lambda$  calculated in Eq. (4.2) derived by the steric mass action isotherm (SMA) model in Eq. (4.3).

$$\alpha = \frac{\lambda_i}{\lambda_j} \quad (4.1)$$

$$\lambda_i = \left( \frac{K_i}{\frac{q_{Displacer}}{c_{Displacer}}} \right)^{\frac{1}{v_i}} \quad (4.2)$$

$$c_{eq,i} = \frac{q_i}{K_{eq,i}} \cdot \left( \frac{c_s}{\Lambda - \sum_{j=1}^n (\sigma_j + v_j) \cdot q_j} \right)^{v_i} \quad (4.3)$$

Previous work of Cramer et. al. is adapted for the identification of competitive binding-based displacement effect during the presented OBE chromatography mode. Rearrangement of Eq. (4.3) leads to the identification of three groups as displayed in Eq. (4.4). T1 ligand availability for the component m, T2 reduction of available ligands by the bound component m and T3 competitive adsorption depending on surface charge, sum of steric hinderance  $\sigma$  and characteristic charge  $v$  of each component. Following this, the interaction strength and thus competitive binding-based displacement rely on the bound components and the applied liquid concentration when compared to Eq. (4.3).

$$q_m = \frac{\Lambda}{\frac{(v_m + \sigma_m)}{T_1}} - \frac{\frac{1}{q_m^{v_m}} \cdot c_s}{\underbrace{(c_{eq,m} \cdot K_{eq,m})^{v_m} \cdot (v_m + \sigma_m)}_{T_2}} - \frac{\sum_{j=2}^n (v_j + \sigma_j) \cdot q_j}{\frac{(v_m + \sigma_m)}{T_3}} \quad (4.4)$$

The identification of competitive adsorption-based displacement effects can be conducted by reducing Eq. (4.4) for a two-component system in Eq. (4.5). This said, the salt molecule is not considered as a component in this case, which would be needed for an analytically correct correlation.

$$q_1 = \frac{\Lambda}{\frac{(v_1 + \sigma_1)}{T_1}} - \frac{\frac{1}{q_1^{v_1}} \cdot c_s}{\underbrace{(c_{eq,1} \cdot K_{eq,1})^{v_1} \cdot (v_1 + \sigma_1)}_{T_2}} - \frac{(v_2 + \sigma_2)}{\frac{(v_1 + \sigma_1)}{T_3}} \cdot q_2 \quad (4.5)$$

However, in Eq. (4.5), the two terms T2 and T3 can have an impact on displacement effects. Based on the parameters given, T3 specifies the steric and charged-based differences between the components and thus be used for the displacement identification. The two-component interaction strength increases with the difference between the components. Following this, with a high interaction strength component 1 will be displaced by component 2. Therefore, T3 is defined as delta interaction strength in Eq. (4.6).

$$\text{delta interaction strength} = \frac{(v_2 + \sigma_2)}{(v_1 + \sigma_1)} \quad (4.6)$$

## 4.2.2.3 Mechanistic model analysis

To validate the above deduction, the outcome of two case studies based on the separation of ribonuclease A and cytochrome C as well as IgG monomer and its HMWS is examined. The differences between BE and OBE chromatography mode, are evaluated by a detailed equilibrium-dispersive mechanistic model analysis applying an SMA isotherm, each by means of locally resolved stationary interaction, column profile and isothermal behavior. The investigated stationary phase for both scenarios is a MA of 8.34 mL, a porosity of 0.75 and a bed height of 13.75 mm. The respective fluid dynamics of the system and MA were characterized with a step function acetone tracer experiment. The ionic capacity for the used Sartobind® S was determined by titration of the module using an Äkta™ Explorer. The used flow rate was 14 mL/min. In Table 4.1, the competent parameters are listed for Ribonuclease A and Cytochrome C obtained from Osberghaus et al.<sup>168</sup> The kinetics were assumed to be equal and comparable to IgG. The IgG and HMWS SMA isotherm parameters were assessed using the HTS BE results published earlier<sup>181</sup> (results not shown here).

Table 4.1: Simulation parameters

	Unit	Ribonuclease A	Cytochrome C	IgG	IgG HMWS
Feed concentration	[M]	1.3e-04	8.0e-06	1.2e-05	3.3e-07
Kinetic	[s(M) <sup>n</sup> ]	0.013	0.013	0.013	0.066
Equilibrium	[-]	0.148	0.307	9.91	14.4
Charge	[-]	5.11	5	4.4	4.93
Steric	[-]	28.88	28.7	513.8	12915.5
Ionic capacity	[M]	0.8	0.8	0.5	0.5

4.2.2.4 High throughput screening – HTS<sub>OBE</sub>

The developed screening procedure leading to the application of OBE chromatography suitable for classical process range determination and difficult to assess and /or identify effects such as displacement. The procedure can be described by a repeated BE mode with partial elution. The HTS<sub>OBE</sub> procedure and the resulting chromatograms are depicted in Table 4.2 and Figure 4.2.

Table 4.2: OBE screening procedure

Step [-]	Step size [mL]	Total volume [mL]	Conductivity (CD) [mS/cm]
L1	2 – 4	28	10
W1	2 – 4	10 – 12	10
E1	4	8	20
L2	2 – 4	14	20
W2	2 – 4	10 – 12	20
E2	4	8	30
L3	2 – 4	14	30
W3	2 – 4	10 – 12	30
E3	4	8	40

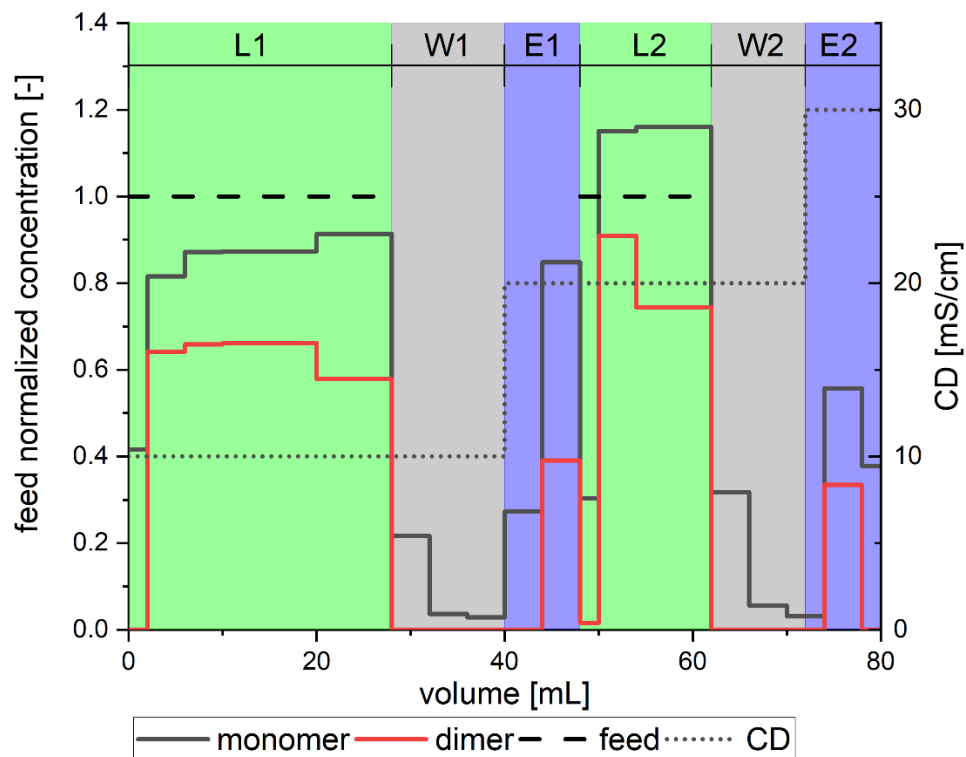


Figure 4.2: Exemplary OBE mode with two phases of a BE mode as loading phases L1, L2 (green areas), wash phases W1,W2 (gray areas) and elution phases E1, E2 (blue areas). The OBE mode comprises a sequence of load (L), wash (W), and elution (E) steps. The parameters used are listed in Table 4.2 and Table 4.3. If a component concentration exceeds its loading concentration in the loading step while the other component concentration remains below, its loading concentration displacement effects are identified

In contrast to the HTS<sub>BE</sub> mode discussed earlier<sup>181</sup>, the equilibrated MA is purposely overloaded by adding a load mass of twice the by estimated static binding capacity (prior knowledge), here in 2 mL – 4 mL steps up to 28 mL load (L1). Subsequently, the MA is washed with 10 mL - 12 mL in 2 mL- 4 mL steps (W1) and partially eluted with 8 mL in 4 mL steps (E1) with one conductivity (CD) step. This is followed by loading the MA (L2) containing 14 mL load in 2 mL - 4 mL steps with the same conditions as the elution step (E1) before. After the anew loading, the procedure is repeated. The approach is completed with an 8 mL regeneration and 12 mL re-equilibration storage step in 4 mL steps. Liquid dispensing velocity was set to 500  $\mu$ L/s. The loading concentration for each pH and conductivity value is listed in Table 4.3. Every pipetting step eluate is collected in a cavity of a movable well plate and analyzed by SEC. Based on prior knowledge the conductivity was set to observe a high, medium, and low binding capacity range. For unknown binding conditions of a stationary phase the conductivity range might be extended, and/or smaller conductivity steps could be used.

Table 4.3: OBE screening procedure

pH	CD 10 [mS/cm]		Loading concentration			CD 30 [mS/cm]	
	IgG Monomer	HMWS	IgG Monomer	HMWS	IgG Monomer	HMWS	
5.0	4.92	0.16	4.84	0.15	3.89	0.11	
5.5	5.65	0.16	5.01	0.20	4.80	0.17	
6.0	5.03	0.15	5.11	0.16	3.83	0.15	
6.5	5.36	0.20	5.30	0.19	4.92	0.16	
7.0	5.34	0.24	5.07	0.21	4.94	0.20	

Limitations of the HTS<sub>OBE</sub> mode: In presence of competitive adsorption displacement effects, the static binding capacity may not be determined with absolute certainty, based on the unknown loading duration needed. However, the HTS<sub>OBE</sub> mode for displacement effect evaluation is capable to identified competitive adsorption, thereby increasing contaminant binding capacity, optimal process conditions enhancing utilization and recovery.

### a) Binding capacity

An outcome of the HTS<sub>OBE</sub> results are static binding capacities for process maps. HTS<sub>BE</sub> and HTS<sub>OBE</sub> will lead to the same static binding capacity if no displacement effects are present. If displacement effects are present, the dependency of the static binding capacity with the loaded mass will lead to differences in the static binding capacity between the HTS<sub>BE</sub> and HTS<sub>OBE</sub>. The static binding capacity at the initial CD at a given pH value is calculated using Eq. (4.7). In Eq. (4.7), the sum difference of each component loaded mass and flow through fraction mass equals the static binding capacity respectively.

$$q_{FT MaxLoad,i} = \frac{1}{V_{MA}} \cdot \left( \sum_{k=1}^l \sum_{i=1}^n c_{FT Load,i,k} \cdot V_{FT Load,k} - \sum_{k=1}^l \sum_{i=1}^n c_{FT i,k} \cdot V_{FT,k} \right) \quad (4.7)$$

### b) Identification of competitive adsorption-based displacement

Raw data obtained by a HTS<sub>OBE</sub> procedure is analyzed by means of a term named displacement identifier (DI). In Eq. (4.8), each component concentration  $c_i$  is normalized by the loading concentration  $c_{feed,i}$ . The normalization thus allows to highlight two distinct situations: 1) the normalized component concentration is bigger than one and thus indicates displacement 2) the normalized component concentration of the component is below one and thus indicates the action of a competitive higher attracted molecule. With this in mind, the DI in Eq. (4.9) is the product of each normalized concentration reduced by one and is considered when the Phase  $k$  is equal to load phase as well as the absolute deviation to the step before is less than 10 %. Consequently, a DI below zero indicates displacement effects and a DI equal or higher than zero indicates no competitive adsorption-based displacement. Applying the DI for competitive adsorption-based displacement effect analysis in HTS<sub>OBE</sub> loading phase requires a stationary phase saturation of at least one component.

$$c_{Norm,i,k} = \frac{c_i}{c_{feed,i}} \quad (4.8)$$

$$DI_k = (c_{Norm,i,k} - 1) \cdot (c_{Norm,i+1,k} - 1) \Big|_{=Load \wedge ABS\left(\frac{\partial c}{\partial V}\right) \leq 10 \%} \quad (4.9)$$

#### 4.2.2.5 Scale-up

For a scale-up validation of the HTS<sub>OBE</sub> data shown in Figure 4.3, benchtop experiments were conducted as follows. Initially, a 4.6 mL prototype Sartobind® S was used with a volume of 500 mL recycled twice over the MA. In addition, an 8.2 mL device was used for recycling and a single FT experiment. The equilibrated MA is loaded, and the flowthrough fractionated into 5 mL samples until reaching a total of 10 membrane volumes (MV). Following this, each 100 mL, a 5 mL - 10 mL sample was collected. All samples were analyzed by SEC. If not sampled, the liquid is recycled into the storage tank. In the recycling experiments feedstock solutions of 1.8 g/L - 3.4 g/L IgG monomer, 0.2 g/L - 0.96 g/L dimer and 0 g/L - 0.04 g/L IgG oligomer were loaded at pH 5 and 5.5 and CDs of 10 mS/cm, 11 mS/cm, and 18 mS/cm. A mass balance is used to determine the concentration in eluate and stirred tank. To do so, load is weighed at the beginning and at the end of the experiment; the states in between were calculated with the taken SEC samples.

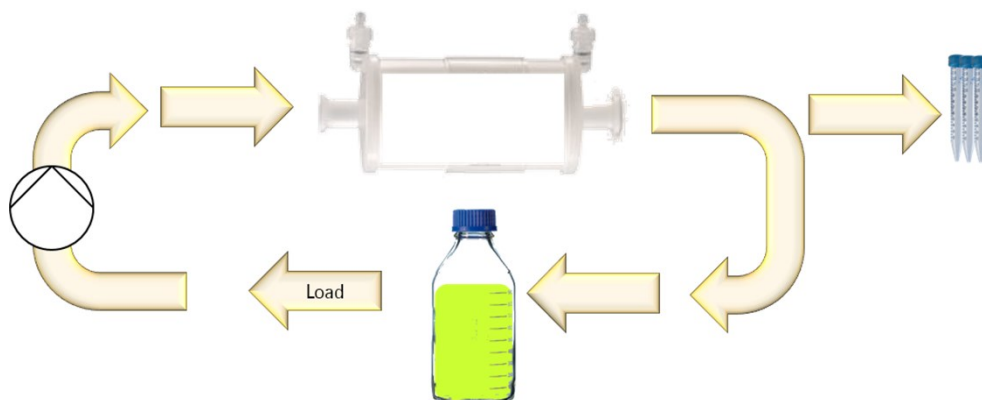


Figure 4.3: Schematic recycling experiments, the load is pumped from the loading vessel over the MA and recycled in the loading vessel. Fractions are analyzed via SEC.

## 4.3 Results and discussion

### 4.3.1 Mechanistic process understanding

Addressing the standardized biopharmaceutical mAb process with its protein A purification step and typically small levels of impurities, both subsequent purification strategies - BE and / or MA FT mode - are currently used.

The typical challenge in a mAb platform process is the separation of the target molecule (IgG) showing a higher feed concentration but lower charge / affinity to CEX ligands (component 1) and an impurity (i.e. aggregates) showing a low feed concentration but usually higher charge / affinity to CEX ligands (component 2). Based on the highlighted correlations between SMA parameters and possible displacement identification (Eq. (4.4)), the introduced interaction strength (Eq. (4.6)) is initially used for a theoretical assessment.

Competitive adsorption-based displacement effects occur now when the difference / delta between these surface-charge related affinities increases. A schematic illustration of these effects at BE and OBE chromatography modes is shown in Figure 4.4. Initially, the higher concentrated molecule (component 1, mAb) will occupy the available surface of the stationary phase, but upon further loading will – in the case displacement takes place – eventually be displaced by the lower concentrated impurity (component 2, aggregate). In BE mode potential displacement effects are hardly seen during load and elution. This said, displacement effects will change the internal ‘column profile’ independent of process mode. In OBE chromatography potential displacement effects, however, can be exploited to increase utilization of the stationary phase and feedstock purity. Thus, the column / membrane load determines the process mode - BE or OBE - while the delta interaction strength determines molecular processes determining the occurrence and strength of displacement effects.

### 4.3 Results and discussion

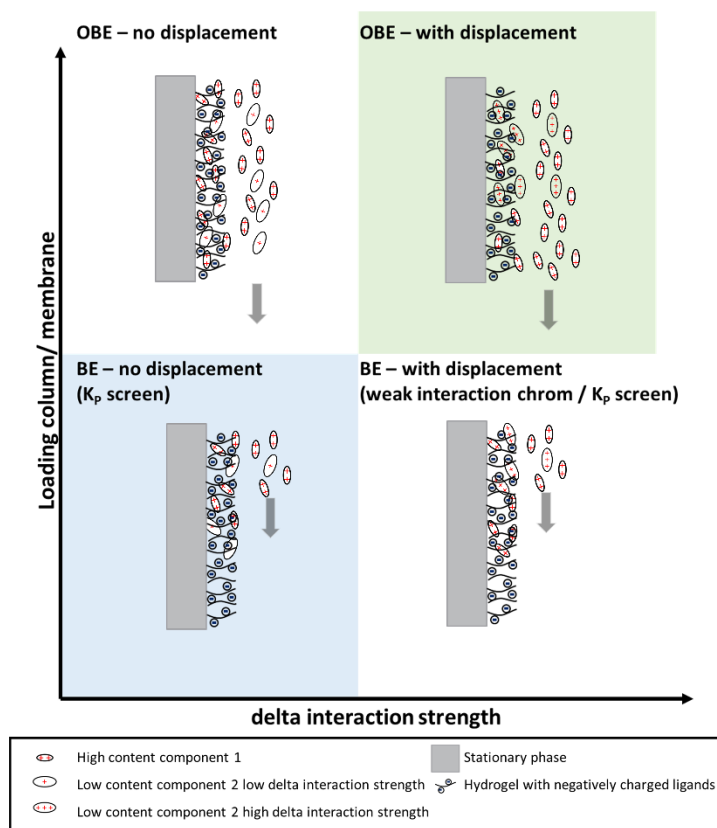


Figure 4.4: Schematic illustrations of the molecular processes along the stationary phase length. The process mode is a function of column load, FT mode for high column load and BE mode for low column load. Displacement effects between two components are governed by the delta interaction strength.

The above presented Figure 4.4 is validated by the two presented mechanistic model-based analysis of two high load FT mode simulation using isotherm data from ribonuclease A and cytochrome C as well as IgG monomer and its HMWS (see Table 4.1) in Figure 4.5. The separation of ribonuclease A and cytochrome C with a delta interaction strength of 0.99 shows no significant displacement effects whereas IgG monomer and its HMWS with a delta interaction strength of 25 clearly shows displacement effects.

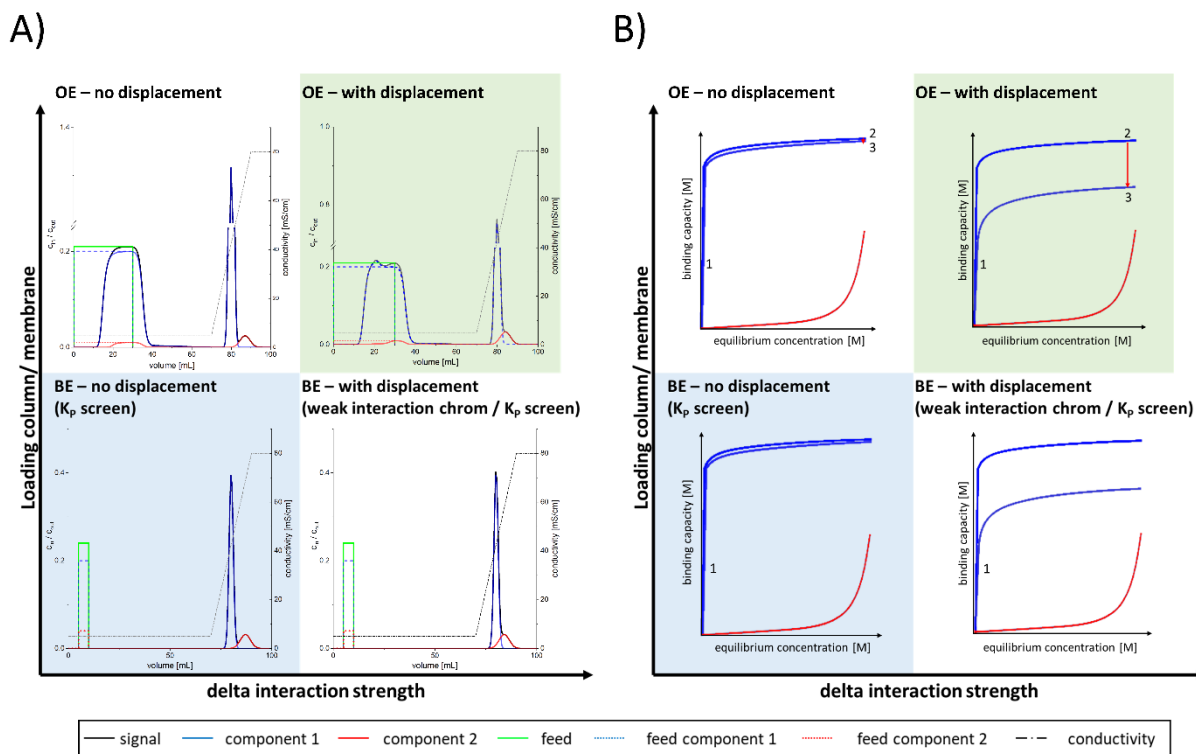


Figure 4.5: Visualization of the obtained process signal in terms of chromatograms (A) and the respective isotherm shapes (B). The signals are sorted compared to the schematic description in Figure 4.4 highlighting the process mode – BE or FT – being a function of column saturation and the underlying molecular processes being a function of the delta interaction strength. The most prominent indicator for displacement effects is clearly seen in the load behavior under FT conditions.

Figure 4.5 A) reviews the resulting process signals in terms of obtained chromatograms and Figure 4.5 B) highlights the respective isotherms behind this behavior. Assessing the obtained chromatograms in a BE mode it becomes clear, that displacement behavior will only lead to a shift in retention time and slight changes in the shape of the elution peak. The delta interaction strength is only visible in the distance of the resulting peaks as a function of elution conditions. For FT mode where the stationary phase is overloaded with process feedstock potential disassembly becomes visible during load showing a higher  $c_{out}$  than  $c_{in}$  of component 1.

While the actual affinity of a components (either single or in a mixture) remains widely unchanged (Figure 4.5 B(1)), the most prominent difference when assessing the isotherms behind the adsorption behavior is the reduction in binding capacity of component 1 when transitioning from a single component systems to a two component mixture (Figure 4.5 B (2,3)).

The loading phase of ribonuclease A and cytochrome C is dominated by the ligand saturation through ribonuclease A being higher concentrated and exhibiting a higher affinity to the stationary phase. Cytochrome C binds to the stationary phase as expected by its smaller concentration – value but reduces the static binding capacity of ribonuclease A insignificantly with a 5 % decrease at the cytochrome C breakthrough. During further loading, the ribonuclease A liquid concentration strives towards its feed concentration, while no displacement effects could be observed.

For IgG monomer and its HMWS, displacement effects can be assumed solely based on the delta interaction strength. The displacement effects are then observed during the loading phase when the IgG monomer concentration exceeds its feed concentration. This effect was described previously<sup>181</sup>

### 4.3 Results and discussion

---

and is confirmed with the monomer binding capacity reduction by the HMWS concentration breakthrough. The HMWS concentration breakthrough indicates an HMWS saturated phase. The relative IgG binding capacity decreases with over 40 % when the HMWS loading content increases from 1 % to 2 %.

In summary, displacement effects are present if the delta interaction strength is greater than one and thus the process concentration of component 1 exceeds its feed concentration in the loading phase. In addition, the concentration of the component with the higher affinity (component 2) will remain below its feed concentration during active displacement. As the most prominent indicator of displacement processes is found during the load step, a reliable screening procedure is introduced: the overload bind and elute (OBE) mode. While classical screening procedures<sup>181</sup> use several elution steps to determine the process range, displacement effects might be missed, this OBE mode investigates concentration behavior during load at several different salt concentrations.

Both, the  $HTS_{BE}$  and  $HTS_{OBE}$  modes result in the same static binding capacity under the following assumptions: identical loading composition and process conditions and no molecular effects such as displacement present. In this scenario, the OBE mode can also be used for conventional process parameter determination. In contrast to the BE mode, the OBE mode offers the possibility to identify potential dynamic effects. The latter, however, to the cost of a lower economic use of resources during the screening procedure such as higher sample and buffer consumption.

## 4.3.2 High throughput screening - OBE mode

In Figure 4.6 the loading steps (L1, L2) of a Sartobind® S MA in a SDD – HTS set-up applying the OBE mode at pH 5, 6 and 7 are shown. The CD values shown in Figure 4.6 were 10 mS/cm (L1) and 20 mS/cm (L2). All collected fractions are analyzed for monomer and HMWS content using off-line SEC. The MA ligand saturation is achieved in the first loading step L1. When examining L1 at pH value 5, the IgG monomer loading concentration is reached but not exceeded. In addition, the IgG dimer loading concentration is not reached, indicating potential displacement effects by competitive adsorption. However, deviation in the measurement and experimental work cannot be excluded and a clear statement is – for this scenario - not possible. In general, competitive adsorption-based displacement effects are only considered given that the behavior of both components indicates this. Considering the loading phase L2 at pH 5, it is observed that the monomer concentration exceeds the loading concentration while the dimer concentration remains below its start/feed concentration. In this case both components indicate a clear competitive adsorption induced displacement scenario. Based on the experimental quality for pH 7 valid statements are hardly possible, the concentration course in the first loading phase implies competitive adsorption here as well.

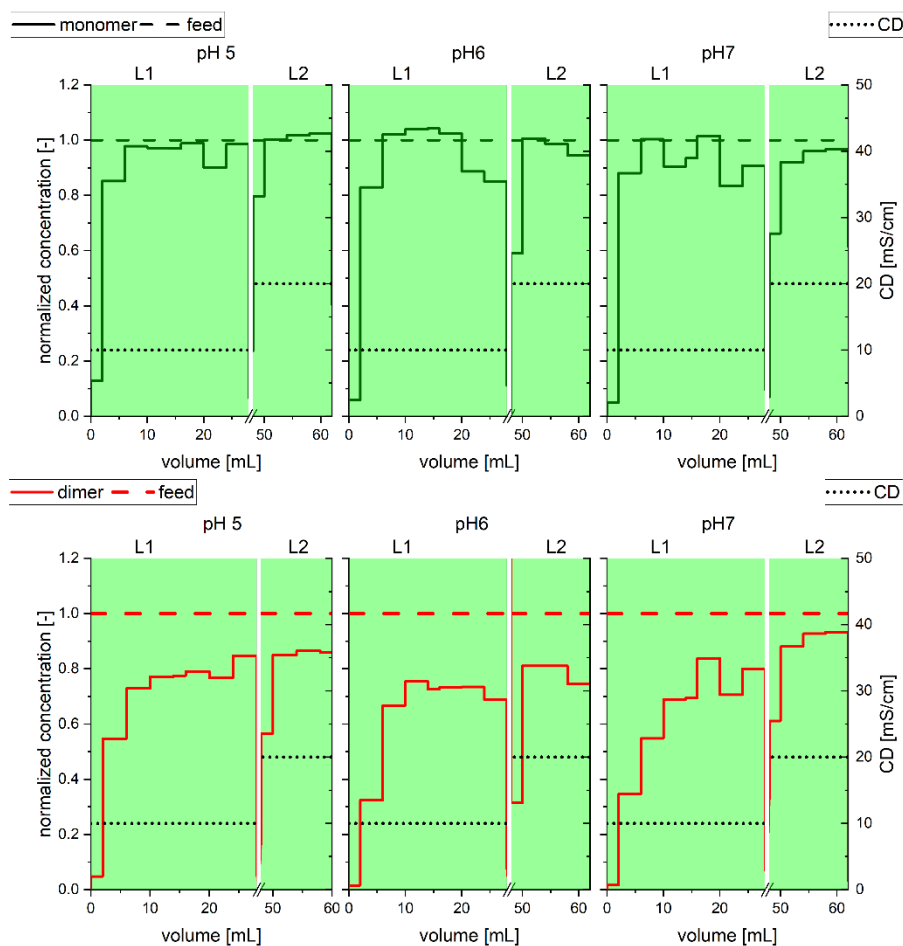


Figure 4.6: Concentration profile of load fraction under OBE mode of Sartobind® S IgG; 1) pH 5; 2) pH 6; 3) pH 7; IgG monomer (top row) and concentration IgG dimer (bottom row); the first loading step L1 is performed at low salt concentration, followed by a wash and stepwise increased salt concentration in the elution step E1. The next loading (L2) is performed at the same salt concentration as chosen for the elution and the procedure is continued as before.

### 4.3 Results and discussion

Even though not directly recognizable looking at the raw data presented in Figure 4.6, applying the OBE leads to an assessment of displacement effects applying a DI map. Figure 4.7 shows the obtained DI values of the screening data presented in Figure 4.6. A DI below 0 displays potential displacement effects. The lowest DI obtained from the different loading fractions is applied for the DI map. Doing so, a DI of -0.01 and -0.027 represents for example an excess of fraction concentration of the IgG over loading concentration of 5 % and 10 %, respectively. For Sartobind® S, IgG displacement effects increase with the salt concentration at decreasing pH value. At neutral to basic pH conditions, no displacement effects are observed. Displacement showed to be a fine interplay between surface charge (distance to isoelectric point of the components) and salt concentration (shielding of electrostatic interactions). The slight differences in DI show the difficulty to determine displacement effects. Decreasing binding capacity also decreases the concentration change of the lower attracted component, leading to detection limitations.

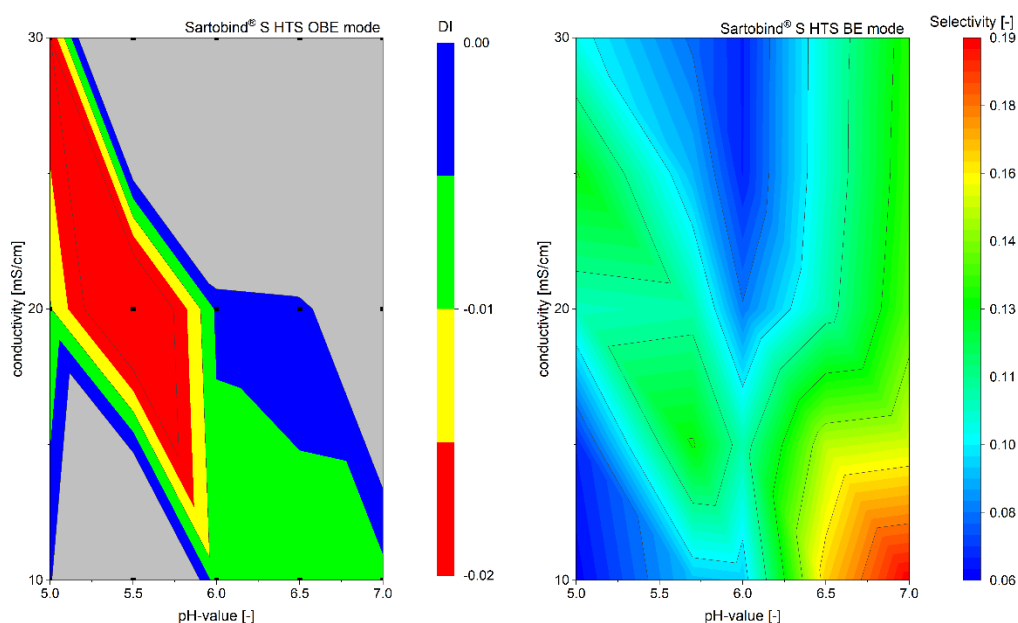


Figure 4.7: OBE DI map for Sartobind® S and IgG in comparison to BE selectivity map. The DI map shows with decreasing pH-value and with the conductivity increasing displacement effects. The colour code for displacement is: grey no displacement detected and increasing displacement effects determined from blue to green over yellow and red. To facilitate the comparison of the determined DI map, the selectivity map of IgG monomer and HMWS, determined in the HTS SDD BE mode published earlier by us<sup>7</sup>, is shown in the upper right corner. The applied BE and OBE mode show similarities in selectivity and Di value respectively.

However, as displacement is a function of different interaction strength and thus the ability to separate two components in BE mode, it is not surprising that the DI course obtained for the OBE mode is comparable with the BE Sartobind® S selectivity band with increasing conductivity and decreasing pH value showed earlier<sup>181</sup>. In addition, S. Vogg et al. have discovered similar process parameters in their investigations of displacement effects on Sartobind® S for a 50 kDA smaller antibody and its aggregate.<sup>136</sup> In additional studies applying the BE mode for pH 5.5 and 20 mS/cm showed binding capacities of 10 mg/mL and 1 mg/mL for a IgG and its HMWS respectively. Applying the OBE mode for the same conditions resulted in binding capacities of 10 mg/mL IgG and 3 mg/mL HMWS respectively. In PD this would result in a 3-time higher load volume. This said, a higher loading volume at reduced IgG product binding enhances yield and productivity when compared to a classical FT approach. Accordingly, the OBE mode is centered between the BE mode facilitating for complex purification / feed impurity variability and the FT mode with high recovery / productivity.

## 4.3.3 OBE recycle chromatography - case study

The OBE results obtained in the HTS set-up were confirmed in an benchtop case studies expressing approximately scale-up factors of 10 and 20. 500 mL feed stock - containing 1.78 g/L IgG monomer, 0.96 g/L dimer and 0.04 g/L IgG HMWS - were loaded/recycled two times on a 4.6 mL Sartobind® S device at pH 5 and CD 11 mS/cm (L1), pH 5.5 and CD 10 mS/cm (L2) also pH 5.5 and CD 18 mS/cm (L3). Additional experiments were conducted with an 8.4 mL device at pH 5 and CD 11 mS/cm (L1), pH 5.5 and CD 11 mS/cm (L2) also pH 5.5 and 18 mS/cm (L3). Figure 4.8 shows the recycle experiment obtained for the 4.6 mL Sartobind® S device at a pH 5.5 and CD 18 mS/cm (L3). The monomer concentration exceeds the loading concentration shortly after the breakthrough started. As a result of the fractionation, the load / vessel concentration decreases with the experimental period not only during adsorption, but also when mass is removed. Shortly after (1-2 MV) the IgG monomer, the IgG dimer breakthrough can be determined. The IgG dimer breakthrough is shallower than that of the IgG monomer. This characteristic can be caused by either strongly deviating isothermal parameters or different adsorption kinetic properties. The start of HMWS breakthrough curve is only detected between 75-110 MV. However, comparing the loading concentration profile between the components show similarities between IgG dimer and HMWS, indicating similarities between the respective components. During the experimental course, the displacement of the IgG monomers decreases as a result of the dimer concentration approaching its loading / vessel concentration. Thereafter, the IgG dimer concentration increases slightly over its loading / vessel concentration which may indicate displacement by IgG HMWS.

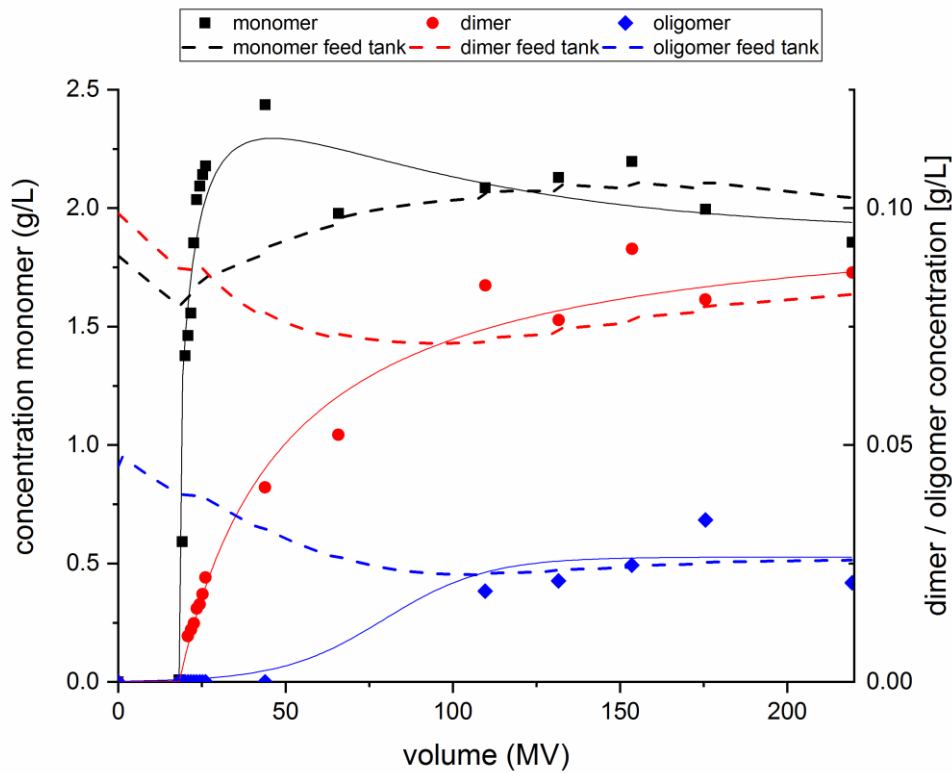


Figure 4.8: Simplified recycle experiment concentration profile at pH 5.5, CD 18 mS/cm. The IgG monomer increases the loading concentration and convergence then the loading concentration. In the range of 20-75 MV, the dimer and HMWS concentration do not reach the loading concentration which conform the displacement of IgG monomer.

## 4.4 Conclusion

---

Based on the recycle experiments described above the presence of displacement effects at the determined OBE conditions could be confirmed. Liua et al. used a Poros™ 50HS resin in column chromatography and gained with 0.3 column volume per minute 36 % less IgG monomer and 66 % higher aggregate binding capacity.<sup>84</sup> For MA processing, we achieved comparable results. Using displacement effects in MA processing leads up to 45% less monomer and 88% higher aggregate binding capacity compared to one-time loading.

Furthermore, the recycle experiment confirms the previous findings of HTS BE and HTS OBE mode at pH 5.5 and a conductivity of 20 mS/cm. The HTS BE mode determined 10 mg/mL IgG and 1 mg/mL HMWS binding capacity while HTS OBE mode and recycle experiment showed capacities of 10 mg/mL IgG, 3 mg/mL HMWS and 14 mg/mL IgG, 3 g/L HMWS binding capacity. The slightly higher binding capacity of the IgG for the HTS OBE mode when comparing to the OBE benchtop experiments is probably due to a lower CD value (18 mS/cm < 20 mS/cm) and an also lower aggregate concentration (5.2 % < 5.7 %).

### 4.4 Conclusion

The applied PD approach targeting displacement effects from investigations on protein adsorption to process design was shown for an example of separating IgG monomer from its HMWS. Theoretical investigations based on SMA isotherm parameter evaluation allow a direct assessment of possible displacement effects in a two-component mixture resulting in the introduction of the delta interaction strength. Following this, the theoretical findings could be verified experimentally leading to a DI process map guiding PD at large scale. The conventional SDD - HTS approach in BE mode<sup>7</sup> has been extended with the OBE approach introduced in this work, allowing the determination of displacement effects. The SDD - HTS OBE approach can be described as a repeated BE mode with partial elution. The OBE approach has been applied to IgG aggregate removal with Sartobind® S and in addition to the successful displacement effect identification, the determination of classical process parameters for FC or OBE chromatography mode has been confirmed. As a result of the recycling experiment, the IgG monomer binding capacity was reduced by 45 % and that of the IgG aggregates increased by 88 %.

### Acknowledgment

The authors wish to acknowledge the Membrane Chromatography & Modification team. Furthermore, we acknowledge Peter Polossek for construction engineering support and the Device Development for 3D printing support of the HTS scale-down model. Our thanks also go to the BioProcessing Group for providing the mAb feed solution. In addition, we especially acknowledge the student Sebastian Hegner for his dedicated effort and excellent laboratory work.

### Conflict of Interest

The authors have declared no conflict of interest.

### List of Symbols

Abbreviations, symbols and indices can be found in Table 4.4, Table 4.5 and Table 4.6.

Table 4.4: Abbreviations

Abbreviations	Meaning	Unit
BE	Bind and Elute	[-]
CD	Conductivity	[-]
CEX	Cation exchange chromatography	[-]
DBC	dynamic breakthrough capacity	[-]
DI	Displacement identifier	[-]
$E_k$	Elution step k	[-]
FC	Frontal Chromatography	[-]
FT	Flow through	[-]
HCP	Host cell protein	[-]
HMWS	Higher molecular weight species	[-]
HTS	High throughput screening	[-]
IgG	Immunoglobulin G	[-]
LC	Liquid chromatography	[-]
$L_k$	Loading step k	[-]
MA	Membrane adsorber	[-]
mAb	Monoclonal antibody	[-]
MM	Mixed mode	[-]
MV	Membrane volume	[-]
OBE	Overload bind and elute	[-]
SDD	Scale-down device	[-]
SEC	size exclusion chromatography	[-]
SMA	Steric mass action	[-]
$W_k$	Wash step k	[-]

Table 4.5: Symbol

Abbreviations	Meaning	Unit
$c_i^*$	Concentration of component i	[g/L]
cFeed	Feed concentration	[M]
$c_i$	Concentration of component i	[M]
$c^{Norm}$	Feed normalized concentration	[-]
$c_s$	Salt concentration	[M]
DI	Displacement identifier	[-]
Delta interaction strength	Two component displacement quantifier interaction strength	[-]
K	Equilibrium constant	[-]
M	Molar mass	[g/mol]
MV	Membrane volume	[MV]
$MV_0$	Slope center in membrane volume	[-]
q	Binding capacity	[M]
qMaxLoad,i	Static binding capacity calculated by the difference between loaded and unbound mass	[M]
T1	Equation term 1	[M]
T2	Equation term 2	[M]
T3	Equation term 3	[M]
V	Volume	[mL]
$\alpha$	Separation factor	[-]
$\lambda$	Dynamic affinity	[-]
$\Lambda$	Ionic capacity	[-]
$\nu$	Characteristic charge	[-]
$\sigma$	Steric hinderance	[-]

Table 4.6: Indices

Abbreviations	Meaning	Unit
i	Component	[-]
BE	Bind and elute mode	[-]
Dimer	IgG dimer	[-]
HMWS	IgG HMWS	[-]
k	Fraction / dispensing step	[-]
m	Component	[-]
Monomer	IgG monomer	[-]
OBE	Overload bind and elute mode	[-]
Total	Total, Overall value	[-]

## 5 Streamlined PD procedure incorporating the selection of various stationary phase types established in a mAb aggregate reduction study with different mixed mode ligands

Dominik Stein<sup>1,2</sup>, Volkmar Thom<sup>2</sup>, Jürgen Hubbuch<sup>1</sup>

<sup>1</sup> Karlsruhe Institute of Technology (KIT), Institute of Process Engineering in Life Sciences, Section IV: Biomolecular Separation Engineering, Karlsruhe, Germany

<sup>2</sup> Sartorius Stedim Biotech GmbH, August-Spindler-Str. 11, D-37079 Goettingen

### Abstract

In biopharmaceutical PD time, cost and reliability are the relevant keywords. During the development of chromatographic processes these targets are challenged by many possible scaffolds, ligands, and process parameters. The common response to this diversity is the establishment of platform processes in the development of chromatographic unit operations. However, while developing a platform library to simplify and accelerate chromatographic processes, the potential combination of scaffold, ligands and process parameters need to be characterized. This challenge is addressed in a case study on novel mixed mode (MiMo) adsorber for the removal of monoclonal antibody (mAb) aggregates. We propose a rigorous strategy to reduce the various experimental design space resulting from possible combinations in scaffolds, backbones, and ligands. This strategy is based on theoretical considerations, identification of adsorber selectivity and capacity for the identification of a suitable membrane system. For this system, each potential MiMo membrane adsorber (MA) candidate is investigated in its high molecular weight species (HMWS) reduction potential for a given mAb feed stream and referenced to the performance of Cpto™ Adhere. The introduced strategy can reduce the developmental effort in an early stage from three to two possible stationary phases. Thereafter, initial examinations at different ionic capacities enlighten one favorable stationary phase. Finalizing the development strategy procedure by studying five different MiMo ligands by HTS and confirming the study with a 2-3 MV higher dynamic breakthrough capacity in benchtop experiments and provides an insight in the benefits of a living process platform library.

### 5.1 Introduction

In biopharmaceutical PD (PD) productivity, separation performance (selectivity and capacity) as well as robustness are the relevant keywords.<sup>35</sup> For chromatographic processes, these parameters are a function of stationary phase characteristics, ligands and process parameters.<sup>49,140</sup> This said, employing all possible combinations of process parameters is contradictive to a stream-lined set up of a potential design space. The common response to this diversity is the establishment of platform processes.<sup>17,34,169,170</sup> Platform processes use a fixed set of unit-operation and stationary phases minimizing PD effort while at the same time ensuring acceptable selectivity, capacity and robustness. This approach, however, is only feasible for a set of molecules expressing high similarity, such as the classical mAb purification processes. Following the increasing number of new chemical or biological entities by a factor of 1.2 and 1.9, comparing developments in 2004-2008 with 2009-2013 and 2014-2018,<sup>95</sup> however requires a different strategy. Investigating the phase 2 product pipeline of several

biopharmaceutical manufacturers reveals a molecule variability compromising of antibodies, small molecules, bispecific antibodies, antibody agonist, antibody conjugate and recombinant proteins.<sup>194-199</sup> The increasing number of modalities generates the need for more process flexibility. What is thus needed, is a dynamic platform strategy for the development of processes rather than today's more static process platform.

The typical (static) platform PD focuses on a few process parameters only, limiting itself in transferability and its success relies on fragile individual knowledge. Future strategies need to rely on standardized strategies for choosing various unit operations, allowing a more dynamic PD leading to diverse but highly robust and productive processes. One of the most common unit operations in downstream processing is chromatography; usually two to three chromatography steps are implemented in typical mAb platform processes.<sup>13,14,17</sup> The typical classification scheme for chromatographic steps employing a) chromatographic processing mode, b) stationary phase scaffolds, c) backbone structures and d) chromatographic interaction mode and are shown in Figure 5.1 and Figure 5.2.

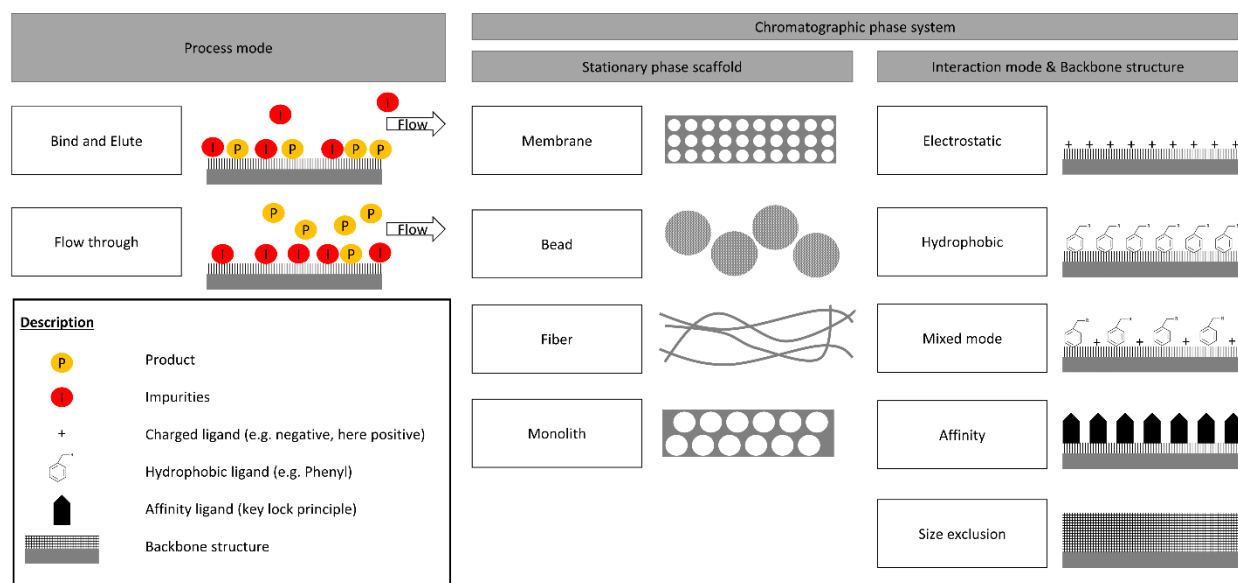


Figure 5.1: Exemplary chromatographic subgroups. Schematic representation of conventional subdivisions in chromatography using process mode, mode of interaction and type of stationary phase scaffolds. Backbone structures investigated in this study are highlighted in more detail in Figure 5.2.

What is needed though is a PD strategy to address chromatographic parameters for a given challenge. This includes a characterization across different combinations of new and existing chromatographic modes, scaffolds, backbones, and ligands resulting in so-called “living knowledge” based libraries.

## 5.1 Introduction

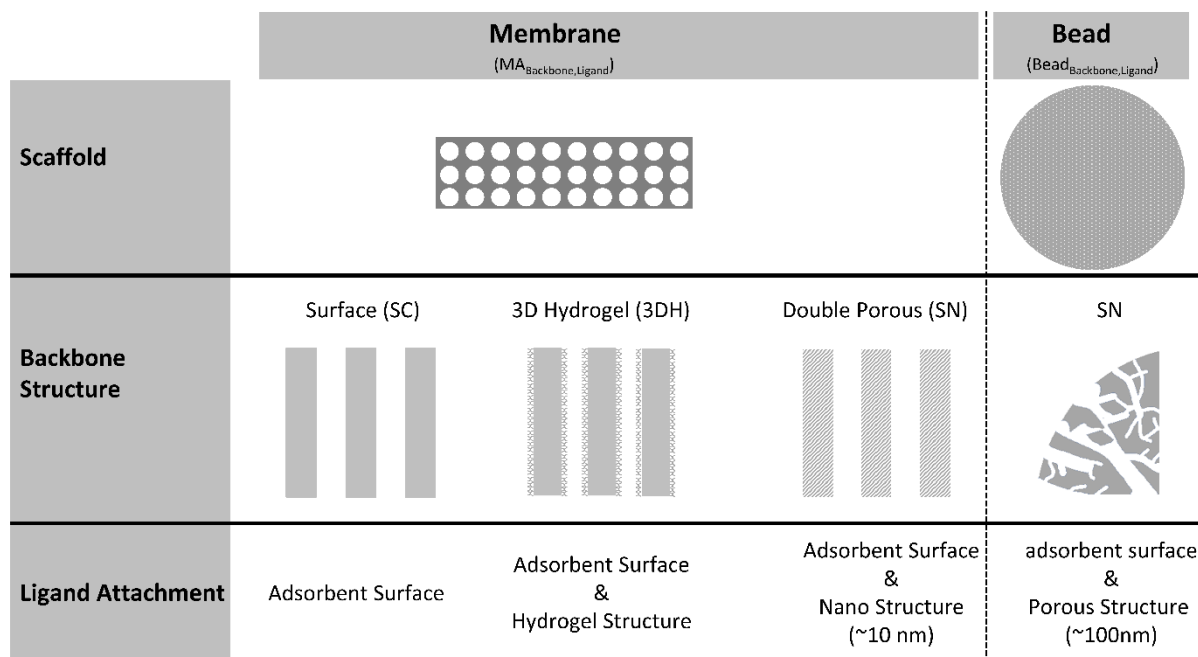


Figure 5.2: Different backbone structure: surface (SC), 3D hydrogel (3DH), and double porous (SN) membrane. The different scaffold types investigated were MA and Bead. Here, the bead is classified as SN to avoid misinterpretation of a nonporous bead with only surface binding.

In general, chromatographic processing modes are bind and elute (BE), flow through (FT) and subgroups thereof. These subgroups are characterized by different load, wash, or elution strategies. The classification of BE and FT is mainly a function of product behavior during the chromatographic process.<sup>14,108,200</sup> In BE mode, the product attaches primarily to the stationary phase while the impurities preferably do not interact with the stationary phase or are separated from the product in the elution, e.g. ion exchange chromatography. For conventional BE mode, stationary phases with high binding capacity are generally preferred. Typically, high binding capacity is associated with optimized pore diameters, resulting in large specific surface areas of the stationary phase; a setting usually leading to diffusion limited mass transfer and thus to long residence- and cycle-time. Operating in FT mode is generally associated with binding the impurities and allowing the product to pass through the stationary phase with as little interaction as possible.<sup>166,201</sup> As a result of the impurity binding, the product concentration of the FT mode is limited to that of the feed. Compensating for this disadvantage the FT mode needs to employ high flow rates and extended loading cycles to reach the desired productivities.<sup>166,201</sup> Scaffolds with non-dominant mass transfer but sufficient binding capacity are thus needed to achieve this.

The optimal process mode for a given challenge is a function of scaffold, backbone, interaction mode and feed stream composition. In order to sort the various properties of the scaffolds, they are grouped into: a) bead, b) monolith, c) fiber and d) membrane adsorber (Figure 5.1). Bead based scaffolds usually have a backbone structures consisting of a particle diameter in the range of 50 – 500  $\mu\text{m}$  and pore diameter of 20 - 160 nm.<sup>106,107</sup> These scaffolds are usually based on silica, polysaccharides, acrylates or methacrylate etc. and can also exhibit additional surface modifications.<sup>141</sup> Numerous researchers have shown a close relationship between molecular size, optimal pore diameter and achievable binding capacity.<sup>108-110</sup> Hunter et al and Svec, among others, point towards an ideal particle pore/protein diameter ratio of  $\sim 10$ -12.<sup>110,143-147</sup> This rule of thumb correlates to the molecule specific accessible surface area and thus available binding sites, nearly independent of the overall ligand density.

Monoliths as bead-based scaffolds can also be characterized by a meso and macro pore structure. The monolith macro pores are called flow channels, with a typical channel size in the range of 1-6  $\mu\text{m}$ <sup>148-150</sup> while the meso pores are in the range of 2-50 nm.<sup>106,148,149</sup> The scaffold of monoliths consists of different materials like silica, polyacrylamide, cellulose, styrene and polyglycidylmethacrylate.<sup>148,151</sup> Monoliths as well as beads tend to express mechanical instability due to the high internal porosity.<sup>106</sup> Depending on the formulation and packing procedure fiber-based backbone structures consist of flow channels in the range of 0.5 – 20  $\mu\text{m}$  and a surface area of 2-20  $\text{m}^2/\text{g}$ . The scaffold can be compared to monoliths and membrane material as e.g. polyethylene terephthalate and cellulose.<sup>152-154</sup> Membrane adsorber backbone structures with its pore sizes of 2-4  $\mu\text{m}$  are known for their high applicable flow range with relatively low pressure drop.<sup>111</sup> These membrane adsorber are usually made of organic material such as cellulose and its derivatives, polyethersulfone, polypropylene and polyvinylidene fluoride exhibiting a surface area of 0.6 – 3  $\text{m}^2/\text{g}$ .<sup>111,155</sup>

Besides the accessible specific surface area for a given molecule – mostly determined by the chosen backbone structure -, the ionic capacity or density can be a variable influencing the binding capacity, selectivity and the mass transfer rate.<sup>141,144,146,157</sup> This said, various backbone structure modifications are available to influence the ionic capacity distribution and/or distance between ligands of a stationary phase such as: a) surface modification, b) grafted polymers and c) gel in a shell.<sup>141</sup> The various modifications can influence the binding capacity and/or mass transfer by changing the ionic forces or ionic charge distribution.

Finally, depending on the type of ligand, the modes shown in Figure 5.1 define the final interaction between the molecules and stationary phase.

The ligand and thus applied interaction mode performance is generally connected to the interplay between molecular surface properties, ligand properties and fluid phase/feed characteristics. Exploiting this interplay, an increasing trend towards the use of so-called mixed-mode ligands has been observed in the last 20 years.<sup>13,71-73</sup> In the past various strategies have been applied in the application of mixed mode interactions: a) a mixture of electrostatic and hydrophobic adsorbent material,<sup>202,203</sup> b) backbone structures with one interaction and the attached ligand with the other interaction as well as c) ligands with mixed chemical/chromatographic interactive regions attached to the backbone structure.<sup>170,185,186</sup> These ligands have at least two different interaction modes, e.g. ionic and hydrophobic interaction respectively. MiMo ligands have shown high potential for mAb HMWS removal<sup>185,186,204</sup> and can be used in classical attraction or ionic repulsion-based FT mode<sup>205</sup>. In the classical BE or FT mode both interactions are used simultaneously, e.g. cation exchange and hydrophobic interactions.<sup>71,72,170,186,206,207</sup> The repulsion mode is used as an alternative to the classical mode, in which an attractive and a repulsive interaction is applied.<sup>71,72,208</sup>

In summary, the increasing variety of feedstocks and stationary phases in PD, which requires high productivity and robustness, necessitates streamlined procedures with fast and flexible screening techniques. Consequently, these screening techniques result in either mapping of the applicable design space or to provide an in-depth characterization of the system in order to allow further PD by in-silico methods.<sup>35,36,39,50</sup>

Addressing the above-mentioned complexity, we introduced screening procedures in the past, allowing the evaluation of MA with different ligands.<sup>181,209</sup> Prior to this screening procedures, the large variability of potential scaffolds and backbone structures in membrane chromatography is reduced by an evaluation scheme using theoretical considerations, and an investigation into selectivity and

capacity. The presented evaluation scheme includes evaluation of different scaffolds, backbones and MiMo ligands. Each candidate is challenged with the target of HMWS reduction of a monoclonal antibody feed stream. Furthermore, this case study investigates the MiMo characterization capability of the scale-down device (SDD) HTS in overload bind and elute (OBE) mode, earlier introduced by us.<sup>209</sup> The approach follows the typical chromatography parameter determination, seen for MiMo chromatography by investigation of adsorbent data (chemical coupling parameters, ligand density, type of backbone structure) and process data - HTS in OBE mode and confirmation in benchtop experiments.

### 5.2 Materials and Methods

In chromatography the separation performance is an interplay between process mode, scaffolds, backbone characteristics, ligand / interaction mode, molecular / biophysical characteristics, and fluid phase properties. The terminology used throughout the study is as follows: Scaffold<sub>Backbone,Ligand</sub>. In the following section, the systems investigated i.e. ligand backbone combinations are presented. Their suitability for HMWS removal is assessed by HTS and benchtop experimentation.

#### 5.2.1 Materials

The material section is divided into the following sections: a) ligand coupling, b) feed and buffer preparation, c) chromatographic experiments, d) analytic and software.

##### a) Ligand coupling

To adjust fluid phase conditions for efficient ligand coupling reactions, a pH probe Portavo® 902 pH from Knick and conductivity probe Cond 330i from Xylem Analytics were used. The reaction solution was prepared by dissolving the ligand and buffer salts in purified water, which was provided by an Arium® Water Purification System from Sartorius Stedim GmbH. The pH-value of the reaction solution was adjusted with sodium hydroxide (NaOH) or hydrochloric acid (HCl), from Carl Roth. Overall, five MiMo ligands (structure confidential) provided by BioRad Laboratories and N-Benzyl-N-methylethanolamine (BMEA) acting as a reference system obtained from Sigma Aldrich were coupled onto membrane backbones. Trimethylamine (40%, TMA) from Merck was used to convert a membrane backbone to an anion exchange MA.

##### b) Feed and buffer preparation

Purified water was provided by an Arium® Water Purification System. Weighing was performed by a Sartorius Master<sup>pro</sup> LP 12000S balance or Sartorius Expert LE225D-OCE from Sartorius Stedim Biotech GmbH. Chemicals used were: sodium chloride (NaCl), sodium hydroxide (NaOH), hydrochloric acid (HCl), glycine, sodium acetate (NaAc), acetic acid, di-potassium hydrogen phosphate, tris(hydroxymethyl)aminomethane (TRIS), di-sodium hydrogen phosphate di-hydrate, sodium di-hydrogen phosphates di-hydrate and ammonium sulfate (NH<sub>4</sub>)<sub>2</sub>SO<sub>4</sub> from Carl Roth, tri-sodium citrate di-hydrate and acetone from VWR chemicals, citric acid monohydrate from Alfa Aesar, ethanol from Sigma Aldrich. The pH value and conductivity of feed and buffer were adjusted with the same probes used for ligand coupling. Buffers used are listed in Table 5.1. Each buffer and feed solution were pre-filtered with a 0.45 µm Sartopure® and a 0.2 µm Sartolab® RF vacuum filter Sartolab® from Sartorius Stedim Biotech GmbH. The applied mAb was produced in a CHO fermentation, harvested and after

filtration with an Sartopore® 2 XLG 0,45/0,2 µm further purified by using a MabSelect™ Sure™ lab column (5 cm diameter, 192 mL volume) provided by Cytiva® UK Limited and a Äkta Prime™ system.

Table 5.1: pH value range dependency of buffers used

Buffer salt [-]	pH value range [-]	Molarity [mM]
Sodium acetate buffer	5.5	20 mM
Potassium phosphate buffer	6-7	150 mM
TRIS HCl buffer	7-8	20 mM

#### c) Chromatographic experiments and material

The MiMo ligand screening was carried out with HTS robot Lissy® 2002 GXXL/8P from Zinsser Analytic and FT experiments using Äkta Prime™ and Äkta™ Explorer from Cytiva© UK Limited. Capto™ Adhere 1 mL column was used for comparison with MiMo MA and process parameter determination. The used MA devices were two prototype set ups, with 3 flat sheet stacked MA with 2.7 cm diameter in plastic housing or a developed lab prototype with 30 flat sheet stacked MA in a silicon housing stabilized by a plastic jacket. The resulting bed volume was 0.46 mL ± 0.05 mL, 4.3 mL ± 0.5 mL respectively.

#### d) Analytic and software

Overall protein concentration was measured by the UV spectrometer at 280 nm wavelength VivaSpec® UV reader from Sartorius Stedim Biotech GmbH. The IgG and its HMWS concentration were determined with a Yarra™ 3 µm SEC 3000 column of 300 x 7.8 mm from Phenomenex using Dionex™ UltiMate™ 3000 HPLC System from Thermo Scientific™ and the software Chromeleon™ 6.80 from Dionex.

The HTS method was carried out with WinLissy (version 7) from Zinsser Analytic. UNICORN® from Cytiva© UK Limited was used for FT experiment code and chromatographic analysis. Experimental results evaluation and chromatographic curve analysis was done by using Origin® 2018b from OriginLab Corporation. MODDE® 12.1 was used for Design of experiments, statistical experimental design, and evaluation. The prototype MiMo ligands were characterized with respect to molecular weight and octanol/water partitioning coefficient using ChemSketch® from Advanced Chemistry Development UK Limited, United Kingdom.

### 5.2.2 Methods

#### 5.2.2.1 Feed preparation

A description of the further treatment for achieving an appropriate aggregate content of the clarified and protein A processed CHO feed solution is given as follows: The protein A eluate contained about 18 g/L mAb and a mAb aggregate level of about 1%. Enrichment of the 0.5-1% aggregate content of the clarified mAb solution to 2-6 % was done by a pH shift. Aggregation by a temporary pH shift is a commonly used method for aggregation.<sup>64,174,175</sup> After diluting the 0.1 M pH 3 glycine buffered mAb solution three times with potassium phosphate buffer (KPi) buffer, to enable aggregation in a mainly unbuffered environment, the pH value is adjusted to pH 3 with 0.5 M H<sub>3</sub>PO<sub>4</sub>. The aggregation time was set to 3 h with stirring at 150 rpm. Additionally, the pH was readjusted to pH 7 with 0.5 M NaOH resulting in an aggregate content between 2-8 %. Hereby, IgG fragments are generated as a byproduct

## 5.2 Materials and Methods

of the pH-Shift, 0.2-0.4 area weighted percentage increase as measured by SEC. To obtain a highly concentrated stock solution, the aggregated mAb solution was concentrated using the protein A column. The stock solutions exhibit mAb concentrations of up to ~18 g/L, 2-8 area weighted % HMWS and 0.5-4 area weighted % LMWS. The final feed solutions in Table 5.2 were prepared by diluting mAb stock solutions with at least three times of the desired buffer volume containing up to 1 M  $(\text{NH}_4)_2\text{SO}_4$  salt concentration. Finally, the feed solutions were filtered through a 0.2  $\mu\text{m}$  Sartolab® RF vacuum filter 62  $\text{cm}^2$  filtration area.

Table 5.2: Feed concentration of the preliminary experiments

Feedstock	pH	Conductivity	$c_{\text{Feed,IgG}}$	HMWS Vol.-%
[-]	[-]	[mS/cm]	[g/L]	[%]
1	6	5	3.3	6.8
	6	15	1.3	6.5
	7	15	3.8	5.3
2	7	15	2.7	4.0
3	7	15	2.8	5.0
4	7	2.2	3.1	5.0
	7	50	2.3	3.0
	7	25	2.4	2.8
	7	15	3.2	3.0
	7	5	2.8	3.4
	7	2.2	2.6	3.0
5	7	15	2.7	4.0

### 5.2.2.2 Coupling procedure

The introduced PD strategy can be described by theoretical evaluation of the stationary phase, followed by an experimental evaluation of the stationary phase and finally confirmation. This said, the theoretical evaluation of the stationary phase is one part of the living library implementation with continuous knowledge increase and refinement.

Five prototype MiMo ligands and one reference MiMo ligand were used. In this work, the chromatographic interactions are induced by the overall constantly positively charged quaternary amino group and the hydrophobic benzene ring. A diversity in ligand hydrophobicity is obtained by different substitutes at the benzene ring. The reference ligand is technical grade BMEA, which is used in the Cytiva© UK Limited product Capto™ Adhere. The five prototype ligands are provided by Bio-Rad Laboratories and are characterized by the molecular weight and the ratio of solubility in octanol/water, which is calculated by the logarithmic partitioning coefficient derived from the ligand concentration in octanol  $c_o$  and water  $c_w$ , the  $\log P$  value. The calculation of the  $\log P$  in Eq. (5.1) is based on the molecular ligand structure and carried out by ChemSketch® (Version 12.01). A high  $\log P$  value indicates a hydrophobic ligand whereas a low  $\log P$  value indicates a hydrophilic ligand.

$$\log P = \frac{\log c_o}{\log c_w} \quad (5.1)$$

The MiMo ligand characteristic values can be found in Table 5.3. The hydrophobicity of the ligands in increasing order is: reference ligand BMEA, L1, L2, L3, L4 and L5.

Table 5.3: MiMo ligand characteristic values

Ligand [-]	log P [-]	MW [g/mol]
BMEA	1.7	165.2
L1	2.1	165.2
L2	2.5	193.3
L3	3.2	255.2
L4	3.7	183.2
L5	4.1	221.3

In order to achieve acceptable ligand coupling parameters, reaction time (1 h – 50 h), temperature (40 °C – 70 °C), ligand density (low – high), ligand to solvent ratio (0.1 – 0.9) and pH value (8 – 11) were investigated. The coupling reaction between all used membrane backbone structures is a nucleophile epoxide ring opening by the tertiary amine of the ligand at basic conditions. All used backbone structures are different epoxide activated precursor Sartobind® membranes. These coupling experiments are carried out with two 4.7 cm and one 7.0 cm diameter Sartobind® hydrogel membranes with a height of 0.025 cm ± 0.003 cm for each coupling.

The ligand mass used is calculated by the product of the ionic capacity  $\Lambda$ , molar mass  $M$  of the ligand, the membrane volume  $V_{MA}$  and the desired ligand excess factor  $E$  (low - high) in Eq. (5.2). This said, the calculated mass should then lead to the target ionic capacity of the modified MA.

$$m_{Ligand} = E \cdot \Lambda \cdot M \cdot V_{MA} \quad (5.2)$$

Investigation of the MiMo ligand coupling parameter space was carried out with design of experiments using Modde 12. The used model was full factorial 2 level with three center points and a total of 19 experiments.

### 5.2.2.3 Biophysical characterization of the stationary phase

The stationary phase system and its separation performance is determined by the combination of scaffold structure, backbone design and applied ligand. In the following, the investigation is grouped in scaffolds and backbone structures followed by the evaluation of the MiMo ligands and stationary phase system performance.

**Scaffolds:** Process parameter and process performance may vary between the scaffolds when applying the same ligand. In order to highlight these effects, the MA<sub>3DH</sub> coupled with the BMEA ligand are compared to the commercial bead based stationary phase ligand, which is attached to capto™ adhere resin, at the very same process parameters with identical feed stocks of different pH and conductivity. Confirmation runs were carried out with a 30-layer stacked MA<sub>3DH</sub> Sartobind® lab prototype module, each layer with a 2.7 cm diameter resulting in a bed volume of 4.3 mL ± 0.5 mL.

**Backbone structure:** Important parameters of the applied backbone structures are surface area, chemical stability, porosity, accessibility, diffusive/convective limitations, and fluid distribution. These parameters define the binding capacity, selectivity, recovery, and productivity of the chromatographic media. The available membrane backbone structures are: surface (SC), 3D hydrogel (3DH) and a double porous (SN) membrane. As a reference we used the commercially available 1 mL Capto™ adhere column from Cytiva® UK Limited applying a volumetric flow of 1 ml/min for all column experiments.

An overview of the different scaffolds and backbone structures used in this study is given in Figure 5.2. The available backbone structures differ in pore diameter and thus surface area and binding capacity, diffusive length, and ligand attachment. In the case of MA<sub>SC</sub>, MA<sub>SN</sub> and Bead<sub>SN, Capto™ Adhere</sub> the ligands are attached to the adsorbent surface. The MA<sub>3DH</sub> exhibits an additional hydrogel of approximately 600-800 nm thickness grafted to the surface. The hydrogel offers an extended coupling space to which the ligands are bound.

Ligand: The chemical properties of the ligand, when coupled to the backbone structure, define the chromatographic interactions. In addition, the distance between the ligands and thus the surface charge distribution influences the chromatography efficiency for the desired separation. One of the state-of-the-art backbone and ligand characterization techniques includes the titration-based ionic capacity determination. In Eq. (5.3), the adsorbed hydroxide ions  $n_{OH^-}$  are calculated by the mass difference between added and measured HCl mass, receiving when integrating the concentration  $c_{Titration,liquid,i}$  and applied volume  $V_{Titration,liquid,i}$ . Dividing the exchanged hydroxide ions by the CV of the investigated device (Eq. (5.4)) leads to the ionic capacity. Resulting from the constantly positively charged ionic amino group and the hydrophobic benzene ring ligand structure, the ionic capacity also notes the number of hydrophobic sites.

$$n_{OH^-} = \int c_{Titration,liquid,2} \cdot \partial V_{Titration,liquid,2} - \int c_{Titration,liquid,1} \cdot \partial V_{Titration,liquid,1} \quad (5.3)$$

$$\Lambda = \frac{n_{OH^-}}{CV} \quad (5.4)$$

Considering the charge similarity of IgG and its HMWS, it is assumed that the distance between two ligands influences the separation. The ligand density of a backbone structure, which is indirectly comparable to ionic capacity, thus influences not only the maximum binding capacity but also the MA selectivity.<sup>141,143,146,157</sup> For the investigated MA a low ligand density reduces the binding capacity but may enhance the larger HMWS selectivity due to the distance between the ligands. With a high ligand density, the distance between the ligands is low and the ligands might interact with one another. This said, the titration based ionic capacity  $\Lambda$  determination in Eq. (5.3) and Eq. (5.4) needs to be transferred to a ligand distance specific parameter. This is given by the specific ionic capacity  $\Lambda^*$  shown in Eq. (5.5).

$$\Lambda^* = \frac{\Lambda}{A_{specific}} \quad (5.5)$$

The ionic capacity is determined by titration of the charged amino group using the benchtop system Äkta™ Explorer (Cytiva©). The membrane device used was set up as follows: fluid distributor mounted before and after three coupled stacked flat sheet membranes with a liquid accessible diameter of 2.7 cm and a height of 0.025 cm ± 0.003 cm resulting in 0.43 mL ± 0.05 mL bed volume. The experimental procedure consisted of an equilibration step with 1 M NaOH, followed by a wash step with purified water and titration with 10 mM HCl until a constant conductivity signal for 5 CV was reached. Subsequently, the membrane was washed again with purified water until the baseline signal is reached, followed by another HCl titration step. The procedure is finalized with a 10 CV 10 mM calcium phosphate buffer KPi wash step at pH 7 followed by 10 mM KPi at pH 7 with 20% ethanol for storage purpose. The measurement was carried out with a flow rate of 10 mL/min and 0.5 mL/min for the

membrane devices and the 1 mL Bead<sub>SN,Capto™ adhere</sub> column, respectively. Establishing the scaffold- and backbone-specific surface area ( $A_{\text{Specific}}$ ) is done for membranes by BET gas adsorption and calculations based on manufacturer information for the Bead<sub>SN,Capto™ adhere</sub>.<sup>210-212</sup> In case of the MA<sub>3DH</sub>, the nitrogen applied by the BET analysis resulted in a collapse of the hydrogel. Consequently, the obtained surface area was erroneously stated too low. The total column porosity  $\varepsilon_{\text{Total}}$  in Eq. (5.6) is determined in a breakthrough tracer experiment performed with 3% to 5% acetone in 10 mM KPi buffer using a benchtop system. The retention volume is corrected by the previously determined void volume, calculated by the first derivative of the acetone breakthrough curve.

$$\varepsilon_{\text{Total}} = \frac{V_{\text{Tracer}}}{V_{\text{MA}}} \quad (5.6)$$

Investigating the most promising stationary phase system for the given mAb aggregate separation application entails investigating different membrane backbone ligand densities. This said, the MA<sub>SC</sub> and MA<sub>3DH</sub> backbones were modified with different coupling parameters achieving three levels of ligand densities: low, medium, and high. Finally, the membrane scaffold evaluation is performed with both SC and 3DH backbone structures, investigating the IgG HMWS reduction of a feed stream containing 2.7 g/L 4 % HMWS aggregates respectively; see Table 5.2 Feedstock 2. The FT process parameters were set to pH 7 and 15 mS/cm. These runs were carried out with the coupled 3-layer MiMo membrane stamps with 2.7 cm diameter stacked in a lab module resulting in a bed volume of roughly 0.46 mL ± 0.03 mL.

#### 5.2.2.4 Initial process parameter – capacity and selectivity

The static and dynamic binding capacities are used to characterize the capture and FT processes. The static binding capacity (SBC) of component  $i$ ,  $q_i$  in Eq. (5.7) is calculated by the difference between the total flow through mass and applied feed mass of a component divided by the volume of adsorber  $V_{\text{MA}}$ . In Eq. (5.8) the component  $i$  corresponding dynamic binding capacity (DBC) of the  $q_{i,10}$  is calculated by the difference between the flow through mass and applied feed mass, both until 10% breakthrough feed concentration is reached, divided by the volume of adsorber  $V_{\text{MA}}$ .

$$q_i = \frac{c_{\text{feed},i} \cdot V_{\text{load}} - \int c_i \cdot \partial V}{V_{\text{MA}}} \quad (5.7)$$

$$q_{i,10} = \frac{c_{\text{feed},i} \cdot V_{\text{load},10} - \int c_i \cdot \partial V}{V_{\text{MA}}} \quad (5.8)$$

Application of HTS<sub>OBE</sub> mode in MA screening provides static and/or dynamic binding capacities and process optimization information<sup>209</sup>; the here evaluated process information are conductivity range and ligand suitability. The maximum binding capacity  $q_i$  in OBE mode at the initial conductivity at the given pH value is calculated by Eq. (5.9), whereas  $k$  indicates the repetitive chromatographic cycle. For accurate binding capacity determination, the MA needs to be fully saturated. The elution step is not only applied to evaluate the influence of conductivity but also prepares the next loading phase if the MiMo interactions increase.

$$q_i = \frac{1}{V_{MA}} \cdot \left( \sum_{k=1}^l \sum_{i=1}^n c_{FT\ load,i,k} \cdot V_{FT\ load,k} - \sum_{k=1}^l \sum_{i=1}^n c_{FT,i,k} \cdot V_{FT,k} \right) \quad (5.9)$$

The commercial reference stationary phase system, the Cytiva® Capto™ Adhere 1 mL column, was screened at pH values 6 - 7 and conductivities 5 – 15 mS/cm guided by the GE application note 29-0237-38AA. This said, the mAb feed solutions with 5.3 % - 6.8 % HMWS content, listed in Table 5.2 Feedstock 1, was loaded in FT mode until at least the feed absorbance was reached for 1 CV.

The binding capacity is converted to the selectivity  $S$ , in Eq. (5.10). The dynamic selectivity  $S_{10}$  is calculated applying the quotient of the binding capacity determined at 10% breakthrough concentration  $q_{10,i}$  in Eq. (5.11).

$$S = \frac{q_{HMWS}}{q_{Monomer}} \quad (5.10)$$

$$S_{10} = \frac{q_{HMWS,10}}{q_{Monomer,10}} \quad (5.11)$$

### 5.2.2.5 Refinement of process parameter – High throughput screening

The used HTS SDD MA set-up in Figure 5.3 was developed for process screening.<sup>181</sup> It comprises eight parallel MA scale-down devices fixed on a holder plate. The HTS SDD MA set-up consist of the robotic needles which penetrate through the septum port and inject the desired liquid in each scale-down device. The liquid is injected by positive pressure and flows through a sandwich consisting of fluid distributor, distribution net, three layers of flat sheet membranes, distribution net and fluid distributor. The flat sheet membrane discs have a liquid accessible diameter of 27 mm and 0.025 cm ± 0.003 μm thickness resulting in 0.46 ml ± 0.05 mL bed volume, respectively. The process fluid is collected in one row of a 12 well plate where each well can hold a maximum of 5 mL solution. Below the SDD holder plate, four movable 12-well plates to collect fractions are placed completing the SDD-HTS. The targeted average pipetted volume accuracy of less than +/- 3% is tested and confirmed with a calibration routine using five different volumes in triplicate for each device before each experiment. In case the targeted accuracy could not be reached, the software WinLissy® volume correction factors of the robotic system Lissy® 2002 GXXL/8P were adjusted.

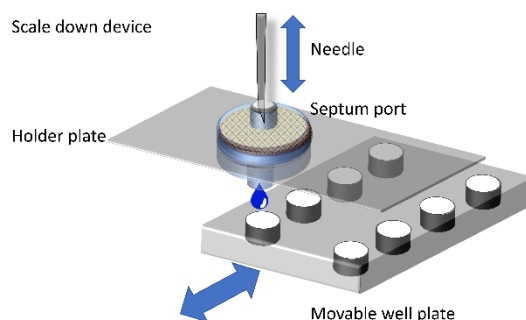


Figure 5.3: HTS MA set-up scheme; The needle injects the liquid through the septum port into the membrane device which is fixed to a holder plate. The liquid passes a fluid distributor followed by a support net and the three membrane layers. The holder plate holds eight membrane devices. Four movable well plates are used for the fractionation, while each well plate collects the fraction for two membrane devices.

For complex stationary phases or entities, the OBE mode is used to determine competitive adsorption-based displacement effects.<sup>209</sup> In this study, we apply the OBE mode to investigate the complex binding regime of MiMo ligands. The OBE can be described as the repetition of feed loading steps at different conductivities enabling the determination of the MiMo ligand binding regime, as shown in Figure 5.4. The procedure is briefly described as follows: Load of the equilibrated MA with feed at a fixed pH value of 6.5 and an initially low salt concentration, wash of the membrane with low salt equilibration buffer, elution at a high conductivity. Thereafter, the membrane is loaded with feed at the high conductivity, washed with the same conductivity and eluted at lower conductivity. Subsequent, the procedure follows a loading at the previous conductivity with decreasing conductivity of the subsequent elution step and repeat of the procedure in the desired process range. Comparing the first initial low salt loading with the last loading step at the same conductivity is used to evaluate the elution efficiency and possible path dependency. The MiMo MA storage procedure is as follows: a final elution step, a pH value shift to pH 3 to inhibit present combined binding effect, washing and subsequent CIP with 0.5 M NaOH, finalized with low salt buffer washing, containing 20% ethanol, of the MA. The procedure enables a HTS screening in which the binding regime will be determined independent of the binding regime.

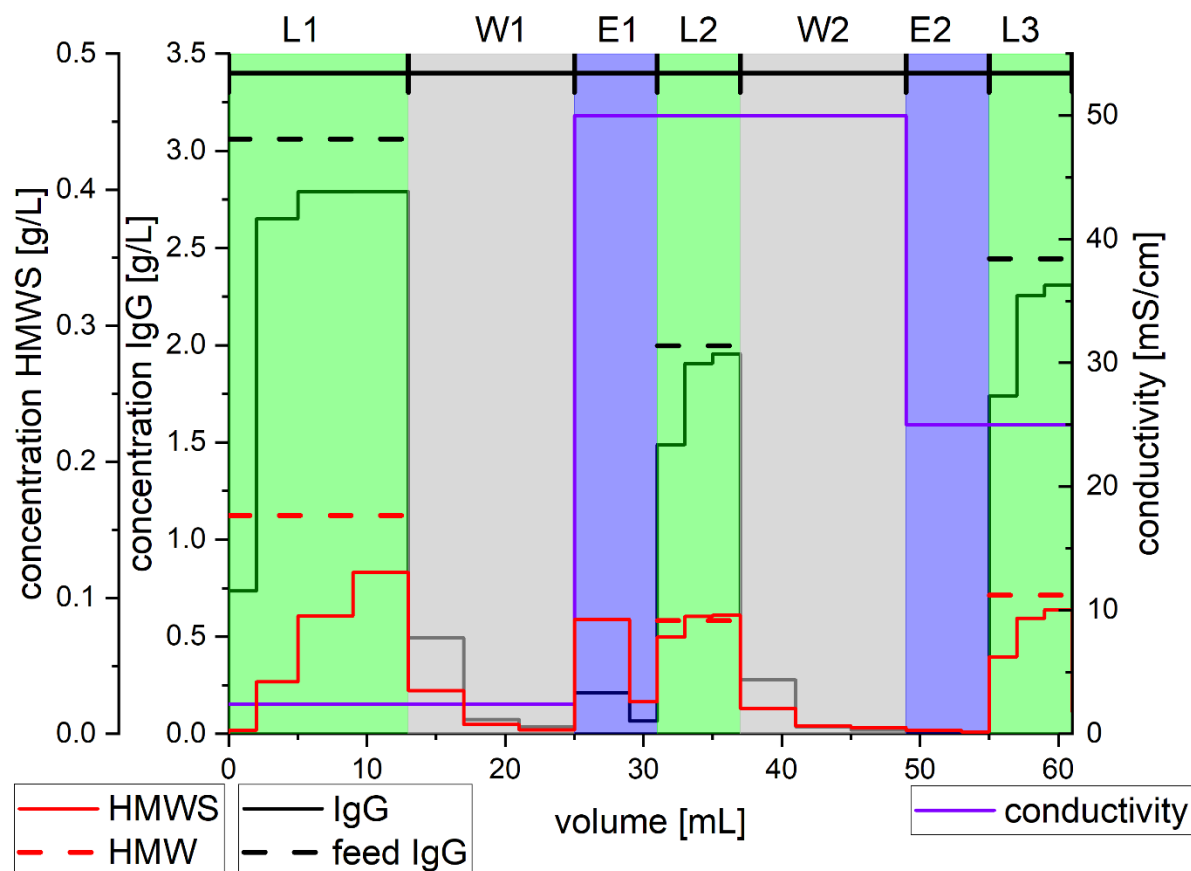


Figure 5.4: Exemplary OBE HTS MiMo MA screening; Green colored feed phase, grey colored wash phase, blue colored elution phase. The procedure follows the chromatographic steps loading, a wash phase at the same salt concentration, an elution step and thereafter a loading phase at the same conditions as the previous elution phase. The initial loading condition of the procedure is without  $(\text{NH}_4)_2\text{SO}_4$  which is equal to the last elution step. Following this, the ionic interactions and challenges elution ability can be evaluated. Thereafter, the loading phases starts with the highest 0.5 M  $(\text{NH}_4)_2\text{SO}_4$  concentration and thereafter decreasing  $(\text{NH}_4)_2\text{SO}_4$  concentration.

## 5.3 Results & Discussion

The procedure involves a saturated MA; therefore the required load volume is estimated by the maximum binding capacity. The obtained fractions, are sequentially analyzed for monomer and aggregate content using off-line SEC at 280 nm and a volumetric flow of 1 mL/min. The HTS<sub>OBE</sub> feed concentration and process parameters are listed in Table 5.2 Feedstock 4.

### 5.2.2.6 Confirmation of process parameter – Bench scale

Confirmation of the HTS<sub>OBE</sub> mode experiments for MiMo MA is carried out with the 3D hydrogel membrane coupled with ligand 1, 2, 3 and 5. All ligands are used in FT benchtop experiments with a bed volume of 4.2 mL, except of ligand 3 which was investigated in a 0.42 mL device due to the limited accessible mass of the ligand. The feed conditions were based on the HTS<sub>OBE</sub> results set to pH 7 and 15 mS/cm for the 4.7 % IgG HMWS removal, listed in Table 5.2 Feedstock 5.

## 5.3 Results & Discussion

### 5.3.1 Ligand densities – Coupling procedure

Ligand densities obtained in the coupling procedure are mainly a function of coupling conditions, namely reaction time, temperature, ligand to solvent ratio and pH. This said, to ease operations, a constant procedure for all MA used throughout this study was sought for. In an initial screening, the reaction conditions of the commercial ligand BMEA were evaluated on a Sartobind® MA<sub>3DH</sub>. The reaction time was set constant for all coupling procedures to 17 h. This period of time was selected based on an initial kinetic evaluation over 50 h using a Sartobind® MA<sub>3DH</sub> with a height of  $0.025 \pm 0.003$  cm for each coupling. After 20 h, the rate of change in ionic capacity reaches almost the asymptotic value zero.

Resulting ionic capacities were ordered into low, medium, and high value clusters. An experimental verification of the ionic capacity based on the coupling conditions let - with exception of L1 considered an outlier - to a variation coefficient of only  $\pm 3$  % between the experimental and predicted ionic capacities, see Table 5.4. In addition, replicates of the coupling procedure showed a deviation of 2 – 9 % in ionic capacity. Thus, the coupling procedure was homogenous, and the dedicated ionic capacity adjustment successfully realized.

Table 5.4: Coupling efficiency for the different ligands investigated

Ligand	Ionic capacity	$\Lambda_{\text{experimental}} / \Lambda_{\text{predicted}}$	Stationary phase system
LBMEA	medium	1.03	MA <sub>3DH,BMAE</sub>
L1	<i>medium-high</i>	<i>1.69</i>	<i>MA<sub>3DH,L1</sub></i>
L2	medium	1.09	MA <sub>3DH,L2</sub>
L3	medium	1.06	MA <sub>3DH,L3</sub>
L4	medium	1.03	MA <sub>3DH,L4</sub>
L5	medium	1.00	MA <sub>3DH,L5</sub>

### 5.3.2 Biophysical characterization of the stationary phase

A comparison in material parameter of the different stationary phase scaffolds and backbones used is given in Table 5.5. A graphical comparison is given in Figure 5.2. The MA<sub>SC</sub> expresses direct surface

binding with a potential ligand density  $\Lambda$  of 10-20  $\mu\text{mol/mL}$  and a specific surface area  $A^*$  of 2  $\text{m}^2/\text{mL}$ . These values result in a specific ligand density  $\Lambda^*$  of 10-30  $\mu\text{mol}/\text{m}^2$ . The  $\text{MA}_{3\text{DH}}$  consists of an extended 3-dimensional hydrogel on top of the membrane surface in order to generate additional binding volume. However, due to the underrated BET measurement with a specific surface area  $A^*$  of 0.8  $\text{m}^2/\text{mL}$ , the  $\text{MA}_{3\text{DH}}$  shows a high specific ligand density  $\Lambda^*$  with 30-80  $\mu\text{mol}/\text{m}^2$ . The  $\text{MA}_{\text{SN}}$  presents additional pore structure in the membrane backbone and thus results in a specific surface area  $A^*$  of 3  $\text{m}^2/\text{mL}$ . The  $\text{Bead}_{\text{SN, Capto}^{\text{TM}} \text{ Adhere}}$  column exhibits with 34  $\text{m}^2/\text{mL}$ , a resin typical high specific surface area  $A^*$  with quite low specific ionic capacity at 2 – 4  $\mu\text{mol}/\text{m}^2$ . Following the properties of the commercially available HMWS reduction application  $\text{Bead}_{\text{SN, Capto}^{\text{TM}} \text{ Adhere}}$ , the initial assumption, that for HMW reduction a lower specific ligand density  $\Lambda^*$  elevates the yield and selectivity, is supported. The different MA properties indicate that the most promising scaffolds in terms of selectivity are the  $\text{MA}_{3\text{DH}} < \text{MA}_{\text{SN}} < \text{MA}_{\text{SC}}$  and for binding capacity  $\text{MA}_{\text{SN}} \leq \text{MA}_{3\text{DH}} < \text{MA}_{\text{SC}}$ . Alongside the purely physical consideration of the backbone, that of the target molecule must also be considered. The hydrodynamic diameter of a mAb is in the range of 11 nm, depending on the surrounding conditions. As stated earlier, a pore/protein diameter below 10 is leading to size exclusion and thus inefficient binding capacity.<sup>110,145-147</sup> Therefore, the  $\text{MA}_{\text{SN}}$  adsorber pore size of 10 nm is too small for efficient protein binding and is neglected as a possible backbone.

Table 5.5: Overview and comparison of different membrane backbones to GE adhere resin. The values are based on manufacturer information.

Stationary Phase	Membrane			Bead
Backbone structure / Ligand coupling	Surface (SC)	3D Hydrogel (3DH)	Double Porous (SN)	Double Porous (SN)
Pore diameter [ $\mu\text{m}$ ]	3-5 <sup>2</sup>	3-5 <sup>2</sup>	3-5 <sup>2</sup>	0.1 <sup>2</sup>
$\Lambda$ [ $\mu\text{mol}/\text{mL}$ ]	10-20 <sup>2</sup>	20-60 <sup>2</sup>	50-120 <sup>2</sup>	80-110 <sup>2</sup>
$q_{10}$ [ $\text{mg}/\text{mL}$ ]	10 <sup>2</sup>	40 <sup>2</sup>	50 <sup>2</sup>	75 <sup>2,4</sup>
$A^*$ [ $\text{m}^2/\text{mL}$ ]	0.8 <sup>1</sup>	0.8 <sup>1</sup>	3 <sup>1</sup>	34 <sup>3</sup>
$\varepsilon$ [-]	0.7-0.8 <sup>1</sup>	0.7-0.8 <sup>1</sup>	0.8-0.9 <sup>1</sup>	0.8-0.99 <sup>3</sup>
$\Lambda^*$ [ $\mu\text{mol}/\text{m}^2$ ]	10-30	30-80	16-40	2-4
Indices	1 = BET analysis / benchtop tracer experiments 2 = Manufacturer information / Manufacturer website 3 = Calculated based on the pressure drop and particle size in the Cytiva© capto® adhere manual 4 = Polishing of monoclonal antibodies using Capto™ adhere ImpRes in bind and elute mode Application note 29-0273-38 AA			

In summary, the theoretical evaluation reduces the experimental effort by one third, indicating that the  $\text{MA}_{\text{SC}}$  is a promising MA backbone and the  $\text{MA}_{3\text{DH}}$  needs further investigation due to eventual misleading BET analysis.

## 5.3 Results & Discussion

### 5.3.3 Initial process parameter – capacity and selectivity

Following the biophysical characterization, the MA<sub>3DH</sub> was selected for process range evaluation. The additional specific surface area of the MA<sub>3DH</sub> hydrogel should exhibit a higher binding capacity when compared to the MA<sub>SC</sub>.

The best selectivity is achieved at pH 6 with low ionic strength and at pH 7 with increased ionic strength, see Table 5.6. Comparing the MA<sub>3DH,BMEA</sub> process parameter at pH 6 and 7 at 5 mS/cm and 15 mS/cm, respectively, reveals an HMWS binding capacity almost doubled with a selectivity only 1.4 times lower at pH 7. Therefore, all further experiments were conducted at pH 7 at increased ionic strength. The reference system Bead<sub>SN,Capto™ Adhere</sub> presents an advantageous dynamic selectivity  $S_{10}$  with high conductivity and decreased pH. However, the higher HMWS binding capacity at pH 7 and increased ionic strength corresponds to data obtained for MA<sub>3DH,BMEA</sub>. Thus, further screening is set to pH 7.

Table 5.6: Comparison run with BMEA coupled Sartobind® MA<sub>3DH,BMEA</sub> with medium ionic capacity and a 1 mL column Bead<sub>SN,Capto™ Adhere</sub>, experimental feed conditions refer to Table 2 Feedstock 1.

Stationary phase [-]	Feedstock [-]	pH [-]	Ionic strength [mS/cm]	$q_{mAb,10}$ [g/L]	$q_{HMWS,10}$ [g/L]	$S_{10}$ [-]
MA <sub>3DH,BMEA</sub>	1	6	5	0.3	0.23	0.69
MA <sub>3DH,BMEA</sub>	1	6	15	0.2	0.07	0.30
MA <sub>3DH,BMEA</sub>	1	7	15	0.9	0.43	0.49
Bead <sub>SN, Capto™ Adhere</sub>	1	6	5	8.6	1.38	0.16
Bead <sub>SN, Capto™ Adhere</sub>	1	6	15	3.0	0.70	0.23
Bead <sub>SN, Capto™ Adhere</sub>	1	7	15	16.5	1.82	0.11

As the MA<sub>3DH,BMEA</sub> exhibiting medium ionic capacity were found to express the highest selectivity, high capacity needs to be assured for economic industrial applications. This said, for the given separation challenge – HMWS vs. mAb – a high HMWS binding capacity and selectivity needs to be assured. We thus evaluated the MA<sub>SC,BMEA</sub> and MA<sub>3DH,BMEA</sub> in comparison to the commercial Bead<sub>SN, Capto™ Adhere</sub>. Aim of this study lies in a high selectivity factor of the chosen membrane. The obtained results are presented in Table 5.7. It was found that the MA<sub>3DH,BMEA</sub> has the highest dynamic selectivity  $S_{10}$  (min. 0.02; max. 0.74) for a medium ionic capacity. In contrast, the MA<sub>SC,BMEA</sub> presents with 0.05 and 0.07 no significant changes in dynamic selectivity with increasing ionic capacity. In addition, the MA<sub>SC,BMEA</sub> dynamic selectivity  $S_{10}$  is significantly lower than that of the MA<sub>3DH,BMEA</sub>. For the commercial reference, a 1mL column Capto™ adhere, a  $S_{10}$  value of 0.2 was found. The lower selectivity of the MA<sub>SC,BMEA</sub> might be induced by different ligand distances or ligand accessibilities when compared to the MA<sub>3DH,BMEA</sub>, indicating different surface areas for the MA<sub>3DH,BMEA</sub> than expected by the BET measurement. Following the obtained dynamic selectivity ( $S_{10}$ ) value of only 0.05-0.07, the MA<sub>SC</sub> is dismissed as potential backbone in further investigations. The range of a 1.6-fold difference in the  $S_{10}$  value obtained for the Sartobind® 3DH membranes shows a clear benefit of custom-made membrane systems with different ligand densities tailored to a given separation problem. All further chemical ligand coupling is carried out based on the developed procedure targeting a medium ionic capacity expressing the highest  $S_{10}$  value.

Table 5.7: Comparison of a Sartobind® MA<sub>3DH</sub>, MA<sub>SC</sub>, and the commercial Bead<sub>SN,Capto™</sub> adhere. The adsorber ligand applied is the BMEA MiMo ligand. Experimental feed conditions refer to Table 5.2 Feedstock 2 and 3.

Stationary phase [-]	Feedstock [-]	pH [-]	Ionic capacity [mmol/mL]	$q_{\text{mAb},10}$ [g/L]	$q_{\text{HMWS},10}$ [g/L]	$S_{10}$ [-]
MA <sub>3DH</sub> ,BMEA	3	7	Low	0.005	0.001	0.02
MA <sub>3DH</sub> ,BMEA	3	7	Medium	0.202	0.150	0.74
MA <sub>3DH</sub> ,BMEA	3	7	High	1.250	0.563	0.45
MA <sub>SC</sub> ,BMEA	2	7	Low	0.027	0.002	0.07
MA <sub>SC</sub> ,BMEA	2	7	Medium	0.081	0.004	0.05
Bead <sub>SN,Capto™</sub> Adhere	3	7	High	10.550	2.156	0.20

The experimental stationary phase evaluation supports the assumption that the MA<sub>3DH</sub> BET measurement is misleading when comparing the binding capacity of MA<sub>SC</sub> and MA<sub>3DH</sub> at similar ionic capacities. This said, at comparable specific surface areas and ionic capacities the resulting binding capacities should be analogous. Consequently, the higher MA<sub>3DH</sub> binding capacities are enabled by more accessible ligands which implies a higher surface area compared to MA<sub>SC</sub>. Following this, the results show that with increasing MA specific surface area the selectivity increases. A lower selectivity with increased binding capacity at the highest specific surface area for Bead<sub>SN,Capto™</sub> Adhere when compared to the MA<sub>3DH</sub> might be related to the higher ionic capacity.

The initial experimental investigation that followed the biophysical characterization avoided the incorrect backbone selection by considering knowledge-based gaps. In addition, the best MA backbone was identified, and a first process parameter space was evaluated.

#### 5.3.4 Refinement of process parameter – High throughput screening

As mixed mode ligands express a fine interplay between electrostatic and hydrophobic interactions, the used salt concentration during processing plays a vital role for the separation performance. We thus applied a screening based on the OBE strategy applying different conductivities during binding.<sup>209</sup>

In Figure 5.5, the HTS SDD OBE results for each system (Table 5.4) MA<sub>3DH,L1-L5</sub> are presented. IgG and IgG HMWS binding capacities follow comparable trends. With increasing conductivity from 2 mS/cm to 5 mS/cm, the binding capacity increases and subsequently decreases with further increasing conductivity. This said, in repulsion mode the ionic repulsive forces decrease with increasing salt concentration while the hydrophobic interaction increase. However, as ionic forces decrease, the hydrogel layer/volume formation is weakened, to the point of collapsing. Following this, the additional surface area and accessible ligands are reduced with increasing salt concentration. These opposing effects are responsible for the observed binding capacity course: first increased hydrophobic induced and thereafter based on reduced surface area decreasing binding capacity. In general, all MA exhibit an IgG monomer binding capacity above 15 mg/mL at 5 mS/cm. MA<sub>3DH,L1</sub> shows a higher salt tolerance for IgG monomer when compared to the other ligands. The higher IgG monomer binding capacity might be correlated to the ~ 1.7 times higher ionic capacity of MA<sub>3DH,L1</sub> (Table 5.4). MA<sub>3DH,L1</sub> and MA<sub>3DH,L2</sub> show salt tolerant HMW binding capacities while MA<sub>3DH,L3</sub> to MA<sub>3DH,L5</sub> exhibit only low salt tolerance HMWS binding capacities. The investigated salt concentrations may be too low to promote the higher hydrophobic interaction of MA<sub>3DH,L3</sub> to MA<sub>3DH,L5</sub>, represented by their log P value. However,

### 5.3 Results & Discussion

the HTS screening presents two membrane adsorber with salt tolerant binding capacity: MA<sub>3DH,L1</sub> and MA<sub>3DH,L2</sub>. During experimentation, all mass balances closed to a value of over 90% except for MA<sub>3DH,L5</sub> with 77 %. Considering the high deviation of MA<sub>3DH,L5</sub> in the HTS experiments, but also the target hydrophobicity range, MA<sub>3DH,L5</sub> was included in the confirmation test plan. However, the experimental elution needs to be optimized with an average of 1.8 times higher binding capacity when compared to the two low conductivity at the beginning and end of the procedure. This was expected due to the complex screening and elution regime as well as analytical error.

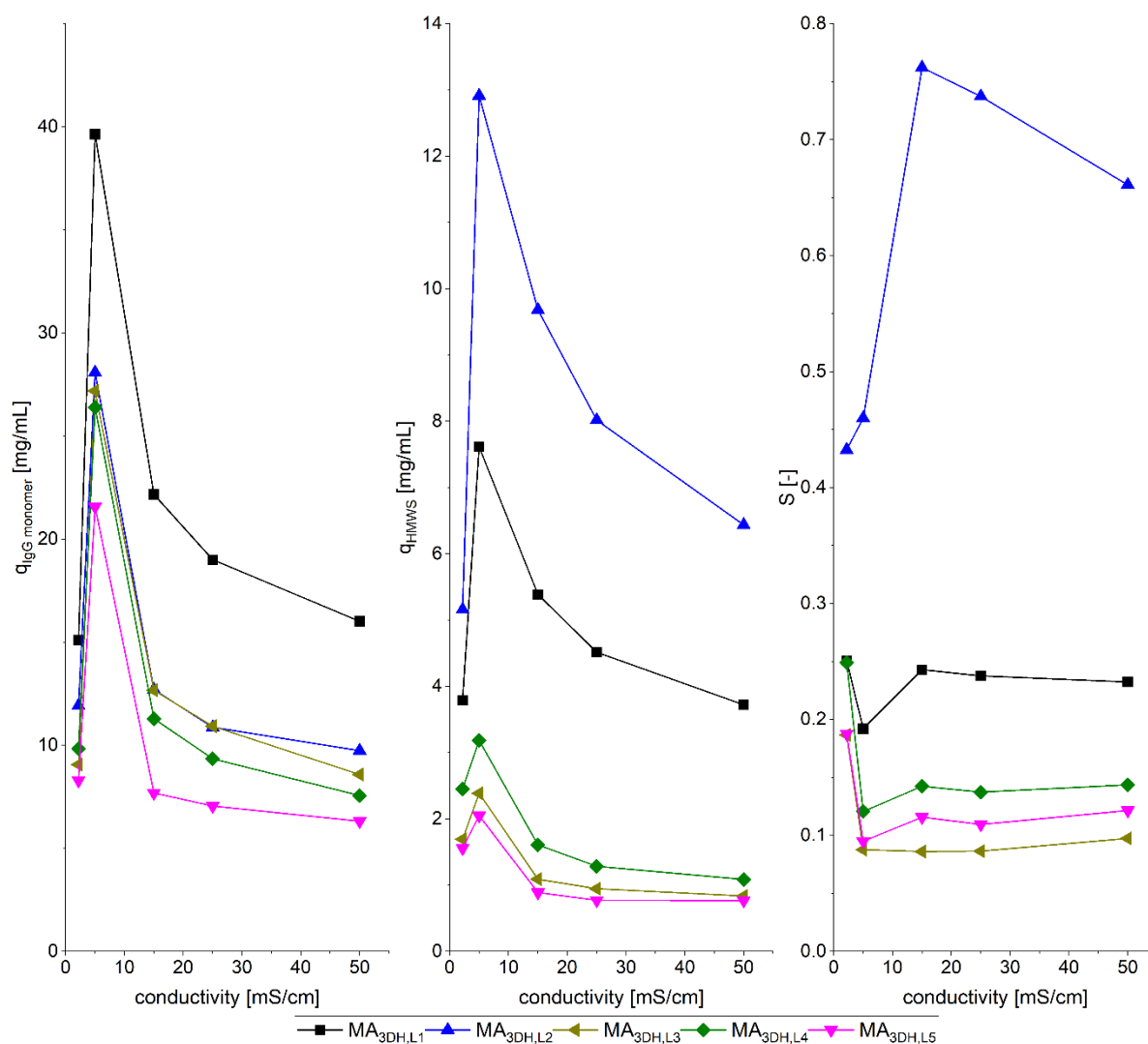


Figure 5.5: HTS SDD OBE screening results for the different Membrane Systems MA<sub>3DH,L1-L5</sub> at pH 7 and varying conductivity / salt concentration. The binding capacity for IgG monomer is presented in the left graph and its HMWS binding capacity in the middle graph. For IgG monomer binding capacity, all ligands show an increased binding capacity from 2 mS/cm to 5 mS/cm conductivity. Furthermore, all ligands follow the same trend of reduced binding capacity at increasing conductivity. Selectivity S is depicted in the right graph. The selectivity decreases with increasing hydrophobic ligands. MA<sub>3DH,L2</sub> shows the highest selectivity in general and with respect to the salt concentration.

The value of selectivity  $S$  ranks the HMWS reduction ability of the ligands in Table 5.8. Except for L2, the selectivity of all ligands is almost independent of the conductivity - except for 5 mS/cm. The selectivity decrease at 5 mS/cm is correlated to the higher binding capacity of IgG and HMWS which can be observed in Figure 5.5. Following this, L1 is promising for an application in B&E mode. Comparing L1 and L2, the differences are predominant in the range from 5 mS/cm to 20 mS/cm. L1 selectivity product decreases from 5 mS/cm to 20 mS/cm while L2 shows an optimum at 15 mS/cm. Comparing HMWS binding capacity and  $S_{10}$  suits different process strategy evaluations. The process feasibility is ranked in descending order: ligands L2 < L1 < L4 < L5 < L3, see Table 5.8. The most promising ligands for the HMWS reduction are L1 and L2. Considering the usual high productivity of MA when applied in FT mode, L2 is the preferred choice at a pH of 7.

Table 5.8: System comparison between the different Ligand hydrophobicity (log P) and selectivity  $S_{10}$  at 15 mS/cm.

Stationary phase [-]	Feedstock [-]	pH [-]	Ionic strength [mS/cm]	$q_{mAb,10}$ [g/L]	$q_{HMWS,10}$ [g/L]	Log P [-]	$S_{10}$ [-]
MA <sub>3DH,L1</sub>	4	7	15	22.2	5.4	2.1	0.24
MA <sub>3DH,L2</sub>	4	7	15	12.7	9.7	2.5	0.76
MA <sub>3DH,L3</sub>	4	7	15	12.7	1.1	3.2	0.09
MA <sub>3DH,L4</sub>	4	7	15	11.3	1.6	3.7	0.14
MA <sub>3DH,L5</sub>	4	7	15	7.7	0.9	4.1	0.12

In Figure 5.6, a possible correlation between log P value, binding capacity and selectivity is presented. The IgG binding capacity can be simplified described as a linear equation, increasing log P value results in a decreased binding capacity. Based on the presented screening results, a log P value-based hydrophobicity between 2.1 and 3.1 (L2 = 2.53) presents a local optimum for a salt tolerant HMWS binding capacity and selectivity. The screening parameters and five different ligands are noted in Table 5.8.

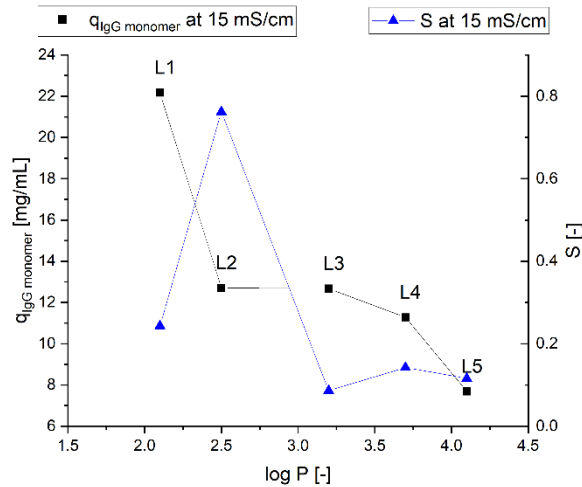


Figure 5.6: HTS SDD OBE screening results for the different Membrane Systems MA<sub>3DH,L1-5</sub> represented by the partitioning coefficient (log P) at pH 7 and a conductivity of 15 mS/cm. The IgG monomer binding capacity can be simplified described as a linear equation, decreasing with increasing log P value. However, the selectivity or HMWS binding capacity indicates a nonlinear correlation with the log P value, for the presented screening a log p value between 2.1 and 3.1 presents a local optimum.

### 5.3 Results & Discussion

Summarizing the sequential strategy, accounting for possible knowledge-based gaps reduced the backbone selection by one and avoided the incorrect backbone selection. In addition, the best MA backbone was identified, and a first process parameter space evaluated in the initial screening. Thereafter, the ligand screening revealed in addition to the most promising ligands a correlation between the ligand property and the target process parameters, a description of the feed variation to be worked out provided. However, incorporation of this information into the platform library leads to a possible evaluation of new MiMo ligands in the future before binding experiments need to be performed.

#### 5.3.5 Confirmation of process parameter – Bench scale

In order to confirm the HTS results L1, L2, L3 and L5 to MA<sub>3DH</sub> were coupled and investigated into using FT benchtop experiments in Figure 5.7. All ligands were screened in FT benchtop experiments with a bed volume of 4.2 mL, except for MA<sub>3DH,L2</sub> which was investigated with a 0.42 mL device. For L2 the ligand amount available was limited and thus a coupling for a 4.2 mL bed volume device was not possible. Reference column used was a 1 mL column Bead<sub>SN,Capto™</sub> Adhere. In Figure 5.7 (left and center) the feed normalized concentration profiles of the FT confirmation experiments are shown. The IgG monomer and HMWS breakthrough concentration at 1% sequence for the different systems investigated is: MA<sub>3DH,L3</sub> ≤ MA<sub>3DH,L5</sub> < MA<sub>3DH,L1</sub> ≤ Bead<sub>SN,Capto™</sub> adhere < MA<sub>3DH,L2</sub>. The result confirms the HTS screening results in which the binding capacity of MA<sub>3DH,L3</sub> and MA<sub>3DH,L5</sub> is low for IgG monomer and its HMWS. The binding capacity of MA<sub>3DH,L2</sub> for IgG monomer is higher than for MA<sub>3DH,L1</sub> which was not predicted by the HTS. This deviation may be induced due to the differences in the bed volume. The FT reduction between HMWS feed and HMWS pool content is shown in Figure 5.7 right hand site. Ligand 1 is based on the log P value comparable to the column Cytiva® adhere™ and shows also similar HMWS breakthrough concentration in the product pool. The pool concentration profile between the different ligands confirms the HTS<sub>OBE</sub> result in terms of ligands HMW reduction potential.

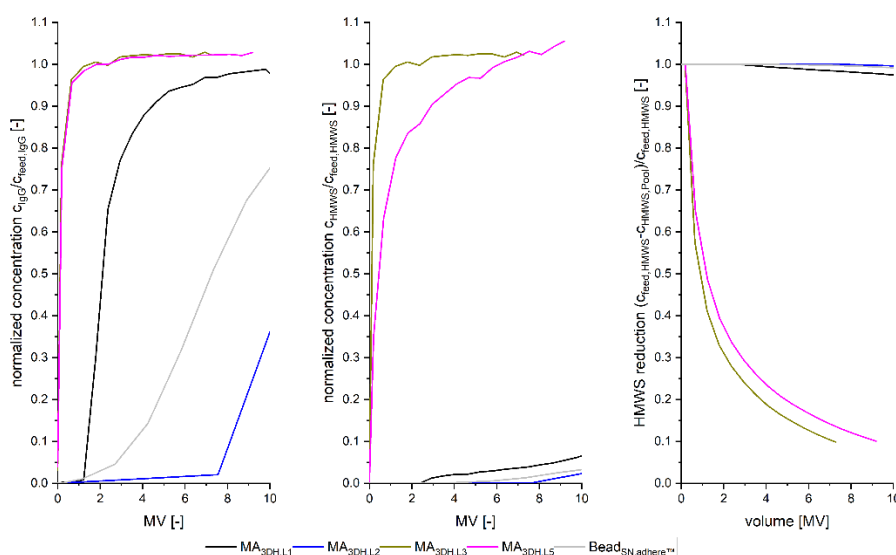


Figure 5.7: Confirmation experiments at pH 7 and 150 mM salt concentration for HMWS removal with MiMo MA. The feed normalized breakthrough concentration is presented for IgG on the left-hand site and its HMWS in the center. The right-hand site graph shows the calculated HMWS product pool concentration. Investigating the IgG and HMWS breakthrough sequence for the different systems shows: MA<sub>3DH,L3</sub> = MA<sub>3DH,L5</sub> < MA<sub>3DH,L1</sub> = Bead<sub>SN,Capto™</sub> adhere < MA<sub>3DH,L2</sub>. The FT reduction between HMWS feed and HMWS pool content is shown right hand site. Considering a HMWS reduction process step, the HMWS reduction in the product pool is reduced last for L3, L5, L1, Capto™ Adhere and L2. MA<sub>3DH,L5</sub> = MA<sub>3DH,L3</sub> < MA<sub>3DH,L1</sub> = Bead<sub>SN,Capto™</sub> adhere < MA<sub>3DH,L2</sub>.

## 5.4 Conclusions

The needs in biopharmaceutical PD are time, cost and reliability while facing different stationary phase system including various scaffolds, backbones and interactions leading to different advantageously processing strategies in chromatography. In fact, there are several new applications available, and emphasis is placed on the fact that platform knowledge needs to be kept up to date to remain competitive. These challenges have been addressed by a case study. The case study included the investigation for the IgG HMW reduction of five different MiMo ligands, three different ionic capacities and three different backbones. This strategy combined the knowledge on ligand coupling and ligand properties, experimental and prior knowledge-based backbone assessment, and is finalized by a screening using a HTS SDD OBE methodology.<sup>209</sup> Based on a thorough chemical coupling study, three different ligand densities were investigated for the IgG HMW reduction. These examinations led to an IgG HMW reduction optimum at medium ionic capacity. Following this, an efficient platform library requires that different ionic capacities are considered. The initial biophysical characterization of the stationary phases helped to reduce the experimental effort by one third. Initial experimental stationary phase evaluation avoided the incorrect backbone selection while providing the best MA backbone and a process parameter range. Thereafter, the ligand HTS revealed in addition to the most promising ligands a correlation between the ligand property and the target process parameters, when incorporated into a platform library enables MiMo ligand evaluation without experiments. Thereafter, the approach is confirmed by benchtop experiments and results in an identified chromatographic media which enables 2-3 MV times later IgG HMWS breakthrough (0.46 mL device) when compared with the reference bead (1 mL device). Comparing a ligand with similar log p values at a MA<sub>3DH</sub> (4.3 mL) with a Bead<sub>SN, Capto™ adhere</sub> (1 mL device) shows similar process performance. In addition, at identical attached ligand, membrane adsorber showed a higher aggregate removal potential when compared to the bead backbone. In summary, the case study showed a time and material reduced living platform library workflow with the demonstration of important chromatographic media parameters.

### Acknowledgment

The authors wish to acknowledge the Membrane Chromatography and Modification team. Our thanks also go to the BioProcessing Group for providing the mAb feed solution. In addition, we especially acknowledge the students Sebastian Hegner and Niklas Eisele for their dedicated effort and excellent laboratory work. In addition, we especially acknowledge Christopher Belisle and team from BioRad Laboratories for providing the MiMo ligands.

## 6 Full train product development from lab 2 production procedure – incorporating a living library with mechanistic modeling - from HTS Scale to pilot scale of Membrane Chromatography in aggregate Removal of Monoclonal Antibodies

Dominik Stein<sup>1,2</sup>, Volkmar Thom<sup>2</sup>, Jürgen Hubbuch<sup>1</sup>

<sup>1</sup> Karlsruhe Institute of Technology (KIT), Institute of Process Engineering in Life Sciences, Section IV: Biomolecular Separation Engineering, Karlsruhe, Germany

<sup>2</sup> Sartorius Stedim Biotech GmbH, August-Spindler-Str. 11, D-37079 Goettingen

### Abstract

The recent global SARS-CoV-2 pandemic intensified the ongoing trend to accelerate product development (PD) in the biopharmaceutical industry. Following this, biopharmaceutical process development is challenged by time, cost, and reliability. During the development of chromatographic processes, these targets are challenged by various possible process parameters and screening techniques. Empirical approaches have addressed these challenges by performing numerous wet lab experiments in the past. As a result, the process development toolbox has evolved from static batch experiments, high throughput screening, and benchtop experiments to statistical and mechanistic modeling to more dynamic assessments. In this paper, we introduce a PD procedure facilitating a guide to transit from partially connected development tools to a fully integrated process development living library approach. The investigated process tools are linked by three case studies in which mechanistic modeling enables the preservation and further investigation of process information. Initially, lab modules are investigated, newly developed, and successfully transferred in scale as well as fluid flow differences. The second case study presents the determination of apparent SMA isotherm parameter from historical HTS data for an IgG HMWS separation. Finally, the third case study successfully transferred the achieved process information from a 0.46 mL small-scale device with axial fluid flow to a 150 mL pilot scale device in radial fluid flow with a deviation in DBC below 10 %.

### 6.1 Introduction

The supply of drugs in a short time and cost sustainable for the individual or the social system is a constant demand for the pharmaceutical manufacturer. Based on the recent global SARS-CoV-2 pandemic, product development (PD) acceleration in the biopharmaceutical industry was urged.<sup>8-11</sup> In addition to the demand of a potent vaccine in a short time, future challenges such as market competition by alternative drugs or generic products, in general, must be considered. This said, the PD is challenged by time, regulatory requirements, market competition, and for the typically applied unit operation chromatography, a variety of stationary phases, processing modes, ligands, and process parameters.<sup>35,49,213</sup>

Pharmaceutical manufacturing typically consists of upstream – cell cultivation – and downstream – product purification.<sup>12,16,17</sup> This said, the product purification, among other unit operations, typically incorporates one to three chromatography purification steps.<sup>21,22,93</sup> The development of a

chromatography unit operation challenges PD in selecting various operation modes, stationary phases, interaction, and process parameters. These challenges have been addressed in the past by empirical approaches by performing numerous benchtop experiments on the milliliter scale. Thereafter, the needed amount of material, feed solution, and time was reduced by developing small-scale static experiments and applying statistical experimental evaluation such as Design of Experiments (DoE).<sup>57,214,215</sup> These small-scale experiments were further optimized by applying robotic platforms for high throughput screening (HTS) evaluating process range determination, see Figure 6.1. However, the rather static process range determination was complemented in performance screening by applying robotic column experiments assessing dynamic effects. The process range determination and performance screening could then effectively evaluate various stationary phases. Following this, the reduced amount of suitable stationary phases would then be investigated within the detailed benchtop experiments. The detailed experiments typically provide production comparable sensor signals such as UV, conductivity, and pH values. Following the detailed experiments, the scale-up is performed, either to pilot scale or directly to production scale.

The empirical approach has been optimized, incorporating a library approach.<sup>17,34,169</sup> In detail, the different methods mentioned are applied to characterize different stationary phases, ligands, and operation modes. The successful candidates and process parameters are transferred to a library incorporating all needed information. Doing so reduces the process development effort for equal or similar molecules due to the existing parameter space, stationary phase, and all manufacturing procedures. This said, cleaning procedures, standard operation procedures (SOP), and training effort is drastically reduced. However, the drawback of a library approach is the self-limitation to investigating candidates and processing modes mentioned early by us.<sup>216</sup> This drawback could be overcome with a truly living library, including comparable data for different stationary phases, investigation methods, operation modes, and prior knowledge. Mechanistic modeling could provide the missing link with its possibility to derive digital twins of different scales while preserving the information in mathematical equations and parameters.

Recently, mechanistic modeling has gained interest in pharmaceutical PD.<sup>1-6</sup> The wet lab reduced simulative approach promises, after correct parameter determination, the development of a digital twin allowing an easier on up to direct scale-up. In addition to the established simulative approaches, which investigate molecular interaction, the current mechanistic modeling research focuses on simplification, methodology, and process knowledge investigations.<sup>1,4</sup> Furthermore, new software is available broadening the distribution of mechanistic modeling into pharmaceutical PD.<sup>217,218</sup>

The simplification of mechanistic modeling is also connected to the newly available software, which incorporates fluid dynamic investigation guidelines and methods to reduce the effort in Isotherm determination. Fluid dynamic investigations focus on acetone tracers, while more sophisticated tracers with different sizes are mentioned for sophisticated stationary phases or separations.<sup>21,102,117,120</sup> The isotherm determination is eased in a few benchtop experiments, e.g., by applying the Yamamoto method.<sup>164</sup> This said, the experimental reduction of benchtop experiments might neglect small-scale set-ups with fewer experimental details. However, the proof of the previously mentioned benefits is up to date, limited to a few success stories.

In this study, we introduce a PD procedure facilitating a guide to transit from partially connected development tools to a fully integrable process development living library approach. The process tools are linked by three case studies in which mechanistic modeling enables the preservation and further

## 6.1 Introduction

investigation of information. Following this, the procedure presents a workflow from small-scale to production guiding through fluid dynamic and adsorption parameter determination. In the first case study, chromatographic devices are developed and characterized. In addition, the devices are successfully transferred in scale, considering fluid flow differences. Thereafter, the second case study presents the determination of apparent SMA isotherm parameter from historical HTS data for an IgG HMWS separation. Finally, the third case study successfully transferred the achieved process information from a 0.46 mL small-scale device with axial fluid flow to a 150 mL pilot scale device with radial fluid flow.

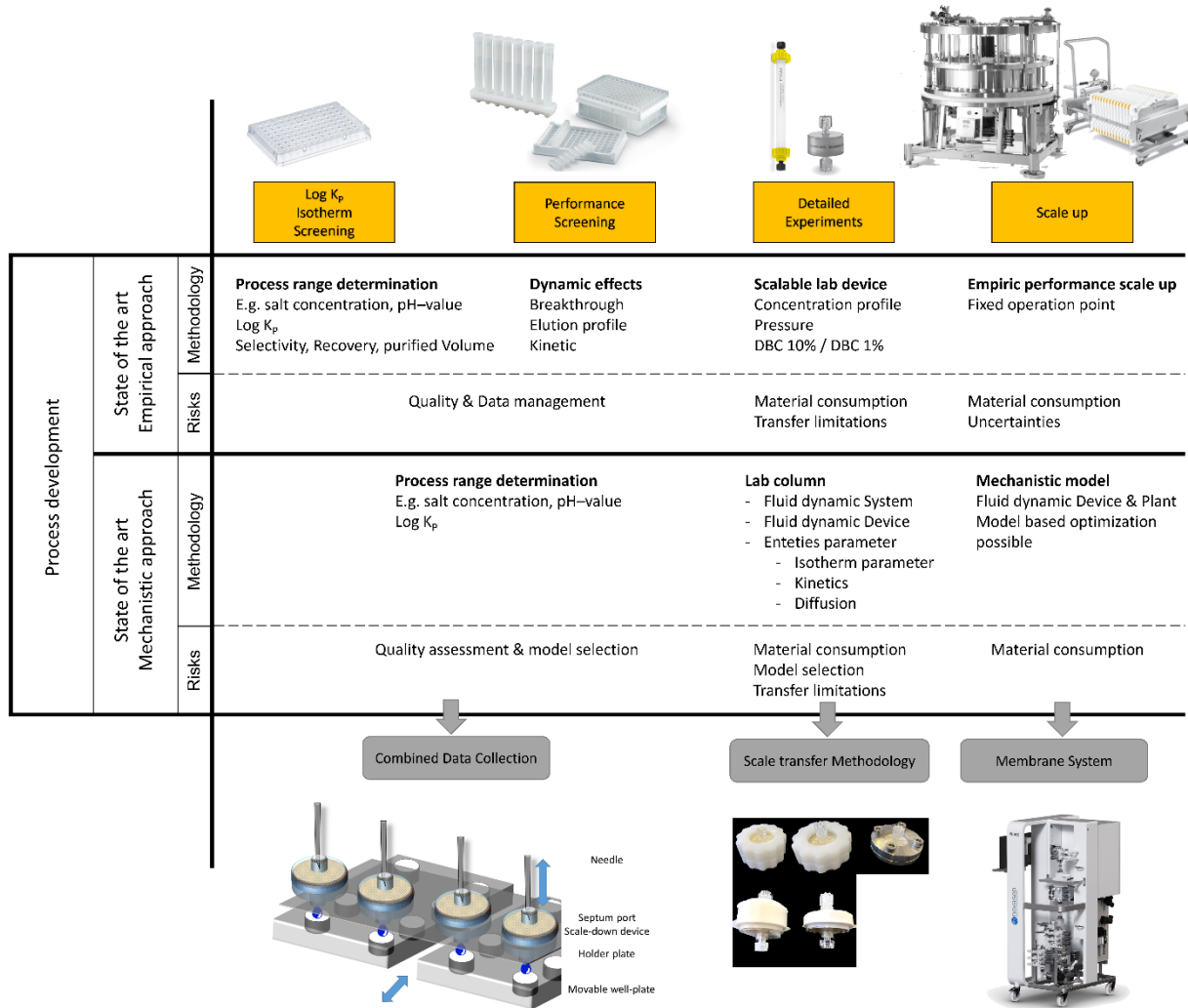


Figure 6.1: Schematic process development tools for empirical and mechanistic modeling procedures. The graphics highlight typical methodologies and risks of the procedures. In addition, the different screening scales from lab to production are presented. Finally, the challenges in mechanistic modeling incorporating a digital twin for scale-up are presented at the bottom figure, along with an eventual approach to address these challenges.<sup>181</sup>

## 6.2 Materials and Methods

The applications for material used in this study are subdivided into the following: buffer preparation, feed preparation, full train product development from lab to production, analytics, and data handling as well as mechanistic modeling (MM) including a full train scale-up approach from lab to production.

### 6.2.1 Buffer preparation

The buffer was prepared by dissolving buffer salts in purified water produced by the arium<sup>®</sup> lab water purification system manufactured by Sartorius Stedim GmbH. Weighing of the components was performed on a Sartorius Master<sup>pro</sup> LP 12000S balance or a Sartorius Expert LE225D-OCE balance provided by Sartorius Lab Instruments GmbH. Salts used were: Sodium chloride (NaCl), hydrochloric acid (HCl), glycine, sodium acetate (NaAc), acetic acid, dipotassium hydrogen phosphate, potassium dihydrogen phosphate, Tris-(hydroxymethyl)-aminomethane (TRIS), di-sodium hydrogen phosphate dihydrate and sodium dihydrogen phosphate dihydrate from Carl Roth, tri-sodium citrate dihydrate purchased from VWR Chemicals, citric acid monohydrate supplied from Alfa Aesar, ethanol purchased from Sigma Aldrich and acetone supplied from Carl Roth GmbH & Co. KG. Sodium hydroxide (NaOH) or hydrochloric acid (HCl) was used to adjust the pH. Each buffer and feed solution are prefiltered through a 0.45 µm Sartopure<sup>®</sup> and a 0.2 µm Sartolab<sup>®</sup> RF vacuum filter supplied by Sartorius Stedim Biotech GmbH.<sup>181</sup>

### 6.2.2 Feed preparation

The CHO-fermented monoclonal antibody was an internal Sartorius Stedim Biotech GmbH feed solution. Further purification was done by using a MabSelect™ Sure™ lab column (5 cm diameter, 192 mL volume) provided by GE Healthcare and by an Äkta Prime™ system. The eluate contained about 18 g/L mAb and a mAb aggregate level of about 0.5-1%. Enrichment of the aggregate content of the clarified mAb solution to 2-6% was done by a pH shift process. Aggregation by a temporary pH shift is a commonly used method for aggregation.<sup>64,174,219</sup> After diluting the 0.1 M pH 3 glycine-buffered mAb solution three times with KPi buffer, the pH was adjusted to 3 with 0.5 M HCl. The aggregation time was set to 3 h with stirring at 150 rpm. Afterwards, the pH was readjusted to pH 7 with 0.5 M NaOH, which resulted in an aggregate content between 6-12 %. Afterwards, the aggregated mAb solution was diafiltrated against the desired buffer using the Sartoflow<sup>®</sup> Smart system (Sartorius Stedim Biotech GmbH) using a 200 cm<sup>2</sup> Sartocoon<sup>®</sup> Slice 200 Hydrosart<sup>®</sup> 30 kDa cassette. Diafiltration was carried out until the buffer conductivity and/or pH of the diafiltered solution reached a constant value. These solutions exhibited a mAb concentrations of up to 10 g/L. The final feed solutions were prepared by diluting of the 10 g/L aggregated mAb solution with the corresponding buffer. Each buffer at each pH was prepared using 0 mol/L and 1 mol/L NaCl. The pH and conductivity (CD) were adjusted by mixing the solution with the corresponding buffer, followed by an incubation period of one hour at room temperature. For the screening procedures, different protein feed solutions were used: (1) 1-5 g/L bovine serum albumin dissolved in KPi buffer at pH 7 with an NaCl concentration of 0-0.3 mol/L, (2) 1-3 g/L lysozyme dissolved in 10 mmol KPi buffer at pH 7 with an NaCl concentration of 0-0.3 mol/L and (3) 1-6 g/l diafiltered mAb solution with a 0-0.3 mol/L NaCl concentration.<sup>181</sup>

## 6.2 Materials and Methods

### 6.2.3 Full train product development from lab to production procedure

Developing a living library approach, including mechanistic modeling, requires a dedicated procedure and tools to include new but also historical data. In addition, the experimental set-ups which provide scale-up relevant parameters need to be incorporated. Consequently, static experiments will be considered in modeling parameters such as isotherms, while dynamic experiments need a more sophisticated approach. Set-ups with combined effects can be investigated up to a digital twin representation to avoid misinterpretation.

The proposed mechanistic modeling procedure here investigates different experimental set-ups and scales applying MA. Following this, the proposed procedure is comparable to state-of-the-art approaches in mechanistic modeling, separating fluid dynamics and thermodynamics/adsorption.<sup>1,15,61,68,99,181</sup> In Figure 6.2, a schematic representation of the model library development is presented. In addition to the general model development<sup>113,114,120</sup>, the approach focuses on scale-up model development Figure 6.2 A) and incorporation of prior knowledge with reduction of the non-significant parameter in Figure 6.2 B). Assessing the relevant parameters would reduce the effort and enable the focus on in-depth needed parameters. Following this, the currently time-consuming mechanistic model development (parameter determination and validation) could be reduced by reusing standardized models preserved in a living library.

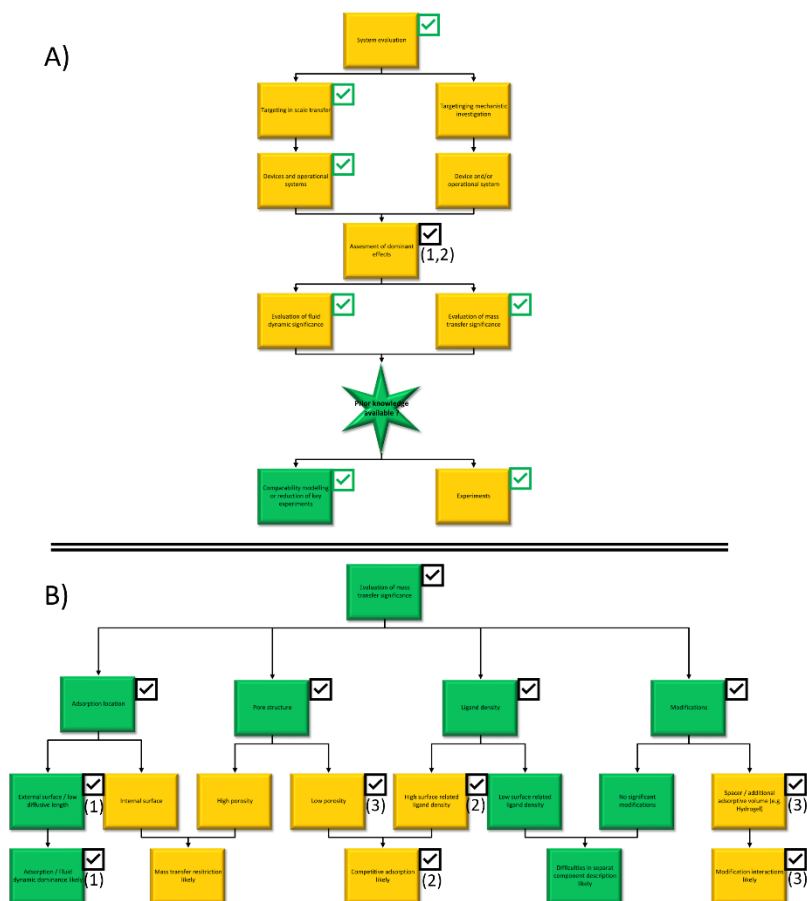


Figure 6.2: Schematic system evaluation for the reduction in modeling effort within the prior knowledge library. Following the overview in A), the experimental and modeling depth can be assessed with the in B) identified significant effects. The green checkmarks were performed within the presented work. Moreover, the black checkmarks identify parameters/information which were already integrated into a library, (1)<sup>181</sup>, (2)<sup>209</sup>, and (3)<sup>181</sup>.

Following the pursued modeling approach, standardized models need to be developed. Additional effort is needed to characterize the available devices at different scales. In addition to the different experimental scales investigated, the separation from axial to radial lab module and the first approach for device and stationary phase separation is given. The procedure presented in Figure 6.3 enables the integration of historical and new data by mechanistic modeling as well as an approach to extrapolate these results to the pilot scale. However, the quality and amount of historical data must be sufficient to extract the information into the model.

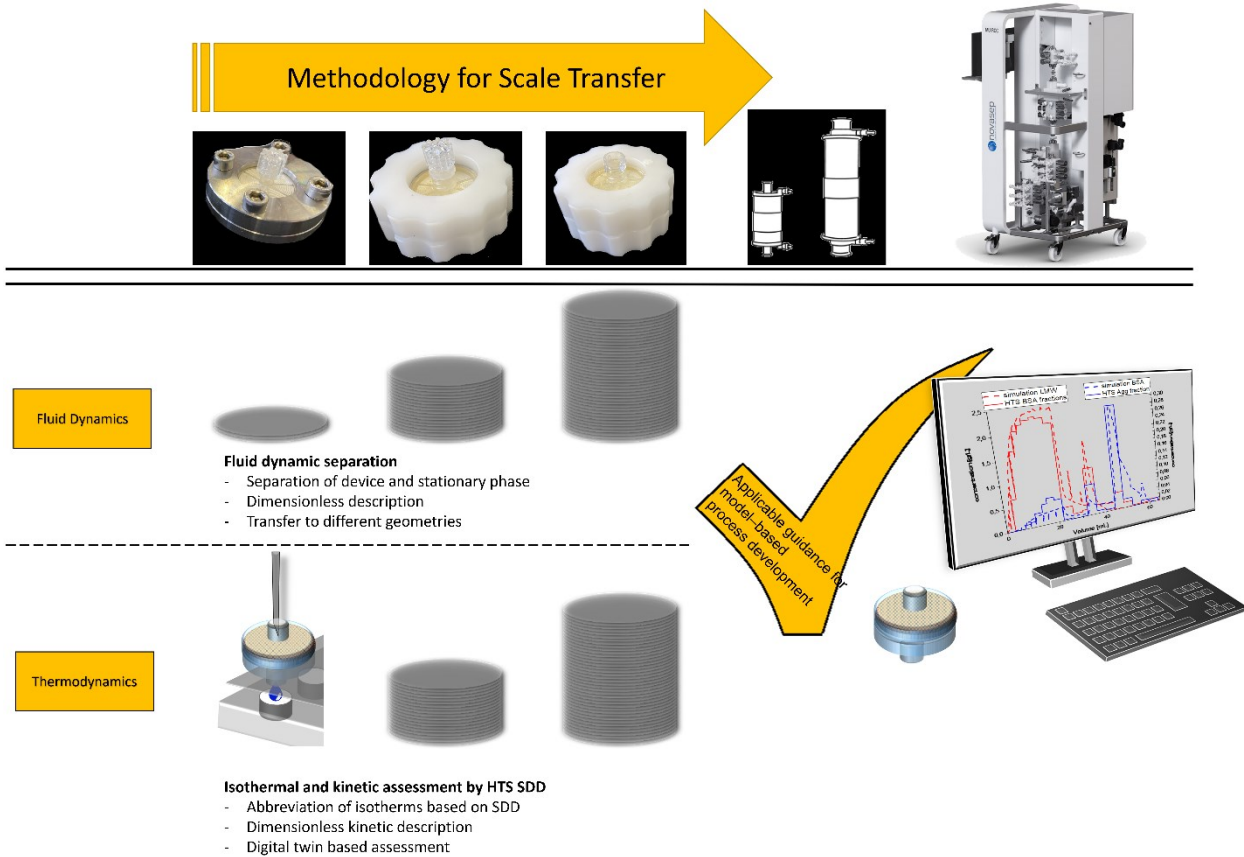


Figure 6.3: Full train approach from lab to production. Initially, scalable devices are developed to investigate the fluid dynamic.<sup>181</sup> Thereafter, information such as batch isotherms or apparent isotherms from small-scale historical experiments is assessed. Finally, the derived mechanistic model is verified for scale-up purposes.

Three case studies support the full train from lab to production procedure. Initially, the fluid dynamic investigation of different devices is presented. Thereafter, small-scale experiments are used as possible historical data to derive adsorption modeling parameters for the scale-up. Finally, the third case study compares the derived mechanistic model with a pilot scale mAb HMWS reduction process.

### 6.2.3.1 Case study 1: Fluid dynamic scale transfer

The fluid dynamic investigation covers the investigation of systems used, device investigation, and development for scale-up. Thereafter, these investigations are used to formulate a universal simulative device description by selecting a suitable model and separating the fluid dynamic effect of the device and the stationary phase. Assuming a successful fluid dynamic scale transfer would lead to reduced effort in PD, neglecting the need for system and device investigation.

### System investigation

The HTS, benchtop, and pilot scale systems were investigated at different velocities and tracer application forms. Therefore, the different velocities were set to represent the device's working range within 0.1 MV/min - 10 MV/min, applying tracer injection and sum functions for the benchtop and pilot system. HTS was carried out with a Lissy® 2002 GXXL/8P HTS robot manufactured by Zinsser Analytic applying Cellstar® 12-wellplates supplied by Greiner Bio-one International GmbH were used for fractionation of process streams. The FT experiments were performed using Äkta Prime™ and Äkta™ Explorer supplied by Cytiva© UK. The pilot scale system was conducted with the multi-use rapid cycling chromatography (MU RCC) system prototype B (to this state under development), provided by Sartorius Chromatography Equipment SAS. The HTS device was investigated earlier, applying tracer sum function signals.<sup>216</sup> Acetone purchased from VWR Chemicals was used as a tracer for all fluid dynamic investigations acetone was dissolved in the respective buffer system to 2 % - 5 %. Two CSTR models performed the system description. The two models facilitate the fluid dynamic before and after the stationary phase. However, the characterization of systems is state-of-the-art, and the results are not presented here.<sup>118,119,127</sup>

### Device investigation and development

The SDD development included investigating the septum port, device fluid distributor, and supporting materials. This said, the septum ports used were HPLC vial caps, 3D printed caps with silicone inlay, and luer lock syringe TLL septum adapter with septa high temp 7.0 DIA from Hamilton Company. Subsequently, the standard device fluid distributor was investigated. The different newly designed fluid distributors were then 3D printed and tested. In addition, several PE distributor nets and membranes were tested to improve the fluid distribution. Following this, the set-up consisted partially of the inlet to outlet of fluid distributor, distributor net, membrane, MA layers, membrane distributor net, and fluid distributor.

SDD characterization includes fluid dynamic investigations with qualitative dyeing- and acetone tracer experiments. In addition, the determination of the overall binding capacity with lyophilized BSA for Sartobind® Q and lysozyme for Sartobind® S. Following the IEX MA properties, dyeing experiments were conducted at low and high salt conditions (1 mS/cm – 80 mS/cm). The dye used was coomassie blue from Thermo Fisher Scientific. The binding capacity experiments evaluated the mass balance between bound and eluted mass. BSA supplied by Kraeber, and lysozyme purchased from Sigma Aldrich were utilized. Sartorius Stedim Biotech GmbH manufactures the Sartobind® MAs employed in our studies.

The scale transfer from axial to radial flow was performed with newly developed devices. Therefore, the SDD development newly designed fluid distributor at the inlet and outlet was applied in the lab module (LM) 30 and 60. In addition, the LM design consisted of a PP housing greater than the dedicated flat-sheet membrane diameter. This said, the free space between PP housing and stacked flat-sheet membrane was sealed with bioburden-reduced silicone. The silicone distribution to the inside of the MA was limited to the outer membrane surface by applying 4 bar pressure at the stacked flat-sheet membrane. In addition, the silicone was inserted with a maximum pressure of 6 bar.

Except for the commercially available Sartobind® Nano and Capsule devices, the MA devices used were prototype set-ups. These prototype devices followed the principle set-up of a 3D printed flow distribution followed by a distribution net and flat-sheet-stacked Sartobind® S or QMAs of a diameter

of 2.8 cm in a plastic housing. This said, we built the device with 3, 30, or 60 flat-sheet-stacked MA stabilized by a plastic jacket. The devices used in this study are summarized in Table 6.1.

Table 6.1: Overview of the used Devices.

Identifier [-]	Category [-]	Flow direction [-]	Void volume [mL]	Membrane volume [mL]	Porosity [-]	Ratio [-]
LM15	HTS SDD	Axial	0.76	0.43	0.75	0.6
LM15	Lab Device	Axial	0.51	0.43	0.75	0.8
LM 30	Lab Device	Axial	0.51	4.6	0.75	9.0
LM 60	Lab Device	Axial	0.51	8.3	0.75	16.3
Nano	Lab Device	Radial	1.55	2.9	0.75	1.9
Sartobind® Q Capsule	Pilot Scale	Radial	90	150	0.75	1.7
Sartobind® Q Capsule	Pilot Scale	Radial	440	400	0.75	0.9

### Model selection

In the course of model building, several iterations of model selection and parameters determination, evaluation, and assessment are needed to be performed.<sup>94,113,114</sup> The parameter assessment includes the parameter determination within an error minimization procedure for parameters that are not directly accessible with experiments.<sup>115,116</sup> This said, increasing the model depth leads to additional parameters. Following this, a higher model depth with potential additional not needed/present parameter (NNP) will accumulate the model errors in these NNP if they are derived by error minimization. This said, these error minimizations will lead to an apparent accuracy between the model and experiments, which does not represent the correctness of the model. Furthermore, the overweight models will almost certainly fail when transferred to another scale; the hidden inaccuracy within the NNP is physically irrelevant and thus increases the inaccuracy in scale transfer. Finally, aiming for a scalable representation of the investigated system includes the continuous evaluation of the selected model adequacy.

The fluid dynamic acetone experiments were performed at different velocities and tracer profiles, see, Table 6.2. This said, injection- and step tracers were performed to evaluate the model suitability. The models used were combinations of equilibrium constant model (EQ), plug flow reactor (PFR) and continuous stirred tank reactor (CSTR). This said, the following combination investigated were: PFR/EQ, PFR/EQ/PFR, CSTR/EQ, CSTR/EQ/CSTR, PFR/EQ/CSTR and CSTR/EQ/PFR.

## 6.2 Materials and Methods

Table 6.2: Summary of the applied volumetric flow in the axial device acetone tracer experiments

Identifier	Applied volumetric flow					
	[-]	[mL/min]				
LM15	5.0	4.3	2.2	1.3		
LM30	14.0	9.0	7.5	5.0	3.7	2.2
LM60	45.0	33.0	16.5	9.0	6.5	2.15

The EQ model in Eq. (6.1) describes the time-dependent concentration change by convective, dispersive, and mass transfer concentration changes.<sup>68</sup> First named convective concentration changes characterize the molecule concentration change through the column length / length coordinate, e.g., when pumping a liquid through a pipe. This said, the velocity  $u$  is divided by the porosity  $\varepsilon$ , which is 1 for the device and smaller than 1 for the stationary phase. The dispersive term is represented by the diffusive-based apparent axial dispersion coefficient  $D_{ax}$  considering the change in concentration due to different resistance as wall effects, diffusion effects, or the separation of fluid elements by physical deflection in the device or in the stationary phase, thus broadening the concentration profile. For adsorption processes, the mass transfer term reflects the change in concentration over time by adsorption of the molecules onto the stationary phase represented by the binding capacity  $q$ . The binding capacity is corrected by the porosity  $\varepsilon$  considering a lower stationary phase volume when reduced by the non-adsorptive pore volume. In Eq. (6.2) the porosity is determined by the interstitial porosity  $\varepsilon_{Device}$ , representing for instance, different-sized resin particles and the pore porosity of the individual particle  $\varepsilon_p$ .

$$\frac{\partial c_i}{\partial t} = - \underbrace{\frac{u}{\varepsilon} \cdot \frac{\partial c_i}{\partial x}}_{convective} + \underbrace{D_{ax} \cdot \frac{\partial^2 c_i}{\partial x^2}}_{dispersive} - \underbrace{\frac{1 - \varepsilon}{\varepsilon} \cdot \frac{\partial q_i}{\partial t}}_{mass\ transfer} \quad (6.1)$$

$$\varepsilon = \varepsilon_{Device} + \varepsilon_p \cdot (1 - \varepsilon_{Device}) \quad (6.2)$$

When comparing the PFR model in Eq. (6.3) with the equilibrium dispersive model in Eq. (6.1), it is reduced by the stationary phase's properties and mass transfer parameter. On the other hand, the CSTR model in Eq. (6.4) assumes ideal mixing while the change of component concentration  $c_i(t)$  is a function of the residence time. This said, the residence time is defined by the reactor length  $L_{CSTR}$  and the velocity  $u$ .

$$\frac{\partial c_i(t)}{\partial t} = -u \cdot \frac{\partial c_i}{\partial x} + D_{ax} \cdot \frac{\partial^2 c_i}{\partial x^2} \quad (6.3)$$

$$\frac{\partial c_i(t)}{\partial t} = -\frac{u}{L_{CSTR}} (c_{in,i}(t) - c_i(t)) \quad (6.4)$$

The Danckwerts boundary conditions complete the model by adding inlet conditions in Eq. (6.5) and outlet conditions in Eq. (6.6).<sup>101</sup> Furthermore, the inlet concentration is described by velocity-induced dispersion with the quotient of velocity  $u$ , axial dispersion coefficient ( $D_{ax}$ ), the concentration difference between inlet concentration ( $c_{in}$ ) and concentration at the first length coordinate of the column ( $c(0,t)$ ).<sup>102</sup> The outlet concentration, e.g., at the stationary phase or device/investigated system end, is equal to that of the length coordinate before.

$$\frac{\partial c_i}{\partial x}(x = 0, t) = \frac{u}{D_{ax}} \cdot (c(x, t) - c_{in}) \quad (6.5)$$

$$\frac{\partial c_i}{\partial x}(x = L, t) = 0 \quad (6.6)$$

The best model is evaluated by error minimization of the axial dispersion coefficient (EQ, PFR) and the mixing factor (CSTR). Furthermore, the device model combinations and its parameter are collectively adjusted to the different acetone tracer experiments. This said, each model combinations were at least 100 iterations given for the parameter adjustment by applying a CMinpack generic minimization algorithm. In addition to the L2 error ranking, the model degree of freedom is calculated. The model degree of freedom is calculated by multiplying the L2Error with the number of parameters and the transferability steps. This said, the number of parameters represents the possibility of blending model inaccuracies into model effects that are not present, thus misleading a higher accuracy than given. In addition, the transferability steps describe the needed scale transfer description for each model parameter. Consequently, the transferability steps are equal to the number of parameters when each mode parameter needs a separate mathematically scale transfer description.

### Fluid dynamic separation

Following the model selection, the two best model combinations are selected for the fluid dynamic device and MA separation. Consequently, the acetone tracer experiments of the different developed axial devices were used to determine the Bodenstein number. The dimensionless Bodenstein number in Eq. (6.7) describes the ratio of convective and axial dispersion. Consequently, a low Bodenstein number represents a high back mixing.

$$Bo = \frac{u \cdot L}{D_{ax}} \quad (6.7)$$

The simultaneously error minimized model parameters represented thus represent the device inlet and/or outlet, respectively. Furthermore, the equilibrium constant model parameter represents the stationary phase effect. Consequently, the different velocities and stationary phase volume (LM3, LM 30, and LM 60) facilitate the separation of the device and stationary phase. In addition, the Bodenstein number delivers a scale-independent description of the fluid dynamic effects of the device and stationary phase.

### Fluid dynamic scale transfer

The fluid dynamic scale transfer is grouped into model selection, verification for the axial LM, and the prediction of the radial devices. Initially, all experimental data were simulated by applying the originally predicted values of the axial dispersion coefficient of the Bodenstein number. Following this, a second error minimization with at least 100 iterations was performed applying an ASA minimization algorithm. This algorithm generates randomized values presenting possible derivation in the Bodenstein number prediction. Thereafter, the radial devices are investigated. Based on the radial flow, the velocity increases with decreasing radius. Consequently, the average velocity of these radial

## 6.2 Materials and Methods

devices was calculated and applied for the axial dispersion coefficient calculation. The applied volumetric flow for the radial device investigation is presented in Table 6.3.

Table 6.3: Summary of the applied volumetric flow in the radial device acetone tracer experiments

Identifier [-]	Applied volumetric flow [mL/min]			
	Nano	15.0	9.0	3.0
150	750			
400	750			

Following device differences between the Nano and pilot scale devices, model deviations are suspected in the pilot scale. The pilot/production scale capsules consist of an inner plastic core in the outlet, which is not the case with the Nano device due to manufacturing limitations. Following this, the capsule void volume is reduced, and back mixing effects in the bigger capsules are reduced.

### 6.2.3.2 Case study 2: Adsorption parameter determination

The second case study investigates the incorporation of imperfect historical data for apparent isotherm parameter determination. This said, simulation parameter determination is, among others, state-of-the-art for batch- or benchtop experiments.<sup>68,164</sup> However, integrating historical knowledge/data into a living library approach would facilitate a fast library setup and enable additional investigation of existing processes.

However, integrating historical data in living library conditions stationary phase properties, which either need to be experimental determined or extracted by the manufacturer. This said, these parameters are described below. Subsequently, the HTS modes are briefly described, and the apparent dynamic isotherm determination procedure is described.

### MA characterization

#### *Ionic capacity*

The ionic capacity is determined by preconditioning the MA for 10 MV with 1 M NaOH. Subsequently, equilibration is carried out with water for injection and titrated with 10 mM HCl. Afterward, the MA is washed with water for injection, and the titration procedure is repeated. In Eq. (6.8), the difference between the resulting CD areas is used to calculate the amount of titration substance used.<sup>181</sup>

$$\Lambda = \frac{\int c_{Titration,liquid,2} \cdot \partial V_{Titration,liquid,2}}{V_{MA} \cdot (1 - \varepsilon)} - \frac{\int c_{Titration,liquid,1} \cdot \partial V_{Titration,liquid,1}}{V_{MA} \cdot (1 - \varepsilon)} \quad (6.8)$$

#### **Porosity**

The device development information in the void volume of the device and the stationary phase is complemented by tracer experiments. This said, the stationary phase volume is 0.43 mL ± 0.05 mL (small-scale LM), 4.6 mL ± 0.2 mL (LM30) and 8.4 mL ± 0.2 mL (LM60). The total column porosity  $\varepsilon_{Total}$  in Eq. (6.9) is determined by a breakthrough tracer experiment with 3% to 5% acetone in 10 mM KPi buffer using a benchtop system. The retention volume is corrected by the previously determined void volume, calculated by the first derivative of the acetone breakthrough curve. In addition to the presented information here, the detailed HTS system characterization was discussed earlier by us.<sup>181</sup>

$$\varepsilon_{Total} = \frac{V_{Tracer}}{V_{MA}} \quad (6.9)$$

### Historical data integration – HTS apparent dynamic isotherm determination

Historical data for the apparent dynamic isotherm parameter determination was derived from our work earlier.<sup>181,209</sup> The applied HTS methods were the bind and elute (BE) mode and overload bind and elute mode (OBE). This said, the BE mode follows a classical bind and elute operation performed in several pipetting steps. Following this, the mode consists of loading-, wash-, several elution-, and regeneration phases. In contrast, the OBE mode intentionally overloads the stationary phase followed by wash and elution step. Thereafter, the stationary phase is overloaded with the same conditions as the before applied elution step. Accordingly, the OBE mode consists of repeatedly loading, wash and elution phases.

The HTS results can be clustered into experimental accuracy, selectivity, recovery, and binding capacity. Following this, the mass balance in Eq. (6.10) with Eq. (6.11) is applied to obtain the experimental accuracy. Here, the index  $i$  is the observed component in the pipetting step. Finally, the deviation  $D$  is determined by the ratio of loaded feed mass to the accumulated mass determined in the eluate, wash, and elution step in.<sup>181</sup>

$$0 = m_{Loading,i} - \sum_{k=1}^n m_{k,i} \quad (6.10)$$

$$D_i = \frac{m_{Loading,i}}{\sum_{k=1}^n m_{k,i}} \quad (6.11)$$

The typical process condition evaluation is performed by selectivity and recovery process maps. Therefore, the selectivity is calculated by the ratio of the bound dimer mass and bound monomer mass in elution step  $i$  in Eq. (6.12). Besides selectivity, product recovery is a parameter of interest for process development, which is calculated by Eq. (6.13).

$$Selectivity_i = \frac{m_{Dimer,i}}{m_{Monomer,i}} \quad (6.12)$$

$$Recovery_i = \frac{m_i}{m_{MA,i}} \quad (6.13)$$

In addition to the more global wellness and process parameter, static binding capacities can be determined. The HTS BE, and OBE mode results were initially used to determine the maximum binding capacity at the initial CD at a given pH by Eq. (6.14), Eq. (6.15) (BE), and Eq. (6.16) (OBE). In Eq. (6.14), the difference between the loaded and the accumulated mass in the flow-through fraction mass of each component equals the static binding capacity. Likewise, the sum of the mass elution fraction is used to determine the static binding capacity. Both procedures should lead to the same results and indicate a closed mass balance. The HTS BE approach also includes several elution salt steps, which are generally used for process maps. Static binding capacity at a given pH and as a function of CD is determined by the sum of component eluate masses, including the elution fraction. In addition, the HTS OBE mode calculates the binding capacity depending on all performed OBE phases before and the current investigated phase  $k$  in Eq. (6.16).<sup>209</sup>

$$q_i = \frac{1}{V_{MA}} \cdot \left( c_{Feed} \cdot V_{Feed} - \sum_{k=1}^l \sum_{i=1}^n c_{i,k} \cdot V_k \right) \quad (6.14)$$

$$q_{MaxElu,i,k} = \frac{1}{V_{MA}} \cdot \sum_{k=1}^l \sum_{i=1}^n c_{i,k} \cdot V_k \quad (6.15)$$

$$q_{i,k} = \frac{1}{V_{MA}} \cdot \left( \sum_{k=1}^l \sum_{i=1}^n c_{Feed,i,k} \cdot V_{Feed,k} - \sum_{k=1}^l \sum_{i=1}^n c_{i,k} \cdot V_{,k} \right) \quad (6.16)$$

The apparent dynamic isotherm parameter determination is compared to a classical batch isotherm parameter determination in Figure 6.4. In 1) a general procedure of isotherm determination is presented. For example, the equilibration, adsorption in 1) A), optional wash in B) and elution step. In contrast, dynamic isotherm assessment within the HTS method is presented in 2).

In the loading phase (Figure 6.4 1 A, 2 L), the dynamic isotherm assessment procedure is comparable to the one obtained in batch isotherm determination. Following this, an isotherm with several apparent equilibrium states at different liquid feed concentrations can be obtained for the initial conditions. However, the stepwise step elution delivers only the saturation equilibrium concentration at the given salt concentration. In addition, several assumptions and limitations must be considered when a dynamic isotherm assessment is carried out. The assumptions can be grouped in stationary phase (A), set-up (B and C), and procedure (D) limitations. Following this, a dynamic investigation must be carried out to prevent kinetic limitation. This said, HTS will blend isotherm results with kinetic effects based on the dedicated process comparable screening procedure. In addition, the HTS set-up differs from that of a classical batch isotherm determination. In contrast to the defined volumes in batch experiments, the HTS set-up consists of the device and stationary phase volume as well as the well plate volume. Following this, the applied volume will be reduced by the void volume of the device and summarized in the next pipetting step. In addition, the HTS SDD fluid dynamic must be considered when not optimized. For example, the batch isotherm determination might exclude the wash step, reducing partial elution, while the dynamic approach is easier to evaluate with the wash step. This said, the wash step ensures a defined application in the elution step and partially neglects the device void volume.

Due to the intended process representation, the dynamic isotherm assessment will not deliver the actual isotherm parameter. However, applying a thoroughly developed HTS set-up will reduce the influences mentioned above and delivers valuable information from purely historical data.

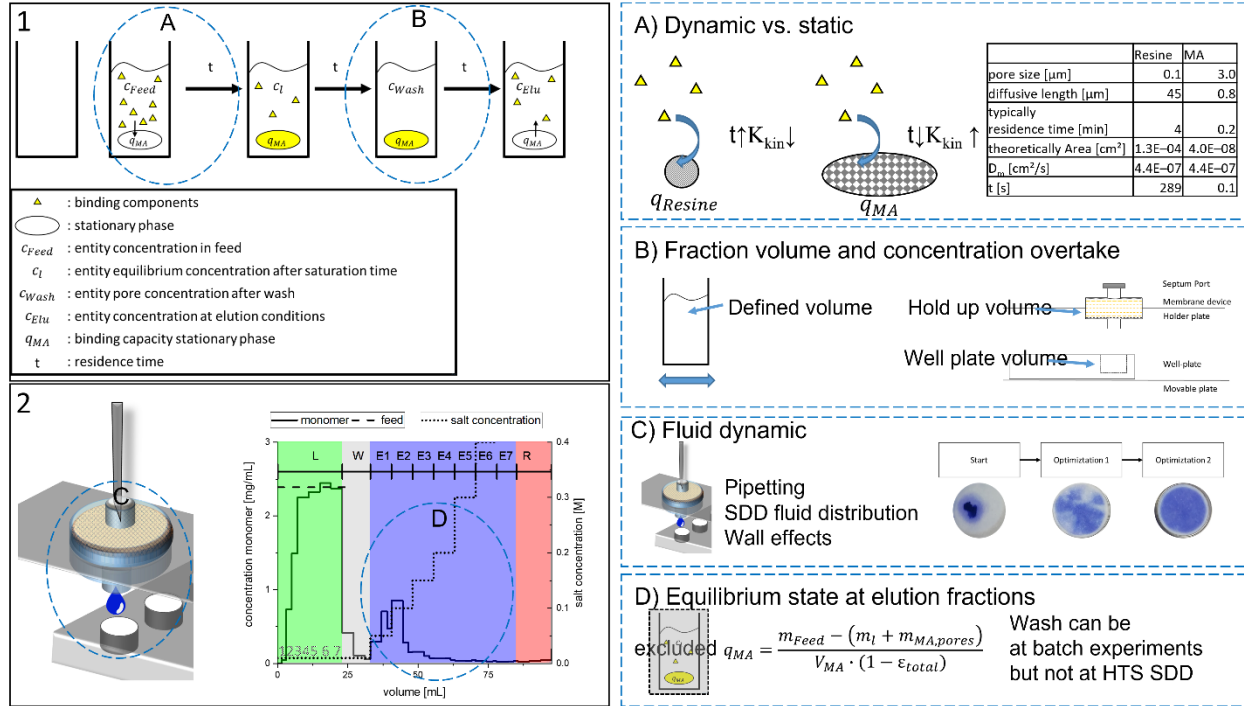


Figure 6.4: Comparison of classical batch and dynamic isotherm determination/assessment. In 1) a general procedure of isotherm determination is presented. The equilibration, adsorption in 1) A, optional wash in B) and elution step. In contrast, dynamic isotherm assessment within the HTS method is presented in 2). The isotherm assessment is comparable in the loading phase, obtaining a full isotherm at different liquid feed concentrations. However, the stepwise step elution delivers only the saturation equilibrium concentration at the given salt concentration. In addition, several assumptions and limitations must be considered when a dynamic isotherm assessment is carried out. The assumptions can be grouped in stationary phase (A), set-up (B and C), and procedure (D) limitations.<sup>181</sup>

### SMA parameter determination

The BE and OBE experiments at pH 5, 5.5, 6 and, 7 were used to determine the apparent isotherm parameter. In addition, BE and OBE elution steps were considered at 0.1 and 0.2 M sodium chloride. Subsequently, the applied equations and boundary conditions are noted.

Eq. (6.17) to Eq. (6.19) presents the ionic capacity in dependence on the steric factor  $\sigma$ , characteristic charge  $\nu$ , and binding capacity of counter ions  $q_1$  as well as the binding capacity  $\bar{q}$  of the components  $q_i$ . For a rapid equilibrium or in the equilibrium state, the SMA isotherm can be expressed as shown in Eq. (6.20).

$$\Lambda = q_1 + \sum_{i=2}^{n+1} (\nu_i + \sigma_i) q_i \quad (6.17)$$

$$\Lambda = q_1 + \sum_{i=2}^{n+1} \nu_i \cdot q_i \quad (6.18)$$

$$\bar{q} = q_1 - \sum_{i=2}^{n+1} \sigma_i \cdot q_i \quad (6.19)$$

$$c_{eq,i} = \frac{q_i}{k_{eq}} \cdot \left( \frac{c_1}{\Lambda - \sum_{i=2}^{n+1} (\nu_i + \sigma_i) q_i} \right)^\nu \quad (6.20)$$

The charge and equilibrium constant are determined by the curve evaluation of  $\log k$  using Eq. (6.21) and Eq. (6.22). A linear regression of the logarithmic capacity factor over the logarithmic salt concentration results in the charge  $v$  and equilibrium  $k_{eq}$  constant by slope and intercept.<sup>100</sup> The presented application of the capacity factor holds only true for single component evaluation. However, the capacity factor values were determined for the IgG and HMWS mixture and applied as initial values. Thereafter, the SMA parameters were adjusted by error minimization. In addition, the calculated error was normalized to facilitate an even weighed IgG and HMWS error minimization.

$$K = \frac{1 - \varepsilon}{\varepsilon} \cdot \left( \frac{q_i}{c_i} \right) \quad (6.21)$$

$$\log k' = \log \left( \frac{1 - \varepsilon}{\varepsilon} \cdot k_{eq_{1,i}} \cdot A^{v_i} \right) - v_i \cdot \log(c_1) \quad (6.22)$$

### Small scale confirmation

The HTS SDD experiments evaluate the obtained apparent dynamic isotherm parameter. Following this, BE and OBE experiments at a pH of 5, 5.5, 6, and 7. In addition to the isotherm parameter determination, all BE salt steps were simulated. On the one hand, the apparent isotherm parameter determination partially blends kinetic effects; on the other hand, the pooling of fractions dilutes the kinetic effects. Following this, the kinetic factor was determined by error minimization.

#### 6.2.3.3 Case study 3: Approach evaluation and scale-up

The full train product development approach is evaluated by determining, comparing, and scaling up the fluid dynamic and by historical data obtained adsorption parameter determination approach. Initially, the apparent dynamic isotherm parameter is assessed, and the kinetic coefficient is evaluated. Subsequently, the approach is transferred to the pilot scale separation of IgG and HMWS. In addition to the pure simulative approach evaluation, the results are compared to the scale factor application. This said, the approach is not only evaluated in quality but also to a second state-of-the-art scale transfer methodology.

### Kinetic evaluation

The HTS SDD assessed kinetic coefficient in chapter 6.2.3.2 is transferred to the larger lab devices using the Peclet number in Eq. (6.23). Following Eq. (6.23), the Peclet number transfers the scale effects of the convective transport rate to the diffusive transport rate. Here, the diffusive transport rate is assumed as summarized in the kinetic constant. The kinetic comparison is performed by comparing the experimental and error minimized simulative results of the lab modules SDD, LM 30, LM 60 at pH 5 and 10 mM sodium chloride.

$$Pe = \frac{L \cdot u}{K_{kin}} \quad (6.23)$$

Assuming an ideal isothermal parameter, the Peclet number equals all different scales. However, deviations may be expected based on the assumptions and imperfections of historical data. The scale comparison will thus lead to an error evaluation.

In addition to the error evaluation, the Peclet number pH value dependency is determined by the HTS SDD experiments. Thus, the kinetic coefficient can be calculated for the scale-up experiments at pH 6.4.

### Scale-up

The SDD experiments result in a range of applicable process parameters. Two approaches have investigated the ability to transfer this information to a larger scale: a) mechanistic modeling(SDD – MM) and b) SDD direct parameter transfer by applying a scale factor.

The mechanistic modeling scale-up is performed with a 150 mL Sartobind® S capsule module. In addition, the prototype pilot scale MU RCC system at a volumetric flow of 45 L/h is used. The applied process conditions were pH 6.4 with 0.1M sodium chloride. Finally, the determined fluid dynamic and adsorption equations were applied to scale-up the HTS SDD results.

The evaluation is performed by comparing the experimental UV/concentration course and the fractions taken in the experiment with the simulative predicted results. Fractions with 150 mL volume were taken in the loading- and wash phase from 1350 mL to 2700 mL, as well as in the elution phase from 4050 mL to 4650 mL. The IgG and HMWS fractions concentration were determined by SEC analysis.

### Direct scale factor

The direct scale factor is used as a fast scale transfer method. For instants, the experimental breakthrough concentration at, e.g., 10% dynamic breakthrough capacity is determined. Thereafter, the scale factor can be calculated with Eq. (6.24) and Eq. (6.25). The HTS SDD experimental results are used to determine the scale factor and extrapolated to the Sartobind® S IgG HMWS separation. The direct scale factor assumes homogeneous binding capacity and fluid dynamics in the different scales. Furthermore, the direct scale factor is not suitable for scale-up of competitive adsorption effects.

$$\Gamma = \frac{V_{DBC10}}{V_{MA,lab\ device}} \cdot c_{Feed} \quad (6.24)$$

$$V_{DBC10,\Gamma} = V_{MA,\Gamma} \cdot \frac{\Gamma}{c_{Feed}} Pe = \frac{L \cdot u}{K_{kin}} \quad (6.25)$$

#### 6.2.4 Analytical methods

A UV spectrometer measured the overall protein concentration at a wavelength of 280 nm using the VivaSpec® UV reader provided by Sartorius Stedim Biotech GmbH. In addition, IgG and its HMWS concentration were measured using a Yarra™ 3 µm SEC 3000 column of 300 x 7.8 mm supplied by Phenomenex using the Thermo Scientific™ Dionex™ UltiMate™ 3000 HPLC System from at a flow rate of 1 mL/min.

## 6.3 Results and Discussion

---

### 6.2.5 Data handling, automation, and mechanistic modeling

Automated HTS was performed using Zinsser Analytic WinLissy (version 7). UNICORN® supplied by GE Healthcare was used for FT experiment recipe writing and chromatographic analysis. The concentration of IgG and its HMW aggregates was quantified by the Dinoex Chromleon™ 6.80. Evaluation of the experimental results and analysis of the chromatographic curves were performed using Origin® 2018b software supplied by OriginLab Corporation. MM was done with the software ChromX™ provided by GoSilico GmbH.

## 6.3 Results and Discussion

The result and discussion for the full train product development from lab to production approaches are grouped into the three case studies. Initially, the fluid dynamic scale transfer is investigated, followed by the adsorption parameter determination for historical data. Finally, the approach is evaluated by comparing the model predicted and experimentally derived pilot scale mAb HMWS separation.

### 6.3.1 Case study 1: Fluid dynamic scale transfer

In this chapter, classical fluid dynamic transfer challenges are addressed and summarized in: Device investigation and development and model selection for the fluid dynamic investigation. In addition, transfer of different device types within fluid dynamic separation and the fluid dynamic scale transfer.

#### 6.3.1.1 Device investigation and development

Aiming for a scalable model and implementing historical data includes investigating the data quality and differences between the devices. This said, the HTS SDD and lab devices were investigated for their feasibility as chromatographic devices. In addition, the applied small-scale axial lab device deviates in fluid dynamics compared to the radial lab and production device.

In Figure 6.5, lefthanded A)-D) the development of the HTS set-up device is presented. In A) 1-7, different distribution nets and support materials are tested in dyeing experiments to improve the fluid dynamic distribution throughout the device. Following the unsatisfying results from Figure 6.5 A) 1-7, the lab module fluid distributor was optimized, presented in B), presenting sufficient improvement in A) 8 and 9. In addition to the lab module optimization, the injection port was optimized in several iteration steps as represented in D) to the final SDD set-up in C). These improvements lead to comparable signals between HTS SDD and benchtop system.<sup>181</sup> In summary, the historical device development presented itself as suitable for the dedicated scalable mechanistic model building.

Transferring the fluid dynamic from axial to radial flow urges for a general approach, enabling the transfer in future investigations. The lab modules presented in Figure 6.5 E) – H) were developed to facilitate different numbers of membrane stamps. Following this, the variation of the membrane sheet numbers should facilitate the differentiation of membrane and device impact. Initially, the lab module consisted of several stainless-steel parts like the stamp, sealing ring, and baseplate in Figure 6.5 F). The puk was made of polypropylene and could be used in a different device after completion. In the membrane puk making process, the different number of distribution nets and membrane layers are placed in between the puk, which is fixed on the baseplate. Thereafter, position rods are placed

through the stamp and seal ring, centralizing the layers. Next, the stamp is placed under an air-supplied plunger, and a defined pressure is applied. The best compression pressure was investigated by acetone tracer and dyeing experiments, not presented here. Subsequent to the compression of the layers, the seal ring is fixed, followed by the adhesion and sealing of the membrane layers and the puk with silicone through the dedicated drill. The silicone pressure for optimal adhesion investigation, as exemplary presented in E), is not detailed here. After the sealing process, the complete set-up is dried for 48 h. Afterward, the set-up is opened, and the finished puk is removed. The finished puk can then be placed in a separate holder and used as a chromatography device. This set-up had several disadvantages, including time constraints, handling difficulties, and occasional leakage when the puk is transferred to the chromatographic device.

The final design in Figure 6.5 H) includes the fluid distributor presented in B) and offers the benefit of the puk being used in the device or removed and stored. In addition, several devices can be prepared in series. The stamp applies the pressure; the outer upper handle is closed until resistance is sensed and the stamp can be removed. Qualification is given by optical inspection if the fluid distributor shows any movement indicating incomplete compression when the pressurized air is removed. Thereafter, the device can be sealed while the next device can be compressed. Following the procedure above, the device is dried for at least 48 h.

In summary, the set-up enables the investigation of several different membrane layers within the same fluid dynamic basis. In the present work, 30 and 60 membrane layer pucks are used. The additional wall effects cannot be separated. However, the device enables the mechanistic modeling investigation of device and membrane impact, which can then be used to transfer to radial devices.

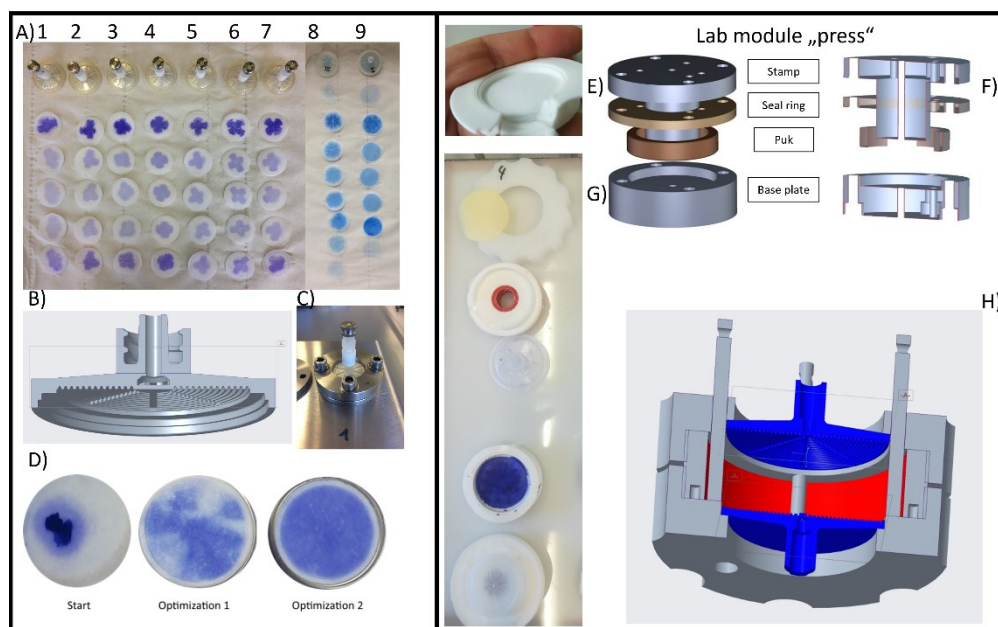


Figure 6.5: Different device development steps. The Figure is split into half, lefthanded A)-D) HTS SDD<sup>181</sup> and righthanded Lab module E)-H). In A) 1-7 different, the distribution nets and the support material are tested in dyeing experiments to improve the fluid dynamic distribution throughout the device. The small-scale device was optimized after the unsatisfying results from A) 1-7. In A) 8 and 9, sufficient improvements resulted in the modified fluid distributor in B. In addition to the small-scale device fluid distributor optimization, the injection port was optimized in several iteration steps, as represented in D) to the final set-up in C). The lab module was designed to facilitate different numbers of membrane stamps, presented right-handed from E)-H).

## 6.3 Results and Discussion

### 6.3.1.2 Model selection

The fluid dynamic model selection is guided by the number of models applied and minimized error. Therefore, three different devices are investigated by acetone breakthrough experiments. The device model selection investigation includes the following model combination: PFR/EQ, PFR/EQ/PFR, CSTR/EQ, CSTR/EQ/CSTR, PFR/EQ/CSTR, and CSTR/EQ/PFR. In addition, the axial dispersion coefficient and mixing factor are error minimized and adjusted to the different experimental results.

In Figure 6.6 A), 100 different error minimization steps for a lab device of 30 MA layers are presented. The lefthanded presents a PFR and CSTR model including two parameters, and righthanded a one PFR model parameter adjustment is presented. In Figure 6.6 B) selected simulation results are presented, enabling a better comparison between the PFR&CSTR and PFR models. This said, both model approaches deliver feasible error minimization between experimental and simulative acetone courses.

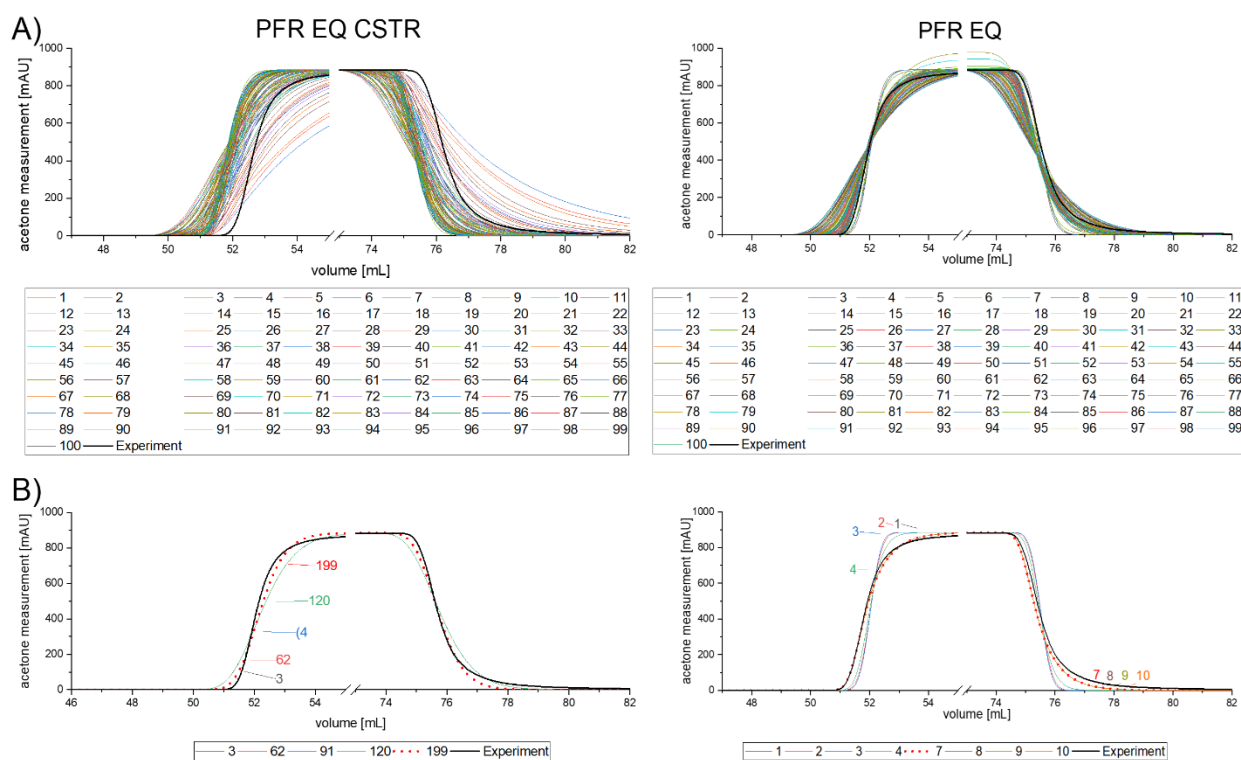


Figure 6.6: Model selection examples: PFR EQ CSTR and PFR EQ. A) shows the 100 error minimization iterations and B) selected results. The red dotted line in B) shows the iteration with the lowest error respectively.

In Table 6.4 presents the different error minimization results of the 30 MA layer lab device at 9 ml/min. The modeling results follow in decreasing suitability  $PFR < PFR^2 < CSTR < CSTR^2 < PFR/CSTR < CSTR/PFR$ . In general, the number of iteration steps should also be verified. This said, two model parameters might need different numbers of iterations compared to one model parameter. Following this, the PFR/CSTR model parameters were error minimized and adjusted to the experimental results by an additional 50 simulations without a significant decrease in the model error ( $\leq 3\%$ ). Accordingly, the iteration amount is assumed to be sufficient for the approach. Following the model evaluation for one velocity, the evaluation is extended to two more velocities.

Table 6.4: Results of model investigation at 9 mL/min step acetone signal

	PFR / EQ	PFR2 / EQ	CSTR / EQ	CSTR2 / EQ	PFR CSTR / EQ	CSTR / EQ / PFR
Dax/mixing factor Device	24385.0	1836.2	1.47	0.44	0.07	0.34
Dax MA	0.0022	0.0056	0.0101	0.0011	0.0138	0.0010
Dax/mixing factor Device	X	9440.9	X	0.55	0.74	0.66
L2 Error	42652	48019	163039	61929	49441	59214
L2 Error normalized	1.0	1.1	3.8	1.5	1.2	1.4

In Table 6.5, the model evaluation for three different velocities of the two most promising model approaches is presented. In addition, the number of parameters, transferability steps, and model error is presented. This said, in contrast to Table 6.4, the transferability steps describe the needed correlation of parameter to scale the model. Furthermore, to avoid error accumulation in NNPs, the number of parameters and the transferability steps are multiplied by the model error. This said, the two-parameter model PFR/EQ is deemed to be better suitable for a scalable approach than the PFR/EQ/CSTR model with lower model error.

Table 6.5: Proof of principle in model selection at different velocities and tracer signals. LM 30 at 3 velocities for different step and pulse injection.

Model combination	Number of parameters	Transferability steps	Residual L2Error	Selection value L2Error x (Transfer+Number)	Ranking
PFR & EQ	2	2	163325	653300	1
PFR & EQ & CSTR	3	3	151871	911226	2

### 6.3.1.3 Fluid dynamic separation

Subsequent to the model selection procedure, the fluid dynamic separation is performed. Therefore, the two selected models are used to separate the device and membrane fluid dynamic. This said, the small-scale (0.43 mL) and two lab-scale (4.6 mL and 8.3 mL) devices are investigated within injection and step acetone tracer experiments. Three different velocities are applied in the experiments. The selected models are then applied to minimize the axial dispersion coefficients for each device.

In Figure 6.7, the comparison of experimental and simulative (PFR EQ) results are presented, A) to C) step- and D) to F) injection signal. In addition, the applied volumetric flow/velocity decreases from top to bottom. The simulative results are visually in good agreement with the experimental signals. Comparing experimental and simulative results is performed by the ratio of integrated measurement and integrated subtracted measurement and simulation values. This said, a good agreement between experimental and simulative results is achieved for deviations below 6 %. The deviation between Figure 6.7 B and F is below 1.9 % and 5.5 %. The deviation for the 150 mL and 400 mL capsules is below 6 %. However, for the injection experiments, the modeling accordance decreases from D) to E). The decreasing accordance might be induced due to the lower velocity, either an efficiency limitation in

### 6.3 Results and Discussion

the fluid distributor/device or a modeling error induced by not considered influences. Nevertheless, the device simulation results are considered sufficient.

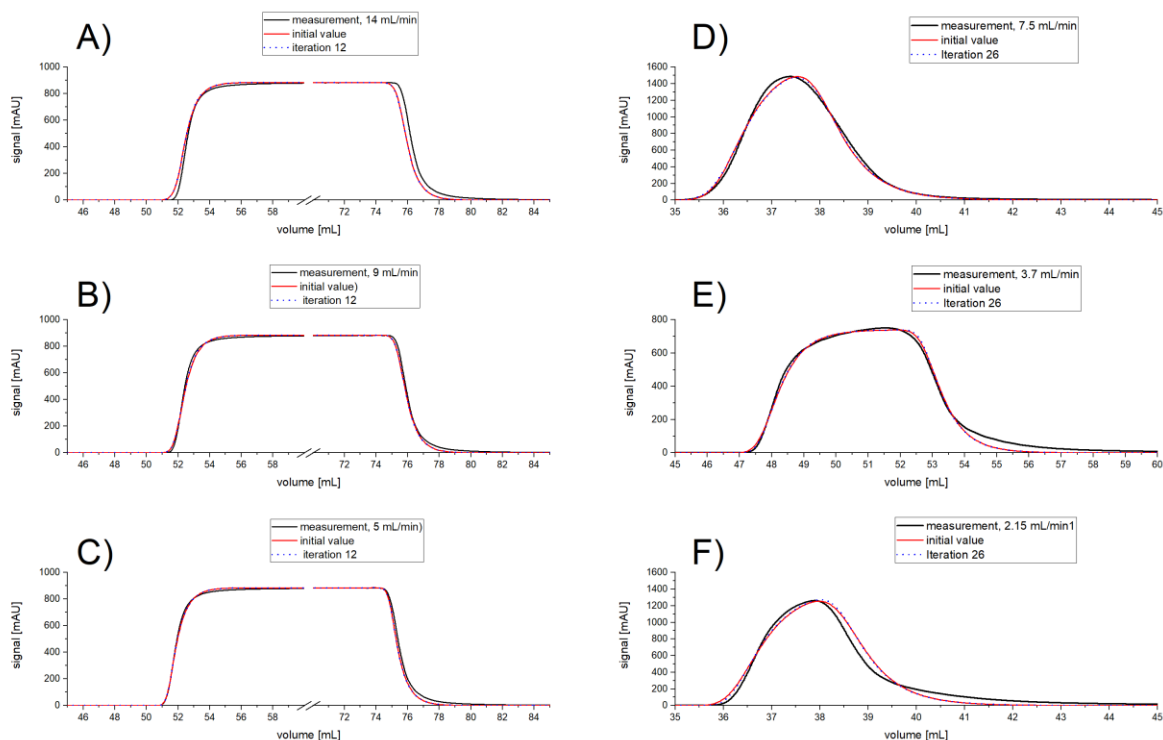


Figure 6.7: Comparison of the lab module with 30 membrane layer experimental and PFR EQ model results after error minimization. The left-handed graphs present the step signal and right-handed injection signal comparison. From top to bottom, the velocity decreases. The simulative step signals results in A) - C) are in good agreement with the experimental data. Comparatively, the modeling and experimental accordance decrease from D) to E). The decreasing accordance might be induced due to the lower velocity, either an efficient limitation in the fluid distributor/device or a modeling error induced by not considered influences.

The 30-membrane layer device PFR EQ CSTR model evaluation is presented in Figure 6.8. Following the previous evaluation, the experiments are similarly presented. The step signals in Figure 6.8 present comparable experimental accordance when compared to Figure 6.7 A) - C). Accordingly, the deviation in Figure 6.8 C) is below 3 %. However, the simulative tracer injection results present a significant deviation between experimental and simulation results (D) - F)). Consequently, the deviation in Figure 6.8 D) is 45 %. This said, the additional model/model parameter does not increase the model accuracy. The controversial increasing model inaccuracy with an increased model parameter is either due to an inadequate model or to low iteration process in the simulative parameter determination. However, the reduced PFR EQ model presents itself once more as sufficient to describe the device.

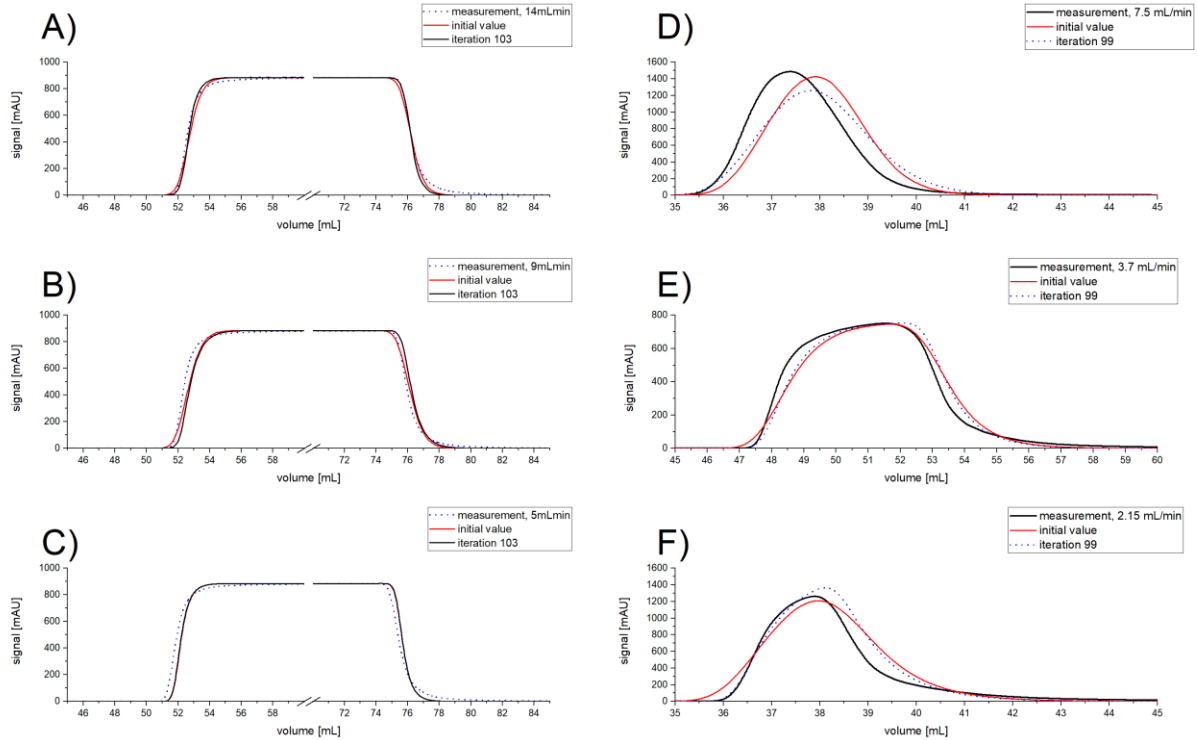


Figure 6.8: Comparison of the lab device with 30 membrane layer experimental and PFR EQ CSTR model results after error minimization. The left-handed graphs present the step signal and right-handed injection signal comparison. From top to bottom, the velocity decreases. The simulative step signal A) to C) and experimental results present visually comparable accordance when compared to the in Figure 6.7 presented results. However, the tracers are less accurate in experimental data description when compared to the step signal results in Figure 6.7 D)-F).

Following the model confirmation, the axial dispersion coefficients for each device are determined simulative. In Figure 6.9, the axial dispersion coefficient of the 30 MA lab module is presented. In Figure 6.9 A) presented EQ model represents the membrane effect, and in B) shown results of the PFR device model. This said, the lab module presents itself as a sufficient fluid distributor. In addition, the result can be used to calculate the Bodenstein number enabling the scale transfer. The device and membrane Bodenstein numbers are calculated as 0.017 and 617.3, respectively.

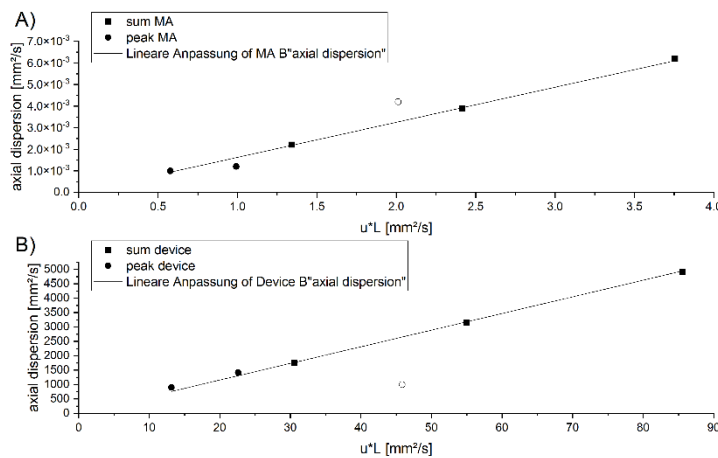


Figure 6.9: Fluid dynamic separation of LM 30. The membrane correlation between axial dispersion coefficient and velocity times length is presented in A), the respectively device correlation is shown in B).

## 6.3 Results and Discussion

### 6.3.1.4 Fluid dynamic scale transfer

The obtained dimensionless device description is evaluated within the different devices. Therefore, tracer signals at different velocities are compared to the general dimensionless prediction, and an individual error minimized model prediction. This said, the deviation between the simulation and experiment will present model error in general. Furthermore, the deviation between dimensionless and error minimized prediction will present scale transfer procedure limitations.

In Figure 6.10, the small-scale device comparison is presented. The applied volumetric flows are A) 5.0 mL/min, B) 4.3 mL/min, C) 2.15 mL/min, D) 1.3 mL/min. In general, the error minimized- and dimensionless model predictions are hardly distinguishable from each other. In addition, the experimental and simulative results are in good agreement with each other, so deviations in the step injection A) can be observed. However, the experimental- and error minimized results are in good agreement with the dimensionless prediction; thus, scale transfer was successfully here.

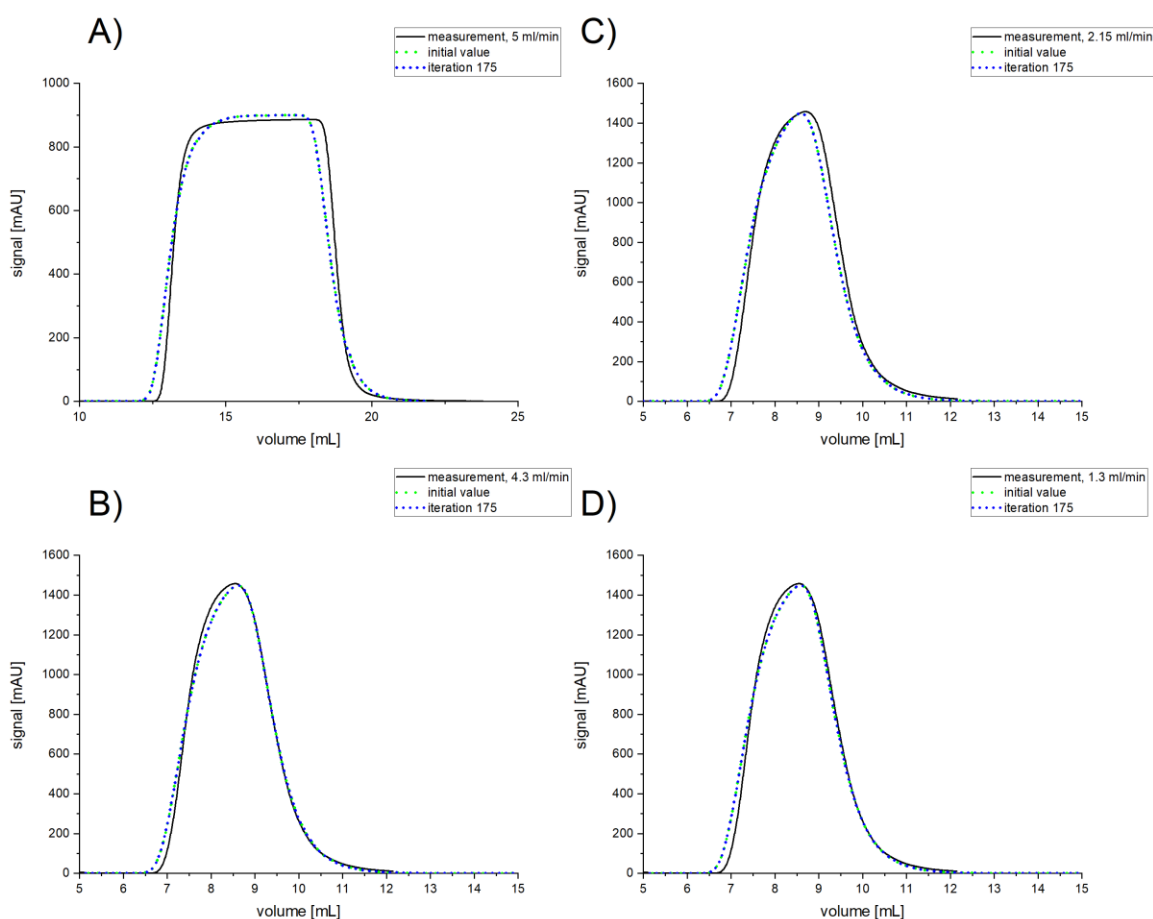


Figure 6.10: Comparison between dimensionless predicted and error minimized model and experimental result of the LM15 device. A) 5.0 mL/min, B) 4.3 mL/min, C) 2.15 mL/min, D) 1.3 mL/min. The error is minimized, and dimensionless model predictions are hardly distinguishable. In addition, the experimental and simulative results are in good agreement with each other; even so, deviations in the step injection observation in A) can be observed. However, generally, the scale transfer was successful.

Following the small-scale device, the LM60 is presented in Figure 6.11, as the LM30 has already been discussed in chapter 6.3.1.3. Applied volumetric flows were A) 45.0 mL/min, B) 33.0 mL/min, C) 9.0 mL/min, D) 6.5 mL/min, E) 16.5 mL/min and F) 2.15 mL/min. Comparable to the small-scale device results in Figure 6.10, the error minimized and dimensionless model predictions are hardly distinguishable in A), B), and C). However, deviations between error minimized, and dimensionless results are visible in the step injection signals E) and F). Furthermore, the first acetone uptake, in A) and B) is sharper predicted in the simulation than observed. Regardless of the initial acetone uptake the injection results agree with the experimental observation. Following this, the experimental results are with minor deviations, and the error minimized results are in good comparison with the dimensionless prediction. The scale transfer can be interpreted as a success with some possible limitations.

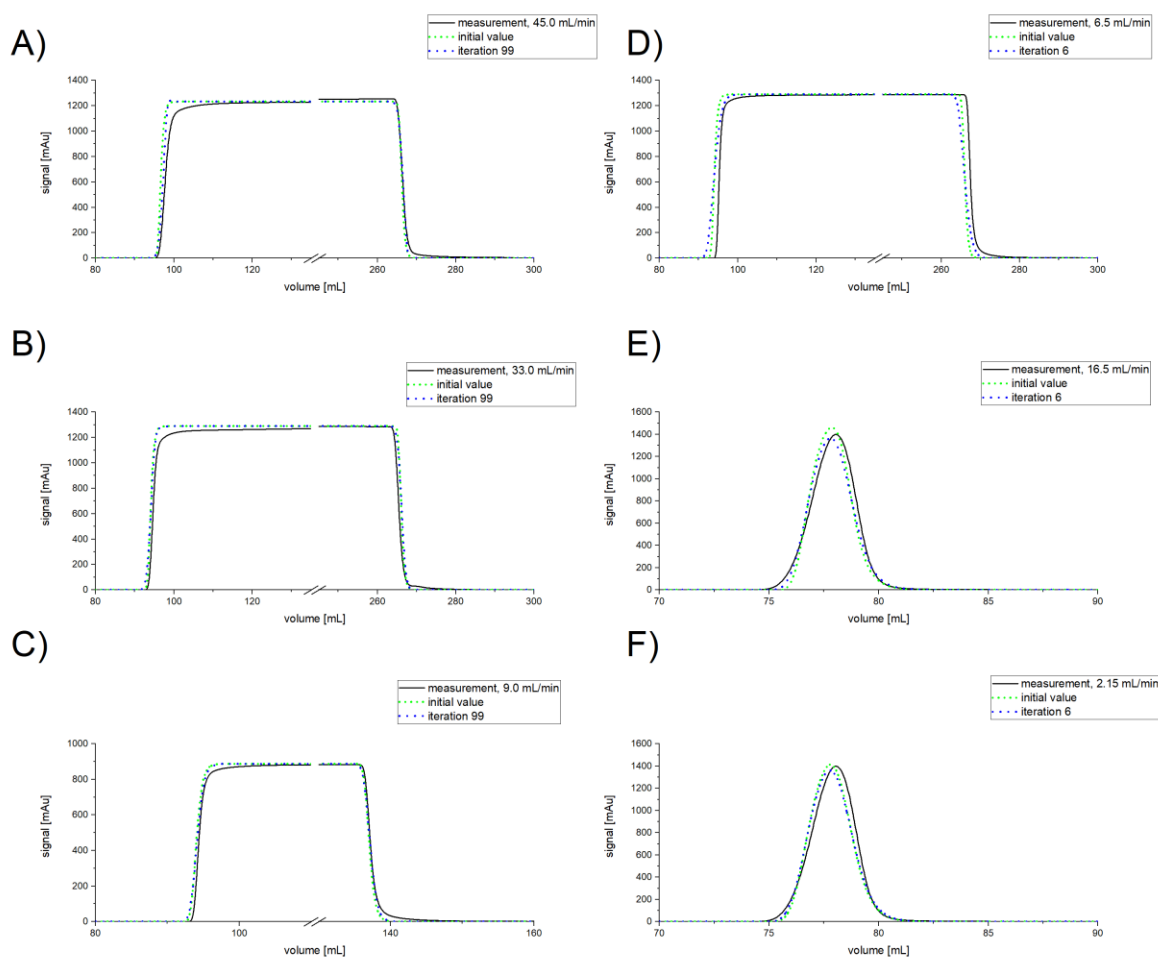


Figure 6.11: Comparison between dimensionless predicted and error minimized model and experimental result of LM60 module. A) 45.0 mL/min, B) 33.0 mL/min, C) 9.0 mL/min, D) 6.5 mL/min, E) 16.5 mL/min and F) 2.15 mL/min. The error is minimized, and dimensionless model predictions are hardly distinguishable in A), B), and C). However, deviations between experimental and simulation results are visible, especially in the step injection signal. This said, the first acetone uptake is sharper predicted in the simulation than observed. Regardless of the initial acetone uptake, the injection results are in good agreement to each other. Therefore, the scale transfer can be interpreted as a success with some possible limitations.

### 6.3 Results and Discussion

Figure 6.12 compares the experimental- and simulative radial Nano device results. The applied volumetric flow at different injection volumes was A) 3.0 mL/min, B) 15.0 mL/min, C) 9.0 mL/min and D) 3.0 mL/min. The dimensionless predicted model results are in good agreement with the experimentally derived results. The simulations in A) and C) indicate possible volumetric shifts while the signal course is correctly predicted. This said, the scale and axial to radial fluid flow transfer were successfully performed by applying the dimensionless approach.

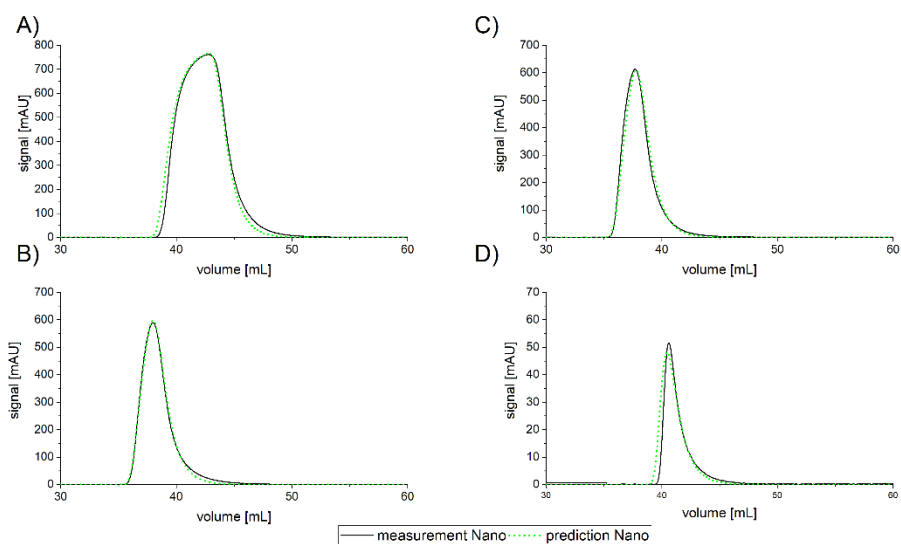


Figure 6.12: Comparison between dimensionless predicted model and experimental result of Nano module. The different following experimental parameter are grouped in volumetric flow and injection volume: A) 3.0 mL/min, 5.0 mL; B) 15.0 mL/min, 0.5 mL; C) 9.0 mL/min 0.5 mL; D) 3.0 mL/min, 0.5 mL. The dimensionless predicted model results are in good agreement with the experimentally derived results. The simulations in A) and D) indicate possible volumetric shifts while predicting the signal course correctly. This said, the scale and axial to radial fluid flow transfer were successfully performed.

The presented dimensionless description was successfully applied in the lab-scale devices and is transferred to the pilot/manufacturing scale in Figure 6.13. Applied volumetric flows were 750 mL/min for the 150 mL capsule as well as for the 400 mL capsule in A) and B), respectively. The dimensionless predicted model results agree with the experimentally derived results. Comparing experimental and simulative results is performed by the ratio of integrated measurement and integrated subtracted measurement and simulation values. The deviations for the 150 mL and 400 mL capsules are below 6%. However, a higher simulative deviation to the experimental results is presented in Figure 6.13 compared to the results in Figure 6.10 and Figure 6.11, and Figure 6.12. The simulative results predict higher dispersion than the experimental observed. This said, the model is only partially applicable, or the devices present some discontinuity that was not observed in the dimensionless approach. Accordingly, the device was investigated, presenting a design deviation between the lab scale Nano and the bigger-sized capsules. The pilot/production scale capsules consist of an inner plastic core in the outlet, which is not the case with the Nano device due to manufacturing limitations. Following this, the capsule void volume is reduced, and back mixing effects in the bigger capsules are reduced. This said, the model correctly predicts the higher axial distribution/back mixing. In general, for better experimental and simulative results, this discontinuity would need further investigation. However, the model accuracy is considered sufficient here.

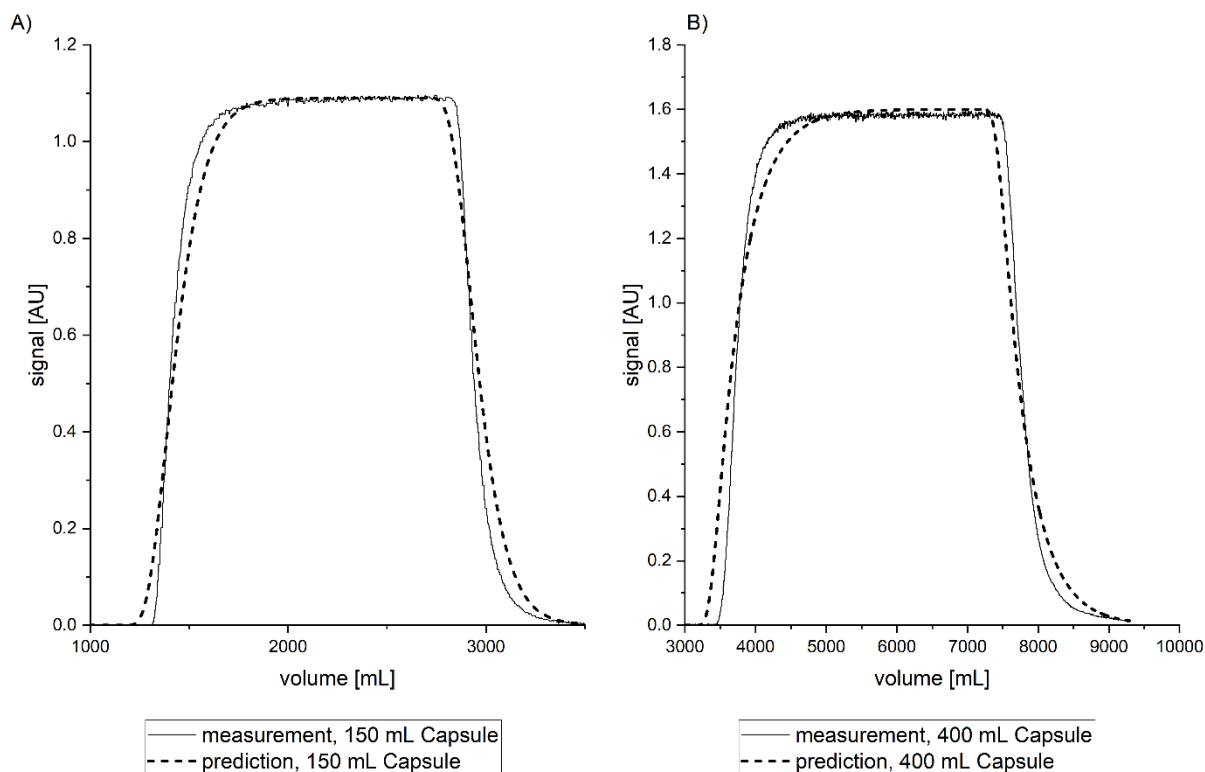


Figure 6.13: Fluid dynamic scale transfer for 150 mL A) and 400 mL B) Sartobind S Capsule. The dimensionless predicted model results agree with the experimentally derived results. However, a higher deviation in the simulative results can be observed compared to the results in Figure 6.10, Figure 6.11, and Figure 6.12. The simulative results predict higher dispersion than experimentally observed. This said, the 150 mL and 400 mL capsule designs differ from the investigated Nano design. However, the model accuracy is considered sufficient, while this discontinuity would need further investigation for more precise results.

### 6.3.2 Case study 2: Adsorption parameter determination

The second case study investigates the determination of adsorption parameter determination based on non-optimal conditions. While batch isotherm determination is state-of-the-art and can be easily integrated with mechanistic PD procedures, historical HTS results are considered more challenging. The living library approach is applied to HTS BE and OBE investigation, determining the initial adsorption parameter. Following the fluid dynamic dimensionless approach in chapter 6.3.1, the isotherm parameter assessment is transferred to a scalable dimensionless description. Thereafter, the approach is confirmed by a comparison of experimental and simulative HTS results.

#### 6.3.2.1 Isotherm assessment

Following the fluid dynamic evaluation, the isotherm parameter assessment is investigated. The determination of batch isotherm parameters for mechanistic modeling is state-of-the-art. However, integrating historical data into a living library would allow for incorporating stationary phases that have been investigated but not selected for a process. Following this, the initial data for the living library development would be greater, and the information content is already for great use in PD. However, due to the intended process condition representation in HTS, the historical isotherm parameter assessment will not deliver the actual isotherm parameter. As mentioned in chapter 6.2.3.2, three factors for the deviation can be named: stationary phase properties, set-up, and evaluation

### 6.3 Results and Discussion

---

procedure. However, applying a thoroughly developed HTS set-up will reduce the mentioned influences and deliver valuable information from purely historical data. The requested accuracy will then determine whether the information is sufficient or whether further experimental data needs to be added.

The dynamically HTS isotherm parameter determination included investigating different process conditions and procedures. The varying process conditions were salt concentration and pH values. In addition, the HTS BE results and a combination of HTS BE and OBE results were investigated. The HTS OBE results were added to complete the SMA determination within competitive adsorption phenomena. Figure 6.14 compares the dynamically assessed HTS BE SMA isotherm results to the experimental data. This said, Figure 6.14 presents the lowest accuracy while the not shown combined BE, and OBE data points increased accuracy. The IgG monomer results are left-handed, and IgG HMWS results are right-handed.

Furthermore, the isotherm parameters were determined by HTS experiments at different pH values of 5, 5.5, 6, and 7, corresponding to Figure 6.14 A, B, C, and D. According to the HTS BE procedure, a full isotherm assessment is derived only for the initial loading phase while for higher salt concentration the respective single point elution fractions are available. The full isotherm assessment for IgG left-handed is in good agreement with the experimental data; even so, pH 7 (D) presents a deviation in the first measurement point. This said, the equilibration constant might present a deviation for this pH value range. Following the IgG isotherm evaluation, the single-point salt elution results present a higher deviation when compared to the overall isotherm, increasing from pH 5 to 7 (A to C). However, the determined SMA parameter for IgG suites the dynamic assessed results.

Conversely, the HMWS full isotherms are visible in less accordance compared to the experimental results than the IgG evaluation, see Figure 6.14. The highest deviation can be observed for pH 5 and 6. Otherwise, the single-point salt elution results deviations are comparable to thus of the IgG evaluation. This said, the HMWS limitations in MA binding capacity and thus analytical determination probably induce higher uncertainties when compared to the IgG investigation. Accordingly, the dynamic isotherm determination is not exempt from the challenges of the classical batch isotherm determination. However, the procedure enables isotherm parameter determination while the application needs to be proven.

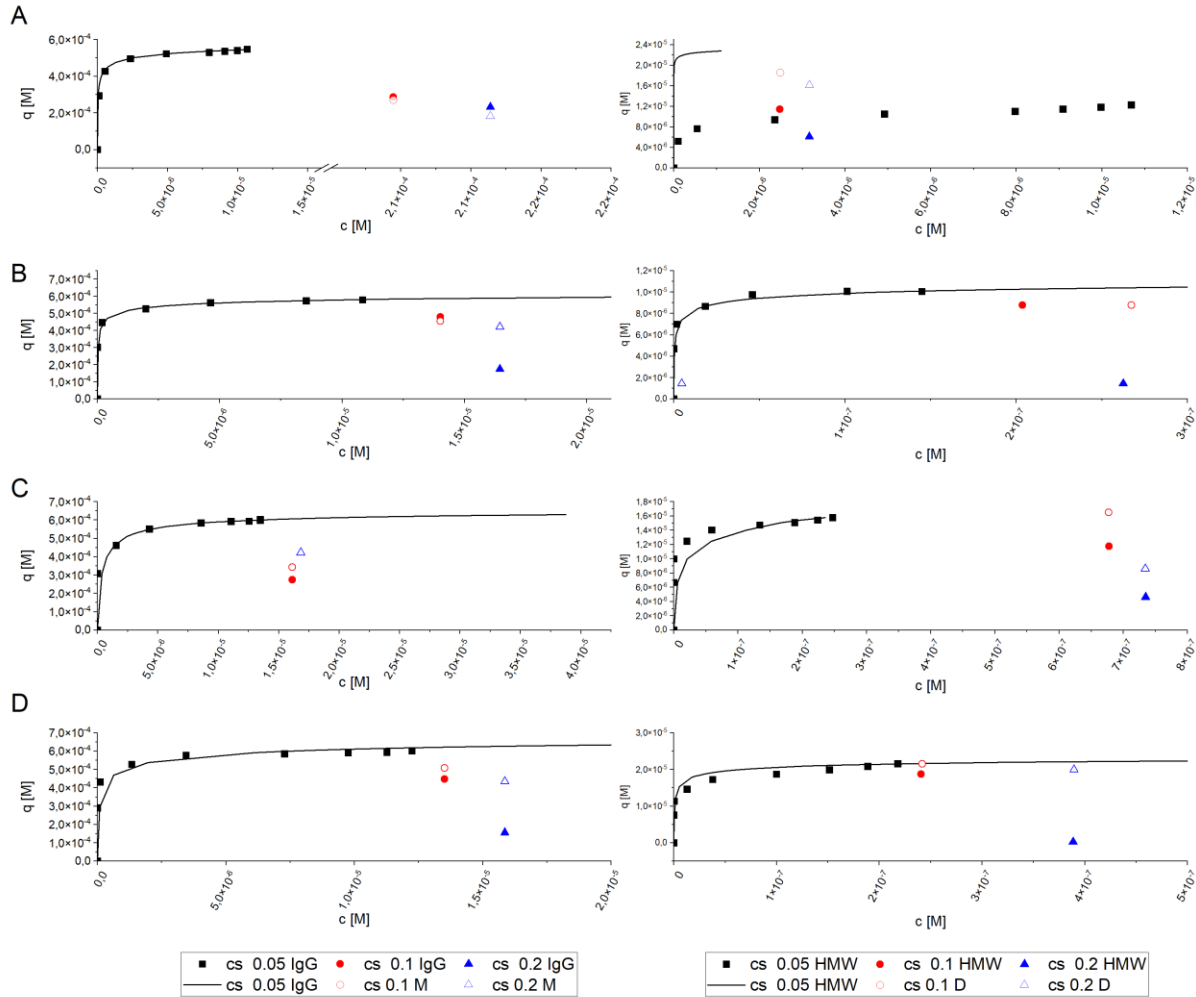


Figure 6.14: Dynamically HTS SMA isotherm parameter assessment. The IgG monomer results are left-handed, and IgG HMWS results are right-handed. Furthermore, the isotherm parameters were determined by HTS experiments at different pH values 5, 5.5, 6, and 7, corresponding to A, B, C, and D. According to the HTS SDD BE mode, a full isotherm assessment is only possible for the initial loading phase while for higher salt concentration the respective single elution fractions are available.

The description of the pH influence on the isotherm parameter can either be included in the SMA equation<sup>1</sup> or simplified with linear and quadratic equations. In Figure 6.15, the pH-induced change of the dynamic derived isotherm parameters is presented. In addition to the in Figure 6.14 presented dynamic isotherm assessment, the competitive adsorption effects obtained by the HTS OBE method were also used to refine the dynamic isotherm parameter determination (not shown here). This said, the course of the isotherm parameter equilibrium and charge change when adding HTS OBE results. Although, the steric parameters are comparable between HTS BE and OBE methods. The course of IgG and HMWS for all isotherm parameters are comparable and present the similarity between these components. In addition, small differences emphasize chromatographic separation while the steric disparity indicates competitive binding.

Following the living library approach, additional information, such as molecular information, can be included in the isotherm assessment. This said, the isoelectric point might be included in the parameter assessment adding a near zero value for the characteristic charge, as demonstrated in Figure 6.15.

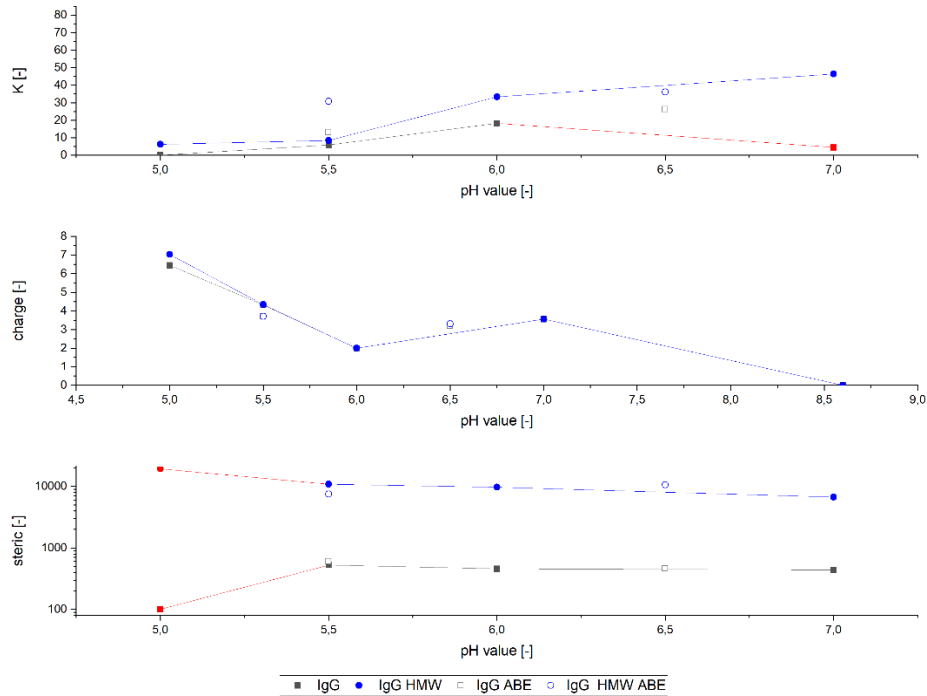


Figure 6.15: Overview dynamic assessed SMA parameter at different pH values. In addition to the in Figure 6.14 presented dynamic isotherm assessment, the competitive adsorption effects obtained by the HTS OBE method are shown as blank markers.

The derived dynamic assessed SMA parameter and pH effects are then preserved in Eq. (6.26) - Eq. (6.31). Following this, these equations can then be applied to calculate the SMA parameter for each component. In addition, a certain parameter space can be obtained when comparing linear and nonlinear equations, see Eq. (6.32) and Eq. (6.33).

$$K_{1,1} = 16.43 \cdot pH - 80.5 \quad (6.26)$$

$$K_{2,1} = 21.6 \cdot pH - 104.6 \quad (6.27)$$

$$v_1 = -1.5 \cdot pH + 13.0 \quad (6.28)$$

$$v_2 = -1.2 \cdot pH + 10.7 \quad (6.29)$$

$$\sigma_1 = -54.5 \cdot pH + 813.5 \quad (6.30)$$

$$\sigma_2 = -5970.3 \cdot pH + 46960 \quad (6.31)$$

$$K_{1,2} = -11,235 \cdot pH^2 + 137,86 \cdot pH - 409,47 \quad (6.32)$$

$$K_{2,2} = -8,5413 \cdot pH^2 + 114,64 \cdot pH - 350,44 \quad (6.33)$$

In summary, the dynamic HTS SMA isotherm parameter assessment presents a possible limitation in accuracy. However, historical data can be transferred and preserved in the isotherm-like parameter. In addition, either a holistic isotherm or simplified equations can be applied to represent the global process condition range. Therefore, assuming the dynamic HTS SMA isotherm parameter assessment would be successful, the historical data could provide a valuable contribution to PD.

## 6.3.2.2 Small scale confirmation

The dynamic HTS SMA isotherm parameters are applied for experiments within pH 5, 5.5, 6, and 7, including BE and OBE procedures. In addition, the different dynamic HTS SMA isotherm parameter determination with and without additional OBE data are compared. The kinetic factor is derived by error minimization of the kinetic factor while the determined SMA parameters were kept fixed.

In Figure 6.16 the comparison of experimental and simulative HTS BE & OBE results is presented. The exemplary comparison for the HTS OBE procedure at pH 5.5 for IgG and HMWS is presented in A) and B). In addition, C) and D) present IgG and HMWS comparison for BE results at pH 7, respectively. The simulation describes the principal OBE concentration course for IgG and HMWS. In the IgG simulation, a good accuracy for the IgG breakthrough is achieved, while the elution profile differs from the experimental observation. However, the HMWS simulated concentration profile varies significantly for the presented OBE experiment at pH 5.5. The breakthrough and elution profile shows too low HMWS binding capacity. Admittedly, the pH 5.5 comparison presented here shows 75 % for IgG (A) and 67 % for HMWS (B), the worst achieved accuracy. Comparative, the experimental and simulative results at pH 7 for IgG (C) and HMWS (D) are with over 75% accuracy in accordance. In general, the IgG accuracy is in all simulations above 75 %, while the HMWS accuracy is above 61 %, see Table 6.6.

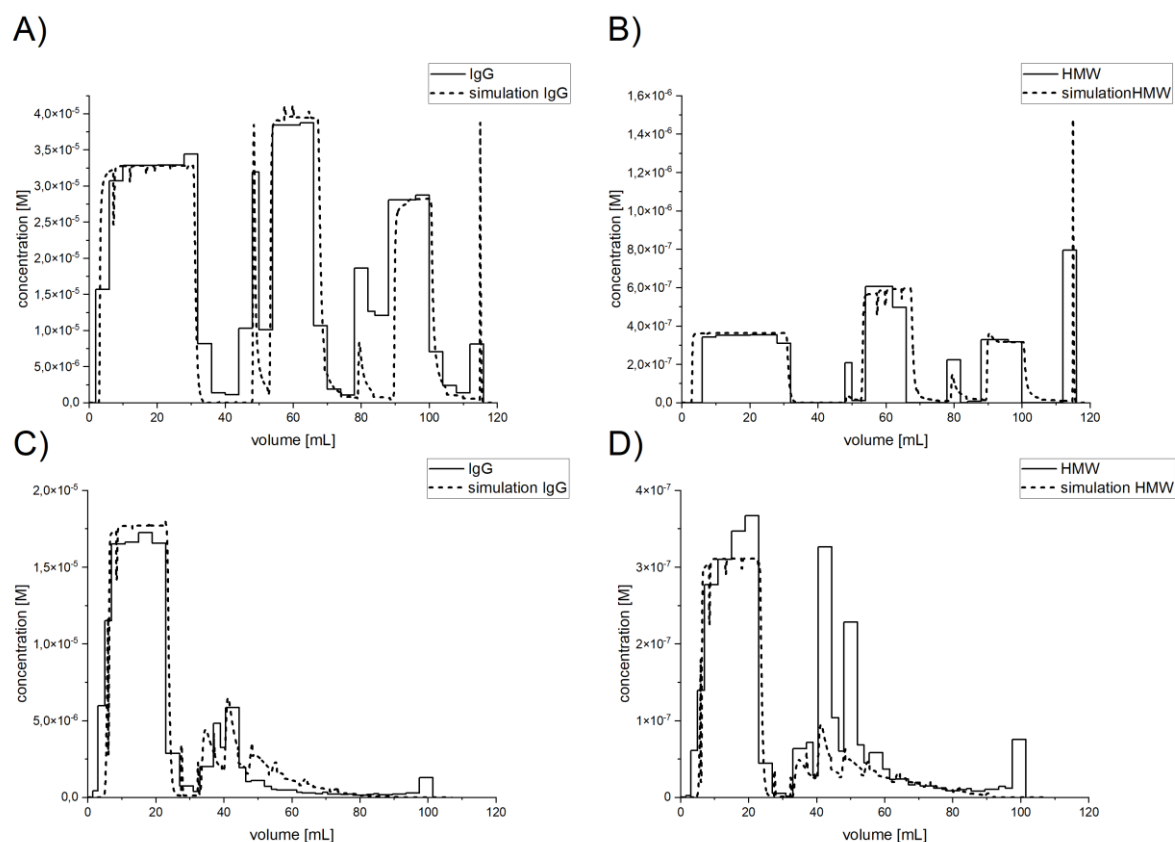


Figure 6.16: Exemplary comparison of experimental and simulative HTS BE & OBE results applying dynamic assessed SMA parameter. The exemplary comparison for the HTS OBE for IgG and HMWS is presented in A) and B). In addition, C) and D) present IgG and HMWS comparison for BE results, respectively. The principal OBE concentration course is described for IgG and HMWS. However, the HMWS concentration profile differs significantly for the presented OBE experiments at pH 5.5. Admittedly, the here presented (A-B) pH 5.5 comparison is with 75 % for IgG and 67 % for HMWS accuracy the worst. Comparative, the experimental and simulative results at pH 7 for IgG (C) and HMWS (D) are with over 75% accuracy in good accordance.

### 6.3 Results and Discussion

The summarized comparison between experimental and simulative HTS results is presented in Table 6.6. The IgG accuracy is evenly distributed in the 75 – 101 % range. Although, the HMWS simulation signal accuracy increases with increasing pH value from 61 %- 117 %. The accuracy thus indicates experimental protein loss and limitations of the kinetic and apparent isotherm transfer. In addition, adding dynamic assesses OBE apparent isotherm information for the parameter determination increases the IgG and HMWS accuracy with increasing pH value. For instance, competitive binding might be more demonstrable in the isotherm parameter assessment at higher differences close to the isoelectric point.

Table 6.6: Comparison between experimental and simulative HTS results applying dynamic HTS SMA isotherm parameters

pH [-]	HTS Methode [-]	Parameter [-]	Overall Fit IgG [%]	Overall Fit HMWS [%]
5	BE	BE	86	77
5	OBE	BE	86	61
5.5	BE	BE	83	67
5.5	OBE	BE	75	67
5.5	BE	OBE	83	67
5.5	OBE	OBE	75	67
6	BE	BE	101	117
6	OBE	BE	93	65
7	BE	BE	96	117
7	OBE	BE	75	89

In addition to the concentration profile and accuracy summary, Figure 6.17 compares experimental and simulative derived process maps. The experimental and simulative comparison for HTS BE IgG binding capacity is presented in Figure 6.17 A) and B). Furthermore, the comparison for HMWS binding capacity is presented in C) and D). In addition, in E) and F), experimental and simulative displacement identifier maps for the HTS OBE mode are compared. Simulative and experimental IgG binding capacities follow the same conductivity and pH profile. However, the simulative binding capacity is with 26 mg/mL overestimated. The simulative and experimental HMWS binding capacity profile is also in good accordance with each other. In addition, the simulative predicted HMWS binding capacity is lower than the experimental.

Furthermore, in Figure 6.17 an HMWS binding capacity deviation can be observed at pH ~5.6 and 15-30 mS/cm. The sudden change in binding capacity might present an outlier. Comparatively, the displacement identifies map profile is well met by the simulation. The simulative predicted displacement effects at a higher pH value. This effect was experimentally suspected but could not be confirmed with certainties. Further investigations in this pH range would be needed to confirm the simulative results.

In summary, the historical data dynamic isotherm SMA parameter determination provides valuable information and delivers similar concentration profiles and process maps. The IgG simulation accordance above 75 % indicates a suitable procedure for historical data. In addition, the HMWS process maps present themselves in good comparison to the experimental results, even though the concentration profile is only above 61 %. The historical data inclusion approach does not aim for exact isotherm determination but includes historical data. This historical data inclusion can be useful to increase living library utility for extrapolation to other products and initial simulation of processes where no isotherms were determined. Aiming to include historical data in a living library should include the accuracy of the different model

parameters. Thus, the extrapolation uncertainties could be considered in the predictions. The living library would then, either manually or with artificial intelligence, be able to group component similarities and, at a final state, predict simulation parameters for unknown components.

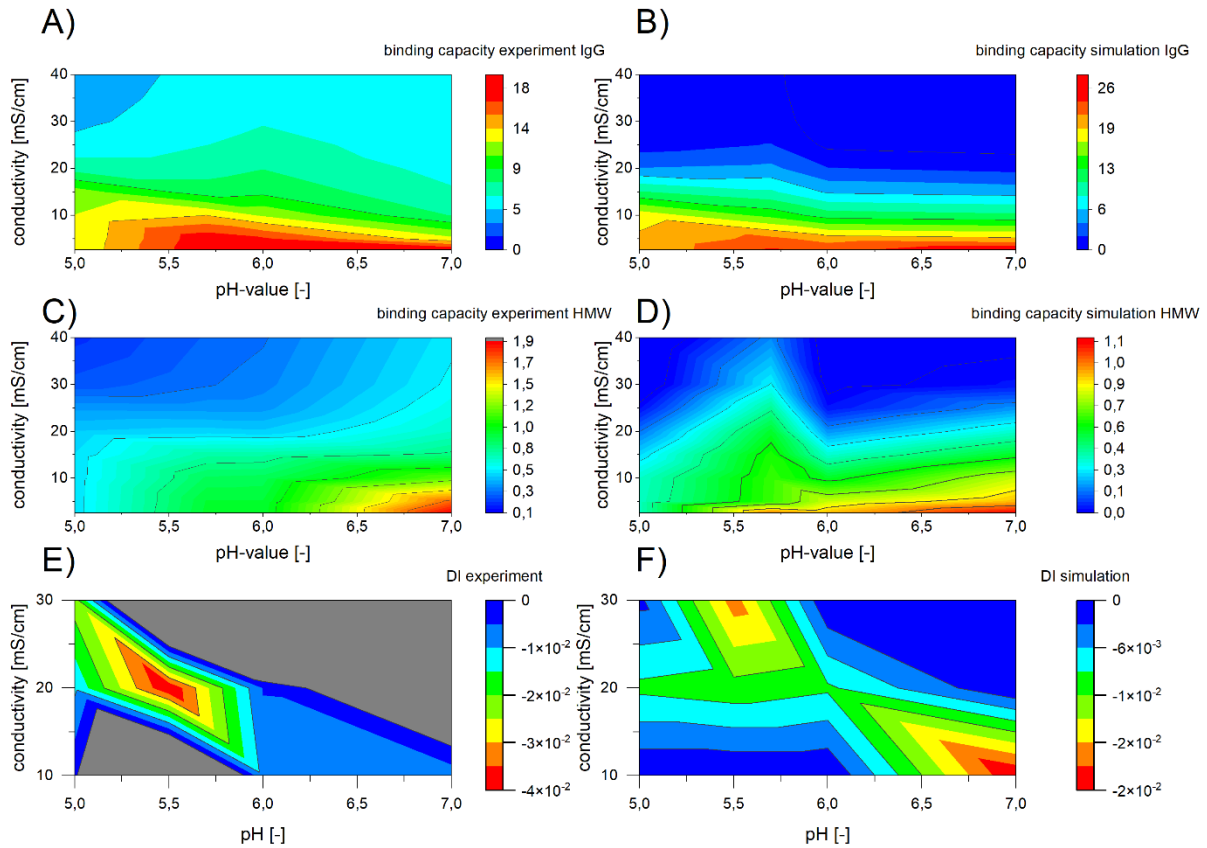


Figure 6.17: HTS SDD BE and OBE mode comparison between simulation and experimental results. The experimental and simulative comparison for HTS BE IgG is presented in A) and B). Furthermore, the comparison for HMWS is presented in C) and D). In addition, in E) and F), the comparison between experimental and simulative displacement identifier maps for the HTS OBE mode are presented. Simulative and experimental IgG binding capacities follow the same conductivity and pH course. However, the simulative binding capacity is with 26 mg/mL overestimated. The simulative and experimental HMWS binding capacity profile is also in good accordance with each other. However, a deviation can be observed at pH  $\sim$ 5.6 and 15-30 mS/cm. The sudden change in binding capacity might present an outlier. Comparatively, the displacement identifies map profile is well met by the simulation. The simulative predicted displacement effects at higher pH values were experimentally suspected but not confirmed with certainties. Further investigations in this pH range would be needed to confirm the simulative results.<sup>209</sup>

### 6.3.3 Case study 3: Approach evaluation and scale-up

The obtained fluid dynamic and adsorption parameter determination are evaluated within a scale-up from 8.3 mL axial lab device to 150 mL capsule device. The resulting scale factor is 18 for the 150 mL device. Furthermore, the IgG and HMWS separation are performed as a bind and elute process with a dedicated component breakthrough. Following this, the experiment includes a breakthrough concentration profile, competitive adsorption, and elution, which are then compared to the simulative results.

In addition to the dimensionless fluid dynamic scale transfer and SMA parameter, the kinetic effects also require a scalable approach. Subsequent to the kinetic effect investigation, the process is evaluated within the earlier by us introduced direct scale factor and mechanistic modeling accuracy.<sup>181</sup>

#### 6.3.3.1 Kinetic evaluation

The kinetic interactions are transferred in scale based on the state-of-the-art Peclet number determination. In addition, the historical HTS results are used to investigate the change of the kinetic factor/ Peclet number within the different pH values. In addition to the Peclet number determination by historical data, separation at different lab device scales is investigated regarding the scale consistency.

In Figure 6.18, the kinetic simulation results are presented. Initially, the different device Peclet numbers are presented in A). Initially, the different device Peclet numbers are presented in A). The investigated devices were the small-scale SDD, LM30, and LM60. Following the Sartobind S® pH 5 at 0.02 M salt IgG experiments, a significant deviation of the Peclet number can be observed in the box diagram. Although the Peclet number presents a range of ~140 – 550 for IgG and ~100 – 170 for HMWS, the small-scale device kinetic factor is with 0.003 – 0.013 for IgG and 0.0025 – 0.066 for HMWS in a reasonable range. The deviation might indicate uncertainties in the SMA parameter. This said, the deviation could be accumulated in the kinetic factor. These limitations in the dynamic isotherm assessment were already discussed. However, the determined deviations are then applied to the Peclet number pH dependency investigation, presented in Figure 6.18. In the evaluation of the assumed relative scale deviation at different pH values, the simulative error minimized BE, and OBE model results were predicted by applying an exponential decrease function (B, C). The investigation presents a reduction of the Peclet number with an increasing pH value. Following this, mass transfer restriction increases with the pH value. Hence, the convergence towards the isoelectric point reduces the attractive ionic forces leading to a lower mass transfer rate.

In summary, the dimensionless kinetic evaluation presents a pH dependency of the Peclet number. The dependency is described with an allomeric and exponential decrease function facilitation the consideration of a scale-up for the whole process range. Admittedly, the different scale device investigation presents a deviation for the dimensionless Peclet number. This said, the dynamic isotherm parameter determination might limit the validity, including blending of isotherm parameter and partially kinetic effects. However, the assessment delivers a limiting range for the upper kinetic factor facilitation a simpler model parameter determination when additional information is available.

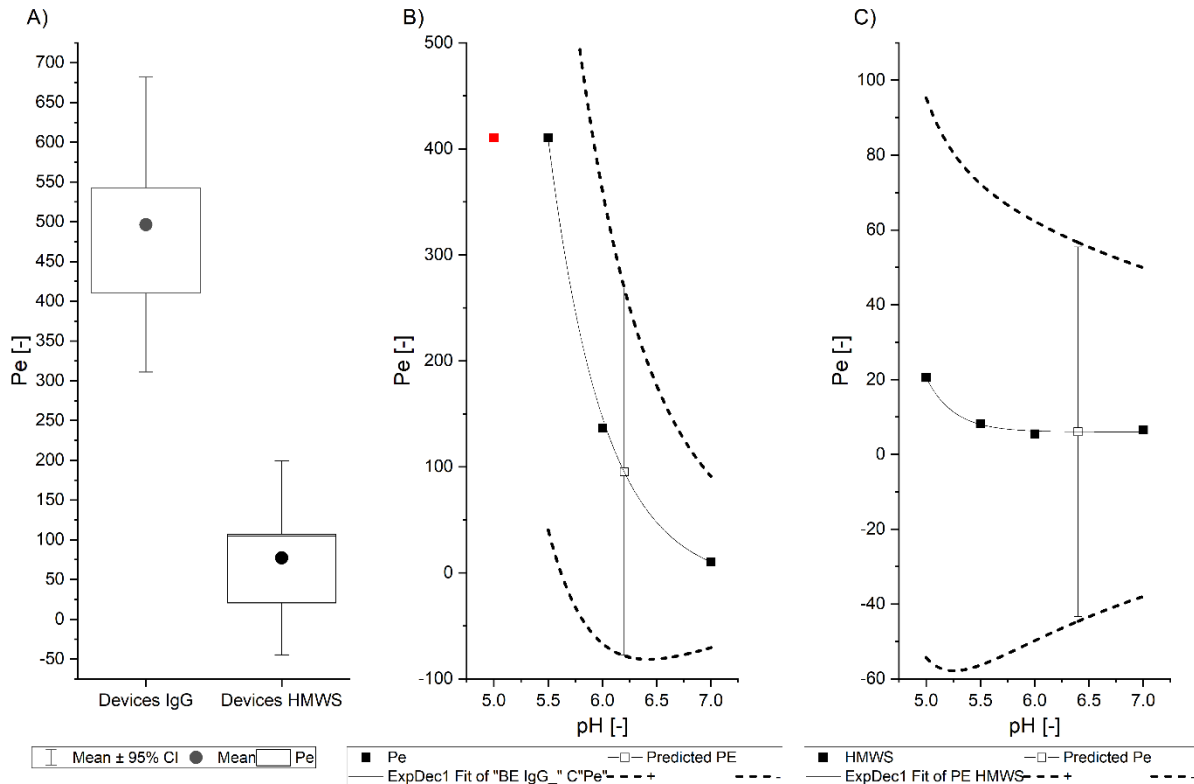


Figure 6.18: In A) a Box diagram of the Peclet number range for HTS SDD, LM30, and LM60. The Peclet number was determined by simulative error minimization of the kinetic factor for different experiments with Sartobind® S. The experiments used were conducted at pH 5 and 0.02 M for all scales. The kinetic factor was determined by simulative error minimization. Assuming relative scale deviation at different pH values, the simulative error minimized BE and OBE experiments results were predicted by applying an exponential decrease function (B, C). The red square (B) is not considered in the PE determination. In B), the Peclet number for IgG with a misleading negatively Peclet number is presented. The Peclet number range of HMWS in C) also presents a negatively Peclet number. This said, the resulting range limits the possible upper kinetic factor, while the lower kinetic factor cannot be narrowed.

### 6.3.3.2 Scale-up

The scale-up is performed with the dynamic assessed isotherm parameter, and the HTS SDD determined kinetic coefficient applying the derived Bodenstein and Peclet number. Figure 6.19 shows a comparison between experimental and simulative signal course for an IgG and HWMS separation at pH 6.4 and 0.1 M salt using a 150 mL Sartobind® S Capsule. The experimental and simulative accumulative signal is presented in A). In addition, the experimental fractions concentrations are shown in B) and the simulative fraction concentration in C), respectively.

Comparing the simulative and experimental results in Figure 6.19 A) presents an offset in the initial breakthrough concentration of approximately 1 MV. In addition, the simulation elution peak starts at a lower volume when compared to the experimental results. Furthermore, the elution peak is predicted to be higher than observed in the experiment. Thus, the components adsorption is predicted to be higher than in the experiment observed. The fraction concentration comparison in B) and C) present comparable results in the initial breakthrough profile. However, the simulation predicts the HMWS breakthrough earlier and is sharper in form. Following the earlier predicted HMWS breakthrough concentration, the HMWS fraction concentration is predicted to be too low in the elution. The observed deviations are most likely a result of the dynamic isotherm assessment, blending isotherm parameter, and kinetic effects, as well as limitations in the kinetic parameter determination

### 6.3 Results and Discussion

based on historical HTS parameter. However, considering a scale factor of  $\sim 320$  (0.46ml - 150 mL) presents a good comparison between experimental and simulative results applying historical HTS experiments. In addition, the breakthrough concentration and elution peak are predicted with a deviation of 150 mL within a safety margin below 10 %.

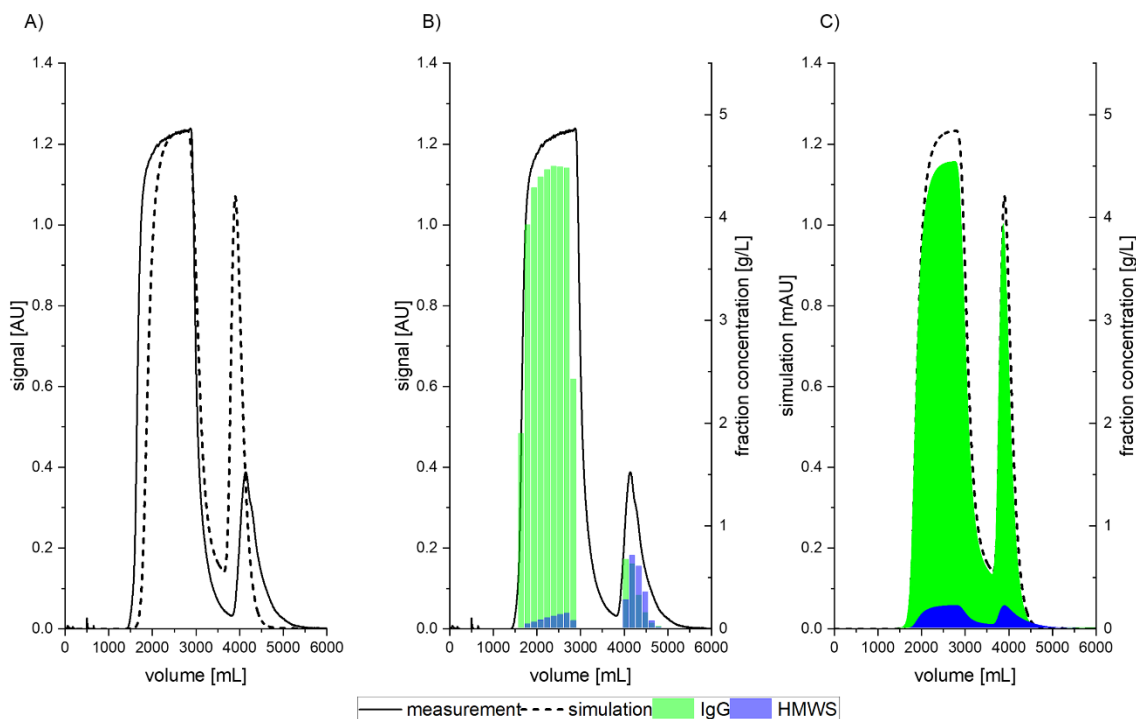


Figure 6.19: Comparison between experimental and simulative signal course for an IgG and HMWS separation at pH 6.4 and 0.1 M salt applying a 150 mL Sartobind® S Capsule. The experimental and simulative accumulative signal is presented in A). In addition, the experimental fractions concentrations are shown in B) and the simulative fraction concentration in C), respectively.

When introducing a new method, the derived advantages and disadvantages must be considered to evaluate the benefit compared to existing methods. This said, the presented simulative method is simplified compared to the most easily scale-factor method. The scale-factor method uses the DBC at a certain volume and predicts the larger scale breakthrough based on the stationary phase volume.

In general, this method's scale-factor simplicity and low needed effort make it so appealing to other methods. Furthermore, in this case study, the simulative and scale-factor predicted DBC deviation are quite comparative, see Table 6.7.

However, the introduced simulative approach reduces the simulative effort drastically after device and system characterization. This said, the fluid dynamic investigation would be neglected, and the isotherm parameters could be determined within the same experiments needed for the scale-factor determination. However, reducing simulative information to that of the scale-factor naturally presents a disadvantage for the simulative investigation. Following this, the benefits of the simulation approach facilitating a living library are the additional information, preservation, and transferability. In contrast to the scale-factor, the simulative approach can be extended/transferred with the device, stationary phase, component information, and different processing modes.

In summary, the scale-factor scale-up delivers a simple and fast scale-up prediction facilitating a fast PD. Comparatively, the introduced simulative approach reduces the efforts in parameter

determination and inclusion of historical data. The additional information facilitates a faster PD by applying, preserving, and adapting information for future separation challenging. Furthermore, the previous and subsequent unit operation can be included in a holistic PD approach, facilitating process control strategies, robustness, and Quality by Design description. Thus, the simulative living library approach enables future proven competition in manufacturing.

Table 6.7: Comparison of experimental, scale factor and simulation results for an IgG and HMWS separation applying a 150 mL Sartobind® S Capsule.

	DBC <sub>10</sub>		Binding capacity	
Prediction Scale Factor	1570	[mL]	-	[mg/mL]
Prediction Simulation	1760	[mL]	2.1	[mg/mL]
Experimental Result	1650	[mL]	1.8	[mg/mL]
<b>Ratio Scale Factor / Experiment</b>	<b>0.95</b>	<b>[-]</b>	<b>-</b>	<b>[-]</b>
<b>Ratio Simulation / Experiment</b>	<b>1.07</b>	<b>[-]</b>	<b>1.17</b>	<b>[-]</b>
Prediction Scale Factor	1985	[mL]	-	[mg/mL]
Prediction Simulation	1842	[mL]	0.4	[mg/mL]
Experimental Result	1800	[mL]	2.0	[mg/mL]
<b>Ratio Scale Factor / Experiment</b>	<b>1.10</b>	<b>[-]</b>	<b>-</b>	<b>[-]</b>
<b>Ratio Simulation / Experiment</b>	<b>1.02</b>	<b>[-]</b>	<b>0.20</b>	<b>[-]</b>

Finally, the presented workflow exemplified the development of standardized, scalable device models, incorporating historical data into a process library and successfully scaling model prediction. In addition, the work can be divided into scale-up model development and reduction in model development effort by historical data. The general model development was refined for the scale-up incorporating historical data in Figure 6.2, including the reduction of the non-significant parameters. The schematic model development presented in Figure 6.2 is divided by the model developed in A) and the reduced parameter determination in B). The green checkmarks were performed within the presented work.

Moreover, the black checkmarks identify parameters/information which were already integrated into the library, (1)<sup>181</sup>, (2)<sup>209</sup> and (3)<sup>181</sup>. Consequently, the presented workflow reduces the effort in model development, facilitating a faster and more comprehensive PD. Furthermore, the device models can be transferred to historical or future investigations. Nevertheless, the transfer of adsorption parameter would need further investigation for other species. However, building a living model library and implementing the necessary workflows could allow the study of transferring adsorption parameters to other species. This said, the current challenges in PD could be overcome, and needed drugs could be delivered more quickly and cost-effectively.

### 6.3.4 Conclusion

The introduction of the from lab to production method provides procedures to simplify mechanistic model approaches for use in a living library approach. Initially, the used devices at all scales are investigated to facilitate a dimensionless description and transfer among the scales and flow direction. Following this, future MM approaches would not need fluid dynamic investigations reducing the experimental and simulative workload. The fluid dynamic dimensionless procedure facilitates a good transfer from HTS SDD to pilot scale, while consideration of physical changes in the pilot device would leave room for improvement. Thereafter, historical HTS data is applied to assess the apparent isotherm parameters. In addition to classical BE data, a comparison with additive OBE experiments that provided further competitive binding information was conducted. The dynamic isotherm parameter determination was then used to compare the HTS data at different pH values. This said, the simulated concentration course and process maps delivered good agreements with the experimental results; even so, isotherm parameter and kinetic effects are blended. After the isotherm parameter determination, the kinetic coefficient is determined at different pH values with the HTS experiments and transferred to a dimensionless PE number description. The kinetic coefficient investigation presents reasonable kinetic information, increasing the kinetic coefficient with the pH value but also high uncertainties in the actual parameter. Following this, the dynamic isotherm determination and kinetic coefficient determination might need further refinement. However, the scale-up by a factor of  $\sim 320$  presents good accordance (below 10 %) between experiments and simulative IgG and HMWS results.

In summary, the presented methodology adapts existing tools (wet lab and simulation) in PD and delivers a simplified holistic mechanistic modeling approach. The received information could then be used to develop a PD living library, including stationary phase, component, process parameter, and process mode information. Furthermore, by continuously increasing the information content, the living library could provide information on separation asks that have not yet been investigated. This said, uncertainties of the determined parameter and model accuracy need to be considered to facilitate a manual or artificial intelligence-enabled extrapolation. Consequently, the future PD work could strengthen the overall process development considering the investigation of previous and subsequent unit operations, optimizing process design, process control strategies, robustness, and Quality by Design.

### 7 Conclusion and Outlook

The limiting toolbox in product development to overcome the present challenges in the pharmaceutical industry is addressed in this Ph.D. thesis. Here it is aimed at a holistic approach in the form of a living library for chromatography process development to address the challenges of different stationary phases, operation modes, and process parameters. Following this, a living library summarizes all information as a single point of truth. However, screening techniques and workflows have historically been shaped for resins and show imbalance for other stationary phases. The existing library approaches are typically self-limiting, maintaining a manageable complexity and neglecting new stationary phases and operation modes. However, new and comprehensive methods are needed to comply with the shortened timescales and to facilitate long-term competitiveness. Process parameters are determined by various established techniques such as wet lab experiments and models. However, the wet lab experimental result preservation and transfer are limited until now. Therefore, statistical- and mechanistic models have been implemented. While academia established simulation and mechanistic modeling and supports the industrial application with qualification methods, the industry is challenged to integrate the new powerful tool in existing PD workflows. These challenges are addressed by establishing a level-playing field for convective material in the wet lab workflow. In addition, incorporating new processing modes, considering competitive adsorption processes and stationary phases, as well as developing a digital twin, are considered.

Furthermore, comparing different processing modes and stationary phases is facilitated by considering theoretical and experimental information. In addition, a holistic living library workflow is presented for the mAb HMWS purification step. Finally, ensuring a level-playing field for different stationary phases, including new processing modes and stationary phases comparability, allows the elaboration of a living library concept developed. The fluid dynamic transfer, apparent adsorption parameter determination with historical data, and the scale-up from small-scale HTS to pilot scale by mechanistic modeling were shown in three case studies. Following this, the first complete data point for the living library approach was generated.

Initially, an HTS SDD was developed for convective stationary phases. The HTS SDD was then investigated to facilitate a digital twin applying mechanistic modeling for the applied BE mode. Next, the performed case studies aimed to align HTS applications for MAs with those established for column chromatography enabling a level-playing field. Following this, the investigations focused on experimental HTS characterization, process parameter determination, and mechanistic model development and verification.

The experimental HTS characterization included robotic parameter evaluation, SDD optimization, and characterization by comparing the HTS SDD set-up with benchtop results. Consequently, deviations between HTS and benchtop scale were identified and minimized. In addition, process parameter range evaluation was performed in a bind and elute mode, obtaining process operation windows by pH and salt concentration variations. In addition, the ion-exchange MAs Sartobind S and Q were investigated for their HMWS reduction potential in a mAb purification step. Benchtop experiments verified these process windows. Accordingly, the HTS SDD representation of benchtop results was successfully confirmed. In a sub-case study, we successfully developed a mechanistic model based on parameters obtained from the SDD - HTS set-up. The results proved to validate the use of the SDD developed for parameter estimation and thus model-based PD. In addition, it was shown that the transferability and

scalability of data from the SDD - HTS set-up using both a direct scale factor and mechanistic modeling. The developed digital twin presented itself sufficient, with deviations less than 20 % for HTS and scale-up predictions. The obtained HTS SDD set-up and digital twin facilitated a deeper understanding of the convective material and narrowed the differences between convective MA and resin PD workflow.

The second part of this thesis applies the developed HTS SDD set-up to achieve a level-playing field for convective material in the PD toolbox. Accordingly, the HTS SDD feasibility of evaluating a new process operation mode is investigated. Therefore, competitive adsorption-based displacement effects were investigated theoretically by mechanistic modeling. Subsequently, a novel HTS screening procedure was developed, including determining competitive adsorption-based displacement effects and key parameter identification. Finally, the screening procedure employing an OBE mode is presented in a case study dealing with IgG HMWS removal in a typical monoclonal antibody purification step, applying a Sartobind® S membrane adsorber (MA).

Correspondingly to the above-described approach, the mechanistic modeling investigation of competitive adsorption-based displacement effects enabled the development of a new HTS screening mode. The OBE mode allows the determination of classical process parameters and dynamic effects, such as displacement effects. Competitive adsorption-based displacement effects are visualized by introducing a displacement identifier (DI), leading to a displacement process map. In addition, the OBE results were confirmed by benchtop recycle experiments proving the representation of different operation modes with the developed HTS SDD set-up. Furthermore, the mechanistic modeling evaluation resulted in an isotherm-based assessment of competitive adsorption-based effects.

Thereafter, the comparison of different stationary phases and backbones by HTS is performed. The various possible scaffolds, ligands, and process parameters challenge the PD efficiency. This said, the common response to this diversity is the establishment of platform processes to develop chromatographic unit operations. However, the general generated library information is reduced to manageable information such as typical process parameters of selected stationary phases. We propose a rigorous strategy to reduce the various experimental design space resulting from possible combinations in scaffolds, backbones, and ligands.

The strategy is addressed in a case study on a novel MiMo adsorber for removing mAb HMWS and compared to the performance of Capto™ Adhere. Moreover, the proposed strategy is based on theoretical considerations, identification of adsorber selectivity, and capacity to identify a suitable membrane system. Subsequent to the theoretical evaluation, the evaluation is supported by HTS SDD and benchtop wet lab experiments. The initial theoretical evaluation reduced the stationary phase backbones and confirmed one investigated ligand in a benchtop confirmation run. In addition to practical results, the introduced PD strategy presents the effectiveness of a living library considering theoretical information. Consequently, incorporating theoretical information and transferring it to a manageable amount of data, e.g., represented by model information, would support the PD's effectiveness.

Finalized is this thesis by investigating the linkage of PD tools facilitating a more universal approach. The connection between the introduced approaches and the mentioned PD tools is needed to overcome the current limitation in PD. Consequently, we introduce a PD procedure facilitating a guide to transit from partially connected development tools to a fully integrable process development living library approach. The process tools are linked by three case studies in which mechanistic modeling enables the preservation and further investigation of information. Generally, the typical mechanistic

modeling chromatography characterization process is performed but here focused on the scale transfer to the pilot scale. Hence, the devices at different scales are precisely investigated. In addition, the implementation of imperfect historical data into a living library is represented by an apparent isotherm parameter determination based on HTS results.

The initially performed fluid dynamic investigations presented imperfection in the lab-scale device fluid distribution. Following this, the fluid distributor was optimized. The challenges in different fluid distribution between axial and radial devices are overcome by developing a new lab module. This said, the new lab module facilitates different membrane layers in one module within the same device set-up. Thus, the separation of membrane layers and device were separated and successfully transferred to the radial device. Consequently, different stationary phases could be included in the library by the known fluid dynamic impact of the device. Thereafter, historical HTS data for an IgG HMWS separation derived an apparent SMA isotherm parameter. The investigation presented imperfections due to adsorption and kinetic parameter blending. However, the scale transfer from the 0.46 mL HTS small-scale device with axial fluid flow to a 150 mL pilot scale device with a radial fluid flow was proven successful, with a deviation below 10 % for the DBC prediction.

Eventually, this thesis contributes with its individual chapters to understanding convective material in HTS, competitive adsorption processes, effects of different stationary phase properties induced, and challenges in the present PD toolbox. The different chapters are supported by mechanistic modeling, facilitating deeper understanding. In addition, incorporating the chapters present a thorough methodology to develop a living library that links all tools in PD. Furthermore, the achieved level-playing field between different stationary phases enables process investigation and a deeper understanding of chromatographic effects. The transfer from lab to pilot scale presented detailed information on different scale effects but also delivered a simplified approach for a broad audience. Accordingly, the methodology could be transferred to other unit operations by adjusting the models and dimensionless numbers. However, further investigation is needed in parameter determination, modeling, and utilization of a living library. The parameter determination, especially in isotherm and kinetic parameters, is challenged by competitive adsorption processes, low entity concentration, and the possible failure even by a sufficient error minimization fit. Given a profound analysis of the correct modeling parameter would facilitate a better and faster scale transfer reducing the experimental effort further. The applied models presented simplifications in fluid dynamics and mass transfer. In radial devices, the axial dispersion coefficient was kept constant while the velocity changed with the radius. In addition, the MA applied consists of a hydrogel volume which changes with the salt and pH value. These effects should be evaluated regarding significance for the scale transfer. Furthermore, the hydrogel volume change might also imply adsorptive or steric changes that need to be investigated. Given these examples in model simplification, new materials and devices should also be sufficiently represented by a model to be included in the living library. Regarding the living library utilization, general approaches should be developed to structure, organize, and add the obtained process and molecule information. Furthermore, recent developments in molecular modeling should be included as well.

8 Verification of the contribution from the co-authors

Title: HTS setup of a Scale-down Device for Membrane Chromatography - Aggregate Removal of Monoclonal Antibodies

Journal: Biotechnology Progress

Authors: Dominik Stein, Volkmar Thom, Jürgen Hubbuch

**Position in the dissertation:**

The content of this paper has been included in Chapter 3

Contribution of "Dominik Stein"

Conceptualization

Formal analysis

Investigation

Methodology

Supervision

Visualization

Manuscript preparation – original draft

Manuscript revision and final approval of the manuscript

Contribution of "Volkmar Thom"

Supervision

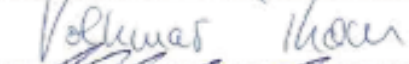
Manuscript revision - review

Contribution of "Jürgen Hubbuch"

Supervision

Manuscript revision – review & editing

**Signature of the authors:**

Author	Signature
(Dominik Stein)	
(Dr. Volkmar Thom)	
(Prof. Dr. Jürgen Hubbuch)	

## Verification of the contribution from the co-authors

---

Title: PD exploiting competitive adsorption-based displacement effects in monoclonal antibody aggregate removal - a new high throughput screening procedure for membrane chromatography

Journal: Biotechnology and applied biochemistry

Authors: Dominik Stein, Volkmar Thom, Jürgen Hubbuch

### Position in the dissertation:

The content of this paper has been included in Chapter 4

### Contribution of "Dominik Stein"

Conceptualization  
Formal analysis  
Investigation  
Methodology  
Supervision  
Visualization  
Manuscript preparation – original draft  
Manuscript revision and final approval of the manuscript

### Contribution of "Volkmar Thom"

Supervision  
Manuscript revision - review

### Contribution of "Jürgen Hubbuch"

Methodology  
Supervision  
Manuscript revision – review & editing

### Signature of the authors:

Author	Signature
(Dominik Stein)	
(Dr. Volkmar Thom)	
(Prof. Dr. Jürgen Hubbuch)	

Title: Streamlined PD procedure incorporating the selection of various stationary phase types established in a mAb aggregate reduction study with different mixed mode ligands

Journal: Biotechnology Progress

Authors: Dominik Stein, Volkmar Thom, Jürgen Hubbuch

**Position in the dissertation:**

The content of this paper has been included in Chapter 5

**Contribution of "Dominik Stein"**

Conceptualization

Formal analysis

Investigation

Methodology

Supervision

Visualization

Manuscript preparation – original draft

Manuscript revision and final approval of the manuscript

**Contribution of "Volkmar Thom"**

Supervision

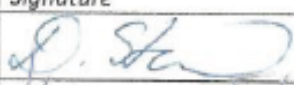
Manuscript revision - review

**Contribution of "Jürgen Hubbuch"**

Supervision

Manuscript revision – review & editing

**Signature of the authors:**

<i>Author</i>	<i>Signature</i>
(Dominik Stein)	
(Dr. Volkmar Thom)	
(Prof. Dr. Jürgen Hubbuch)	

## 9 References

1. Saleh D, Wang G, Mueller B, et al. Cross-scale quality assessment of a mechanistic cation exchange chromatography model. *Biotechnol Prog*. 2021;37(1):e3081. doi:10.1002/btpr.3081.
2. Narayanan H, Luna MF, Stosch M von, et al. Bioprocessing in the Digital Age: The Role of Process Models. *Biotechnol J*. 2020;15(1):e1900172. doi:10.1002/biot.201900172.
3. Baumann P, Hubbuch J. Downstream process development strategies for effective bioprocesses: Trends, progress, and combinatorial approaches. *Eng Life Sci*. 2017;17(11):1142-1158. doi:10.1002/elsc.201600033.
4. Hahn T, Huuk T, Osberghaus A, et al. Calibration-free inverse modeling of ion-exchange chromatography in industrial antibody purification. *Eng Life Sci*. 2016;16(2):107-113. doi:10.1002/elsc.201400248.
5. Zobel-Roos S, Schmidt A, Mestmäcker F, et al. Accelerating Biologics Manufacturing by Modeling: Is Approval under the QbD and PAT Approaches Demanded by Authorities Acceptable Without a Digital-Twin? *Processes*. 2019;7(2):94. doi:10.3390/pr7020094.
6. Herwig C. *Digital Twins: Tools and Concepts for Smart Biomanufacturing*. Cham: Springer International Publishing AG; 2021. Advances in Biochemical Engineering/Biotechnology Ser; v.176. <https://ebookcentral.proquest.com/lib/kxp/detail.action?docID=6568330>.
7. Google Ireland Limited. Google Trends search term "vaccine production". <https://trends.google.de/trends/explore?date=2010-01-01%202021-10-11&gprop=news&q=vaccine%20production>. Accessed November 14, 2021.
8. European Commission. European Vaccine Research and Development Infrastructure. <https://cordis.europa.eu/project/id/730964>. Accessed June 25, 2022.
9. European Commission, iMi. ADVANCE (Accelerated development of vaccine benefit-risk collaboration in Europe). <https://www.imi.europa.eu/projects-results/project-factsheets/advance>.
10. European Union, iMi, efpia. ADAPTSMART. <http://adaptsmart.eu/work-packages/>. Accessed June 25, 2022.
11. IMI CARE, European Commission. CARE / (Corona Accelerated R&D in Europe). <https://www.imi-care.eu/legal-notice/>.
12. Jungbauer A. Continuous downstream processing of biopharmaceuticals. *Trends Biotechnol*. 2013;31(8):479-492. doi:10.1016/j.tibtech.2013.05.011.
13. Shukla AA, Hubbard B, Tressel T, Guhan S, Low D. Downstream processing of monoclonal antibodies--application of platform approaches. *J Chromatogr B Analyt Technol Biomed Life Sci*. 2007;848(1):28-39. doi:10.1016/j.jchromb.2006.09.026.
14. Liu HF, Ma J, Winter C, Bayer R. Recovery and purification process development for monoclonal antibody production. *MAbs*. 2010;2(5):480-499. doi:10.4161/mabs.2.5.12645.
15. Brestrich N, Sanden A, Kraft A, McCann K, Bertolini J, Hubbuch J. Advances in inline quantification of co-eluting proteins in chromatography: Process-data-based model calibration and application towards real-life separation issues. *Biotechnol Bioeng*. 2015;112(7):1406-1416. doi:10.1002/bit.25546.

16. Tripathi NK, Shrivastava A. Recent Developments in Bioprocessing of Recombinant Proteins: Expression Hosts and Process Development. *Front Bioeng Biotechnol.* 2019;7:420. doi:10.3389/fbioe.2019.00420.
17. Shukla AA, Thömmes J. Recent advances in large-scale production of monoclonal antibodies and related proteins. *Trends Biotechnol.* 2010;28(5):253-261. doi:10.1016/j.tibtech.2010.02.001.
18. Walther J, Godawat R, Hwang C, Abe Y, Sinclair A, Konstantinov K. The business impact of an integrated continuous biomanufacturing platform for recombinant protein production. *J Biotechnol.* 2015;213:3-12. doi:10.1016/j.jbiotec.2015.05.010.
19. Kelley B. DOWNSTREAM PROCESSING OF MONOCLONAL ANTIBODIES: CURRENT PRACTICES AND FUTURE OPPORTUNITIES. In: Gottschalk U, ed. *Process Scale Purification of Antibodies*. Vol. 25. Hoboken, NJ, USA: John Wiley & Sons, Inc; 2017:1-21.
20. Mollerup JM, Hansen TB, Kidal S, Sejergaard L, Staby A. Development, modeling, optimisation and scale-up of chromatographic purification of a therapeutic protein. *Fluid Phase Equilibria.* 2007;261(1-2):133-139. doi:10.1016/j.fluid.2007.07.047.
21. Hahn R. Methods for characterization of biochromatography media. *J Sep Sci.* 2012;35(22):3001-3032. doi:10.1002/jssc.201200770.
22. Oelmeier SA, Ladd Effio C, Hubbuch J. High throughput screening based selection of phases for aqueous two-phase system-centrifugal partitioning chromatography of monoclonal antibodies. *J Chromatogr A.* 2012;1252:104-114. doi:10.1016/j.chroma.2012.06.075.
23. Ken Broeckhoven, Jelle De Vos, Gert Desmet. ressure, Particles, and System Contribution: The Holy Trinity of Ultrahigh-Performance Liquid Chromatography. <https://www.chromatographyonline.com/view/particles-pressure-and-system-contribution-holy-trinity-ultrahigh-performance-liquid-chromatograph-0>. Accessed June 28, 2022.
24. Tale uzzam an M, Ali S, Gilan i SJ, Imam SS, Hafez A. Ultra Performance Liquid Chromatography (UPLC) - A Review. *Austin J Anal Pharm Chem.* 2015;(Vol. 2 Issue 6). [https://d1wqtxts1xzle7.cloudfront.net/64357302/Ultra%20Performance%20Liquid%20Chromatography%20\(UPLC\)%20-%20A-with-cover-page-v2.pdf?Expires=1656404057&Signature=Cc1vA3-VLjSdYbC8NYuDAyJrqbhbbyQ59NpNIznxOqGyo0ADtL-X5XM3mCJtEyN0rwHVdiXcZkt~s5p-DVf1QicqoRs3hVg3F-dUJm0WUx05E0499WskBpkiCUL2ch7FAUloYbX~23IbTtbe7sHFMD4HEQt3yVTY2NN5ut-MxGyJ0n2UylicczocE6~CKXegAsPe~LNZOeCUAB2bcs3lPS~RAUp80-3KKGpioo68rkmlMahNR-oWaZOONPOyqODXvaln7XOjXySKSFV2F9xLEnjBw0KVJczgMOUfRsm0itcRYVWk~QQiY1vtHJOW1D aqzhRvMU4K43Pifw0~Y7Ncw\\_\\_&Key-Pair-Id=APKAJLOHF5GGSLRBV4ZA](https://d1wqtxts1xzle7.cloudfront.net/64357302/Ultra%20Performance%20Liquid%20Chromatography%20(UPLC)%20-%20A-with-cover-page-v2.pdf?Expires=1656404057&Signature=Cc1vA3-VLjSdYbC8NYuDAyJrqbhbbyQ59NpNIznxOqGyo0ADtL-X5XM3mCJtEyN0rwHVdiXcZkt~s5p-DVf1QicqoRs3hVg3F-dUJm0WUx05E0499WskBpkiCUL2ch7FAUloYbX~23IbTtbe7sHFMD4HEQt3yVTY2NN5ut-MxGyJ0n2UylicczocE6~CKXegAsPe~LNZOeCUAB2bcs3lPS~RAUp80-3KKGpioo68rkmlMahNR-oWaZOONPOyqODXvaln7XOjXySKSFV2F9xLEnjBw0KVJczgMOUfRsm0itcRYVWk~QQiY1vtHJOW1D aqzhRvMU4K43Pifw0~Y7Ncw__&Key-Pair-Id=APKAJLOHF5GGSLRBV4ZA). Published December 31, 2015.
25. Snyder LR, Dolan JW. Milestones in the development of liquid chromatography. In: *Liquid Chromatography*. Vol. 21. Elsevier; 2017:1-15.
26. Coskun O. Separation techniques: Chromatography. *North Clin Istanbul.* 2016;3(2):156-160. doi:10.14744/nci.2016.32757.
27. LoBrutto R, Kazakevich Y, eds. *HPLC for pharmaceutical scientists*. Hoboken, N.J.: Wiley-Interscience; 2007. <https://onlinelibrary.wiley.com/doi/book/10.1002/0470087951>.
28. Isane SP, Waghmare SA, Kamble HV. A Review on Method Development, Validation, Optimization and Applications of HPLC. *IJRASET.* 2022;10(5):1860-1867. doi:10.22214/ijraset.2022.42685.
29. Aguilar M-I. HPLC of peptides and proteins: basic theory and methodology. *Methods Mol Biol.* 2004;251:3-8. doi:10.1385/1-59259-742-4:3.

30. Morley R, Minceva M. Liquid-Liquid Chromatography: Current Design Approaches and Future Pathways. *Annu Rev Chem Biomol Eng.* 2021;12:495-518. doi:10.1146/annurev-chembioeng-101420-033548.
31. Marchal L, Legrand J, Foucault A. Centrifugal partition chromatography: a survey of its history, and our recent advances in the field. *Chem Rec.* 2003;3(3):133-143. doi:10.1002/tcr.10057.
32. DiMasi JA, Hansen RW, Grabowski HG. The price of innovation: new estimates of drug development costs. *J Health Econ.* 2003;22(2):151-185. doi:10.1016/S0167-6296(02)00126-1.
33. DiMasi JA, Grabowski HG, Hansen RW. Innovation in the pharmaceutical industry: New estimates of R&D costs. *J Health Econ.* 2016;47:20-33. doi:10.1016/j.jhealeco.2016.01.012.
34. Gottschalk U. *Process Scale Purification of Antibodies.* Hoboken, NJ, USA: John Wiley & Sons, Inc; 2017.
35. Keller WR, Evans ST, Ferreira G, Robbins D, Cramer SM. Use of MiniColumns for linear isotherm parameter estimation and prediction of benchtop column performance. *J Chromatogr A.* 2015;1418:94-102. doi:10.1016/j.chroma.2015.09.038.
36. Kistler C, Pollard J, Ng LS, Streefland M. High-Throughput Bioprocess Development. *Genetic Engineering & Biotechnology News.* 2016;36(7):30-31. doi:10.1089/gen.36.07.15.
37. Shukla AA, Rameez S, Wolfe LS, Oien N. High-Throughput Process Development for Biopharmaceuticals. *Adv Biochem Eng Biotechnol.* 2018;165:401-441. doi:10.1007/10\_2017\_20.
38. Bareither R, Bargh N, Oakeshott R, Watts K, Pollard D. Automated disposable small-scale reactor for high throughput bioprocess development: a proof of concept study. *Biotechnol Bioeng.* 2013;110(12):3126-3138. doi:10.1002/bit.24978.
39. Wiendahl M, Schulze Wierling P, Nielsen J, et al. High Throughput Screening for the Design and Optimization of Chromatographic Processes – Miniaturization, Automation and Parallelization of Breakthrough and Elution Studies. *Chem Eng Technol.* 2008;31(6):893-903. doi:10.1002/ceat.200800167.
40. Collins, L. A., and Scott G. Franzblau. *Microplate alamar blue assay versus BACTEC 460 system for high-throughput screening of compounds against Mycobacterium tuberculosis and Mycobacterium avium.* Antimicrobial agents and chemotherapy; 1997.
41. Gupta PB, Onder TT, Jiang G, et al. Identification of selective inhibitors of cancer stem cells by high-throughput screening. *Cell.* 2009;138(4):645-659. doi:10.1016/j.cell.2009.06.034.
42. Wambaugh MA, Shakya VPS, Lewis AJ, Mulvey MA, Brown JCS. High-throughput identification and rational design of synergistic small-molecule pairs for combating and bypassing antibiotic resistance. *PLoS Biol.* 2017;15(6):e2001644. doi:10.1371/journal.pbio.2001644.
43. Langer R, Tirrell DA. Designing materials for biology and medicine. *Nature.* 2004;428(6982):487-492. doi:10.1038/nature02388.
44. Zhou Y, Zhu S, Cai C, et al. High-throughput screening of a CRISPR/Cas9 library for functional genomics in human cells. *Nature.* 2014;509(7501):487-491. doi:10.1038/nature13166.
45. Ladd Effio C, Baumann P, Weigel C, Vormittag P, Middelberg A, Hubbuch J. High-throughput process development of an alternative platform for the production of virus-like particles in Escherichia coli. *J Biotechnol.* 2016;219:7-19. doi:10.1016/j.jbiotec.2015.12.018.
46. Lindström S, Larsson R, Svahn HA. Towards high-throughput single cell/clone cultivation and analysis. *Electrophoresis.* 2008;29(6):1219-1227. doi:10.1002/elps.200700536.
47. Bensch M, Selbach B, Hubbuch J. High throughput screening techniques in downstream processing: Preparation, characterization and optimization of aqueous two-phase systems. *Chemical Engineering Science.* 2007;62(7):2011-2021. doi:10.1016/j.ces.2006.12.053.

48. Diederich P, Hoffmann M, Hubbuch J. High-throughput process development of purification alternatives for the protein avidin. *Biotechnol Prog.* 2015;31(4):957-973. doi:10.1002/btpr.2104.
49. Coffman JL, Kramarczyk JF, Kelley BD. High-throughput screening of chromatographic separations: I. Method development and column modeling. *Biotechnol Bioeng.* 2008;100(4):605-618. doi:10.1002/bit.21904.
50. Bensch M, Schulze Wierling P, Lieres E von, Hubbuch J. High Throughput Screening of Chromatographic Phases for Rapid Process Development. *Chem Eng Technol.* 2005;28(11):1274-1284. doi:10.1002/ceat.200500153.
51. Dorsey JG. Editorial on "Mass transfer kinetics, band broadening and column efficiency" by F. Gritti and G. Guiochon. *J Chromatogr A.* 2012;1221:1. doi:10.1016/j.chroma.2011.11.004.
52. Tsuneda S, Saito K, Furusaki S, Sugo T. High-throughput processing of proteins using a porous and tentacle anion-exchange membrane. *Journal of Chromatography A.* 1995;689(2):211-218. doi:10.1016/0021-9673(94)00911-R.
53. Osberghaus A, Drechsel K, Hansen S, et al. Model-integrated process development demonstrated on the optimization of a robotic cation exchange step. *Chemical Engineering Science.* 2012;76(1):129-139. doi:10.1016/j.ces.2012.04.004.
54. Leuthold M. *Characterization of Membrane Adsorbers for Contaminant Removal.* 1. Aufl. Saarbrücken: Südwestdeutscher Verlag für Hochschulschriften; 2014. Accessed June 18, 2018.
55. Nfor BK, Noverraz M, Chilamkurthi S, Verhaert PDEM, van der Wielen LAM, Ottens M. High-throughput isotherm determination and thermodynamic modeling of protein adsorption on mixed mode adsorbents. *J Chromatogr A.* 2010;1217(44):6829-6850. doi:10.1016/j.chroma.2010.07.069.
56. Keller WR, Evans ST, Ferreira G, Robbins D, Cramer SM. Understanding operational system differences for transfer of miniaturized chromatography column data using simulations. *J Chromatogr A.* 2017;1515:154-163. doi:10.1016/j.chroma.2017.07.091.
57. Łacki KM. High-throughput process development of chromatography steps: advantages and limitations of different formats used. *Biotechnol J.* 2012;7(10):1192-1202. doi:10.1002/biot.201100475.
58. Benner SW, Welsh JP, Rauscher MA, Pollard JM. Prediction of lab and manufacturing scale chromatography performance using mini-columns and mechanistic modeling. *J Chromatogr A.* 2019;1593:54-62. doi:10.1016/j.chroma.2019.01.063.
59. Bergander T, Nilsson-Välímáa K, Oberg K, Lacki KM. High-throughput process development: determination of dynamic binding capacity using microtiter filter plates filled with chromatography resin. *Biotechnol Prog.* 2008;24(3):632-639. doi:10.1021/bp0704687.
60. Bellot JC, Condoret JS. Liquid chromatography modeling: A review. *Process Biochemistry.* 1991;26(6):363-376. doi:10.1016/0032-9592(91)85027-L.
61. Chen Y, Yang O, Sampat C, Bhalode P, Ramachandran R, Ierapetritou M. Digital Twins in Pharmaceutical and Biopharmaceutical Manufacturing: A Literature Review. *Processes.* 2020;8(9):1088. doi:10.3390/pr8091088.
62. Ruppach H. Viral safety for biotherapeutics and biosimilar. *Drug Discovery Today: Technologies.* 2020;395(1):565. doi:10.1016/j.ddtec.2020.08.001.
63. Wang W, Nema S, Teagarden D. Protein aggregation--pathways and influencing factors. *Int J Pharm.* 2010;390(2):89-99. doi:10.1016/j.ijpharm.2010.02.025.
64. Vázquez-Rey M, Lang DA. Aggregates in monoclonal antibody manufacturing processes. *Biotechnol Bioeng.* 2011;108(7):1494-1508. doi:10.1002/bit.23155.

65. Adamíková J, Antošová M, Polakovič M. Chromatographic purification of recombinant human erythropoietin. *Biotechnol Lett.* 2019;41(4-5):483-493. doi:10.1007/s10529-019-02656-8.
66. Guiochon G, Beaver LA. Separation science is the key to successful biopharmaceuticals. *J Chromatogr A.* 2011;1218(49):8836-8858. doi:10.1016/j.chroma.2011.09.008.
67. Ajish S.R. Potty, Alex Xenopoulos. Stress-Induced Antibody Aggregates. *BioProcess International.* <https://bioprocessintl.com/upstream-processing/bioreactors/stress-induced-antibody-aggregates-340657/>. Published March 1, 2013. Accessed July 3, 2022.
68. Guiochon G, Felinger A, Shirazi DG, Katti AM. *Fundamentals of preparative and nonlinear chromatography.* Second edition. Amsterdam, Boston, Heidelberg, London, New York, Oxford, Paris, San Diego, San Francisco, Singapore, Sydney, Tokyo: Elsevier Academic Press; 2006.
69. Kröner F, Hubbuch J. Systematic generation of buffer systems for pH gradient ion exchange chromatography and their application. *J Chromatogr A.* 2013;1285:78-87. doi:10.1016/j.chroma.2013.02.017.
70. Eriksson KO. Hydrophobic Interaction Chromatography. In: *Biopharmaceutical Processing.* Vol. 87. Elsevier; 2018:401-408.
71. Sýkora D, Řezanka P, Záruba K, Král V. Recent advances in mixed-mode chromatographic stationary phases. *J Sep Sci.* 2019;42(1):89-129. doi:10.1002/jssc.201801048.
72. Zhang K, Liu X. Mixed-mode chromatography in pharmaceutical and biopharmaceutical applications. *J Pharm Biomed Anal.* 2016;128:73-88. doi:10.1016/j.jpba.2016.05.007.
73. Yang Y, Geng X. Mixed-mode chromatography and its applications to biopolymers. *J Chromatogr A.* 2011;1218(49):8813-8825. doi:10.1016/j.chroma.2011.10.009.
74. Cytivia. MabSelect SuRe, 1 L. <https://www.cytivalifesciences.com/en/us/shop/chromatography/resins/affinity-antibody/mabselect-sure-antibody-purification-resin-p-00700#order>. Accessed May 14, 2022.
75. Cytivia Global Life Sciences Solutions USA LLC. Butyl Sepharose High Performance. <https://www.cytivalifesciences.com/en/us/shop/chromatography/resins/hydrophobic-interaction/butyl-sepharose-high-performance-p-05569>. Accessed May 14, 2022.
76. Cytivia Global Life Sciences Solutions USA LLC. Capto Butyl ImpRes hydrophobic interaction chromatography resin. <https://www.cytivalifesciences.com/en/us/shop/chromatography/resins/multimodal/capto-mmc-multimodal-chromatography-resin-p-05538>. Accessed May 14, 2022.
77. Cytivia Global Life Sciences Solutions USA LLC. Capto MMC multimodal chromatography resin. <https://www.cytivalifesciences.com/en/us/shop/chromatography/resins/multimodal/capto-mmc-multimodal-chromatography-resin-p-05538>. Accessed May 14, 2022.
78. Cytivia Global Life Sciences Solutions USA LLC. Capto Q ImpRes ion exchange chromatography resin. <https://www.cytivalifesciences.com/en/us/shop/chromatography/resins/ion-exchange/capto-q-impres-ion-exchange-chromatography-resin-p-00612>. Accessed May 14, 2022.
79. Cytivia Global Life Sciences Solutions USA LLC. Capto Q XP ion exchange chromatography resin | Cytiva (cytivalifesciences.com). <https://www.cytivalifesciences.com/en/us/shop/chromatography/resins/ion-exchange/capto-q-xp-ion-exchange-chromatography-resin-p-00595>. Accessed May 14, 2022.
80. Cytivia Global Life Sciences Solutions USA LLC. Capto S ion exchange chromatography resin. <https://www.cytivalifesciences.com/en/us/shop/chromatography/resins/ion-exchange/capto-s-ion-exchange-chromatography-resin-p-00721>. Accessed May 14, 2022.

81. Cytivia Global Life Sciences Solutions USA LLC. Capto adhere ImpRes multimodal chromatography resin.  
<https://www.cytivalifesciences.com/en/us/shop/chromatography/resins/multimodal/capto-adhere-impres-multimodal-chromatography-resin-p-06142>. Updated May 14, 2022.
82. Cytivia Global Life Sciences Solutions USA LLC. Capto Butyl ImpRes hydrophobic interaction chromatography resin.  
<https://www.cytivalifesciences.com/en/us/shop/chromatography/resins/hydrophobic-interaction/capto-butyl-impres-hydrophobic-interaction-chromatography-resin-p-05678>. Updated May 14, 2022.
83. Thermo Fisher Scientific. POROS™ Ethyl Hydrophobic Interaction Chromatography (HIC) Resin.  
<https://www.thermofisher.com/order/catalog/product/A32554>. Accessed May 14, 2022.
84. Liu HF, McCooey B, Duarte T, et al. Exploration of overloaded cation exchange chromatography for monoclonal antibody purification. *J Chromatogr A*. 2011;1218(39):6943-6952. doi:10.1016/j.chroma.2011.08.008.
85. Stone MT, Cotoni KA, Stoner JL. Cation exchange frontal chromatography for the removal of monoclonal antibody aggregates. *J Chromatogr A*. 2019;1599:152-160. doi:10.1016/j.chroma.2019.04.020.
86. Ichihara T, Ito T, Kurisu Y, Galipeau K, Gillespie C. Integrated flow-through purification for therapeutic monoclonal antibodies processing. *MAbs*. 2018;10(2):325-334. doi:10.1080/19420862.2017.1417717.
87. Bloomingburg GF, Carta G. Separation of protein mixtures by continuous annular chromatography with step elution. *The Chemical Engineering Journal and the Biochemical Engineering Journal*. 1994;55(1-2):B19-B27. doi:10.1016/0923-0467(94)87013-6.
88. Ng CKS, Rousset F, Valery E, Bracewell DG, Sorensen E. Design of high productivity sequential multi-column chromatography for antibody capture. *Food and Bioproducts Processing*. 2014;92(2):233-241. doi:10.1016/j.fbp.2013.10.003.
89. Arve BH, Liapis AI. Biospecific adsorption in fixed and periodic countercurrent beds. *Biotechnol Bioeng*. 1988;32(5):616-627. doi:10.1002/bit.260320506.
90. Aumann L, Morbidelli M. A continuous multicolumn countercurrent solvent gradient purification (MCSGP) process. *Biotechnol Bioeng*. 2007;98(5):1043-1055. doi:10.1002/bit.21527.
91. Zobel S, Helling C, Ditz R, Strube J. Design and Operation of Continuous Countercurrent Chromatography in Biotechnological Production. *Ind Eng Chem Res*. 2014;53(22):9169-9185. doi:10.1021/ie403103c.
92. Behere K, Yoon S. Chromatography bioseparation technologies and in-silico modelings for continuous production of biotherapeutics. *J Chromatogr A*. 2020;1627:461376. doi:10.1016/j.chroma.2020.461376.
93. Mollerup JM. The thermodynamic principles of ligand binding in chromatography and biology. *J Biotechnol*. 2007;132(2):187-195. doi:10.1016/j.jbiotec.2007.05.036.
94. Nicoud R-M. *Chromatographic processes: Modeling, simulation, and design*. Cambridge: Cambridge University Press; 2015. Cambridge series in chemical engineering.
95. www.efpia.eu. The pharmaceutical industry in figures. <https://efpia.eu/publications/downloads/>. Accessed May 31, 2020.
96. Bellot JC, Condoret JS. Liquid chromatography modeling: a review. *Process Biochemistry*. 1991;26(6):363-376. doi:10.1016/0032-9592(91)85027-L.

## References

---

97. Thoma JU, Ould Bouamama B. *Modeling and simulation in thermal and chemical engineering: A bond graph approach*. Berlin, Heidelberg: Springer; 2000. <http://www.loc.gov/catdir/enhancements/fy0816/99058791-d.html>.
98. Hagemann F, Wypysek D, Baitalow K, Adametz P, Thom V, Wessling M. Why device design is crucial for membrane adsorbers. *Journal of Chromatography Open*. 2022;2(4):100029. doi:10.1016/j.jcoa.2021.100029.
99. Schmidt-Traub H, Schulte M, Seidel-Morgenstern A, eds. *Preparative chromatography*. Third edition. Weinheim, Hoboken, NJ: Wiley-VCH; John Wiley & Sons Inc; 2020. <https://onlinelibrary.wiley.com/doi/book/10.1002/9783527816347>.
100. Brooks CA, Cramer SM. Steric mass-action ion exchange: Displacement profiles and induced salt gradients. *AIChE J*. 1992;38(12):1969-1978. doi:10.1002/aic.690381212.
101. Danckwerts PV. Continuous flow systems. Distribution of residence times. *Chemical Engineering Science*. 1995;50(24):3855. doi:10.1016/0009-2509(96)81810-0.
102. Levenspiel O. *Tracer Technology: Modeling the Flow of Fluids*. Boston, MA: Springer US; 2012. SpringerLink Bücher; 96. Accessed February 20, 2022.
103. Miyabe K, Cavazzini A, Gritti F, Kele M, Guiochon G. Moment analysis of mass-transfer kinetics in C18-silica monolithic columns. *Anal Chem*. 2003;75(24):6975-6986. doi:10.1021/ac0302206.
104. Foo SC, Rice RG. On the prediction of ultimate separation in parametric pumps. *AIChE J*. 1975;21(6):1149-1158. doi:10.1002/aic.690210615.
105. KATAOKA T, YOSHIDA H, UYAMA K. MASS TRANSFER IN LAMINAR REGION BETWEEN LIQUID AND PACKING MATERIAL SURFACE IN THE PACKED BED. *J Chem Eng Japan / JCEJ*. 1972;5(2):132-136. doi:10.1252/jcej.5.132.
106. Teepakorn C, Fiaty K, Charcosset C. Comparison of Membrane Chromatography and Monolith Chromatography for Lactoferrin and Bovine Serum Albumin Separation. *Processes*. 2016;4(3):31. doi:10.3390/pr4030031.
107. Johan Avallin, Anders Nilsson, Magnus Asplund, Niklas Pettersson, Tony Searle, and Christina Jägersen. Columns up to 1600 mm in diameter packed with protein A chromatography medium using axial mechanical compression. <http://www.processdevelopmentforum.com/posters/columns-up-to-1600-mm-in-diameter-packed-with-protein-a-chromatography-medium-using-axial-mechanical-compression/>. Accessed May 11, 2020.
108. Zhou JX, Tressel T. Basic concepts in Q membrane chromatography for large-scale antibody production. *Biotechnol Prog*. 2006;22(2):341-349. doi:10.1021/bp050425v.
109. Specht R, Han B, Wickramasinghe SR, et al. Densonucleosis virus purification by ion exchange membranes. *Biotechnol Bioeng*. 2004;88(4):465-473. doi:10.1002/bit.20270.
110. Yu M, Li Y, Zhang S, et al. Improving stability of virus-like particles by ion-exchange chromatographic supports with large pore size: advantages of gigaporous media beyond enhanced binding capacity. *J Chromatogr A*. 2014;1331:69-79. doi:10.1016/j.chroma.2014.01.027.
111. Catherine Charcosset. *Membrane processes in biotechnologies and pharmaceuticals*. Amsterdam, Boston: Elsevier; 2012. <http://www.sciencedirect.com/science/book/9780444563347>.
112. van Reis R, Zydney A. Bioprocess membrane technology. *Journal of Membrane Science*. 2007;297(1-2):16-50. doi:10.1016/j.memsci.2007.02.045.
113. Shekhawat LK, Rathore AS. An overview of mechanistic modeling of liquid chromatography. *Prep Biochem Biotechnol*. 2019;49(6):623-638. doi:10.1080/10826068.2019.1615504.

114. Close EJ, Salm JR, Bracewell DG, Sorensen E. Modeling of industrial biopharmaceutical multicomponent chromatography. *Chemical Engineering Research and Design*. 2014;92(7):1304-1314. doi:10.1016/j.cherd.2013.10.022.
115. Rischawy F, Saleh D, Hahn T, Oelmeier S, Spitz J, Kluters S. Good modeling practice for industrial chromatography: Mechanistic modeling of ion exchange chromatography of a bispecific antibody. *Computers & Chemical Engineering*. 2019;130(3):106532. doi:10.1016/j.compchemeng.2019.106532.
116. Saleh D, Wang G, Müller B, et al. Straightforward method for calibration of mechanistic cation exchange chromatography models for industrial applications. *Biotechnol Prog*. 2020;36(4):e2984. doi:10.1002/btpr.2984.
117. Schwellenbach J, Taft F, Villain L, Strube J. Preparation and characterization of high capacity, strong cation-exchange fiber based adsorbents. *J Chromatogr A*. 2016;1447:92-106. doi:10.1016/j.chroma.2016.04.019.
118. Roper DK, Lightfoot EN. Estimating plate heights in stacked-membrane chromatography by flow reversal. *Journal of Chromatography A*. 1995;702(1-2):69-80. doi:10.1016/0021-9673(94)01068-P.
119. Francis P, Lieres E von, Haynes CA. Zonal rate model for stacked membrane chromatography. I: characterizing solute dispersion under flow-through conditions. *J Chromatogr A*. 2011;1218(31):5071-5078. doi:10.1016/j.chroma.2011.05.017.
120. Zobel-Roos S, Stein D, Strube J. Evaluation of Continuous Membrane Chromatography Concepts with an Enhanced Process Simulation Approach. *Antibodies (Basel)*. 2018;7(1). doi:10.3390/antib7010013.
121. Dwivedi PN, Upadhyay SN. Particle-Fluid Mass Transfer in Fixed and Fluidized Beds. *Ind Eng Chem Proc Des Dev*. 1977;16(2):157-165. doi:10.1021/i260062a001.
122. Williamson JE, Bazaire KE, Geankoplis CJ. Liquid-Phase Mass Transfer at Low Reynolds Numbers. *Ind Eng Chem Fund*. 1963;2(2):126-129. doi:10.1021/i160006a007.
123. Carta G, Jungbauer A. *Protein chromatography: Process development and scale-up*. 2nd edition. Weinheim: Wiley-VCH; 2020. <https://onlinelibrary.wiley.com/doi/book/10.1002/9783527824045>.
124. Susanto A, Herrmann T, Hubbuch J. Short-cut method for the correction of light attenuation influences in the experimental data obtained from confocal laser scanning microscopy. *Journal of Chromatography A*. 2006;1136(1):29-38. doi:10.1016/j.chroma.2006.09.053.
125. Hubbuch J, Linden T, Knieps E, Thömmes J, Kula M-R. Mechanism and kinetics of protein transport in chromatographic media studied by confocal laser scanning microscopy. Part II. Impact on chromatographic separations. *Journal of Chromatography A*. 2003;1021(1-2):105-115. doi:10.1016/j.chroma.2003.08.092.
126. Ljunglöf A, Thömmes J. Visualising intraparticle protein transport in porous adsorbents by confocal microscopy. *Journal of Chromatography A*. 1998;813(2):387-395. doi:10.1016/s0021-9673(98)00378-1.
127. Boi C. Membrane adsorbents as purification tools for monoclonal antibody purification. *J Chromatogr B Analyt Technol Biomed Life Sci*. 2007;848(1):19-27. doi:10.1016/j.jchromb.2006.08.044.
128. Lan Q, Bassi AS, Zhu J-X, Margaritis A. A modified Langmuir model for the prediction of the effects of ionic strength on the equilibrium characteristics of protein adsorption onto ion

## References

---

- exchange/affinity adsorbents. *Chemical Engineering Journal*. 2001;81(1-3):179-186. doi:10.1016/S1385-8947(00)00197-2.
129. LeVan MD, Vermeulen T. Binary Langmuir and Freundlich isotherms for ideal adsorbed solutions. *J Phys Chem*. 1981;85(22):3247-3250. doi:10.1021/j150622a009.
130. Brooks CA, Cramer SM. Solute affinity in ion-exchange displacement chromatography. *Chemical Engineering Science*. 1996;51(15):3847-3860. doi:10.1016/0009-2509(95)00287-1.
131. Natarajan V, Cramer SM. Optimization of ion-exchange displacement separations. *Journal of Chromatography A*. 2000;876(1-2):63-73. doi:10.1016/S0021-9673(00)00139-4.
132. Gerstner JA, Cramer SM. Cation-exchange displacement chromatography of proteins with protamine displacers: effect of induced salt gradients. *Biotechnol Prog*. 1992;8(6):540-545. doi:10.1021/bp00018a011.
133. Guiochon G. *Fundamentals of preparative and nonlinear chromatography*. 2. ed. Amsterdam: Elsevier Acad. Press; 2006.
134. Katti AM, Dose EV, Guiochon G. Comparison of the performances of overloaded elution and displacement chromatography for a given column. *Journal of Chromatography A*. 1991;540:1-20. doi:10.1016/S0021-9673(01)88795-1.
135. Felinger A, Guiochon G. Optimization of the experimental conditions and the column design parameters in overloaded elution chromatography. *Journal of Chromatography A*. 1992;591(1-2):31-45. doi:10.1016/0021-9673(92)80220-O.
136. Vogg S, Pfeifer F, Ulmer N, Morbidelli M. Process intensification by frontal chromatography: Performance comparison of resin and membrane adsorber for monovalent antibody aggregate removal. *Biotechnol Bioeng*. 2020;117(3):662-672. doi:10.1002/bit.27235.
137. Morbidelli M, Servida A, Storti G, Carra S. Simulation of multicomponent adsorption beds. Model analysis and numerical solution. *Ind Eng Chem Fund*. 1982;21(2):123-131. doi:10.1021/i100006a005.
138. Kaczmarek K, Mazzotti M, Storti G, Morbidelli M. Modeling fixed-bed adsorption columns through orthogonal collocations on moving finite elements. *Computers & Chemical Engineering*. 1997;21(6):641-660. doi:10.1016/S0098-1354(96)00300-6.
139. Abramov YA, Sun G, Zeng Q. Emerging Landscape of Computational Modeling in Pharmaceutical Development. *J Chem Inf Model*. 2022;62(5):1160-1171. doi:10.1021/acs.jcim.1c01580.
140. Lye G, Hubbuch J, Schroeder T, Willmann E. Shrinking the Costs of Bioprocess Development - BioProcess International. <https://bioprocessintl.com/analytical/downstream-development/shrinking-the-costs-of-bioprocess-development-185354/>. Updated July 27, 2021. Accessed July 29, 2021.
141. Lenhoff AM. Protein adsorption and transport in polymer-functionalized ion-exchangers. *J Chromatogr A*. 2011;1218(49):8748-8759. doi:10.1016/j.chroma.2011.06.061.
142. Schmoltdt A, Benthe HF, Haberland G. Digitoxin metabolism by rat liver microsomes. *Biochemical Pharmacology*. 1975;24(17):1639-1641. doi:10.1016/0006-2952(75)90094-5.
143. Hunter AK, Carta G. Protein adsorption on novel acrylamido-based polymeric ion-exchangers. *Journal of Chromatography A*. 2000;897(1-2):65-80. doi:10.1016/S0021-9673(00)00864-5.
144. Hunter AK, Carta G. Protein adsorption on novel acrylamido-based polymeric ion-exchangers. *Journal of Chromatography A*. 2002;971(1-2):105-116. doi:10.1016/S0021-9673(02)01027-0.

145. Elsevier Science B.V., ed. *Monolithic materials: Preparation, properties, and applications*. 1st ed. Amsterdam: Elsevier; 2003. Journal of chromatography library; v. 67. <https://ebookcentral.proquest.com/lib/kxp/detail.action?docID=318202>.
146. Müller E. Properties and Characterization of High Capacity Resins for Biochromatography. *Chem Eng Technol*. 2005;28(11):1295-1305. doi:10.1002/ceat.200500161.
147. Orr V, Zhong L, Moo-Young M, Chou CP. Recent advances in bioprocessing application of membrane chromatography. *Biotechnol Adv*. 2013;31(4):450-465. doi:10.1016/j.biotechadv.2013.01.007.
148. Strancar A, Podgornik A, Barut M, Necina R. Short monolithic columns as stationary phases for biochromatography. *Adv Biochem Eng Biotechnol*. 2002;76:49-85. doi:10.1007/3-540-45345-8\_2.
149. BIA Separations. Architecture of chromatography media and devices. <https://www.biaseparations.com/en/technology/architecture-of-chromatography-media-and-devices>. Accessed May 12, 2020.
150. Díaz-Bao M, Barreiro R, Miranda J, Cepeda A, Regal P. Recent Advances and Uses of Monolithic Columns for the Analysis of Residues and Contaminants in Food. *Chromatography*. 2015;2(1):79-95. doi:10.3390/chromatography2010079.
151. Giese RW. Editorial on "Polymethacrylate monoliths for preparative and industrial separation of biomolecular assemblies" by A. Jungbauer and R. Hahn. *Journal of Chromatography A*. 2008;1184(1-2):61. doi:10.1016/j.chroma.2007.12.057.
152. Schwellenbach J, Zobel S, Taft F, Villain L, Strube J. Purification of Monoclonal Antibodies Using a Fiber Based Cation-Exchange Stationary Phase: Parameter Determination and Modeling. *Bioengineering (Basel)*. 2016;3(4). doi:10.3390/bioengineering3040024.
153. Cytiva. HiTrap Fibro Prisma units. <https://www.cytivalifesciences.com/en/us/shop/chromatography/membranes/hitrap-hiscreen-fibro-prisma-units-for-research-and-process-development-p-23550#related-documents>. Accessed June 1, 2020.
154. Nelson DM, Stanelle RD, Brown P, Marcus RK. Capillary-Channeled Polymer (C-CP) fibers: a novel platform for liquid-phase separations;. <https://www.americanlaboratory.com/913-Technical-Articles/19170-Capillary-Channeled-Polymer-C-CP-Fibers-A-Novel-Platform-for-Liquid-Phase-Separations/>. Accessed June 1, 2020.
155. Schwellenbach J, Kosiol P, Sölter B, Taft F, Villain L, Strube J. Controlling the polymer-nanolayer architecture on anion-exchange membrane adsorbers via surface-initiated atom transfer radical polymerization. *Reactive and Functional Polymers*. 2016;106:32-42. doi:10.1016/j.reactfunctpolym.2016.07.005.
156. Ley A, Altschuh P, Thom V, Selzer M, Nestler B, Vana P. Characterization of a macro porous polymer membrane at micron-scale by Confocal-Laser-Scanning Microscopy and 3D image analysis. *Journal of Membrane Science*. 2018;564(2):543-551. doi:10.1016/j.memsci.2018.07.062.
157. Hardin AM, Harinarayan C, Malmquist G, Axén A, van Reis R. Ion exchange chromatography of monoclonal antibodies: effect of resin ligand density on dynamic binding capacity. *J Chromatogr A*. 2009;1216(20):4366-4371. doi:10.1016/j.chroma.2008.08.047.
158. Suen S-Y, Etzel MR. A mathematical analysis of affinity membrane bioseparations. *Chemical Engineering Science*. 1992;47(6):1355-1364. doi:10.1016/0009-2509(92)80281-G.
159. Boi C, Dimartino S, Sarti GC. Modeling and simulation of affinity membrane adsorption. *Journal of Chromatography A*. 2007;1162(1):24-33. doi:10.1016/j.chroma.2007.02.008.

160. Legras A, Kondor A, Heitzmann MT, Truss RW. Inverse gas chromatography for natural fibre characterisation: Identification of the critical parameters to determine the Brunauer-Emmett-Teller specific surface area. *J Chromatogr A*. 2015;1425:273-279. doi:10.1016/j.chroma.2015.11.033.
161. Gelb LD, Gubbins KE. Characterization of Porous Glasses: Simulation Models, Adsorption Isotherms, and the Brunauer-Emmett-Teller Analysis Method. *Langmuir*. 1998;14(8):2097-2111. doi:10.1021/la9710379.
162. Baumann P, Huuk T, Hahn T, Osberghaus A, Hubbuch J. Deconvolution of high-throughput multicomponent isotherms using multivariate data analysis of protein spectra. *Eng Life Sci*. 2016;16(2):194-201. doi:10.1002/elsc.201400243.
163. Hahn T, Baumann P, Huuk T, Heuveline V, Hubbuch J. UV absorption-based inverse modeling of protein chromatography. *Eng Life Sci*. 2016;16(2):99-106. doi:10.1002/elsc.201400247.
164. Yamamoto S, Nakanishi K, Matsuno R, Kamikubo T. Ion exchange chromatography of proteins-prediction of elution curves and operating conditions. I. Theoretical considerations. *Biotechnol Bioeng*. 1983;25(6):1465-1483. doi:10.1002/bit.260250605.
165. Azevedo AM, Rosa PAJ, Ferreira IF, Aires-Barros MR. Chromatography-free recovery of biopharmaceuticals through aqueous two-phase processing. *Trends Biotechnol*. 2009;27(4):240-247. doi:10.1016/j.tibtech.2009.01.004.
166. Kuczewski M, Fraud N, Faber R, Zarbis-Papastoitsis G. Development of a polishing step using a hydrophobic interaction membrane adsorber with a PER.C6-derived recombinant antibody. *Biotechnol Bioeng*. 2010;105(2):296-305. doi:10.1002/bit.22538.
167. Charcosset C. Review: Purification of proteins by membrane chromatography. *J Chem Technol Biotechnol*. 1998;71(2):95-110. doi:10.1002/(SICI)1097-4660(199802)71:2<95:AID-JCTB823>3.0.CO;2-J.
168. Osberghaus A, Hepbildikler S, Nath S, Haindl M, Lieres E von, Hubbuch J. Determination of parameters for the steric mass action model--a comparison between two approaches. *J Chromatogr A*. 2012;1233:54-65. doi:10.1016/j.chroma.2012.02.004.
169. Gottschalk U, Brorson K, Shukla AA. Innovation in biomanufacturing: the only way forward. *Pharmaceutical Bioprocessing*. 2013;1(2):141-157. doi:10.4155/pbp.13.17.
170. Wolfe LS, Barringer CP, Mostafa SS, Shukla AA. Multimodal chromatography: Characterization of protein binding and selectivity enhancement through mobile phase modulators. *J Chromatogr A*. 2014;1340:151-156. doi:10.1016/j.chroma.2014.02.086.
171. Collins L, Franzblau SG. Microplate alamar blue assay versus BACTEC 460 system for high-throughput screening of compounds against Mycobacterium tuberculosis and Mycobacterium avium. *Antimicrob Agents Chemother*. 1997;41(5):1004-1009. doi:10.1128/AAC.41.5.1004.
172. Bensch M, Selbach B, Hubbuch J. High throughput screening techniques in downstream processing: Preparation, characterization and optimization of aqueous two-phase systems. *Chemical Engineering Science*. 2007;62(7):2011-2021. doi:10.1016/j.ces.2006.12.053.
173. Leuthold M. *Characterization of membrane adsorbers for contaminant removal*. Hannover : Gottfried Wilhelm Leibniz Universität Hannover; 2012.
174. Cromwell MEM, Hilario E, Jacobson F. Protein aggregation and bioprocessing. *AAPS J*. 2006;8(3):E572-9. doi:10.1208/aapsj080366.
175. Chi EY, Krishnan S, Randolph TW, Carpenter JF. Physical stability of proteins in aqueous solution: mechanism and driving forces in nonnative protein aggregation. *Pharm Res*. 2003;20(9):1325-1336. doi:10.1023/A:1025771421906.

176. Diederich P, Hubbuch J. High-Throughput Column Chromatography Performed on Liquid Handling Stations. In: Staby A, Rathore AS, Ahuja S, eds. *Preparative Chromatography for Separation of Proteins*. Vol. 100. Hoboken, NJ, USA: John Wiley & Sons, Inc; 2017:293-332.
177. Stefan Fischer-Frühholz, Florian Taft, Louis Villain, Amélie Boulais, R. Köhler, Sebastian van Teeffelen, Michael W. Wolff, Udo Reichl, A. Raquel Fortuna. Influenza virus capture using membrane chromatography: Improving selectivity by matrix design and pseudo-affinity ligand interactions. In: *Vaccine Technology VII*. ECI Symposium Series.
178. Hilterhaus L, Liese A, Kettling U, Antranikian G, eds. *Applied biocatalysis: From fundamental science to industrial applications*. Weinheim: Wiley-VCH Verlag GmbH & Co. KGaA; 2016. <http://gbv.ebib.com/patron/FullRecord.aspx?p=4558130>.
179. Rathore AS. *Process Validation in Manufacturing of Biopharmaceuticals*. 3rd ed. Hoboken: CRC Press; 2012. Biotechnology and Bioprocessing. <http://site.ebrary.com/lib/alltitles/docDetail.action?docID=10558381>.
180. *Biopharmaceutical Processing*. Elsevier; 2018.
181. Stein D, Thom V, Hubbuch J. High throughput screening setup of a scale-down device for membrane chromatography-aggregate removal of monoclonal antibodies. *Biotechnol Prog*. 2020;36(6):e3055. doi:10.1002/btpr.3055.
182. Nadarajah D, Mehta A, inventors; Genentech, Inc. OVERLOAD AND ELUTE CHROMATOGRAPHY. US20140301977.
183. Brown A, Bill J, Tully T, Radhamohan A, Dowd C. Overloading ion-exchange membranes as a purification step for monoclonal antibodies. *Biotechnol Appl Biochem*. 2010;56(2):59-70. doi:10.1042/BA20090369.
184. Reck JM, Pabst TM, Hunter AK, Carta G. Separation of antibody monomer-dimer mixtures by frontal analysis. *J Chromatogr A*. 2017;1500:96-104. doi:10.1016/j.chroma.2017.04.014.
185. Toueille M, Uzel A, Depoisier J-F, Gantier R. Designing new monoclonal antibody purification processes using mixed-mode chromatography sorbents. *J Chromatogr B Analyt Technol Biomed Life Sci*. 2011;879(13-14):836-843. doi:10.1016/j.jchromb.2011.02.047.
186. Voitl A, Müller-Späth T, Morbidelli M. Application of mixed mode resins for the purification of antibodies. *J Chromatogr A*. 2010;1217(37):5753-5760. doi:10.1016/j.chroma.2010.06.047.
187. Dieter Melzner, Rene Faber, H.-H. Hörl, Wolfgang Demmer, Stefan Fischer-Frühholz, Miyako Hirai. *New HIC and AEX membrane adsorbers*.
188. Mehta KK, Vedantham G. Next-Generation Process Design for Monoclonal Antibody Purification. In: *Biopharmaceutical Processing*. Vol. 127. Elsevier; 2018:793-811.
189. Wang J, Zhou J, Gowtham YK, Harcum SW, Husson SM. Antibody purification from CHO cell supernatant using new multimodal membranes. *Biotechnol Prog*. 2017;33(3):658-665. doi:10.1002/btpr.2454.
190. Khanal O, Kumar V, Lenhoff AM. Displacement to separate host-cell proteins and aggregates in cation-exchange chromatography of monoclonal antibodies. *Biotechnol Bioeng*. 2021;118(1):164-174. doi:10.1002/bit.27559.
191. Khanal O, Kumar V, Westerberg K, Schlegel F, Lenhoff AM. Multi-column displacement chromatography for separation of charge variants of monoclonal antibodies. *J Chromatogr A*. 2019;1586:40-51. doi:10.1016/j.chroma.2018.11.074.
192. Brgles M, Clifton J, Walsh R, et al. Selectivity of monolithic supports under overloading conditions and their use for separation of human plasma and isolation of low abundance proteins. *J Chromatogr A*. 2011;1218(17):2389-2395. doi:10.1016/j.chroma.2010.11.059.

## References

---

193. Chi EY, Krishnan S, Randolph TW, Carpenter JF. Physical Stability of Proteins in Aqueous Solution: Mechanism and Driving Forces in Nonnative Protein Aggregation. *Pharm Res*. 2003;20(9):1325-1336. doi:10.1023/A:1025771421906.
194. F. Hoffmann-La Roche AG. Roche Product Development Portfolio. [https://www.roche.com/de/research\\_and\\_development/who\\_we\\_are\\_how\\_we\\_work/pipeline.htm](https://www.roche.com/de/research_and_development/who_we_are_how_we_work/pipeline.htm). Accessed February 13, 2020.
195. AbbVie Inc. North Chicago. Our-Science/Pipeline. <https://www.abbvie.com/our-science/pipeline.html>. Accessed February 13, 2020.
196. GlaxoSmithKline plc. Our pipeline | GSK. <https://www.gsk.com/en-gb/research-and-development/our-pipeline/>. Accessed February 13, 2020.
197. Novartis International AG. Novartis Global Pipeline | Novartis. [https://www.novartis.com/our-science/novartis-global-pipeline?field\\_pipeline\\_therapeutic\\_area=2121&field\\_pipeline\\_therapeutic\\_area=2616&field\\_pipeline\\_therapeutic\\_area=2126&field\\_pipeline\\_therapeutic\\_area=2131&field\\_pipeline\\_therapeutic\\_area=2136&field\\_pipeline\\_therapeutic\\_area=2141&field\\_pipeline\\_therapeutic\\_area=2146&field\\_pipeline\\_therapeutic\\_area=2151&field\\_pipeline\\_filing\\_date=All](https://www.novartis.com/our-science/novartis-global-pipeline?field_pipeline_therapeutic_area=2121&field_pipeline_therapeutic_area=2616&field_pipeline_therapeutic_area=2126&field_pipeline_therapeutic_area=2131&field_pipeline_therapeutic_area=2136&field_pipeline_therapeutic_area=2141&field_pipeline_therapeutic_area=2146&field_pipeline_therapeutic_area=2151&field_pipeline_filing_date=All). Accessed February 13, 2020.
198. Pfizer Inc. Product Pipeline | Pfizer. <https://www.pfizer.com/science/drug-product-pipeline>. Accessed February 13, 2020.
199. SANOFI. Product Pipeline SANOFI. <https://www.sanofi.com/en/science-and-innovation/research-and-development>. Accessed February 13, 2020.
200. Knudsen HL, Fahrner RL, Xu Y, Norling LA, Blank GS. Membrane ion-exchange chromatography for process-scale antibody purification. *Journal of Chromatography A*. 2001;907(1-2):145-154. doi:10.1016/S0021-9673(00)01041-4.
201. Dieter Melzner. New HIC and AEX membrane Adsorber; September 6, 2009; Montpellier, France.
202. Washburn MP, Wolters D, Yates JR. Large-scale analysis of the yeast proteome by multidimensional protein identification technology. *Nat Biotechnol*. 2001;19(3):242-247. doi:10.1038/85686.
203. Link AJ, Eng J, Schieltz DM, et al. Direct analysis of protein complexes using mass spectrometry. *Nat Biotechnol*. 1999;17(7):676-682. doi:10.1038/10890.
204. Wang J, Jenkins EW, Robinson JR, Wilson A, Husson SM. A new multimodal membrane adsorber for monoclonal antibody purifications. *Journal of Membrane Science*. 2015;492:137-146. doi:10.1016/j.memsci.2015.05.013.
205. Pezzini J, Joucla G, Gantier R, et al. Antibody capture by mixed-mode chromatography: a comprehensive study from determination of optimal purification conditions to identification of contaminating host cell proteins. *J Chromatogr A*. 2011;1218(45):8197-8208. doi:10.1016/j.chroma.2011.09.036.
206. Kallberg K, Johansson H-O, Bulow L. Multimodal chromatography: an efficient tool in downstream processing of proteins. *Biotechnol J*. 2012;7(12):1485-1495. doi:10.1002/biot.201200074.
207. Kaleas KA, Schmelzer CH, Pizarro SA. Industrial case study: evaluation of a mixed-mode resin for selective capture of a human growth factor recombinantly expressed in *E. coli*. *J Chromatogr A*. 2010;1217(2):235-242. doi:10.1016/j.chroma.2009.07.023.

208. Alpert AJ. Electrostatic repulsion hydrophilic interaction chromatography for isocratic separation of charged solutes and selective isolation of phosphopeptides. *Anal Chem.* 2008;80(1):62-76. doi:10.1021/ac070997p.
209. Stein D, Thom V, Hubbuch J. Process development exploiting competitive adsorption-based displacement effects in monoclonal antibody aggregate removal-A new high-throughput screening procedure for membrane chromatography. *Biotechnol Appl Biochem.* 2021. doi:10.1002/bab.2236.
210. GE Healthcare. Capto adhere multimodal chromatography resin: GE Healthcare Life Sciences. <https://www.gelifesciences.com/en/us/shop/chromatography/resins/multimodal/capto-adhere-multimodal-chromatography-resin-p-05643#tech-spec-table>. Accessed February 3, 2020.
211. GE Healthcare. Process development HiScreen™ prepacked columns. <https://www.gelifesciences.com/en/us/shop/chromatography/prepacked-columns/multimodal/hiscreen-capto-adhere-p-00615#related-documents>. Accessed February 3, 2020.
212. GE Healthcare. Purification of monoclonal antibodies using modern chromatography media and membranes: 29094443 AB. Accessed February 3, 2020.
213. Gary Lye, Jürgen Hubbuch, Tim Schroeder, and Eric Willmann. Shrinking the Costs of Bioprocess Development. *BioProcess International.* 2009;Case Study Automation. <https://pdfs.semanticscholar.org/c690/f2a1a845c282dbe8baee734bf65378a02393.pdf>. Accessed February 3, 2019.
214. Stamatis C, Goldrick S, Gruber D, Turner R, Titchener-Hooker NJ, Farid SS. High throughput process development workflow with advanced decision-support for antibody purification. *J Chromatogr A.* 2019;1596:104-116. doi:10.1016/j.chroma.2019.03.005.
215. Utturkar A, Gillette K, Sun C-Y, Pagkaliwangan M, Quesenberry R, Schofield M. A Direct Approach for Process Development Using Single Column Experiments Results in Predictable Streamlined Multi-Column Chromatography Bioprocesses. *Biotechnol J.* 2019;14(4). doi:10.1002/biot.201800243.
216. Stein D, Thom V, Hubbuch J. Streamlined process development procedure incorporating the selection of various stationary phase types established in a mAb aggregate reduction study with different mixed mode ligands. *Biotechnol Prog.* 2022;38(2):e3230. doi:10.1002/btpr.3230.
217. Cytivia Global Life Sciences Solutions USA LLC. GoSilico™ Chromatography Modeling Software. <https://www.cytivalifesciences.com/en/de/shop/chromatography/chromatography-modeling/gosilico-chromatography-modeling-software-p-28023>. Accessed May 18, 2022.
218. Jülich Forschungszentrum. CADET for process chain simulation including, but not limited to, fermentation, filtration and chromatograph. [https://www.fz-juelich.de/ibg/ibg-1/EN/Research/SystemsBiotechnology/modsim/modsim\\_research.html?nn=982498](https://www.fz-juelich.de/ibg/ibg-1/EN/Research/SystemsBiotechnology/modsim/modsim_research.html?nn=982498).
219. Chi EY, Krishnan S, Randolph TW, Carpenter JF. Physical Stability of Proteins in Aqueous Solution: Mechanism and Driving Forces in Nonnative Protein Aggregation. *Pharm Res.* 2003;20(9):1325-1336. doi:10.1023/A:1025771421906.

## 10 Appendix

### 10.1 HTS setup of a Scale-down Device for Membrane Chromatography - Aggregate Removal of Monoclonal Antibodies

The supplementary material for Chapter 3 is presented below, additional HTS information.

#### 10.1.1 HTS set-up development of a scale-down device

The HTS set-up development included the development of the SDD and additional parts to facilitate the dedicated chromatographic processing mimic. Figure 10.1 presents one HTS set-up consisting of the pipetting arm, buffer stock, shaker and interim storage for well-plates already used, the rack stock, and a UV well plate reader. Initially, the Gripper arm will adjust the moveable SDD well plate holder and place four well plates on it. Thereafter, the moveable SDD well plate holder will be moved to the operation position. Next, the pipetting arm will perform all liquid supplies taken by the buffer stock, which can either be a 50 mL or 15 mL falcon tube holder. Following the liquid uptake, the pipetting arm will dispense the liquid through the SDD injection port. Afterward, the gripper arm will move the SDD well plate holder and repeat the liquid handling according to the programmed recipe. For example, if four pipetting steps were performed, the well plates were moved to the shaker and interim well plate storage. The procedure is repeated until the method is completed. Thereafter, the gripper sorts the well plate according to its pipetting steps, completing the chromatographic method. The robotic platform can then be changed to support the analytical preparation by mounting an HPLC vial holder. Furthermore, the well plate fractions are automatically mixed by liquid aspiration, dispensing, and transferred to the HPLC vials. Finally, the HPLC vials are capped and transferred to the SEC.

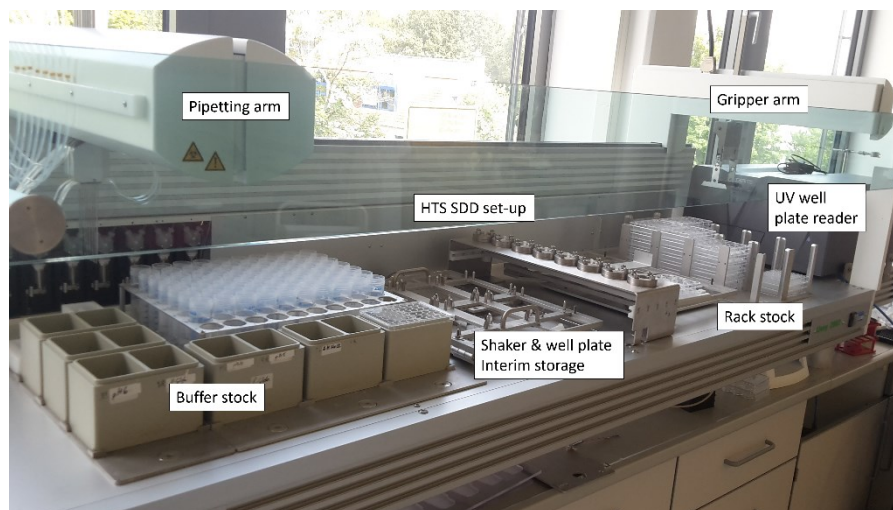


Figure 10.1: Overview of the robotic platform

The above-mentioned chromatographic process is performed in Figure 10.2 presented SDD. The SDD parts are specified in Table 10.1. Specifically, the SDD consists of a base frame (3) added by a small-scale lab module holder (1) that supports the 3D printed and optimized small-scale device. Furthermore, the well plates (4) are held and positioned by the moveable slide in the well plate holder and positioner (5) sliding in the rail (2). The slide-in well plate holder nose (6) allows the gripper to move the well plate holder and enable the fractionation between the pipetting steps.

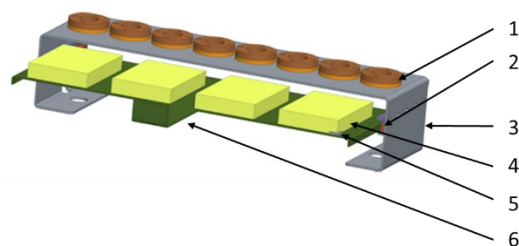
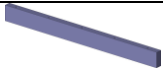


Figure 10.2: Schematic HTS set-up

Table 10.1: HTS parts description

Part	Number	Exemplary design	Description
Lab module holder	1	-	Holder for lab module
Guiding rail	2.1		Guiding rail for the slide-in module, enables movement and thus fractionation
Cover guiding rail	2.2		Holds the slide-in module horizontal
Stopper	2.3		Prevents the slide-in module from leaving the guiding rail
Base frame	3		Frame for the HTS set up
Well plate	4	-	Contains fractions of the experiments
Glue elbow	5		Exact positioning of the well plates and thus preventing misalignment between the lab module outlet and the well plate fraction position.
Slide-in module	6		Enables the fractionation and holds the well plates. The bending provides the movement by the robotic arm

The additional robotic platform parts for more buffer supply and HPLC analytic preparation are presented in Figure 10.3 A) and B). respectively.

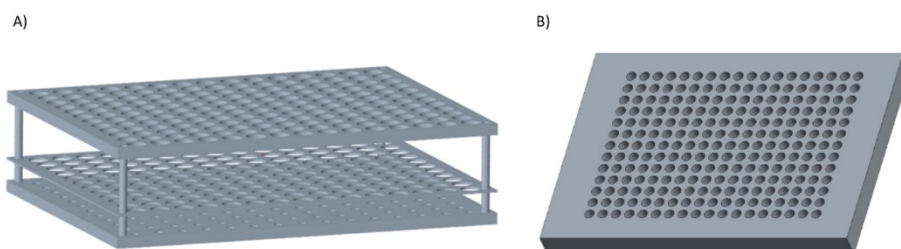


Figure 10.3: In A) the 15 mL falcon tube holder for buffers and in B) the HPLC holder for automated probe preparation are presented.

10.1.2 Robotic parameters

he liquid handling parameter is subdivided into component properties and volume correction parameters. In the typical range of 0-6 g/L protein content and 0-0.3 M buffer salt content, no significant effect was observed on the viscosity and density of the total solution. The viscosity and density were measured in the range of 0-6 g/L absolute protein concentration, pH 4-7, and 0-1 molar sodium chloride concentration in PBS. Additionally, KPi buffer was investigated in a range of 0-6 g/L absolute protein concentration and 0-1 molar sodium chloride concentration. Density measurement was performed by a DMA 38 from Anton Paar GmbH, and the viscosity was measured by an Ubbelohde capillary type 50110 viscometer from SI Analytics GmbH. All measurements were tempered by 20 °C. Comparing the density results in Table 10.2 with water (0.9982 g/cm<sup>3</sup>, 1.03 mPa·s) presents a deviation below 6 % for the density and below 16 % in viscosity.

Furthermore, the deviation between density and viscosity of the PBS and KPi buffer is below 5 % and 14 %, respectively. The maximum deviation between the experimental replicas was 2 %. The maximum viscosity change can be compared to the viscosity of ethanol. The deviation for dispensed volumes equal to or above 200 µL was in the calibration error noise.

Table 10.2: Overview of density and viscosity results for PBS and KPi buffer

		Density [g/cm <sup>3</sup> ]				Viscosity [mPa·s]			
		pH-value [-]		Salt concentration [mol/L]		pH-value [-]		Salt concentration [mol/L]	
<i>PBS Buffer</i>		4	7	0	1	4	7	0	1
Protein [g/L]	0	1.0081	1.0053	1.0049	1.0438	1.05	1.03	1.03	1.11
	6	1.0083	1.0084	1.0064	1.0346	1.08	1.1	1.08	1.15
<i>KPI Buffer</i>									
Protein [g/L]	0	-	-	1.0114	1.0494	-	-	1.07	1.15
	6	-	-	1.0110	1.0387	-	-	1.13	1.19

Accordingly, the HTS component liquid handling parameters were kept constants for all runs. The volume correction factors were adjusted if the accuracy of the dispensed volume at 500 µL/s was greater than 3%, see Figure 10.4. In addition, deviations above 10% were used to identify mechanical inadequacies such as defective needles or pump gaskets. The calibration procedure was automated by writing a procedure in the internal provided “Calibration worker” program in Figure 10.5. Furthermore, the connection to the weighing device was facilitated. Thereafter, the HTS method pipetting interval, number of checked syringes, number of measurements, and lower limit to acquire weight entered. Based on the pipetting interval, the weight change was checked each 10th of an interval time, and if it exceeds the lower limit to acquire, the weight is taken when constant. Direct integration of a weighing device was not possible at the used robotic set-up.

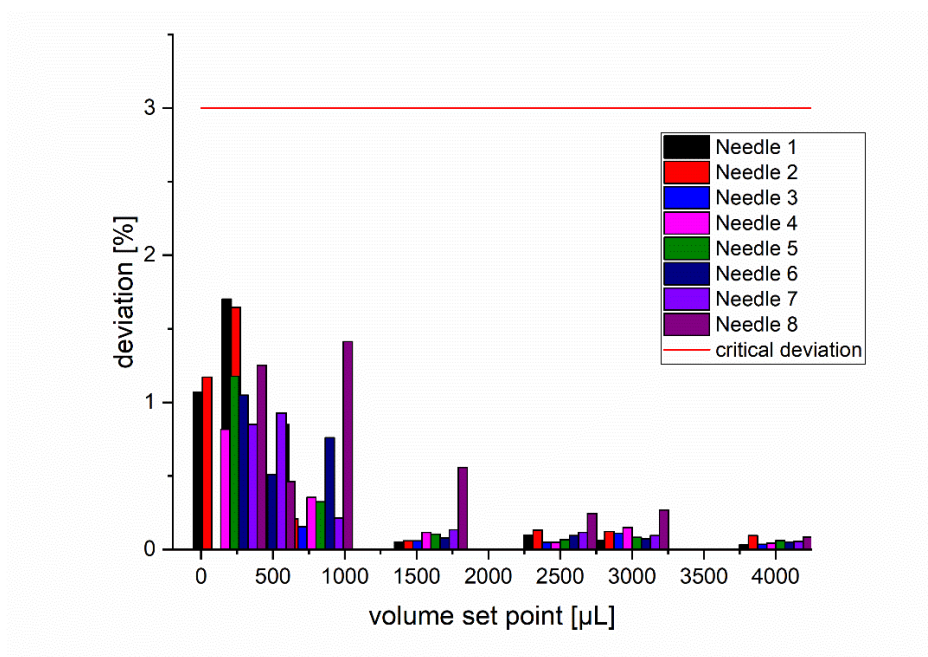


Figure 10.4: Exemplary calibration routine. All dispensing steps show a deviation of less than 3% from the specified values. The volume correction factors remain unchanged.

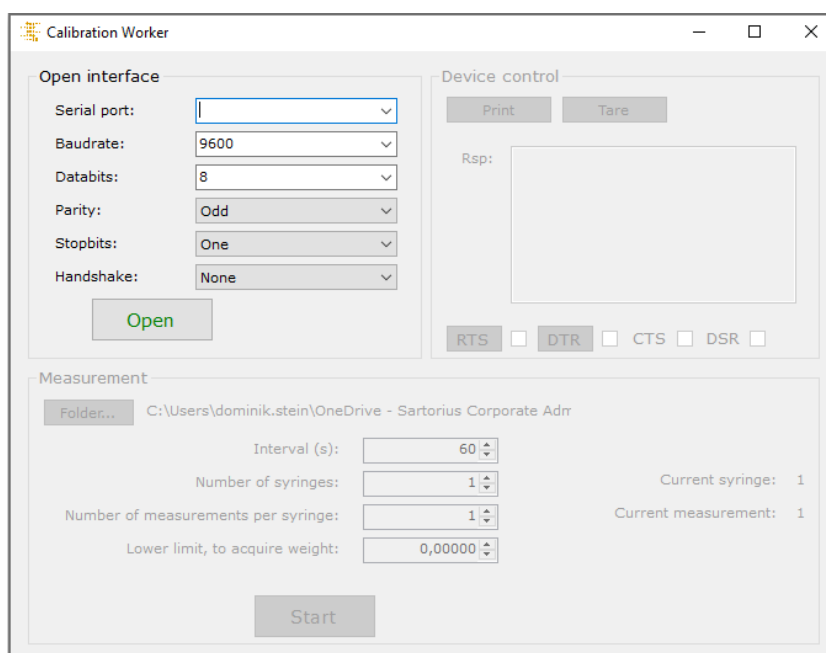


Figure 10.5: User Interface for the developed pipetting calibration procedure by a weighing device.

The aspirating and dispensing speed can influence the pipetted volume and binding capacity. Following this, we conducted the calibration routine and IgG SDD – HTS bind and elute experiments with IgG at 100 and 500  $\mu\text{L}/\text{s}$ . The calibration routine showed no significant differences between the two investigated velocities. The corresponding IgG bind and elute experiments show deviations of 1.7% and 8.6% for the monomer and dimer binding capacity; these deviations are supposed to be negligible.

## 10.2 Appendix - Full train product development from lab 2 production procedure – incorporating a living library with mechanistic modeling - from HTS Scale to pilot scale of Membrane Chromatography in aggregate Removal of Monoclonal Antibodies

The supplementary material for Chapter 6 is presented below, additional modeling information.

### 10.2.1 Mechanistic modeling

In Table 10.3, the apparent isotherm parameter along with the Peclet numbers are presented. The apparent isotherm parameter was used in chapter 6 to assess the kinetic parameter. Thereafter, mechanistic modeling applied the Peclet number to facilitate the scale-up.

Table 10.3: Applied SMA isotherm parameters

	IgG	HMWS
$K_{kin}$	0.07	0.74
$K_{EQ}$	26.34	36.02
$v$	3.20	3.32
$\sigma$	459.28	10556.80
Pe	95.4	8.6

Table 10.4 notes the applied models for the system description. Subsequent to the device optimization, the HTS set-up presented itself with no significant influence on the separation. This was shown by the comparison of HTS and benchtop results in chapter 3. The benchtop systems used were all characterized by PFR models. Unlike small-scale systems, the pilot scale model development presented itself as more complex. The system was split into five sections: two pump lines, system until UV detector pre-MA, MA Pipes and System until post-MA. All sections were investigated by acetone and salt tracer at different flow rates (45, 80, and 150 L/h). In addition, the pump regulation parameter interference with the accurate model building. Therefore, the pump work – output per time – was measured. Following this, the determined pump work correlation was used to calculate the resulting switch from one pump to the second. The received pump transition profile presented the buffer to tracer/protein transition when switching from one pump to another. The difference between the ramp on and ramp off profile was investigated, and the pump work correlation was assessed. Finally, a sufficient model quality was achieved.

Table 10.4: Applied System models

System	Model Identifier	Model
HTS	Device	PFR
	MA	Equilibrium dispersive
Benchtop	Elution Buffer	PFR
	Buffer & Feed	PFR
	Device	PFR
	MA	Equilibrium dispersive
Pilot Scale	Pump line I	PFR
	Pump line II	PFR
	UV Pre MA	PFR
	MA Pipes	PFR
	Device	PFR
	MA	Equilibrium dispersive
	UV Post MA	PFR